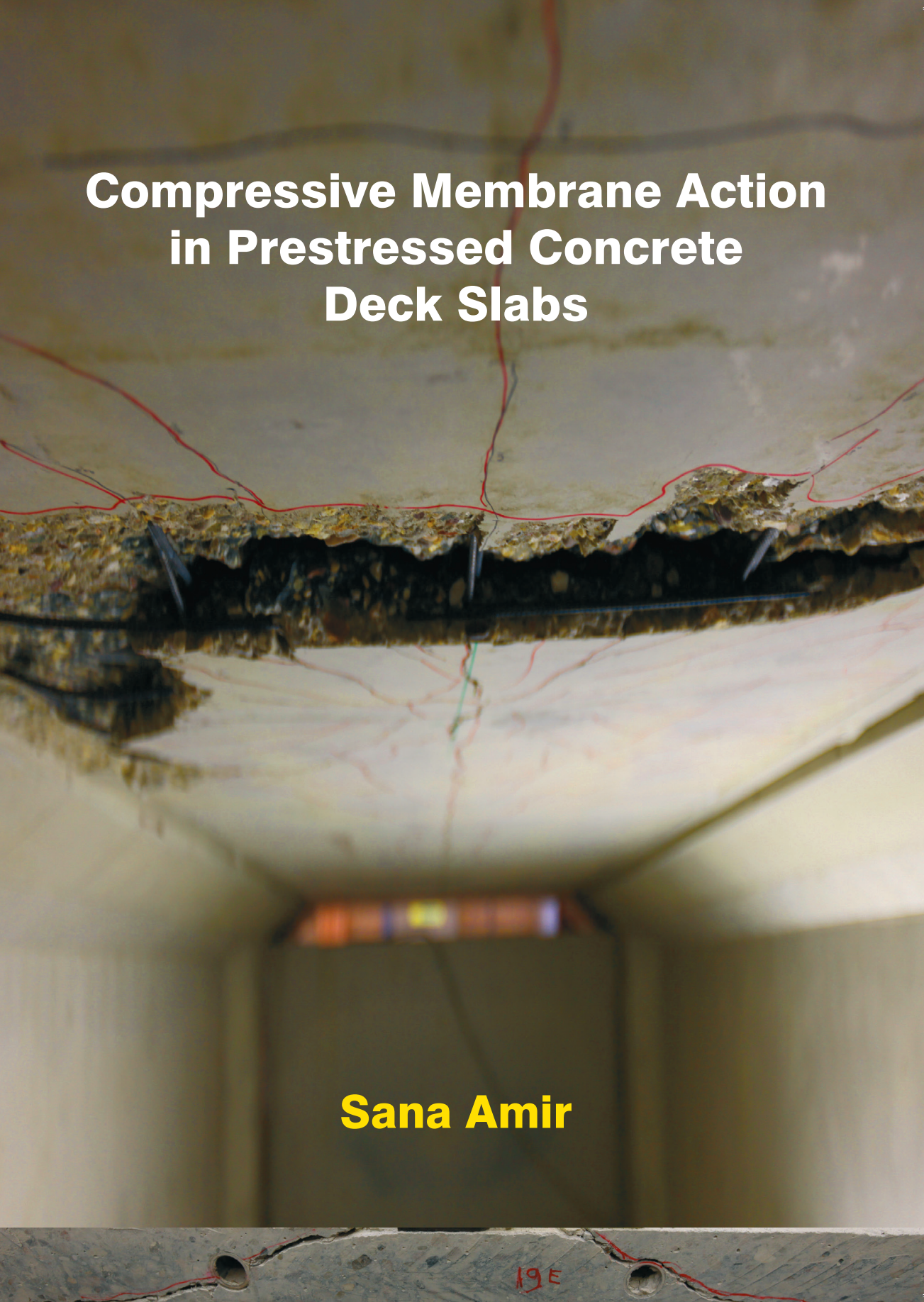


# Compressive Membrane Action in Prestressed Concrete Deck Slabs



**Sana Amir**

# Propositions

Accompanying the Ph.D. Thesis

## *Compressive Membrane Action in Prestressed Concrete Deck Slabs*

Sana Amir

1. The in-plane compressive forces resulting from transverse prestressing in combination with the compressive membrane forces arising from the lateral restraint can enhance the bearing capacity of bridge decks considerably.
2. The contribution of compressive membrane action to the punching shear capacity of prestressed concrete slabs is independent of the level of prestressing. The effects of prestressing and lateral confinement can be added when calculating the punching shear capacity of the slab.
3. The Level of Approximation V proposed in this research implies that the critical shear crack theory becomes redundant when a nonlinear analysis with a 3D solid finite element model is carried out.
4. The Critical Shear Crack Theory is a discovery, not an invention.
5. From scientific models to life in general, the more complexities we introduce, the more sources of error we generate.
6. Working women must believe in themselves first before expecting that others will do, because self-confidence is the key to success, especially when you are outnumbered in a male-dominated field.
7. The hottest places in hell are reserved for those who, in a period of moral crisis, maintain their neutrality.  
(An interpretation of Dante Alighieri's *La Comedia Divina*, Inferno, canto 3)
8. To transform a society, both political and social elements must work together as the one element can't have an impact without the contribution of the another.
9. The world can be a better place without the concept of nationalism.
10. Intelligence + Hard work → PhD, where Luck acts as a catalyst.

*These propositions are regarded as opposable and defensible, and have been approved as such by the supervisor Prof. dr. ir. Dr.-Ing. e.h. J.C. Walraven.*

# Stellingen

Behorende bij het proefschrift

## *Compressive Membrane Action in Prestressed Concrete Deck Slabs*

Sana Amir

1. In het vlak van de plaat aangrijpende normaaldrukkrachten ten gevolge van voorspanning, in combinatie met membraandrukkrachten ten gevolge van verhinderde zijdelingse uitzetting, kunnen het draagvermogen van betonnen brugdekken aanzienlijk vergroten.
2. De bijdrage van membraandrukwerking aan het ponsdraagvermogen van voorgespannen betonnen dekken is onafhankelijk van het voorspanniveau. De effecten van voorspanning en membraandrukwerking kunnen bij elkaar worden opgeteld bij het berekenen van het ponsdraagvermogen van het dek.
3. Het benaderingsniveau V voorgesteld in deze studie voor de berekening van het ponsdraagvermogen van betonnen platen houdt in dat de Kritische Dwarskracht Scheur Theorie overbodig wordt indien een niet-lineaire numerieke analyse met 3D-volume-elementen wordt uitgevoerd.
4. De Kritische Dwarskracht Scheur Theorie is een ontdekking, geen uitvinding.
5. Wat geldt voor wetenschappelijk modellen geldt ook voor het leven in het algemeen: hoe meer complicaties we er in verwerken, des te groter wordt de kans op falen.
6. Werkende vrouwen moeten in zichzelf geloven voordat zij verwachten dat anderen dat zullen doen, omdat zelfvertrouwen de sleutel tot succes is, speciaal in een door mannen gedomineerd vakgebied waar vrouwen in de minderheid zijn.
7. De heetste plaatsen in de hel zijn gereserveerd voor diegenen die, in een periode van morele crisis, hun neutraliteit behouden.  
(Een interpretatie van Dante Alighieri's *La Comedia Divina*, Inferno, canto 3)
8. Om een maatschappij te hervormen moeten politieke en sociale elementen met elkaar samenwerken, omdat het ene element geen impact heeft zonder het andere.
9. De wereld kan een betere plaats zijn zonder het concept van nationalisme.
10. Intelligentie + Hard werken → Doctorstitel, waarbij de factor geluk als katalysator werkt.

*Deze stellingen worden oponeerbaar en verdedigbaar geacht en zijn als zodanig goedgekeurd door de promotor Prof. dr. ir. Dr.-Ing. e.h. J.C. Walraven.*

# **Compressive Membrane Action in Prestressed Concrete Deck Slabs**



Faculty of Civil Engineering and Geosciences  
Department of Structural and Building Engineering  
Concrete Structures

Delft, the Netherlands



# **Compressive Membrane Action in Prestressed Concrete Deck Slabs**

## **Proefschrift**

ter verkrijging van de graad van doctor  
aan de Technische Universiteit Delft,  
op gezag van de Rector Magnificus prof. ir. K.C.A.M. Luyben,  
voorzitter van het College voor Promoties,  
in het openbaar te verdedigen op woensdag 4 juni 2014 om 12:30 uur

door

**Sana AMIR**

Master of Science in Civil Engineering, University of Engineering and Technology Lahore

geboren te Lahore, Pakistan

Dit proefschrift is goedgekeurd door de promotor:

Prof. dr. ir. J. C. Walraven

Copromotor: Dr. ir. C. van der Veen

Samenstelling promotiecommissie:

Rector Magnificus,	voorzitter
Prof. dr. ir. J. C. Walraven,	Technische Universiteit Delft, promotor
Dr. ir. C. van der Veen,	Technische Universiteit Delft, copromotor
Prof. dr. ir. D. A. Hordijk,	Technische Universiteit Delft
Prof. dr. ir. J. G. Rots,	Technische Universiteit Delft
Prof. dr. M. Hallgren,	Kungliga Tekniska Högskolan (KTH) Royal Institute of Technology
Dr. ir. A. de Boer,	Rijkswaterstaat
Dr. G. I. B. Rankin,	Queen's University Belfast
Prof. Ir. A. Q. C. van der Horst	Technische Universiteit Delft, reservelid

This work is supported by:

Faculty Development Program, University of Engineering and Technology Lahore  
Rijkswaterstaat, Ministry of Infrastructure and the Environment  
SOOB, Stichting Stimulering Onderwijs En Onderzoek Betonconstructies

ISBN: 978-90-8891-895-7

Printed by: Uitgeverij BOXPress

Cover design: Uitgeverij BOXPress

Published by: Uitgeverij BOXPress, 's-Hertogenbosch

Copyright © 2014 S. Amir

Email: sanaamir.1919@gmail.com

*All rights reserved. No part of the material protected by this copyright notice may be reproduced or utilized in any form or by any means, electronic or mechanical, including photocopying, recording or by any information storage and retrieval system, without permission from the author.*

*Dedicated to my parents and grandparents*



## Summary

### **Compressive Membrane Action in Prestressed Concrete Deck Slabs**

One of the most important questions that structural engineers all over the world are dealing with is the safety of the existing structures. In the Netherlands, there are a large number of transversely prestressed bridge decks that have been built in the last century and now need to be investigated for their structural safety under the actual (increased) traffic loads, for the rest of their service life. This research is an attempt to investigate the bearing (punching shear) capacity of such bridge decks under concentrated loads (wheel loads). Using the actual design codes for the verification of the bearing capacity leads to values suggesting that the safety standards are not met. However, since the bridge decks are laterally restrained by the supporting beams it is expected that compressive membrane action (CMA) exists in such deck slabs, and that the transverse prestressing of the deck slab in combination with CMA will enhance the bearing capacity, making thinner deck slabs possible with no problems of serviceability and structural safety.

This thesis begins with an introduction to the research topic, listing briefly the background and the objectives, and concluding with the research strategy. A literature review regarding the punching shear capacity of transversely prestressed concrete decks and compressive membrane action has also been carried out. First, the general mechanism of punching shear and compressive membrane action is explained along with the relevant analysis methods and code provisions and then important experimental investigations done on prestressed deck slabs are briefly described. It is concluded that there is a need to investigate the bearing capacity of transversely prestressed concrete deck slabs supported by and connected to concrete girders using a large scale model since most of the past research is either done on concrete decks with steel girders or on small scale models.

In order to investigate the research problem experimentally, laboratory tests on a 1:2 scale bridge model of a real bridge in the Netherlands have been performed. The model bridge consisted of a thin, transversely prestressed concrete deck (with unbonded tendons), cast in-situ between the flanges of long prestressed concrete girders. Prestressed transverse beams were also provided close to either end of the bridge deck. The interface between the deck slab and the girder flanges was either straight or skewed and two types of loads were applied: single and double. Loads were applied at midspan and close to the deck slab-girder flange interface. All the tests showed failure in punching shear (either brittle punching or flexural punching) regardless of the type and position of the load. Failure always occurred in the span of the slab, whereas the interface remained undamaged. The effect of various

## Summary

parameters, like the transverse prestressing level (TPL), the type and position of the load(s), the inclination of the joint (interface), the size of the loading plate etc., on the bearing capacity were also studied.

As part of the numerical investigation, a 3D solid, 1:2 scale model of the real bridge, similar to the experimental model, was developed in the finite element software DIANA and several nonlinear analyses were carried out. A comparison with the experimental results was made proving that satisfactory results were obtained that validated the finite element model. The normal forces arising from compressive membrane action were determined with the help of composed elements. A detailed parametric study was also carried out involving numerical modeling parameters, like the mesh size, displacement-load step size etc., and the material and geometrical parameters, similar to the experimental parametric study. In addition to that, the size effect was studied by carrying out a nonlinear analysis on a 3D solid model of the real bridge, showing that a size factor of 1.2 is appropriate to convert the results of the model bridge deck with 100 mm thickness to those for the real bridge deck with a thickness of 200 mm.

A theoretical analysis of the model bridge deck was then carried out and it was demonstrated that the ultimate load carrying capacity as found from the experiments and the finite element analysis was much higher than predicted by governing codes and theoretical methods. The discrepancy was attributed to the lack of consideration of CMA in the theoretical approaches. In order to incorporate CMA in the analysis, the normal forces arising from compressive membrane action and determined via the finite element analysis were used in the *fib* Model Code 2010 punching shear provisions (based on the Critical Shear Crack Theory) to determine the ultimate bearing (punching shear) capacity. Calculations were performed at two Levels-of-Approximation (LoA); Elementary LoA (without CMA) and Advanced LoA (with CMA).

Generally, it was observed that an increase in the TPL improved the behavior of the bridge deck with regard to both serviceability and ultimate limit state. An average safety factor of 3.25 was obtained when the projected model bridge design capacity and the real bridge design capacity were compared with the design wheel load. It can be concluded that the existing bridges still have sufficient residual bearing capacity considering the beneficial effect of CMA. Moreover it was shown that appropriate nonlinear finite element models can predict the load bearing capacity quite accurately. The research described in this thesis, resulting in methods for the analysis of bridge decks including compressive membrane action, has the potential to result in considerable cost savings, since the models are able to demonstrate that many existing bridge decks are safe enough, contrary to earlier

## Summary

expectations. A proposal has been prepared to introduce the effect of compressive membrane action into the calculation models for punching shear offered in the *fib* Model Code for Concrete Structures 2010. To this end two more Levels of Approximation are added to the first three given already in the code. The new level IV enables the use of the Critical Shear Crack Theory in combination with the calculation of the curvature of the area around the concentrated load with a nonlinear finite element analysis using shell elements. The level V enables the prediction of the punching shear capacity with a tailored NLFE-program using composed elements.

## Summary

## Samenvatting

### **Membraandrukwerking in voorgespannen betonnen brugdekken**

Een van de belangrijkste vraagstukken waarmee constructieve ingenieurs over de hele wereld te maken hebben is de veiligheid van bestaande constructies. In Nederland zijn een groot aantal in het vlak voorgespannen brugdekken voorhanden die gebouwd zijn in de vorige eeuw en nu moeten worden onderzocht op constructieve veiligheid in relatie tot de (toegenomen) verkeersbelasting, voor de rest van de geplande levensduur. Het uitgevoerde onderzoek richt zich op het ponsdraagvermogen van zulke brugdekken bij hoge geconcentreerde lasten (wiellasten). Het gebruik van de huidige bouwvoorschriften voor het bepalen van het draagvermogen leidt tot waarden, waaruit men zou kunnen concluderen dat de vereiste constructieve veiligheid niet wordt gehaald. Omdat de brugdekken echter niet alleen in hun vlak zijn voorgespannen, maar ook in hun vlak zijn opgesloten door het systeem van dragende brugliggers, kan verwacht worden dat bij belasten door verkeer membraandrukwerking (“gewelf-werking”) ontstaat, waardoor het draagvermogen in werkelijkheid groter is dan berekend met de eerder genoemde rekenmodellen. Hierdoor zijn dunnere dekken mogelijk, zonder dat problemen ten aanzien van de bruikbaarheidsgrenstoestand en de uiterste grenstoestand ontstaan.

De dissertatie begint met een introductie in het onderwerp van het onderzoek, waarbij in het kort de achtergronden en de doelstellingen worden toegelicht, en de strategie van het onderzoek wordt voorgesteld. Tevens worden belangrijke elementen uit de literatuur omtrent het ponsgedrag van in het vlak voorgespannen betonnen dekken behandeld, waarbij ook het onderwerp membraandrukwerking aan de orde komt. Eerst wordt hierbij ingegaan op de bezwijkmechanismen in het algemeen, waarna wordt overgegaan op de relevante methoden voor het analyseren van het gedrag en op bestaande berekeningsmodellen en voorschriften. Vervolgens komen de belangrijkste experimentele onderzoeken die tot nu toe zijn gerapporteerd aan de orde. De conclusie wordt getrokken dat het nodig is het draagvermogen van platen met voorspanning in het vlak, ondersteund door en verbonden aan betonnen draagliggers, door middel van een grootschalige proefneming experimenteel te onderzoeken. De belangrijkste reden hiertoe is dat experimenteel onderzoek tot nu toe vooral is gedaan aan platen op stalen liggers, dan wel met zeer kleinschalige tests, waarbij niet duidelijk is in hoeverre zij de (grootschalige) werkelijkheid representeren.

Om een betrouwbare basis voor de te onderzoeken problematiek te creëren is laboratoriumonderzoek uitgevoerd op een model van een werkelijke Nederlandse brug, nagebouwd op schaal 1:2. Het experimentele model bestond uit een dun, in het vlak

## Samenvatting

voorgespannen betonnen dek (voorspanning zonder aanhechting), waarbij het dek werd gestort tussen de flenzen van lange voorgespannen liggers. Aan beide einden van deze liggers waren dwarsliggers aangebracht. Het aansluitvlak tussen het dek en de liggers was ofwel recht ofwel schuin. De belasting op het dek bestond uit enkele dan wel dubbele geconcentreerde lasten. Bezwijken trad steeds op door pons (ofwel bros, ofwel meer ductiel in combinatie met buiging). De breuk trad steeds op in het veld van het dek tussen de liggers, waarbij het contactvlak niet maatgevend bleek te zijn. Het effect van diverse parameters, zoals het niveau van de voorspanning, the type en de positie van de last(en) alsmede de grootte van het lastvlak en de helling van het aansluitvlak tussen dek en flens op het draagvermogen, was tevens onderwerp van studie.

Als onderdeel van het numerieke onderzoek werd een 3D, schaal 1:2 model van de echte brug, in navolging van het experimentele onderzoek, ontwikkeld, waarbij gebruik werd gemaakt van het FE programma DIANA. Hierbij werd een serie niet-lineaire analyses uitgevoerd. De resultaten van het numerieke onderzoek werden vergeleken met de proefresultaten. Hieruit bleek dat goede resultaten werden verkregen, die de geschiktheid van de benadering met het numerieke programma bevestigden. De normaalkrachten die optraden als gevolg van membraandrukwerking werden bepaald met behulp van samengestelde elementen. Een gedetailleerde parameterstudie werd uitgevoerd, waarbij numerieke parameters werden gevarieerd, zoals het elementennet, de grootte van de belastingstappen, en verder materiaalparameters en geometrische parameters aan de orde kwamen, afgestemd op het experimentele onderzoek. Verder werd het schaaffect bestudeerd via een niet-lineaire analyse met het 3D model van de werkelijke brug, waaruit bleek dat een schaalfactor van 1,2 geschikt is om de resultaten van de proef (met plaatdikte van 100 mm) om te rekenen naar het gedrag van het brugdek op ware grootte (met plaatdikte van 200 mm).

Uit een theoretische analyse van het gemodelleerde brugdek bleek dat het draagvermogen van een betonnen dek met membraandrukwerking veel groter is dan voorspeld op grond van bestaande richtlijnen en theoretische methoden. Om het effect van membraandrukwerking ook in een analytisch model op te nemen werd als basis uitgegaan van de Kritische Dwarskracht Scheur Theorie, zoals gepresenteerd in de *fib* Model Code for Concrete Structures 2010. Het effect van de normaalkrachten in het vlak werd hierbij geïntroduceerd via een analyse met de elementenmethode. Berekeningen werd uitgevoerd met twee niveaus van nauwkeurigheid: elementair (zonder membraandrukwerking) en geavanceerd (met membraandrukwerking).

## Samenvatting

Algemeen werd vastgesteld dat het niveau van de voorspanning in het vlak het gedrag van het dek zowel in de bruikbaarheidsgrenstoestand als in de uiterste grenstoestand verbetert. Een gemiddelde veiligheidsfactor van 3,25 werd verkregen op grond van vergelijkingen tussen de experimenteel verkregen resultaten en de numerieke analyses van het dek op ware grootte. Geconcludeerd kan worden dat de bestaande bruggen van het beschouwde type in Nederland over voldoende extra draagvermogen beschikken door het effect van membraandrukwerking. Verder kan vastgesteld worden dat met een geschikt elementenprogramma het draagvermogen met goede betrouwbaarheid kan worden voorspeld.

Het onderzoek beschreven in de dissertatie, dat resulteerde in methoden voor de analyse van brugdekken rekening houdend met membraandrukwerking, heeft het potentieel om tot aanzienlijke kostenbesparingen te leiden, omdat met de ontwikkelde modellen kan worden aangetoond dat betreffende bruggen veilig genoeg zijn, ondanks de eerdere vermoedens dat dure versterkingsmaatregelen noodzakelijk zouden zijn. Een voorstel is geformuleerd om het effect van membraandrukwerking in de analytische modellen ter bepaling van het ponsdraagvermogen gegeven in de *fib* Model Code 2010 op te nemen.

Daartoe worden twee niveaus van berekening toegevoegd aan de bestaande eerste drie niveaus. Het nieuwe niveau IV maakt het gebruik van de Kritische Dwarskracht Scheur Theorie mogelijk, in combinatie met de berekening van de kromming van de plaat rondom de last met een NLFEM programma. Het nieuwe niveau V maakt de berekening van het ponsdraagvermogen met membraandrukwerking mogelijk via een op maat gesneden NLFEM berekening met samengestelde elementen.

## Samenvatting

# Contents

Summary.....	vii
Samenvatting .....	xi
Contents .....	xv
Notations.....	xxiii
<b>1 Introduction.....</b>	<b>1</b>
1.1 Background .....	2
1.2 Scope of the research and its objectives .....	3
1.3 Research hypothesis and strategy.....	4
1.3.1 Experimental analysis .....	4
1.3.2 Numerical analysis.....	5
1.3.3 Theoretical analysis .....	5
1.3.4 Proving the hypothesis and conclusions .....	5
<b>2 Punching shear capacity of concrete deck slabs considering compressive membrane action (CMA).....</b>	<b>7</b>
2.1 General.....	8
2.2 Punching Shear Failure .....	8
2.2.1 The general mechanism of punching shear .....	8
2.2.2 Analysis of punching shear .....	11
2.2.3 Design code provisions for punching shear strength of prestressed slabs.....	14
2.3 Compressive Membrane Action.....	16
2.3.1 The general mechanism of compressive membrane action.....	16
2.3.2 Analysis of compressive membrane action.....	18
2.3.3 Design code provisions incorporating compressive membrane action .....	22
2.4 Punching shear capacity considering compressive membrane action in prestressed decks.....	26
2.4.1 Introduction.....	26
2.4.2 Past research .....	26

## Contents

2.5	Summary and conclusions.....	30
<b>3</b>	<b>Experimental Program - Design of the Test Setup.....</b>	<b>33</b>
3.1	Introduction.....	34
3.1.1	Real bridge.....	34
3.1.2	Scale factors for the prototype.....	34
3.1.3	Design considerations: Some important lower bounds.....	35
3.1.4	Prototype of the bridge.....	36
3.2	Material properties of the model bridge deck.....	42
3.2.1	Concrete.....	42
3.2.2	Prestressing and ordinary reinforcing steel.....	45
3.3	Construction of the model bridge deck in the laboratory.....	46
3.3.1	Bridge deck.....	46
3.3.2	Transverse beams.....	48
3.3.3	Deck slab panels.....	50
3.3.4	Post tensioning the model bridge deck.....	53
3.4	Experimental program and test setup.....	55
3.4.1	Load assembly.....	55
3.4.2	Instrumentation.....	57
3.4.3	Measurements.....	60
3.5	Conclusions.....	62
<b>4</b>	<b>Experimental Results.....</b>	<b>63</b>
4.1	Introduction.....	64
4.1.1	Testing sequence.....	64
4.2	Description of typical tests.....	65
4.2.1	Important test parameters.....	65
4.2.2	Load application.....	65
4.2.3	Instrumentation.....	66
4.2.4	Test observations.....	67

## Contents

4.2.5	Cracking pattern.....	68
4.2.6	Test results .....	69
4.3	Summary and discussion of test results.....	74
4.3.1	Tests with a single load at midspan .....	76
4.3.2	Tests with a single load close to the interface.....	81
4.3.3	Tests with a double load at midspan .....	85
4.3.4	Tests with a double load close to the interface .....	88
4.4	Conclusions .....	92
<b>5</b>	<b>Experimental Parametric Study .....</b>	<b>93</b>
5.1	Introduction .....	94
5.2	Important experimental parameters.....	94
5.3	Results of parametric analysis.....	94
5.3.1	Transverse Prestressing Level.....	94
5.3.2	Position of the load with regard to the transverse slab panel span.....	97
5.3.3	Position of load with regard to the prestressing ducts: In-between or above the ducts.....	99
5.3.4	Position of the load with regard to the whole deck: Interior or exterior slab panels .....	100
5.3.5	Position of the load with regard to the longitudinal span.....	101
5.3.6	Inclination of the girder flange-deck slab panel joint: Straight or skewed...	102
5.3.7	Number of loads: Single or double loads.....	104
5.3.8	Size of the loading plate.....	105
5.3.9	Influence of previous damage to the deck slab panel.....	103
5.4	Summary and conclusions.....	106
<b>6</b>	<b>Numerical Model - Finite Element Analysis .....</b>	<b>109</b>
6.1	Introduction .....	110
6.2	Finite Element Analysis .....	110
6.2.1	TNO DIANA 9.4.4 finite element software.....	110
6.2.2	Overview of the bridge model .....	111

## Contents

6.2.3	Modeling assumptions and limitations.....	111
6.3	Modeling of material behavior.....	112
6.3.1	Cracking model for concrete.....	113
6.3.2	Modeling of steel behavior.....	116
6.3.3	Material properties input.....	116
6.4	Setup of the finite element model.....	117
6.4.1	Concrete: Element type and mesh.....	118
6.4.2	Steel reinforcement.....	122
6.4.3	Material model input.....	123
6.4.4	Applied loads and support constraints.....	124
6.4.5	Solution method.....	125
6.4.6	Special finite element bridge model with a nonlinear girder flange.....	125
6.5	Basic finite element analysis.....	126
6.5.1	Summary of analysis results.....	128
6.5.2	Ultimate loads and mode of failure.....	128
6.5.3	Deflected shape at failure stage.....	130
6.5.4	Load – Deflection behavior.....	131
6.5.5	Cracking loads and cracking pattern.....	135
6.5.6	Von Mises stress distributions.....	142
6.6	Compressive Membrane Action.....	143
6.6.1	Introduction.....	143
6.6.2	Horizontal edge displacements.....	144
6.6.3	Transverse concrete stresses in the loaded deck slab panel.....	148
6.6.4	Development of compressive membrane force with the applied load.....	151
6.7	Summary and conclusions.....	157
<b>7</b>	<b>Numerical Parametric Study.....</b>	<b>159</b>
7.1	Introduction.....	160
7.2	Important numerical parameters.....	160
7.3	Numerical modeling parametric study.....	161

## Contents

7.3.1	Mesh sensitivity and element size.....	161
7.3.2	Influence of the step size of the displacement load.....	165
7.3.3	Material model for concrete in compression.....	167
7.3.4	Comparison of the finite element modeling parameters in the present study with the recommendations of Rijkswaterstaat for nonlinear finite element analysis .....	168
7.4	Geometrical and material parametric study.....	170
7.4.1	Transverse prestressing level (TPL) .....	170
7.4.2	Position of the load with regard to the transverse deck slab span: Midspan or close to the interface .....	172
7.4.3	Position of the load with regard to the ducts: Above or in-between the ducts ... ..	173
7.4.4	Position of the load with regard to the deck slab panels: Interior or exterior deck slab panels .....	174
7.4.5	Position of the load with regard to the longitudinal span.....	175
7.4.6	Number of loads: Single or double loads.....	176
7.4.7	Size of the loading area (wheel print/loading plate) .....	177
7.4.8	Presence of previous damage to the deck slab panel .....	178
7.4.9	Presence of ducts and size of the ducts .....	179
7.4.10	Fracture energy .....	180
7.4.11	Concrete strength .....	181
7.4.12	Size effect .....	182
7.5	Summary and conclusions.....	187
<b>8</b>	<b>Theoretical Analysis of Transversely Prestressed Deck Slabs .....</b>	<b>191</b>
8.1	Introduction .....	192
8.2	Existing codes and methods .....	192
8.2.1	Important parameters used in the calculations .....	192
8.2.2	Model bridge analyses .....	194
8.2.3	Real bridge analyses .....	199
8.2.4	Discussion.....	201
8.3	The Critical Shear Crack Theory (CSCT).....	203

## Contents

8.3.1	MC2010 punching shear provisions for prestressed slabs .....	204
8.3.2	Application of CSCT to the research problem .....	206
8.3.3	Verification of the failure criterion .....	209
8.3.4	Assessment of the punching shear capacity for the experimental load cases using proposed LoA approach .....	212
8.3.5	Comparison of the theoretical, experimental and FEA punching loads .....	214
8.3.6	Application of the proposed LoA approach using CSCT on test results from past literature.....	214
8.3.7	Ultimate bearing capacity of the real bridge by CSCT .....	215
8.3.8	Conclusion .....	217
8.4	Real bridge ultimate bearing capacity .....	217
8.4.1	The Global Safety format and model uncertainty .....	217
8.4.2	Factor of safety .....	218
8.5	Summary and conclusions.....	222
<b>9</b>	<b>Recommendations for practice .....</b>	<b>223</b>
9.1	Introduction .....	224
9.2	Proposed LoA approach to the critical shear crack theory incorporating compressive membrane action .....	224
9.3	Design formulation of the proposed LoA approach .....	225
9.3.1	Design shear resistance .....	225
9.3.2	Load-rotation relationship.....	226
9.3.3	Analysis procedure .....	228
9.4	Conclusions .....	228
<b>10</b>	<b>Conclusions and Future Recommendations.....</b>	<b>229</b>
10.1	Summary and conclusions.....	230
10.1.1	The scientific hypothesis.....	230
10.1.2	Experimental analysis .....	230
10.1.3	Numerical analysis.....	231
10.1.4	Theoretical analysis .....	233

## Contents

10.1.5	Important research findings and conclusions .....	234
10.2	Recommendations for future research.....	235
	References .....	237
	Appendix A.....	249
	Appendix B.....	261
	Appendix C.....	265
	Appendix D.....	275
	Acknowledgements.....	279
	About the author .....	281

## Contents

## Notations

### Greek lower case

$\alpha_s$	factor accounting for the location of the loaded column (ACI 318)
$\alpha_{BR}$	reduction factor for the required reliability level
$\beta$	the reliability index
$\beta_p$	coefficient depending upon the type of column (ACI 318)
$\gamma_c$	material factor for concrete = 1.5 (Eurocode 2)
$\gamma_m$	partial safety factor for concrete = 1.5 (UK HA BD 81/02)
$\gamma_{GL}$	global resistance factor
$\gamma_Q$	partial factor for traffic actions
$\gamma_T$	resistance factor for test results
$\delta_v$	uniform vertical deflection under the steel loading plate
$\delta_{BR}$	coefficient of variation of the tests results
$\varepsilon$	strain
$\varepsilon_{avg}$	average compressive strain at the bottom of the deck slab panel
$\varepsilon_b$	strain in the real bridge
$\varepsilon_c$	plastic strain of an idealized elastic plastic concrete (UK HA BD 81/02)
$\varepsilon_{C,E}$	compressive strain at the bottom east of the deck slab panel
$\varepsilon_{C,W}$	compressive strain at the bottom west of the deck slab panel
$\varepsilon_p$	strain in the prototype
$\eta$	empirical restraint factor
$\lambda$	scale factor
$\lambda_\varepsilon$	scale factor for strain
$\lambda_\rho$	scale factor for mass density
$\lambda_\sigma$	scale factor for stress
$\lambda_A$	scale factor for area
$\lambda_F$	scale factor for force
$\lambda_I$	scale factor for moment of inertia
$\lambda_L$	scale factor for length
$\lambda_M$	scale factor for moment
$\lambda_S$	scale factor for section modulus
$\mu_{BR}$	mean ratio of the experimental and the calculated <i>load</i>
$\nu$	poisson's ratio
$\rho$	mass density
$\rho_{avg}$	average steel reinforcement ratio

## Notations

$\rho_b$	mass density in the real bridge
$\rho_e$	effective reinforcement ratio (UK HA BD 81/02)
$\rho_{eq}$	equivalent reinforcement ratio
$\rho_l$	longitudinal reinforcement ratio (EC2)
$\rho_{ly}$	bonded steel in the y direction (EC2)
$\rho_{lz}$	bonded steel in the z direction (EC2)
$\rho_p$	mass density in the prototype
$\rho_{ps}$	geometric ratio of the prestressed reinforcement
$\rho_x$	finite element smeared grid reinforcement in the horizontal x direction
$\rho_y$	finite element smeared grid reinforcement in the horizontal y direction
$\rho_z$	finite element smeared grid reinforcement in the vertical z direction
$\sigma$	stress
$\sigma_b$	stress in the real bridge
$\sigma_{cp}$	prestress
$\sigma_{cp}$	the average normal compressive stress in the concrete (EC2, ACI 318)
$\sigma_{cy}$	the normal compressive stress in the concrete in y direction (EC2)
$\sigma_{cz}$	the normal compressive stress in the concrete in z direction (EC2)
$\sigma_b$	stress in the prototype
$\phi$	equivalent diameter of the loaded area (UK HA BD 81/02)
$\phi_{md}$	resistance factor for punching shear (CHBDC)
$\psi$	rotation of the slab (CSCT, MC2010)

## Greek upper case

$\Delta_{H,E}$	global horizontal displacement on the eastern side of the deck slab panel
$\Delta_{H,W}$	global horizontal displacement on the western side of the deck slab panel
$\Delta_{V,E}$	relative vertical eastern joint deflection
$\Delta_{V,W}$	relative vertical western joint deflection
$\Phi$	diameter of reinforcement bar

## Roman lower case

$b$	width of the deck slab (CHBDC), width of the element
$b_c$	transverse length of the loaded area
$c_c$	longitudinal length of the loaded area
$b_0$	length of the control perimeter (CSCT, ACI 318)
$b_{eff}$	effective width
$b_s$	width of the support strip (MC2010)

## Notations

$c$	face of the square columns or the side length of the loaded area
$d$	flexural effective depth
$d$	deck thickness, $t$ (CHBDC)
$d_a$	maximum aggregate size
$d_{avg}$	average effective depth of deck slab (EC2)
$d_g$	reference aggregate size equal to 16 mm (CSCT)
$d_{g0}$	maximum aggregate size (CSCT)
$d_l$	longitudinal effective depth of the deck slab (CHBDC, EC2)
$d_p$	effective depth till the prestressing steel
$d_t$	transverse effective depth of the deck slab (CHBDC, EC2)
$d_v$	shear-resisting effective depth of the member (CSCT)
$f_c$	compressive strength of the concrete, concrete cylinder strength (UK HA BD 81/02)
$f_c'$	specified concrete compressive strength (measured on cylinders)
$f_{ck}$	characteristic cylinder strength of concrete
$f_{cm}$	mean compressive cylinder strength of concrete
$f_{cm28}$	mean compressive cylinder strength of concrete at 28 days
$f_{cm,cube}$	mean compressive cube strength of concrete
$f_{cm,cube28}$	mean compressive cube strength of concrete at 28 days
$f_{csp}$	mean splitting tensile strength of concrete
$f_{csp28}$	mean splitting tensile strength of concrete at 28 days
$f_{ctm}$	mean tensile strength of concrete
$f_{cu}$	characteristic cube strength of concrete (UK HA BD 81/02)
$f_{pe}$	effective prestress
$f_{pk}$	characteristic tensile strength of prestressing steel
$f_{pk0.1}$	characteristic 0.1% proof stress of prestressing steel
$f_{sy}$	mean yield strength of steel
$f_{su}$	mean ultimate tensile strength of steel
$f_y$	yield strength of steel
$f_{yd}$	design yield strength of steel
$f_t$	tensile strength
$h$	overall depth of the slab, height of the element
$h_a$	initial arch height (Rankin's method, Rankin et al. 1982)
$h_a^*$	deflected arch height (Rankin's method, Rankin et al. 1982)
$k$	non-dimensional arching moment coefficient
$k_\psi$	rotation parameter (MC 2010)
$k_l$	contribution of the normal compressive stress in concrete
$k_{dg}$	coefficient to take into account different aggregate sizes (MC2010)

## Notations

$l$	length of the element
$m_s$	the average moment per unit length for the calculation of the flexural reinforcement in the support strip (CSCT)
$m_{sd}$	the average design moment per unit length for the calculation of the flexural reinforcement in the support strip (MC2010)
$m_p$	the average decompression moment over the width of the support strip due to prestressing (CSCT)
$m_{pd}$	the average decompression moment over the width of the support strip due to prestressing (MC2010)
$m_R$	the average flexural strength per unit length in the support strip (CSCT)
$m_{Rd}$	the average design flexural strength per unit length in the support strip (MC2010)
$n$	normal force per unit length (CSCT, MC2010)
$q$	steel reinforcement ratio
$r_c$	half the transverse length of the loading plate
$r_s$	the distance from the column axis to the line of contra-flexure of bending moments (radial bending moments for circular slabs) (CSCT, MC2010)
$r_{sx}$	the distance from the column axis to the line of contra-flexure of the bending moment in x direction (MC2010)
$r_{sy}$	the distance from the column axis to the line of contra-flexure of the bending moment in y direction (MC2010)
$r_w$	half the transverse span of the deck slab panel
$t$	deck thickness (CHBDC)
$u$	the critical shear perimeter (EC2)
$v_{min}$	minimum shear strength (EC2)
$v_{Rd,c}$	punching shear stress (EC2)
$w$	opening of the crack (CSCT, Strauss et al. 2003)
$w$	crack width over which stress cannot be transferred (Strauss et al. 2003)
$x$	scale factor

## Roman upper case

$A$	cross-sectional area of arch leg (Rankin's method, Rankin et al. 1982)
$A$	area
$A$	factor to convert splitting tensile strength into tensile strength
$A_b$	area in the real bridge
$A_p$	area in the prototype
$A_p$	area of the prestressing steel

## Notations

$A_{p,required}$	required area of prestressing steel in the prototype
$A_{sl}$	longitudinal bottom steel area (CHBDC)
$A_{st}$	transverse bottom steel area (CHBDC)
$B$	transverse span of the slab (proposed LoA approach, CSCT)
$C_{Rd,c}$	calibration factor in the shear formula (NEN-EN 1992-1-1:2005)
$E$	Young's modulus
$E_{har}$	hardening modulus
$E_c$	Young's modulus of concrete or modulus of elasticity of concrete
$E_{c28}$	modulus of elasticity of concrete at 28 days
$E_{cm}$	mean modulus of elasticity of concrete
$E_p$	modulus of elasticity of prestressing steel
$E_s$	Young's modulus of steel or modulus of elasticity of steel
$Eknn$	normal crack strain
$F$	force
$F_b$	force in the real bridge
$F_c$	correction factor based on specified concrete strength
$F_d$	the design action
$F_{md}$	scaled down design wheel load for model bridge deck
$F_p$	force in the prototype
$F_p$	prestressing force
$F_p$	in-plane force due to compressive membrane action (proposed LoA approach for CSCT)
$F_q$	correction factor based on the reinforcement ratio (CHBDC)
$G_c$	concrete compression fracture energy
$G_f$	fracture energy
$G_f^I$	mode-I fracture energy
$G_{f0}$	base value of fracture energy (Model code 90)
$H_{eq}$	equivalent length of the element
$I$	moment of inertia
$I_b$	moment of inertia in the real bridge
$I_p$	moment of inertia in the prototype
$L$	length
$L_b$	length in the real bridge
$L_e$	half the span of slab strip with elastic boundary restraint (Rankin's method, Rankin et al. 1982)
$L_{min}$	the minimum span of the slab in x or y-directions (MC2010)
$L_x$	the span of the slab in x direction (MC2010)
$L_y$	the span of the slab in y direction (MC2010)

## Notations

$L_r$	half the span of slab strip with rigid boundary restraint (Rankin's method, Rankin et al. 1982 or UK BD 81/02)
$L_p$	length in the prototype
$L_T$	crack bandwidth (Strauss et al. 2003)
$M$	moment
$M_b$	moment in the real bridge
$M_p$	moment in the prototype
$N_{xx}$	in-plane force distributed force in the finite element analysis
$P$	load
$P_{double}$	punching shear capacity corresponding to single point loads
$P_{p,BD81/02}$	punching capacity (UK HA BD 81/02)
$P_{pd}$	ultimate punching load for axle loading (UK HA BD 81/02)
$P_{ps}$	ultimate punching load (UK HA BD 81/02)
$P_{pr,CSA}$	projected CSCT advanced LoA ultimate punching load for the real bridge (CSCT)
$P_{pr,CSE}$	projected elementary LoA ultimate punching load for the real bridge (CSCT)
$P_{pr,FEA}$	finite element model bridge (2ELEM) projected ultimate load
$P_{pr,T}$	test projected ultimate load
$P_{single}$	punching shear capacity corresponding to double point loads
$P_{BAS}$	basic model used in the finite element analysis (2ELEM)
$P_{CSA}$	advanced LoA ultimate punching load (CSCT)
$P_{CSA,RB}$	advanced LoA ultimate punching load for the real bridge (CSCT)
$P_{CSE}$	elementary LoA ultimate punching load (CSCT)
$P_{CSE,RB}$	elementary LoA ultimate punching load for the real bridge (CSCT)
$P_{CR0.1,T}$	test initial flexural cracking load (0.1 mm wide crack)
$P_{CRi,T}$	test initial flexural cracking load (hairline)
$P_{CR,FEA}$	finite element analysis initial cracking load
$P_{CRS,FEA}$	finite element analysis initial inclined shear cracking load
$P_{CR,T}$	test cracking load
$P_{FEA}$	finite element analysis ultimate load
$P_{FEA,RB}$	real bridge finite element ultimate load
$P_{FP}$	flexural punching load
$P_{MOD}$	ultimate load for a finer mesh in the finite element analysis
$P_T$	test failure load (test ultimate load/test peak load)
PS	prestressing
$Q_K$	characteristic wheel load
$R$	non-dimensional parameter for the arching moment of resistance

## Notations

$R_d$	the design resistance
$R_{d,CSA}$	critical shear crack theory design resistance at an advanced LoA
$R_{d,FEA}$	finite element analysis design resistance
$R_{d,T}$	test design resistance
$R_m$	resistance calculated by using mean values for the material strengths
$R_{md,CSA}$	critical shear crack theory design resistance of model bridge deck at an advanced LoA
$R_{md,FEA}$	finite element analysis design resistance of model bridge deck
$R_{md,T}$	test design resistance of model bridge deck
$R_n$	nominal punching shear resistance (CHBDC)
$R_{n,CHBDC}$	punching capacity of the real bridge (CHBDC)
$R_r$	factored punching shear resistance (CHBDC)
$S$	section modulus
$S_b$	section modulus in the real bridge
$S_p$	section modulus in the prototype
$S_{xx}$	transverse stress distribution in the finite element analysis
$S_{FEA,RB}$	real bridge finite element ultimate deflection
$S_{MT}$	test ultimate deflection at the midspan of the deck slab panel
$S_T$	test ultimate deflection (under the load)
$S_{T,325}$	test ultimate deflection at 325 mm in the transverse direction
$V$	shear force (CSCT), punching load
$V_{flex}$	shear force associated with the flexural capacity of the slab (CSCT)
$V_p$	vertical component of the prestressing force (ACI 318)
$V_{r,ACI}$	punching shear capacity (ACI)
$V_{r,EC2}$	punching shear capacity (background report 25.5-02-37-prENV 1992-1-1 2002)
$V_{rd,EC2}$	punching shear capacity (EC2)
$V_{u,calc}$	calculated punching shear load (background report 25.5-02-37-prENV 1992-1-1 2002)
$V_{u,exp}$	experimental punching shear load (background report 25.5-02-37-prENV 1992-1-1 2002)
$V_{Ed}$	design punching shear force or acting shear (MC2010)
$V_R$	shear strength (CSCT)
$V_{Rd}$	design shear strength (MC2010)
$V_{Rd,c}$	design shear resistance attributed to concrete (MC2010)
$W_{CR,E}$	crack width at the top east of the deck slab panel
$W_{CR,W}$	crack width at the top west of the deck slab panel

## Abbreviations

2D	two dimensional
3D	three dimensional
2ELEM	finite element model bridge deck with two elements over the depth
4ELEM	finite element model bridge deck with four elements over the depth
6ELEM	finite element model bridge deck with six elements over the depth
<i>b</i>	real bridge
<i>p</i>	prototype
A	exterior model bridge deck slab panel on the eastern side
AASHTO	American Association of State Highway and Transportation Officials
ACI	American Concrete Institute
AD	above the duct
B	interior model bridge deck slab panel
BB	real bridge
BD	in-between the ducts
BP	brittle punching
BV	bottom view of the deck slab
C	exterior model bridge deck slab panel on the western side
CHBDC	Canadian Highway Bridge Design Code
CMA	compressive membrane action
CMF	compressive membrane force
COV	coefficient of variation
CSA	Canadian Standards Association
CSCT	Critical Shear Crack Theory
EB	east side bottom edge
EC	Eurocode
EC2	Eurocode 2
ECOV	estimation of coefficient of variation of resistance method
ET	east side top edge
FE	finite element
FEA	finite element analysis
FMODE	failure mode
FOS	factor of safety
FP	prestressing force measured by load cell
FP	flexural punching
FR	reaction force measured by load cell
GFR	global resistance factor method

## Notations

HB	abnormal vehicle loading (UK HA BD 37/01)
J	Joint/Interface
LoA	level of approximation (MC2010)
LV	longitudinal view
M	midspan
MC90	Model code 90
MC2010	Model code 2010
OHBDC	Ontario Highway Bridge Design Code
OMTC	Ontario Ministry of Transportation (MTC)
P1J	single point load acting close to the girder flange-slab interface/joint
P2J	double point loads acting close to the girder flange-slab interface/joint
P1M	single point load acting at midspan of the deck slab panel
P2M	double point loads at the midspan of the deck slab panel
PSF	partial safety factor method
RB4ELEM	real bridge finite element model with four elements over the depth
SK	skewed joint
SLP	small loading plate (115×150 mm)
ST	straight joint
TNZAA	Transit New Zealand Ararau Aotearoa
TPL	transverse prestressing level
TS	transverse section
UK HA BD	United Kingdom Highways Agency Design Manual for Roads and Bridges
ULS	ultimate limit state
WB	west side bottom edge
WT	west side top edge
Xbeam	transverse beam (cross-beam)

## Notations

# **CHAPTER 1**

## **Introduction**

This chapter introduces the research topic to the reader and explains the background, objectives and the scope of work. A working hypothesis of the scientific research is stated and a step-by-step strategy for its evaluation is outlined. A small introduction to each chapter is also given.

## 1.1 Background

*“Are the old structures safe?”, “Do old bridges have sufficient capacity to carry the present traffic loads?”, “If the bridges designed according to old codes and requirements still seem to be in working condition, where is the residual capacity coming from?”*

These are the questions that every structural engineer and designer is facing all over the world after the construction boom of the latter half of the last century has left the world with costly structures that have now become old and may or may not be adequate enough according to modern design requirements. With the on-going economic recession seen by even the developed countries, complete demolition of these expensive structures and replacing them is not only a burden on the economy, but may have a huge negative impact on the environment as well. Therefore, it is an astute approach to check if the existing structures can still be used for a few more decades, provided they are safe and viable. A filter can be developed regarding structures that need to be replaced completely, structures that only need to be retrofitted for functioning, or structures that have sufficient residual capacity that makes them serviceable for another stretch of time.

The current research deals with the problem underlined above, with a focus on the bridges in the Netherlands; in particular, bridges with thin transversely prestressed decks cast in-situ between the flanges of long, precast girders. There are around 70 such bridges in the Netherlands that were constructed in the 60s or 70s of the last century. Since the traffic flow has increased enormously, the safety of old bridges has become questionable according to the modern design codes. Also, the shear capacity as prescribed by the codes is more conservative in the recently implemented EN 1992-1-1:2005 (CEN 2005) than the formerly used Dutch NEN 6720:1995. As a result, many existing bridges are found to be shear-critical when assessed using the Eurocode. In 2006, the Dutch ministry of Infrastructure and the Environment, Rijkswaterstaat, carried out a review of the old bridges of the Netherlands and found out that most of the bridges were in good condition despite being overloaded beyond their calculated capacity. Possible explanations to this anomaly could be the increase in the concrete strength as a result of on-going cement hydration over the years, the transverse load redistribution in slabs and most importantly, the well-recognized but yet to be validated “*Compressive Membrane Action*” or the dome effect.

Compressive Membrane Action (CMA) occurs in laterally restrained concrete slabs and provides enhanced bearing capacity in both flexure and punching shear. As concluded by various researchers, CMA is also the reason that the bridges that are traditionally designed by conservative flexural theories mostly fail in punching shear rather than in flexure under

concentrated wheel loads. Therefore, when analyzing transversely prestressed decks considering compressive membrane action, the punching shear capacity becomes the most critical aspect of the structural behavior.

### 1.2 Scope of the research and its objectives

A lot of research has been done in the past on the subject of compressive membrane action (CMA) in reinforced concrete slabs and deck slabs. Codes like the Canadian Highway Bridge Design Code (CAN/CSA-S6-06 2006), the New Zealand code (TNZAA 2003) and UK Highways Agency Design Manual for Roads and Bridges (UK HA BD81/02 2002) have incorporated membrane action in their analysis and design provisions to some extent. However, not much research has been done on prestressed concrete decks considering CMA, nor have any codes incorporated membrane action in their prestressed slab analysis and design methods. It is worth mentioning here that the codes used in the Netherlands do not consider the beneficial effect of CMA in their design provisions at all. Therefore, the scope of this research work covers *the structural behavior and ultimate bearing capacity, in particular, the punching shear capacity of thin, transversely prestressed decks under concentrated loads considering compressive membrane action.*

For the research investigation, experimental, numerical and theoretical approaches have been employed. The prototype used in the research was based on the “ramp” or “ascent” of the Van Brienenoord bridge that was constructed in 1965 and connects the city of Rotterdam with the southern part of the Netherlands by crossing the Nieuwe Maas (Fig. 1.1). A second bridge was constructed next to the existing one in 1990 to meet the demand of rapidly increasing traffic.



Fig. 1.1 Aerial view of the Van Brienenoord bridge.

Currently, the bridge has 12 lanes and a traffic of over 250,000 vehicles per day making it part of the busiest road network of the Netherlands. It consists of long, prestressed girders

with transversely post tensioned deck slabs panels. The slenderness ratio of the deck slab of the Van Brienenoord bridge is quite high, defying the slenderness limitation for the development of compressive membrane action in codes like CHBDC, TNZAA code and UK BD81/02. However, since these codes are for reinforced concrete deck slabs, it is expected that the transverse prestressing will not only improve the bearing capacity but compensate for the high slenderness ratio, making thinner deck slabs possible with no problems of serviceability and structural safety. Hence, the primary objective of this project is to investigate if bridges like the Van Brienenoord bridge with thin deck slabs and transverse prestressing have sufficient bearing capacity or if they require some strengthening measures.

### **1.3 Research hypothesis and strategy**

Since both transverse prestressing and compressive membrane action create compressive forces in the plane of a prestressed, laterally restrained slab, the hypothesis of this research can be stated as:

*“The in-plane compressive forces from transverse prestressing in combination with the compressive membrane forces arising from the lateral restraint will enhance the bearing capacity of bridge decks.”*

The important empirical methods, mechanical models, experimental programs and numerical approaches relevant to punching shear in prestressed concrete decks considering compressive membrane action are presented in Chapter 2. Based on the literature review, following strategy was decided upon to work on the scientific hypothesis and achieve the objectives of the research while remaining within the scope of work.

#### **1.3.1 Experimental analysis**

An experimental research program was conducted in the Stevin II laboratory, Faculty of Civil Engineering and Geosciences, Delft University of Technology, to investigate the capacity of a 1:2 scaled model of a bridge (based on the Van Brienenoord bridge) with a thin transversely prestressed concrete deck slab, cast between precast concrete girders and subjected to concentrated loads. Nineteen static tests were carried out in order to investigate the effect of different parameters, like the transverse prestressing level (TPL), the geometry of the deck, the type and position of the loading etc., on the punching shear strength and to determine the development of CMA in the deck slab. The experimental program is explained in detail in Chapter 3 and the results are briefly described in Chapter 4. Chapter 5 carries out a parametric analysis based on the experimental results.

### 1.3.2 Numerical analysis

Most of the research work done in the past to study CMA in bridge decks has been focused on small scale experimental programs. However, small scale testing does not necessarily depict true structural behavior because of the size effect, and large scale testing is usually very costly. Therefore, it is essential that calibrated numerical models are developed that are able to predict the actual structural behavior. Furthermore, numerical models can be used to carry out a parametric study which may not be possible experimentally due to high costs associated with the construction and testing of physical models.

Chapter 6 describes the development of the model bridge deck in the finite element software TNO DIANA 9.4.4. A 3D solid model was constructed and analyzed nonlinearly for basic test cases. The development of compressive membrane action was also studied. A detailed parametric analysis was carried out in Chapter 7 to study the effect of various parameters on the punching shear strength. A comparison of the finite element and experimental results was also made for the basic test cases and the parametric analyses, where available. Furthermore, a full scale bridge model was developed to study the size effect on the punching shear capacity.

### 1.3.3 Theoretical analysis

Although the punching shear failure and compressive membrane action can be simulated well by the nonlinear analysis of a 3D finite element structure, it can be cumbersome for complex problems. Therefore, a theoretical approach to study the research problem is explored in Chapter 8. First, the traditional code methods, with or without CMA, are used to assess the punching shear capacity. Then the new Model Code 2010 (*fib* 2012) shear provisions based on the Critical Shear Crack Theory (Muttoni 2008, Clément et al. 2013) are applied on the model bridge deck. A new Level of Approximation approach is introduced that makes use of the compressive membrane action in laterally restrained slabs or deck slabs. At the end, a factor of safety of the full scale bridge against the traffic live loads is established by making use of the experimental, numerical and theoretical results. Recommendations for practice using the proposed LoA approach are given in Chapter 9.

### 1.3.4 Proving the hypothesis and conclusions

The results from the three modes of analyses, experimental, numerical and theoretical, are then brought together to prove the hypothesis of the research in Chapter 10. An overview of the conclusions from each chapter is also given, leading to the final answer regarding the safety and ultimate bearing capacity of transversely prestressed concrete deck bridges.

## Introduction

# **CHAPTER 2**

## **Punching shear capacity of concrete deck slabs considering compressive membrane action (CMA)**

This chapter briefly describes the methods used for the assessment of punching shear capacity of reinforced and prestressed concrete slabs, in particular, the methods that are later used in the theoretical analysis of the research problem. Special attention is given to the historical background of compressive membrane action and how current theories deal with this phenomenon.

## 2.1 General

The main objective of this research is to determine the bearing capacity of transversely prestressed concrete decks. For this purpose, a brief literature review of the subject has been carried out. Since deck slabs tend to fail in punching shear when a concentrated wheel load acts on it (Kirkpatrick et al. 1984, Batchelor 1990, Bakht and Jaeger 1992, Mufti et al. 1993, Fang et al. 1994), focus is on the background and analysis methods of punching shear failure.

A lot of research has been done in the past on Compressive Membrane Action (CMA) in reinforced concrete decks. Both flexural and punching shear behavior have been studied and methods of analysis have been developed. Furthermore, CMA has been introduced in some codes (CHBDC: CAN/CSA-S6-06 2006, New Zealand TNZAA 2003, UK HA BD81/02 2002) for reinforced concrete slabs. Code methods and the background research done in this regard have been summarized and some important experimental studies carried out on *prestressed concrete decks* considering CMA are also presented.

The literature review is divided into three sections: *Punching shear in concrete slabs or deck slabs*, *Compressive membrane action* and *Punching shear capacity considering compressive membrane action in prestressed decks*. The scope of the literature review is limited to slabs without shear reinforcement. Special attention is given to methods or codes later used for the theoretical analysis of the research problem.

## 2.2 Punching Shear Failure

When a slab is subjected to a concentrated load, a conical plug pushes out of the slab directly under the load causing failure. This phenomenon is known as Punching (Fig. 2.1a). Punching shear is also called *two-way shear* and is generally a *brittle punching* failure with no warning in advance; where some warning is shown, the case is classified as *flexural punching*.

### 2.2.1 The general mechanism of punching shear

The mechanical behavior of punching failure can be explained from test observations, although there is always a hindrance to observe the internal cracks in the two-way shear mechanism within a solid block of concrete. The punching shear failure is a combined action of flexure and shear load resulting in combined flexural, radial and inclined shear cracking. The vertical flexural and inclined shear cracking is commonly grouped as

## Punching shear capacity of concrete deck slabs considering CMA

tangential cracking. Fig. 2.1b shows the cracking pattern typically associated with punching shear failure.

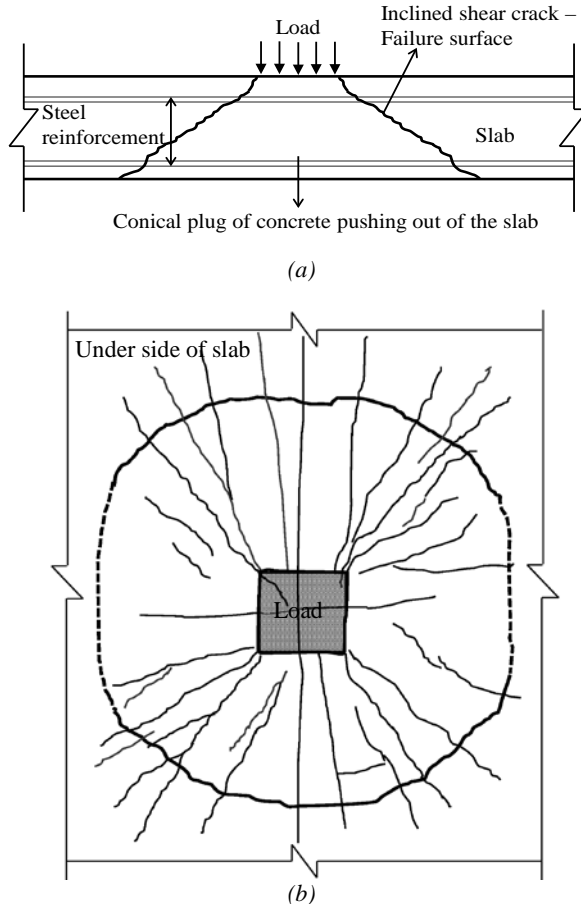


Fig. 2.1 Punching shear failure in a typical concrete deck slab subjected to a concentrated load (wheel print): a) Punching shear cone in cross-section; b) Crack pattern in plan.

Initially, at low load levels, flexural cracks develop at the bottom of the slab directly under the projection of the load, within and around the loading perimeter. Next, radial cracks, caused by tangential moments, spread out from the perimeter of the load projection, dividing the slab into fan-like segments. At further loading, inclined shear cracking, caused by the radial moments, forms from the tangential cracks, and starts building up a cone-like plug. At higher loads, the inclined cracks extend towards the slab edges and appear around the loaded perimeter. For some time, the crack widths are found to increase with very few new cracks and then failure occurs suddenly and in a very brittle manner when the concrete plug is pushed out of the slab at the ultimate punching load. The presence of flexural

reinforcement may act as a hanger for the pushed out cone, preventing complete dislodging of the concrete plug from the slab<sup>1</sup> (Vaz Rodrigues 2007). Test observations and finite element studies from literature on slab-column connections (Kinnunen and Nylander 1960, Shehata 1982, Hallgren 1996) show that the radial strains are higher at the loading point and decrease more rapidly in the radial direction than the tangential strains which are lower at the loading point and decrease more gradually. In RC slabs and in prestressed slabs with bonded tendons, the increase in steel strains also varies inversely with the radius, while the strains of unbonded tendons hardly increase (Shehata 1982).

### Punching failure in bridge deck slabs

The behavior of bridge deck slabs under concentrated loads is not only different from that of slab-column specimens but more complex as well. In deck slabs, the punching shear mechanism may not be truly symmetrical since the flow of inner forces is different from that observed in slab-column specimens. The transverse spans are much smaller than the longitudinal spans and the dashed cracking lines shown in Fig. 2.1b can be longer and sometimes may not even be visible at the underside of the slab depending on the aspect ratio<sup>2</sup>. Bridge deck slabs also differ from the regular slab-column isolated specimens as compressive membrane action can develop in the former due to external lateral restraint (Fig. 2.2). This aspect of the deck slab behavior will be discussed later in section 2.3.

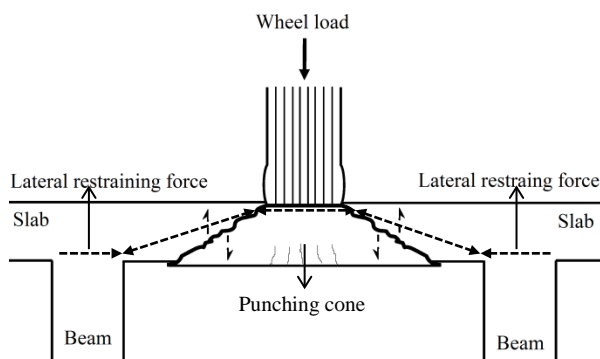


Fig. 2.2 Punching shear failure in laterally restrained slabs or deck slabs (Main concept of the figure is inspired by Kirkpatrick et al. 1984).

<sup>1</sup> In current tests, the unbonded prestressing bars prevented complete collapse of the punching cone.

<sup>2</sup> Such failures were observed in current tests also. The circumferential cracks (projection of punching cone) did not fully extend till the bottom due to the one-way nature of the deck slab.

## 2.2.2 Analysis of punching shear

Generally speaking, the problem of punching shear is solved by empirical equations commonly used in North America or by more rational models favored in Europe. Empirical solutions are based on experimental data and involve the relationship of various parameters with the failure load or stress calculated at a critical section. These parameters include concrete strength, ratio of flexural reinforcement, boundary conditions, size effect etc. The rational methods include mathematical models and constitutive equations determining forces in concrete and steel and defining a failure mechanism. A brief history of research on punching shear is given in the following section.

### Historical Background

The concept of a limiting shear stress on a critical section around the loaded area (critical shear perimeter) was introduced by Talbot (1913) and has served as the basic design approach for most codes of practice. Between 1913 and 1960, major contributions to shear failure in column footings or slabs, in the form of experimentation leading to empirical mathematical expressions to calculate shear stress at a certain critical perimeter, were made by Richart (1948), Hognestad (1953), Elstner and Hognestad (1953, 1956) and Whitney (1957). Some landmark findings in research on punching shear are summarized below.

One of the most important studies carried out on the subject of shear in reinforced concrete slabs and footings under concentrated loads was carried out by Moe (1961). He found that the shear force at the calculated ultimate flexural capacity of the slab was one of the parameters governing the shear strength of slabs and footings. The concrete strength and the ratio of the side length of the loaded area to the slab thickness, were also directly related to the calculation of the ultimate shear strength. According to Moe, to determine the inclined cracking load, stresses should be computed at a distance of  $d/2$  from the periphery of the loaded area, while the stresses on the periphery of the loaded area or column should be used to predict the shear compression failure. He also concluded that the triaxial state of stress in the compression zone at the critical section influenced the shear resistance of the section to a great degree, that inclined cracks in the slabs could develop at loads as low as half of the ultimate loads and that prestressed slabs had a higher shear resistance than ordinary reinforced slabs.

The first rational mechanical model for punching shear was developed by Kinnunen and Nylander (1960) based on equilibrium of forces acting on a sector element of a polar symmetrical slab supported on a column. They performed 61 tests on slab-column specimens and were able to explain the mechanism of punching as well as to predict the

ultimate loads. In the original model, a portion of the slab bounded by the tangential shear crack and the radial cracks rotated as a rigid body and was loaded through a compressed conical shell that developed from the column to the end of the shear crack. The failure criterion was fulfilled when the tangential concrete strain at the bottom of the slab surface reached a critical value. Equations of equilibrium were applied to the slab segment subjected to the external load and internal forces and solved iteratively to reach the ultimate capacity. The original theory was derived for slabs with ring reinforcement and then extended to slabs with two way reinforcement and refinement for dowel action (Kinnunen 1963).

Between 1960 and 2000, considerable research on punching shear was done by various researchers. A few studies are highlighted below:

- Regan (1971) correlated shear in slabs with shear in beams and determined the position of the critical section from the column perimeter. The nominal ultimate shear stress was a function of the reinforcement ratio and the concrete strength. Further, instead of a critical shear perimeter, the concept of a “true failure surface” (inclined fracture surface) was introduced by Regan (1981) to calculate the nominal shear stress. Regan (1985) also carried out tests on post-tensioned slabs to simulate intermediate column support regions of prestressed slab bridges. In order to account for the influence of prestressing, a decompression load was added to the punching resistance of a geometrically similar slab without prestress and the resulting formula gave good correlation between the calculated and the experimental results.
- The mechanical model by Kinnunen and Nylander (1960) was modified by Shehata (1985). Failure was assumed to occur either by splitting under principal tensile stresses or by crushing in the radial or tangential direction (Shehata and Regan 1989).
- Braestrup et al. (1976) used the plasticity theory to develop a model for punching. The failure mechanism consisted of punching-out of a slab portion from a relatively rigid slab. An upper bound solution was given by equating the fracture energy of the conical shell with the work performed by the applied loads.
- Bazant and Cao (1987) based their punching shear formula on laws of fracture mechanics. The failure zone propagated across the structure with the energy dissipation localized into the cracking front. The punching load was calculated based on energy and stability criteria instead of strength.
- In 1996, the mechanical model of Kinnunen and Nylander (1960) was modified by Hallgren by introducing a fracture mechanics based failure criterion. Size effect

and brittleness of concrete were also reflected in the modified model (Hallgren 1996).

### The Critical Shear Crack Theory (CSCT)

The concept of critical shear crack theory (CSCT) was introduced by Muttoni (1985). Over the years the theory was validated with the help of theoretical and experimental studies (Muttoni and Thürlimann 1986, Muttoni 1989 and Muttoni and Schwartz 1991) and formed the basis of the Swiss Code SIA 162 (1993). The theory continues to be extended and improved, for example, for shear in one- and two-way slabs (included in SIA 262 2003), slabs with plastic strains (Guandalini et al. 2009), punching of bridge cantilever slabs (Vaz Rodrigues et al. 2008), punching of slabs without shear reinforcement (Muttoni 2008) and with shear reinforcement (Fernández Ruiz and Muttoni 2009), and prestressed slabs (Clement et al. 2013) to name a few.

The general concept of critical shear crack theory for members without transverse reinforcement is based on the assumption that the shear strength is a function of width and roughness of a shear crack which develops through the inclined compression strut carrying shear (Fig. 2.3a). The shear strength can thus be calculated by integrating the contribution of concrete in tension and aggregate interlock along the failure surface (Guidotti 2010).

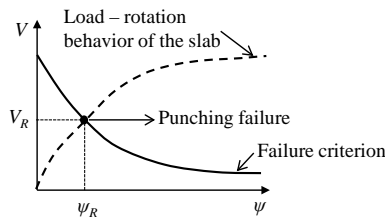
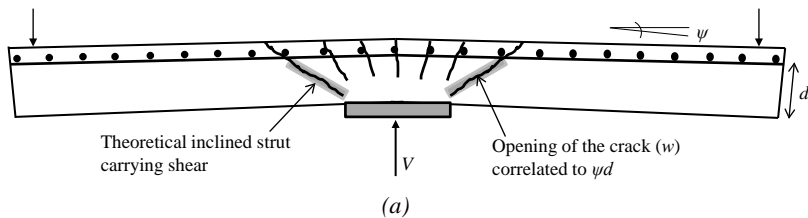


Fig. 2.3 The Critical Shear Crack Theory (CSCT): a) The basic mechanism; b) Calculation of strength and deformation capacity (Muttoni 2008).

For design purposes, Muttoni (2008) proposed a simplified failure criterion. The width of the shear crack is assumed proportional to the product of the slab rotation times the effective depth of the slab ( $w \propto \psi d$ ). The average failure criterion is expressed as follows:

$$\frac{V_R}{b_0 d_v \sqrt{f_c}} = \frac{3/4}{1 + 15 \frac{\psi d}{d_{g0} + d_g}} \quad [SI \text{ Units : } N, mm] \quad (2.1)$$

where,  $V_R$  is the shear strength,  $b_0$  is the length of the control perimeter at  $d_v/2$  of the edge of the supported area,  $d_v$  is the shear-resisting effective depth of the member (distance between the centroid of the flexural reinforcement and the surface at which the slab is supported) and  $f_c$  is the compressive strength of the concrete. The roughness of the critical crack is correlated to the maximum aggregate size and its capacity to carry the shear forces is accounted for by dividing the nominal crack width  $\psi d$  by the quantity  $d_{g0} + d_g$  (Walraven 1981, Vecchio and Collins 1986), where  $d_{g0}$  is the maximum aggregate size and  $d_g$  is the reference aggregate size equal to 16 mm.

The failure load can be found out by intersecting the actual load-rotation behavior of a slab with the failure criterion (Fig. 2.3b). Various methods can be used to estimate the load-rotation behavior as outlined by Muttoni and Fernández Ruiz (2010). A simplified expression to calculate the rotation has been given in Muttoni (2008):

$$\psi = 1.5 \frac{r_s}{d} \frac{f_y}{E_s} \left( \frac{V}{V_{flex}} \right)^{3/2} \quad [SI \text{ Units : } N, mm] \quad (2.2)$$

where,  $V$  is the shear force,  $V_{flex}$  is the shear force associated with the flexural capacity of the slab,  $f_y$  is the yield strength of steel,  $E_s$  is the Young's modulus of steel,  $r_s$  is the distance from the column axis to the line of contra-flexure of radial bending moments (equal to radius of the slab in case of an isolated member) and  $d$  is the flexural effective depth.

Compared to modern design codes like the ACI 318-05 and Eurocode 2, the CSCT gave excellent results when applied to a series of 87 test results with a coefficient of variation of only 8% (Muttoni 2008). The CSCT also grounds the basis of the Model Code 2010 (*fib* 2012) punching shear provisions.

### 2.2.3 Design code provisions for punching shear strength of prestressed slabs

In this section, the design methods for the prediction of punching shear capacity of prestressed slabs given in NEN-EN 1992-1-1:2005 and ACI 318 (2011) are presented. Model Code 2010 (*fib* 2012) punching shear provisions for prestressed slabs are given in detail in section 8.3.1.

## Eurocode 2: NEN-EN 1992-1-1:2005

The punching shear stress and ultimate capacity by Eurocode 2 is expressed in Eq. 2.3 and Eq. 2.4, respectively.

$$v_{Rd,c} = C_{Rd,c} k (100 \rho_l f_{ck})^{1/3} + k_1 \sigma_{cp} \geq (v_{\min} + 0.10 \sigma_{cp}) \quad [SI Units : N, mm] \quad (2.3)$$

$$V_{rd,EC2} = v_{rd,c} u d \quad [SI Units : N, mm] \quad (2.4)$$

where,  $C_{Rd,c} = 0.18/\gamma_c$  ( $\gamma_c = 1.5$ ),  $k = 1 + (200/d)^{1/2} \leq 2$  is the size factor,  $\rho_l = (\rho_{ly} \rho_{lz})^{1/2} \leq 0.02$  is the longitudinal reinforcement ratio,  $f_{ck}$  is the characteristic concrete cylinder strength,  $d$  = average effective depth in each orthogonal direction,  $k_1 = 0.1$ ,  $\sigma_{cp} = (\sigma_{cy} + \sigma_{cz})/2$  is the normal compressive stress in concrete,  $v_{\min} = 0.035 k^{3/2} f_{ck}^{1/2}$  is the minimum shear strength,  $V_{rd,EC2}$  is the punching shear load and  $u = 4c + 4\pi d$  is the critical shear perimeter calculated at  $2d$  from the face of the square column or the loaded area with side length  $c$ .

Note:  $\sigma_{cy}$  and  $\sigma_{cz}$  are the normal concrete stresses from longitudinal forces in the critical section in the y and z-directions respectively.  $\rho_{ly}$  and  $\rho_{lz}$  relate to the bonded steel in the y and z-directions respectively. The values should be calculated as mean values taking into account a slab width equal to the loaded area or column width plus  $3d$  at each side). Where necessary, the punching shear resistance outside the shear reinforced area should be checked by considering further control perimeters.

## ACI 318-11

The punching strength according to ACI 318 is expressed in Eq. 2.5. Contrary to Eurocode 2, the vertical component of the tendons  $V_p$ , calculated at  $d/2$  from the face of the column or the loaded area is added to  $V_{r,ACI}$ . No size effect is considered in the ACI code punching shear expression.

$$V_{r,ACI} = (\beta_p \sqrt{f'_c} + 0.3 \sigma_{cp}) b_0 d + V_p \quad [SI Units : N, mm] \quad (2.5)$$

where,  $\beta_p$  is the smaller of 0.29 and  $0.083 (\alpha_s d/b_0 + 1.5)$ ,  $\alpha_s = 40$  for interior columns, 30 for edge columns and 20 for corner columns,  $f'_c < 35$  MPa is the specified concrete compressive strength measured on cylinders,  $0.9 \text{ MPa} \leq \sigma_{cp} \leq 3.5 \text{ MPa}$  is the average prestressing in each direction,  $b_0 = 4(c + d)$  is the length of the control perimeter at  $d/2$  from the face of the column or the loaded area with side length  $c$ , and  $d$  is the effective depth.

## 2.3 Compressive Membrane Action

In this section, first the mechanism of compressive membrane action (CMA) will be explained and then the experimental and analytical research forming the basis of the design codes (CHBDC 2006, UKBD81/02 2002) that have included CMA in their provisions will be briefly described. Since the current study is on prestressed deck slabs and most of the past research was done with regard to reinforced concrete slabs, the scope of the review includes the effect of CMA on the punching shear capacity of both reinforced and prestressed concrete slabs and deck slabs.

### 2.3.1 The general mechanism of compressive membrane action

#### Introduction

According to Park and Gamble (2000), compressive membrane action (CMA) is a phenomenon that occurs in slabs whose edges are restrained against lateral movement by stiff boundary elements. This restraint induces compressive membrane forces in the plane of the slab. As the slab deflects, changes of geometry cause the slab edges to tend to move outward and to react against the boundary elements as shown in Fig. 2.4. CMA leads to an increase in the bearing capacity of the slab and it fails at a load much higher than predicted by the standard yield line theory. Both the flexural and the punching shear capacity of a restrained slab are enhanced because of this phenomenon, with punching shear being the commonly occurring mode of failure (Kirkpatrick et al. 1984, Batchelor 1990, Bakht and Jaeger 1992, Mufti et al. 1993, Fang et al. 1994).

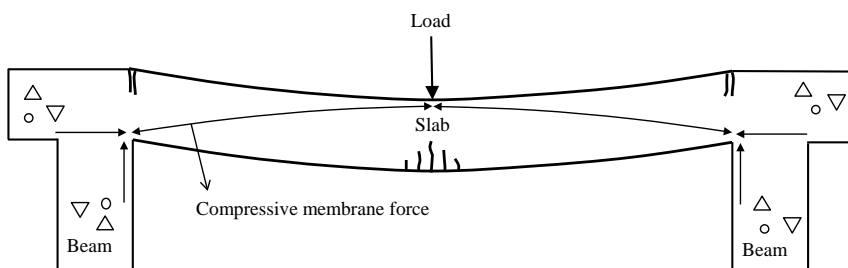


Fig. 2.4 Compressive membrane action in a reinforced concrete bridge deck slab (adapted from Hon et al. 2005).

#### Factors affecting compressive membrane action

According to Hon et al. (2005), the extent of compressive membrane action developed in a system depends on the level of horizontal translational restraint stiffness (Fig. 2.5). This lateral restraint depends on:

## Punching shear capacity of concrete deck slabs considering CMA

- The axial stiffness of the surrounding slab area;
- The horizontal bending stiffness of the edge beams;
- The position of the load with regard to the end cross-beams or the diaphragms. The restraint stiffness increases if the loaded area moves toward the ends of the specimen, closer to the diaphragms.

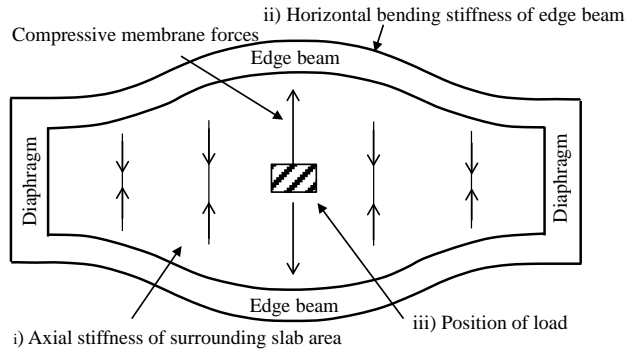


Fig. 2.5 Contributions to horizontal translational restraint stiffness according to Hon et al. (2005).

### Classification of the restraining action

The restraining action in a slab can be classified by Hewitt and Batchelor (1975) into two parts (Fig. 2.6): 1) Compressive membrane action (CMA); 2) Fixed boundary action.

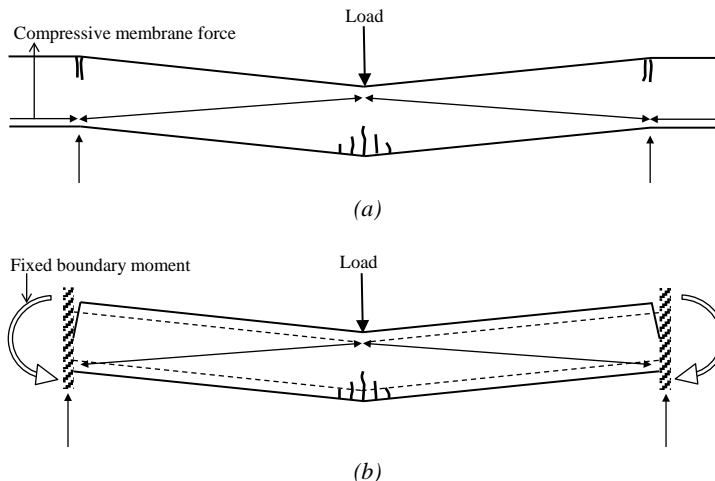


Fig. 2.6 Idealized restrained slab (adapted from Hewitt and Batchelor 1975): a) Compressive membrane action; b) Fixed boundary action.

## Punching shear capacity of concrete deck slabs considering CMA

- Compressive membrane action can develop only after cracking occurs in a slab and gives net in-plane forces at the slab boundaries. This phenomenon cannot occur in slabs with the same strength in tension and compression. Moreover, the presence of reinforcement is not necessary.
- Fixed boundary action can develop in both uncracked and cracked slabs (provided that the tensile reinforcement is present at the slab boundaries) and is due to the moment restraint only. Contrary to the CMA, this phenomenon can occur in slabs with the same tensile and compressive strengths.

Hewitt and Batchelor (1975) explain the development of typical punching shear failure in a restrained slab as follows: 1) Fixed boundary action (FBA); 2) Cracking on the tensile side of the slab; 3) Compressive membrane action (CMA) alone if the slab is unreinforced, or a combination of CMA and FBA if the slab is reinforced; 4) Punching shear failure.

### **2.3.2 Analysis of compressive membrane action**

The first significant observation of compressive membrane action was made by Ockleston (1955) while testing an old dental hospital in Johannesburg where the interior panels of the floor systems showed capacities that were three or four times those according to Johansen's yield line theory. Ockleston (1958) attributed this increase in strength to in-plane compressive membrane forces developed because of the lateral restraint present in the slab panels. This triggered an interest in this subject (Wood 1961, Brotchie 1963, Christiansen 1963, Park 1964, Liebenberg 1966) but mostly with regard to the flexural failure assuming that shear failure does not occur as per the yield line theory.

With regard to punching shear failure, the research on compressive membrane action can be broadly divided into two groups: 1) Research in North America (USA and Canada); 2) Research in the United Kingdom.

#### **Research in North America**

In North America, the majority of highway bridges are composite structures consisting of concrete deck slabs supported by steel or concrete girders. To investigate the load carrying capacity of such structures, a detailed experimental and theoretical research program on bridge deck slabs started at the Queen's university, Kingston, Ontario in the mid 1960's. Initially, Young (1965) performed some experiments on fixed-ended two way slabs subjected to single concentrated loads and Tong and Batchelor (1971) carried out an experimental study on 1/15<sup>th</sup> scale reinforced concrete bridge models and single slab panel models with varying steel reinforcement ratios. The governing mode of failure in all tests

## Punching shear capacity of concrete deck slabs considering CMA

was punching shear except for specimens with low reinforcement ratios. Higher capacities were observed than predicted by yield line theory regardless of the actual mode of failure. The results were presented in the annual convention of American Concrete Institute (ACI) at Denver that also included other works on arching and compressive membrane action in reinforced concrete slabs, mainly focusing on square slab panels (ACI 1971). Punching was recognized as a possible mode of failure resulting from the combined action of shear and flexure.

The Ontario Ministry of Transportation (MTC) sponsored further research at the Queen's University which resulted in an extensive investigation on scaled models of concrete deck slabs of composite steel/concrete bridge under concentrated loads (Hewitt 1972). High factors of safety were obtained leading to the conclusion that under a four wheel truck loading, the girders of a conventionally designed bridge would fail before the deck slab. A minimum isotropic reinforcement of 0.2% was deemed sufficient for ultimate limit states. Based on the experimental work, Hewitt and Batchelor (1975) proposed a rational model for predicting the punching shear capacity of restrained slabs by modifying the punching shear model developed by Kinnunen and Nylander (1960) and introducing lateral restraining forces and moments based on an empirical restraint factor,  $\eta$ , with  $\eta = 0$  for no restraint available and  $\eta = 1$  for fully restrained slabs. By considering the equilibrium of the slab sector element with the addition of the restraining force and moment, and by applying the same failure criterion as in the original Kinnunen and Nylander model, the punching shear capacity was derived through an iterative procedure.

Other experimental programs sponsored by the Ontario Ministry of Transportation include tests on a full scale model bridge (Csagoly et al. 1978) and extensive field tests (Bakht and Csagoly 1979) on 28 existing bridges of varying types (non-composite decks, decks composite with steel girders, decks with reinforced concrete T beams and decks composite with prestressed concrete girders). The restraint factor of these existing bridges varied from 0.43 to 0.93 showing considerable compressive membrane action to be developed in the system.

After extensive studies at Queen's university, Kingston, Ontario, empirical design specifications to account for the development of CMA in bridge deck slabs were introduced in the Ontario Highway Bridge Design Code (OHBDC OMTC 1979) resulting in thinner and lighter deck slabs, requiring a minimum isotropic reinforcement of 0.3% for shrinkage and temperature crack control and giving a 40% reduction in the amount of deck reinforcement over those designed for flexural failure of the deck slab (He 1992).

An extensive experimental, analytical and numerical investigation was conducted in the University at Texas at Austin (Fang et al. 1990, Graddy et al. 1995) regarding the behavior of Ontario-type reinforced concrete bridge decks on steel girders consisting of both cast-in-place and precast prestressed panels with cast-in-place topping. The model bridge decks were subjected to static and fatigue loading and significant compressive membrane action was reported in both flexural and punching shear modes, especially after the initial flexural cracking of the deck slabs. Most importantly, the finite element models were able to predict the contribution of membrane forces in the ultimate capacity.

### Research in the United Kingdom

Apart from the detailed research program in Ontario, Canada, significant development on compressive membrane action was made in Northern Ireland, UK. Some early research (Masterson and Long 1974) indicated that the punching strength of slab-column structures would be enhanced by the development of CMA. Rankin (1982) developed a rational technique for the strength of laterally restrained reinforced concrete slab strips.

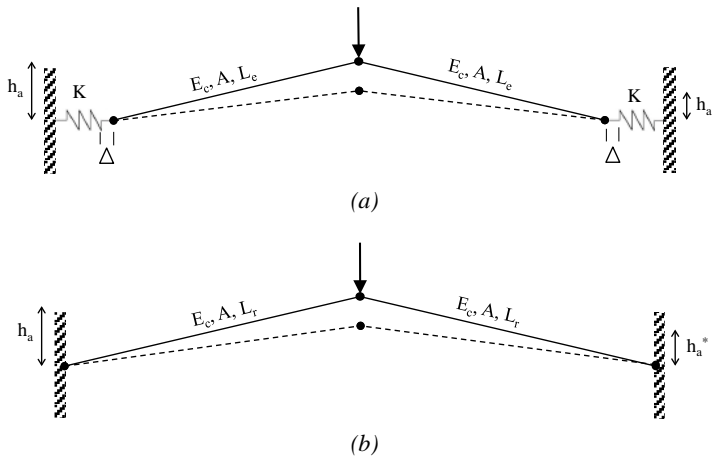


Fig. 2.7 Rankin's (1982) three hinged arch analogy: a) Elastically restrained arch; b) Rigidly restrained arch. where,  $E$  = Young's modulus,  $L$  = Half span of slab strip,  $A$  = cross-sectional area of arch leg,  $h_a$  = Initial arch height,  $h_a^*$  = deflected arch height, for each of the two arches.

The proposed method was based on an arching deformation theory (McDowell et al. 1956) and utilized an elastic plastic stress-strain criterion for concrete. The maximum arching moment of resistance was derived and the ultimate flexural capacity was considered to be the sum of bending and arching load capacities. Fig. 2.7 shows the analogy of a three-hinged arch with linear elastic 'spring' restraints used by Rankin (1982) for less than rigid restraints. The analysis was also extended to two-way slabs under a concentrated load

## Punching shear capacity of concrete deck slabs considering CMA

considering compressive membrane action. Both the enhanced flexural and punching shear capacities were predicted and the ultimate capacity was the lesser of the two.

In a parallel study at Queen's university, Kirkpatrick et al. (1982) carried out field tests as part of a joint research program between the Department of the Environment (NI) Roads Service and the Department of Civil Engineering at Queen's university, Belfast. Load distribution tests on a 11.815 m span M-beam bridge deck with beams spaced at 2 m and 1.5 m and a 160 mm reinforced concrete slab were performed. Later Kirkpatrick et al. (1984) carried out punching shear tests on a 1/3<sup>rd</sup> scale model of the same bridge. The punching shear strength was found to be independent of the level of reinforcement and the beam spacing and was considerably higher than predicted by both the British (BS 5400 1978) and the Canadian (OHBC 1979) code. Subsequently an equivalent steel ratio derived from the arching characteristics of the slab was used in the punching shear equation derived from Long's (1975) "two-phase approach" to calculate the punching shear capacity. The proposed theory gave good correlation with various test results (Kirkpatrick et al. 1984). The limitation of the model include a span to depth ratio of less than 15 and the availability of sufficient restraint in form of edge parapet and fully composite diaphragms. A minimum isotropic reinforcement of 0.5% was deemed necessary to ensure an uncracked slab for serviceability limit state.

Between 1985 to 2000, further progress was made in the area of CMA by developing methods for restrained slabs under uniformly distributed loads (Niblock 1986), in cellular structures (Skates 1987) and laterally restrained rib slab systems (Ruddle 1989). Reviews of the overall experimental and analytical research were also published (Long and Rankin 1989, Long et al. 1995, Rankin and Long 1997).

In 2000, Taylor assessed the degree of lateral restraint by using a restraint model with an effective width concept. The ultimate load carrying capacity of bridge deck slabs was determined by assessing the real restraint arising from the diaphragms, area of slab surrounding the loaded area and the edge beams, and incorporating it in the previously developed flexural capacity by Rankin and Long (1997) and punching shear capacity by Kirkpatrick et al. (1984). A clear distinction was made between the failure modes of flexural punching and brittle punching.

Between 2000 and to date, several laboratory tests on scaled bridge models have been carried out with varying parameters. Use of high performance concrete (Taylor et al. 2003) and addition of polypropylene fibers to reduce shrinkage and enhance long term durability of the concrete (Taylor et al. 2007) in restrained deck slabs have been investigated. An

experimental, analytical and numerical study has also been carried out on steel-concrete composite bridge models (Zheng et al. 2009, 2010). Compressive membrane action has been evident in all the tests and further modifications in the restraint model of Taylor (2000) have been proposed (Zheng et al. 2010).

The research done in Northern Ireland on compressive membrane action has been recognized in the form of code design and assessment provisions of reinforced concrete bridge deck slabs (UKBD 81/02). However, a rational treatment of CMA still needs to be incorporated and the provisions need to be extended for prestressed deck slabs.

### **2.3.3 Design code provisions incorporating compressive membrane action**

To date, none of the existing codes have incorporated compressive membrane action in the design or capacity assessment provisions of prestressed deck slabs. The design codes that have acknowledged CMA in predicting the punching shear capacity for reinforced concrete deck slabs are reviewed in the following sections.

#### **CHBDC: CAN/CSA-S6-06 (2006)**

CHBDC provides a rapid, empirical method of evaluating the load-carrying capacity of existing slabs. Both composite and non-composite deck slabs can be investigated with the help of charts. A similar approach is adopted in the New Zealand code (TNZAA 2003) to estimate the punching shear capacity.

Fig. 2.8 shows the chart for punching shear capacity of composite deck slabs. A similar chart is available in the code for non-composite slabs. These charts are a simplified version of the ones given in the third edition of the OHBDC (MTO 1991) and can be used provided that the slab parameters are within the limitations<sup>3</sup> specified as follows:

- The center-to-center spacing of the supporting beams for a slab panel does not exceed 4.5 m and the slab extends sufficiently beyond the external beams to provide full development length of the bottom transverse reinforcement.
- The ratio of the spacing of the supporting beams to the thickness of the slab does not exceed 20.
- The minimum slab thickness of sound concrete is at least 150 mm (with the minimum slab thickness used for slabs of variable thickness).

---

<sup>3</sup> For detailed clauses, reference is made to section 14.14 of CAN/CSA-S6-06 (2006).

## Punching shear capacity of concrete deck slabs considering CMA

- All cross-frames or diaphragms extend throughout the cross-section of the bridge between external girders and are provided at support lines. The maximum spacing of such cross-frames or diaphragms in case of steel girders or box girders does not exceed 8.0 m c/c.
- The transverse free edges of all deck slabs shall be stiffened by composite edge beams and shall be proportioned for the effects of wheel loads.

If all the limitations are satisfied, the value of the factored resistance  $R_r$  is calculated as follows:

$$R_r = \phi_{md} R_n \text{ [kN]} \quad (2.6)$$

where,  $\phi_{md} = 0.5$ .

The value of  $R_n$  for both composite and non-composite concrete deck slabs is calculated as follows:

$$R_n = R_d F_q F_c \text{ [kN]} \quad (2.7)$$

where,  $R_d$  is taken from Fig. 2.8 for a particular deck thickness  $d$  (or  $t$  in Fig. 2.8) and the corresponding deck span,  $F_q$  is a correction factor based on the reinforcement ratio,  $q = 50(A_{sl} / bd_l + A_{st} / bd_t)$ , with  $0.2\% \leq q \leq 1\%$ ;  $A_{sl}$  and  $A_{st}$  are the longitudinal and transverse bottom steel areas,  $b$  is the width and  $d_l$  and  $d_t$  are the longitudinal and transverse effective depths of the deck slab, respectively.  $F_c$  is a correction factor based on  $f'_c$ , the specified concrete compressive strength measured on cylinders ( $20 \text{ MPa} \leq f'_c \leq 40 \text{ MPa}$ ).

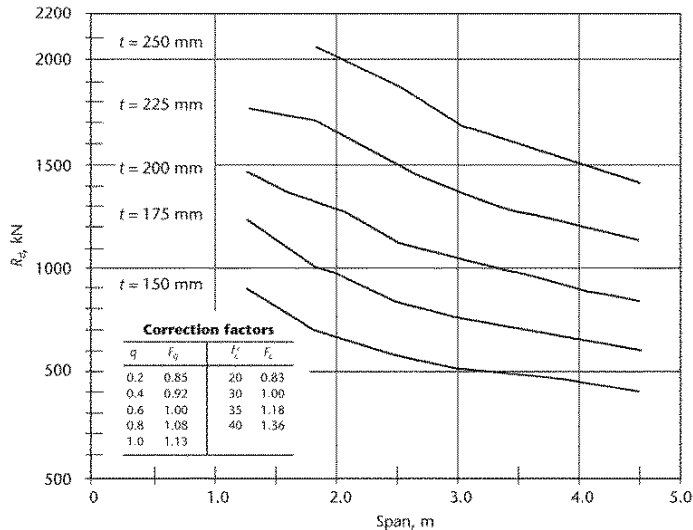


Fig. 2.8 Deck punching shear capacity for composite slab (CAN/CSA-S6-06 2006).

$F_q$  and  $F_c$  are taken from Fig. 2.8 or obtained from the figure by linear interpolation. For deck thicknesses other than those shown in Fig. 2.8, the value of  $R_n$  can be obtained by linear interpolation. This method does not apply to cantilevered slabs. The slab capacities are based on a wheel load at the centerline of the span of the slab panel. The wheel load considered is a dual wheel, consisting of two 250×250 mm areas in contact with the deck, separated by a clear space of 100 mm.

### **UK HA BD81/02 (2002)**

A simplified method for calculating the ultimate local capacity (punching shear) of laterally restrained deck slabs, based on the work of Kirkpatrick et al. (1984, 1986), has been included in the UK highway agency's design manual for roads and bridges (UK HA BD 81/02 2002). It assumes that the slab reinforcement does not contribute to the local load carrying capacity and the local strength may be assumed adequate for up to 45 units<sup>4</sup> of type HB loading (abnormal vehicle unit loading as defined in UK HA BD 37/01 2001). Moreover, the assessed local capacity of the deck slab should not exceed the load carrying capacity of adjacent supporting members. Following limitations<sup>5</sup> must be satisfied to apply the method:

- The slab should be at least 160 mm thick and of at least grade 40 concrete.
- The minimum steel area provided in the deck slab at each face in each direction should be at least 0.3% of the gross concrete section.
- The transverse (primary) span length of a slab panel perpendicular to the direction of the traffic should not be more than 3.7 m.
- The slab should extend at least 1.0 m beyond the center line of the external longitudinal supports of a panel.
- The span length to thickness ratio of the slab should not exceed 15.
- Transverse edges at the ends of the bridge and at intermediate points where the continuity of the slab is broken should be supported by diaphragms designed for the full effects of the wheel loads.
- Cross frames or diaphragms should be provided at the support lines of all bridges. Bridges with steel beams should have cross frames or diaphragms at centers not exceeding 8m or half the span of the bridge. Bridges with concrete beams other than prestressed beams, should have at least one intermediate diaphragm in each span.

---

<sup>4</sup> One unit is equal to 2.5 kN per wheel.

<sup>5</sup> For detailed clauses, reference is made to volume 3, section 4, part 20, "Use of compressive membrane action in bridge decks", of the UK HA BD81/02 (2002).

## Punching shear capacity of concrete deck slabs considering CMA

- Edge beams should be provided for all slabs having main reinforcement parallel to the traffic direction.

If all limitations are satisfied, the ultimate capacity can be calculated as per the code provisions. The plastic strain of an idealized elastic plastic concrete  $\varepsilon_c$  is calculated as:

$$\varepsilon_c = (-400 + 60f_c - 0.33f_c^2) \times 10^{-6} \quad (2.8)$$

The non-dimensional parameter for the arching moment of resistance  $R$  is given by:

$$R = \frac{\varepsilon_c L_r^2}{h^2} \quad (2.9)$$

For the deck slab to be treated as restrained,  $R$  must be less than 0.26. If this condition is not met, the deck slab is considered unrestrained and the benefit from the compressive membrane action to enhance the load capacity of the slab cannot be assumed.

The non-dimensional arching moment coefficient  $k$  is given by:

$$k = 0.0525 \left( 4.3 - 16.1 \sqrt{3.3 \times 10^{-4} + 0.1243R} \right) \quad (2.10)$$

The effective reinforcement ratio  $\rho_e$  is given by:

$$\rho_e = k \left( \frac{f_c}{240} \right) \left( \frac{h}{d} \right)^2 \quad [SI \text{ Units: } N, mm] \quad (2.11)$$

The ultimate load  $P_{ps}$  can be calculated as:

$$P_{ps} = 1.52(\phi + d)d\sqrt{f_c}(100\rho_e)^{0.25} \quad [SI \text{ Units: } N, mm] \quad (2.12)$$

where a deck is subjected to axle loading, either two wheels on one slab or two wheels on adjacent axles, the ultimate predicted wheel load  $P_{pd}$  is taken as:

$$P_{pd} = 0.65P_{ps} \quad [N] \quad (2.13)$$

where,  $d$  is the average effective depth, the concrete cylinder strength is  $f_c = 0.8f_{cu}/\gamma_m$  ( $f_{cu}$  is the characteristic concrete cube strength in MPa,  $\gamma_m$  is the partial safety factor for concrete),  $h$  is the overall slab depth,  $L_r$  is half the span<sup>6</sup> of the slab strip with boundary restraint,  $\phi$  is the equivalent diameter of the loaded area.

---

<sup>6</sup> Clear span for slabs monolithic with beams; distance between beam web center lines for slabs supported on steel or concrete girders.

## **2.4 Punching shear capacity considering compressive membrane action in prestressed decks**

This section deals with a review of experimental programs and finite element studies conducted on transversely prestressed decks considering compressive membrane action. The main focus is on the effect of transversely prestressing and compressive membrane action on the punching shear capacity and the overall behavior of deck slabs. Experimental programs that are similar to the current study are reviewed.

### **2.4.1 Introduction**

The concept of transverse post-tensioning of bridge superstructures was first introduced in Europe during the 1960's. The technique was initially applied to cell-box girder bridges for the following purposes:

- Increase the length of cantilever overhangs
- Reduce the number of webs
- Improve the connection between longitudinal girders
- Provide better and less congested reinforcement layout at pier locations

After witnessing the improved behavior of transversely prestressed box girder bridges, its application was extended to cast-in-place deck slabs on steel or concrete girders as well. Where dead load reduction becomes necessary, like in longer spans, thinner deck slabs can be provided by making use of transverse prestressing. Not only is this technique economical but also leads to an improved durability as slab deformations and cracking are reduced (Tedesco 1976). Transverse prestressing becomes worthwhile for superstructures wider than 12 m and definitely advantageous for widths above 17-18 m since transverse bending generated by the live loads depends on the square of the transverse span or the width of the deck (Rosignoli 2002).

### **2.4.2 Past research**

#### **Design criteria and effectiveness of transverse prestressing**

A comprehensive research program was initiated at the University of Texas at Austin in the 1980's regarding transverse prestressing and is summarized by Poston et al. 1988. A series of tests and finite element analyses were conducted to develop necessary design criteria for transverse prestressing of bridge decks. The prototype was 8.23 m wide and 10.36 m long with a 96 mm thick transversely post-tensioned slab and consisted of seven prestressed

## Punching shear capacity of concrete deck slabs considering CMA

Texas Type-C girders with end and interior diaphragms. Three types of laboratory tests were performed: Lateral stressing tests, vertical load tests and horizontal concentrated edge load tests.

### Test observations

In the lateral stressing experiments, the resulting lateral post-tensioning stress distribution showed that transverse prestressing the deck slab could effectively develop compressive stresses in the slab to counteract tensile stresses due to shrinkage and live loads. Also, the slab transverse stresses were found to be affected by the existence of the diaphragms. It was also observed that stepwise distribution of strand forces should always be used in modeling transverse prestressing forces.

The vertical load test results showed that the deck slab remained in the linear elastic stage under factored load levels and the deck remained uncracked at service load levels. The deck slab was not tested to failure but the cracking pattern indicated a punching failure mode. No substantial difference between the behavior of the deck slab with straight strands only and the deck with a combination of straight and draped strands was found. Also no difference in slab behavior was observed when loading at the interior and the exterior locations.

The horizontal concentrated edge load tests showed that the stresses near the strand anchorage were fairly high and not significantly affected by tensioning of additional strands. Also, it was concluded that because post-tensioning forces were applied to a deck in a discretized manner due to spacing of the strands, there were areas along the edge of the deck between the strands where the prestressing was ineffective.

### Finite element analysis

The 3D finite element model of the bridge deck showed that the presence of diaphragms at the time of transverse prestressing significantly affected the transverse stress distribution in a bridge deck slab resulting in a non-uniform stress distribution. In order to avoid this, additional transverse prestressing strands were recommended in the slab area close to the diaphragm. Another solution was to provide equal prestressing in the diaphragms and the slab. Decreasing the span length was found to increase the restraint due to an increase in the maximum axial force in the diaphragms.

### **Reducing the deck slab thickness by using transverse prestressing**

Parallel to the research described previously at the University of Texas, Moll (1984) proposed that the thickness of bridge decks designed according to OHBDC (1983) be

reduced and that the two layers of normal reinforcement in each direction be replaced by one layer of transverse prestressing. Tests on a composite bridge deck designed according to Moll's proposal proved to be satisfactory in terms of ultimate limit state. Two full scale prototype *concrete bridge decks on steel girders* were tested. The first model deck slab was designed using the empirical approach in the OHBDC (1983) and the second model deck slab was thinner and designed with a single layer of transverse prestressing. Each deck was statically tested to failure under the concentrated load. The second model was first tested to failure near one end in the longitudinal direction with a transverse prestressing level (TPL) of 3.92 MPa and then every second strand was distressed giving a reduced TPL of 2.04 MPa and tested to failure at the other end. All the tests failed in punching shear and at loads well above the OHBDC (1983) design service load.

### **Influence of transverse prestressing level on the punching shear capacity**

An extensive research program was conducted at Queen's University, Ontario, Canada to study the behavior of transversely prestressed composite bridge decks. The individual experimental programs are briefly summarized below.

Savides (1989) conducted static tests by applying a concentrated load on a 1/4.04 scale model of a *concrete bridge deck supported on steel girders*. The model bridge deck slab was 43 mm thick and had a layer of transverse prestressing tendons at the mid-depth of the slab. The deck was prestressed to a transverse prestress level (TPL) of 4.37 MPa. A high degree of compressive membrane action was developed in the deck slab. The first cracking occurred at an average load of 4 times the OHBDC (1983) design service load and punching failure occurred at an average load of 10 times the OHBDC (1983) design service load. The study confirmed the possibility of reducing the thickness of the OHBDC deck slab without compromising serviceability.

A second study was undertaken by He (1992) on two model bridge decks similar to the one used by Savides (1989). The main parameter in the study was the transverse prestressing level. TPLs of 1.84, 2.15, 2.50, 2.91, 3.32 and 3.88 MPa were applied. A linear correlation was found to exist between the punching load and the transverse prestressing level (Fig. 2.9). The higher the transverse prestressing level, the higher was the punching load. The cracking load varied between 23% to 38% of the failure load and was found to increase with the transverse prestressing level. This further showed that transverse prestressing acts as an effective crack controller.

## Punching shear capacity of concrete deck slabs considering CMA

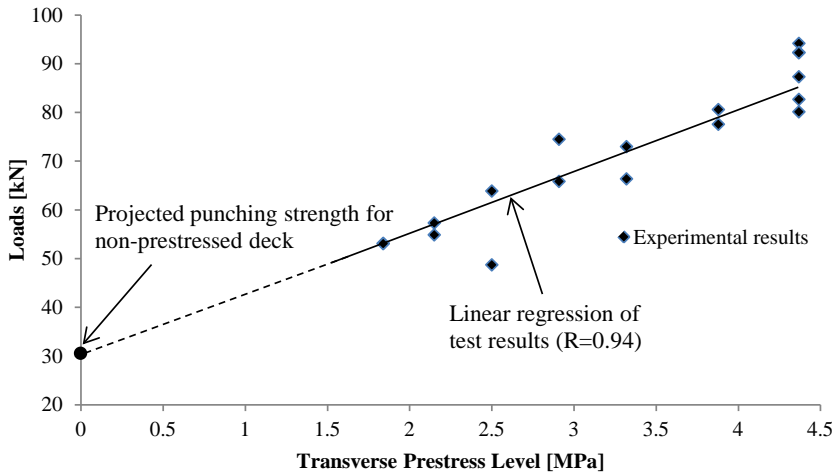


Fig. 2.9 Relationship between TPL and the ultimate punching load (He 1992). Test results of Savides (1989) with a transverse prestress level of 4.37 MPa were also considered by He (1992).

A similar study was also conducted by Marshe (1997) but with CFRP prestressed deck slabs. The TPLs investigated were 2.15, 2.5 and 3.32 MPa. Higher cracking and punching loads were obtained than those by He (1992) on a steel prestressed deck.

### Design specifications and implementation of transverse post-tensioning in concrete bridge decks

Another research on transverse prestressing was conducted at the Purdue university sponsored by Indiana Department of Transportation (INDOT). Initially design specifications for the use of transverse post-tensioning in concrete bridge decks were developed (Ramirez and Smith-Pardo 2002) based on analytical studies. It was found that different application levels of prestressing were required in regions containing the interior and exterior (or outermost) diaphragms. The magnitude of transverse forces was found to be a function of the girder boundary conditions, the axial stiffness of the diaphragms, the skew angle of the deck, and the position of the diaphragms/stiffener with respect to the edge of the deck. Simplified design guidelines were developed for use in INDOT. Further research was conducted by Ramirez and Aguilar (2010) on a rectangular concrete bridge deck supported on precast prestressed concrete girders. The key parameters of the study were the effect of both girder boundary conditions and position of the diaphragms. The number of steel diaphragms was varied from five to none, and the applied transverse stress from 2.75 to 8.27 MPa. Also, the restraining force at one of the support lines was varied to evaluate the effect of end-restraint on the distribution of transverse post-tensioning. The experimental results showed that the presence of diaphragms had some effect on the distribution of transverse strains, however, it was not found to be as large as expected. In

the range of post-tensioning estimated to maintain the uncracked condition under service loads, the use of uniform transverse post-tensioning was deemed appropriate. The effect of end restraint could not be established with sufficient confidence to justify a reduction in the concrete deck stresses resulting from the transverse post-tensioning of the same.

Hwang et al. (2010) investigated the punching shear capacity of long-span prestressed concrete deck slabs on steel girders. Six 1/3<sup>rd</sup> scale specimens were subjected to static tests using a concentrated load and the test results were used to evaluate existing punching shear formulae. The level of prestressing was observed to influence the mode of failure, with low prestressing levels giving *flexural punching* as the failure mode. The punching strength was found linearly proportional to the prestressing level. The Eurocode 2 formula was deemed reasonable for the punching strength estimation, while still being on the conservative side and on average predicting about 75% of the actual strength observed in tests.

## 2.5 Summary and conclusions

In this chapter, the literature related to the ultimate bearing (punching shear) resistance of transversely prestressed concrete decks considering compressive membrane action has been briefly reviewed. First, a historical background of research carried out on punching shear resistance was given and punching shear strength provisions of current codes and the critical shear crack theory were outlined. Next the phenomenon of compressive membrane action was explained and the research programs that led to the development of codes like CHBDC (2006) and UK HA BD81/02 (2002) that consider compressive membrane action in reinforced concrete decks were described. Lastly, the experimental programs conducted in the past to investigate punching shear strength of prestressed decks considering compressive membrane action were reviewed.

Three important conclusions can be derived from the literature review:

- The current codes do not consider compressive membrane action (CMA) in their provisions for estimating the punching shear capacity of *prestressed* slabs or deck slabs.
- Most of the past research on the punching shear capacity considering compressive membrane action has been conducted on reinforced concrete decks. There is a need to expand the investigations regarding CMA to prestressed decks.
- The little research carried out on prestressed deck slabs was either on small-scale specimens, incapable of simulating the true behavior of full-scale real bridge decks; or on concrete decks supported on *steel girders*, possibly leading to a lower

## Punching shear capacity of concrete deck slabs considering CMA

level of restraining action that could otherwise develop fully if concrete girders monolithically connected to the concrete deck were present.

It can be concluded that a reasonably scaled, experimental and analytical research is needed for the in-depth study of the behavior of laterally restrained, transversely prestressed decks subjected to punching shear action. Nonlinear finite element analyses of 3D solid bridge models are also recommended rather than performing investigations on 2D or shell element models so that the phenomena of punching shear and compressive membrane action is properly simulated in prestressed decks.

## Punching shear capacity of concrete deck slabs considering CMA

# **CHAPTER 3**

## **Experimental Program - Design of the Test Setup**

This chapter includes the description of a 1:2 scaled bridge model constructed in the laboratory for the experimental part of this research. The design and construction of the bridge model, the material properties, the experimental program and the test setup are discussed.

### 3.1 Introduction

A comprehensive experimental program was conducted in the laboratory to study the punching behavior of transversely prestressed concrete bridge decks. A 1:2 scaled model of a real approach bridge in the Netherlands was constructed and tested for this purpose. This chapter describes the design and construction of the model bridge deck and the experimental program in detail.

#### 3.1.1 Real bridge

An approach bridge provides a smooth and safe transition of vehicles from a highway road to the main bridge structure. Fig. 3.1 shows the Van Brienoord bridge in the Netherlands that consists of a number of 50 m approach spans having thin, post-tensioned deck slab panels cast-insitu between the flanges of simply supported, post-tensioned girders. The design records of the bridge show that the regular reinforcement ratio of the deck slab is quite low as prestressing reinforcement is already present. The prestressing tendons in the slab are placed in the transverse direction at an average spacing of around 650 mm c/c. In some places this spacing is 800 mm c/c. The transition of the deck to girder flange is realized by an inclined indented interface to generate sufficient shear capacity. Transversely prestressed end transverse beams are present at the supports, along with diaphragms at 1/3 and 2/3 of the span (Amir et al. 2014).



Fig. 3.1 An old draft drawing of the Van Brienoord bridge in Rotterdam, consisting of nine approach spans of 50 m, an arch bridge of 300 m, the bascule bridge, the bascule pit and another nine approach spans of 50 m. Material properties of the deck slab are given in Table 3.1.

Table 3.1 Material properties of the deck slab of Van Brienoord bridge.

Material property	Value	No. of samples - Size	Coefficient of variation
	[MPa]		[MPa]
Concrete characteristic compressive strength	84.6	6 - 100×100 mm cores	8
Concrete mean compressive strength	98.8		
Concrete characteristic splitting tensile strength	4.3	6 - 100×100 mm cores	0.9
Concrete mean splitting tensile strength	5.8		
Reinforcing steel (QR22) characteristic yield strength	220	Not tested. Standard values.	
Prestressing steel (QP150) ultimate tensile strength	1262		

An investigation was carried out by Witteveen+Bos (2009) to determine the concrete properties of the Van Brienoord bridge deck slab. The concrete strength class of the

girders and the deck slab panels was B45 and B35 respectively at the time of casting. Currently the concrete strength is considerably higher as a result of on-going cement hydration over the years. The material properties are given in Table 3.1.

### 3.1.2 Scale factors for the prototype

In order to simulate the actual bridge as closely as possible, a 1:2 scale was used to design the prototype. Linear scale factors based on the geometry and keeping the stress as unity in the real and the prototype bridge were used to derive the scale factors of the prototype. Such an approach was followed in research carried out in Ontario, Canada (Savides 1989, He 1992, Marshe 1997). Appendix A includes the cross sectional details of the approach of the Van Brienenoord bridge. All linear dimensions were scaled down by a factor  $x = 2$ . Rest of the scale factors are given in Table 3.2.

Table 3.2 Scale factors for the prototype bridge for various parameters ( $p$  stands for the prototype and  $b$  for the real bridge).

Parameter	Scale factor, $\lambda$
Stress ( $\sigma$ )	$\lambda_\sigma = \sigma_b/\sigma_p = 1$
Strain ( $\epsilon$ )	$\lambda_\epsilon = \epsilon_b/\epsilon_p = 1$
Length ( $L$ )	$\lambda_L = L_b/L_p = x$
Area ( $A$ )	$\lambda_A = A_b/A_p = x^2$
Force ( $F$ )	$\lambda_F = F_b/F_p = x^2$
Moment ( $M$ )	$\lambda_M = M_b/M_p = x^3$
Section modulus ( $S$ )	$\lambda_S = S_b/S_p = x^3$
Moment of inertia ( $I$ )	$\lambda_I = I_b/I_p = x^4$
Mass density ( $\rho$ )	$\lambda_\rho = \rho_b/\rho_p = 1/x^2$

It should be noted that the scale factors mentioned in Table 3.2 are linear scale factors with the assumption that the nominal strength remains the same with an increase in the structural size. In the current study, the model bridge deck thickness is only 100 mm and a size effect (reduction of strength with an increase in structural size) is expected to occur when the results are projected to larger sizes. This implies that the force scale factor is not exactly  $x^2 = 2^2 = 4$  (as shown in Table 3.2) but lesser than that. The two factors, scale factor and size factor, are dealt with separately in this thesis as the former is a known entity while the latter is unknown and is yet to be identified. This will be discussed later in chapter 7 and 8.

### 3.1.3 Design considerations: Some important lower bounds

The girders and the deck slab were designed in such a way that the failure would occur in the deck slab as it was the main subject of interest in this research. A higher strength concrete was used in the girders than in the deck slab of the prototype. To consider the most

unfavorable effects in the investigation, the following lower bounds were considered during design:

- In a typical real bridge, the interface between the side of the upper flange of the girder and the cast in-situ deck is inclined to 5 degrees at one side of the deck slab but the prototype was provided with inclined interfaces at both sides.
- The spacing of the transverse prestressing was increased from the general spacing of 650 mm c/c in the actual bridge<sup>7</sup> to 800 mm c/c (scaled down to 400 mm c/c) in the prototype.
- Most of the tests were done with a load applied in-between two adjacent transverse prestressing ducts in the deck. This gives a lower bound for the bearing capacity as compared to the capacity when testing directly above a prestressing duct.
- Three transverse prestressing levels (TPLs) were applied: 0.5 MPa, 1.25 MPa and 2.5 MPa. Although the usual TPL in a real bridge is 2.5 MPa, the value of 1.25 was applied to regard the eventual effect of tendon failure. A TPL of 0.5 MPa was applied to simulate a reinforced concrete bridge deck with no prestressing effect.
- In order to adjust the prestressing level, unbonded prestressed bars were applied in the deck slab, whereas in the real bridge only bonded cables are present.

### 3.1.4 Prototype of the bridge

Fig. 3.2 shows the prototype bridge. The deck was 6.4 m wide and 12 m long, with one main span of 10.95 m and a cantilever of 0.525 m at each end. It consisted of four, 1300 mm high, precast concrete girders placed at 1800 mm c/c distance. The three deck slab panels were cast in-situ and post-tensioned in the transverse direction with a clear span of 1050 mm and a thickness of 100 mm. Two transverse beams were provided at the end of the girder-slab assembly, also post-tensioned in the transverse direction. Following sections briefly describe the design of each component of the bridge deck.

---

<sup>7</sup> Note that in the actual bridge, the spacing of the transverse prestressing in the deck slab is 800 mm only at the location of the anchors of the longitudinal cables of the girders.

## Experimental Program – Design of the Test Setup

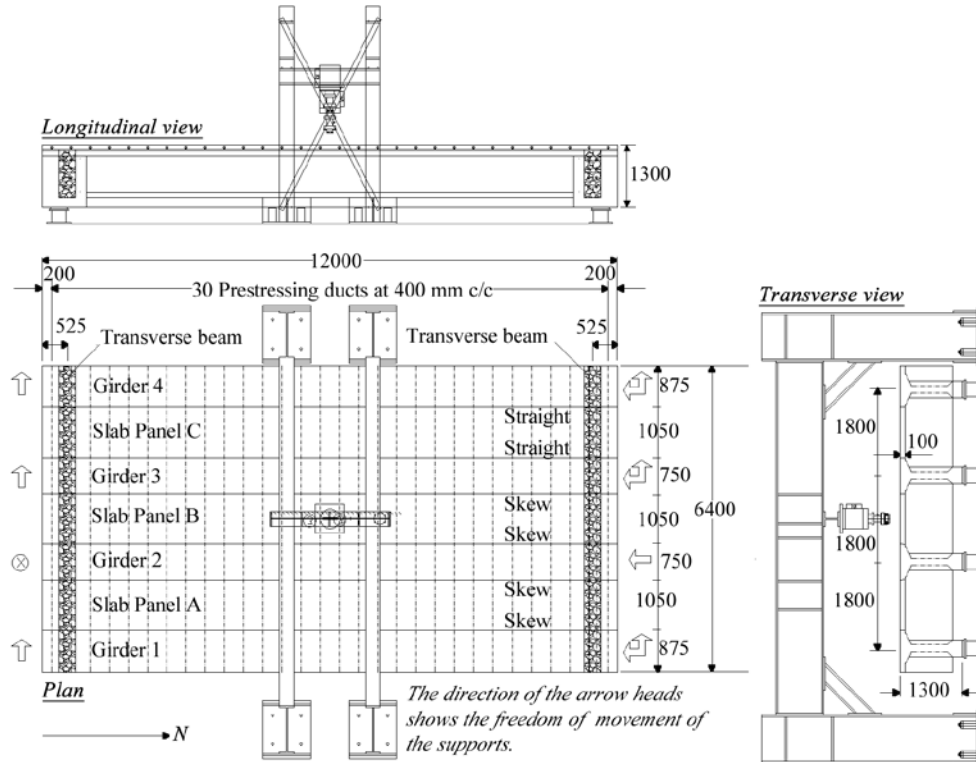


Fig. 3.2 An overview of the test-setup; Longitudinal view, Transverse view and Plan (clockwise from top) from Stevin Report No. 25.5.13-06 (2013).

### Scale model of the girders

#### Cross section

Four 12m long precast-prestressed girders of the model bridge deck were made by Spanbeton, the Netherlands. The shape of the cross section of the girders was determined by that of the real bridge. The cross section of the model bridge interior girder is shown in Fig. 3.3a and old draft drawings of the real bridge are shown in Appendix A. The slab between the girders of the real bridge has a thickness of 200 mm which was scaled down for the prototype/model bridge to 100 mm. Therefore, it was necessary to make the top flange of the girders 100 mm thick. The top flange width was scaled down from 1500 mm to 750 mm. However, not all dimensions of the real bridge girders could be scaled down to exactly 1:2 because instead of making a new mold, a saving in cost was made by adapting to an existing mold of Spanbeton. Some variations are as follows:

## Experimental Program – Design of the Test Setup

- In the real bridge, the height of the girders is 3000 mm but the height of the model bridge girders was kept at 1300 mm.
- The thickness of the web is 150 mm in the original design, but a 150 mm wide web was provided in the prototype girder cross section as this is the minimum practical thickness for casting. The shape and size of the bottom flange slightly differs as well.

The longitudinal moment of inertia of the model cross section was 15% smaller than required but the transverse moment of inertia was more than sufficient. It is worth mentioning that the girders had a thicker web at the overhanging deck edges to introduce prestressing force in the girders. Also, the exterior girders had an extended width of 125 mm at the exterior flanges (Fig. 3.3b) to make sure that the prestressing and the confining effects were introduced adequately into the deck slab. In addition to this, the overhang also provided a smooth surface for the anchor and bearing plates for the prestressing bars in the deck slab and increased the stiffness in the transverse direction. More details on the design of girders are given in the Stevin Report No. 25.5.13-06 (2013) and by Vugts (2012).

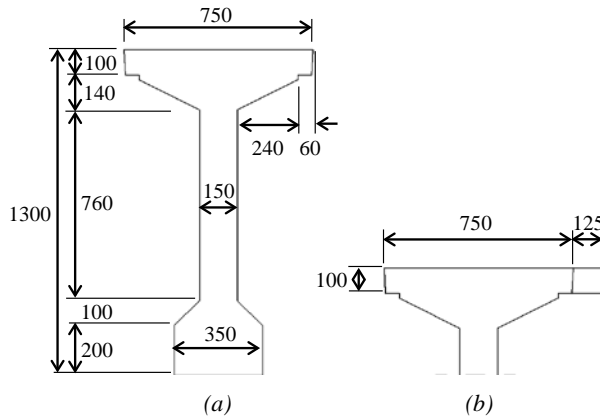


Fig. 3.3 Dimensions of the girders (in mm): a) Model bridge interior girder; b) Model bridge exterior girder overhang.

### Prestressing steel

The girders were designed for a point load of 1100 kN requiring a prestressing force of 4951 kN acting at an eccentricity of 389 mm. The required area of the prestressing steel is:

$$A_{p,required} = \frac{4951 \times 10^3}{1395} = 3549 \text{ mm}^2$$

Hence, 24 strands were provided using 15.7 mm  $\Phi$  strands with an area of 150 mm<sup>2</sup>. The reinforcement detailing of the girders by Spanbeton is provided in Appendix A.

## Scale model of the deck slab panels

### Cross section

The deck slab of the real bridge was scaled down using the factors in Table 3.2. This resulted in a thickness/depth of 100 mm and a span of 1050 mm in the transverse direction. The length of the deck slab panels was kept equal to the overall bridge length of 12 m.

### Prestressing system

The deck slab had to be investigated for varying levels of transverse prestressing. Therefore, unbonded, post tensioned prestressing bars were provided in the transverse direction. The provision of bars instead of strands was due to the easy and cheap system of anchorage required. Steel plates were provided on each side of the deck at the edge of the exterior girder flanges to act as anchor and bearing plates. As compared to the anchorage system of the strands, that would have required a certain length to introduce the prestressing force, and as a result additional concrete to the outer girder flanges, the steel plates did not require any extra length. Furthermore, it is also much easier to prestress a bar as compared to strands at the building site.

### Prestressing steel

As explained in section 3.1.1, the transverse prestressing steel in the real bridge varies from an average spacing of 650 mm c/c to a maximum spacing of 800 mm c/c in some places. In order to simulate the most unfavorable situation, the maximum spacing of 800 mm c/c was selected and scaled down using the length scale factor in Table 3.2. Hence, the resulting spacing of the prestressing bars was 400 mm c/c throughout the model bridge deck slab. With a deck slab of 100 mm thickness, this would mean that one prestressing bar stressed a concrete area of 40,000 mm<sup>2</sup>. The maximum transverse prestressing level (TPL) to be investigated was 2.5 MPa requiring a total working force in one bar of 100 kN. The prestressing steel of DYWIDAG systems was used. A minimum cross-sectional area of 112 mm<sup>2</sup> was required but the smallest bar by DYWIDAG is 15 mm  $\Phi$  with a cross-sectional area of 177 mm<sup>2</sup>. Therefore, the total prestressing steel provided per meter in the deck slab is:

$$A_p = \frac{177 \times 1000}{400 \times 1000} = 0.4425 \text{ mm}^2 / \text{mm}$$

The amount of prestressing force required per bar is given in Table 3.3. More information about the layout of the prestressing steel in the deck slab is given in Appendix B.

## Experimental Program – Design of the Test Setup

Table 3.3 Prestressing force per bar.

Transverse prestressing level (TPL) [MPa]	Prestressing force, $F_p$ [kN]
0.5	25
1.25	50
2.5	100

For the application of post-tensioned bars in the deck, ducts were required. For a 15 mm  $\Phi$  bar, the minimum diameter of the duct is 20 mm but for ease of fitting, a larger diameter of 45 mm was provided. The size of the steel plates used for anchorage of the prestressing bars was 100×170 mm with a thickness of 20 mm.

### Ordinary steel reinforcement

The applied reinforcement in the Van Brienenoord bridge deck slab is 8 mm  $\Phi$  bars @ 200 mm c/c in the longitudinal direction and 8 mm  $\Phi$  bars @ 250 mm c/c in the transverse direction at both top and bottom. Since the smallest available steel bar has a diameter of 6 mm, therefore, in the model bridge deck, the regular steel reinforcement provided was 6 mm  $\Phi$  bars @ 200 mm c/c in the longitudinal direction and 6 mm  $\Phi$  bars @ 250 mm c/c in the transverse direction (Appendix B). A clear cover of 7 mm to the top and bottom reinforcement and 16 mm to the vertical reinforcement is provided.

## Scale model of the transverse beams

### Cross section

Two post-tensioned, transverse beams were provided at 525 mm from each end of the model bridge to provide stiffness in the transverse direction as shown in Fig. 3.2 and 3.4. The height of the transverse beams depended on the height of the girders and therefore the top of the beams was at 190 mm from the top of the girders. In order to provide space for going underneath the deck slab for inspection during the test, the transverse beams were designed to be 300 mm above the bottom of the girders. This resulted in a total height of 810 mm. The width of the transverse beams of the real bridge is 700 mm. Scaling it down by using the length scale factor in Table 3.2 gives a width of 350 mm for the transverse beams of the model bridge. Fig. 3.4 shows the size of the transverse beams with regard to the girders.

### Prestressing steel

Since the deck was transversely prestressed, the transverse beams also required prestressing of the same level for uniform force distribution. For a level of 2.5 MPa, the total force required can be calculated as in Eq. 3.1 and for eight bars in total, the force per bar is

## Experimental Program – Design of the Test Setup

calculated in Eq. 3.2. 15 mm  $\Phi$  prestressing bars were provided in ducts of 65 mm  $\Phi$  (Appendix B includes the reinforcement details).

$$F = A_t \times \sigma_{cp} = 810 \times 350 \times 2.5 = 708.8 \text{ kN} \quad (3.1)$$

$$F_t = \frac{F}{n} = \frac{708.8}{8} = 88.6 \text{ kN} \quad (3.2)$$

### Ordinary steel reinforcement

Ten 12 mm  $\Phi$  bars in four layers were provided in the longitudinal direction and seven 8 mm  $\Phi$  bars were provided as stirrups (Appendix B includes the reinforcement details).

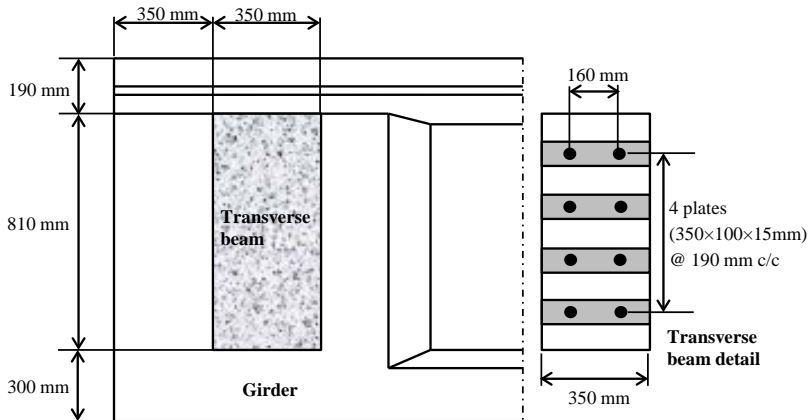


Fig. 3.4 Geometry and position of the end transverse beams (Stevin Report No. 25.5.13-06).

### **Girder flange-slab panel interface**

As explained in section 3.1.1, the upper flanges of the girders and the deck slab panels are connected by an indented concrete interface. The properties of the interface of the Van Brienoord bridge are unknown but since the interface characteristics were expected to influence the bearing capacity, it was simulated in the scale model as best as possible using knowledge of construction methods of that time. Two important parameters had to be designed carefully: the roughness and the skewness of the joint.

### Roughness

Eurocode 2 distinguishes four surface classes for concrete to concrete interface; very smooth, smooth, rough and indented. A teardrop pattern of size 30x10 mm with 1-2 mm depth (Fig. 3.5a) was selected for the interface joint classified as “smooth” according to

Eurocode 2. This pattern was introduced by placing specially formed shear keys in the molds.

### Skewness

In contrast to the real bridge with inclined surfaces on one side of the flange, the prototype was provided with inclined interfaces at both sides (Fig. 3.5b). Two deck slab panels had skewed interfaces and one was designed with a straight (90 degrees) interface to study the effect of the inclination of the joint surface on the bearing capacity.

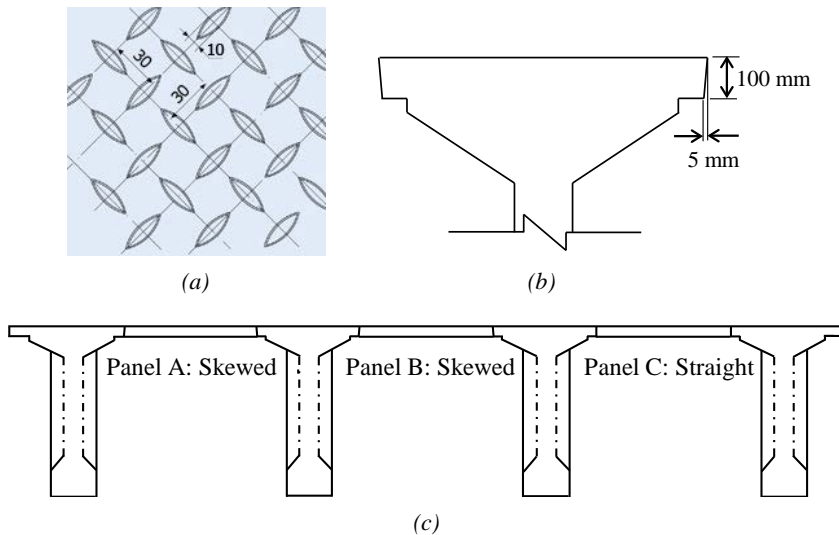


Fig. 3.5 Girder-slab joint/Interface properties: a) Roughness-Ruukki DIN 59220 teardrop pattern; b) Skewness of the girder flange; c) Location of skewed joints in the model bridge deck section.

## 3.2 Material properties of the model bridge deck

The following sections explain the material properties of concrete and steel used in the model bridge deck. Since the investigation is about real old bridges, the material strength being used in the model bridge is approximately simulating current strength of the material when it comes to concrete. The steel properties are simulated as close to actual conditions as possible.

### 3.2.1 Concrete

The compressive and the splitting tensile strength of concrete was measured on 150 mm cubes. Table 3.4 describes the concrete properties used in the bridge model. Each strength value is the mean of tests done on 3 specimens at 28 days of casting. The mean cylinder

## Experimental Program – Design of the Test Setup

strength and the modulus of elasticity are calculated as per the Model Code 2010. For the deck slabs panels, cubes were tested at 28 days and at regular intervals throughout the experimental phase (Fig. 3.6 and 3.7). For the transverse beams, cubes were tested at 7, 14 and 28 days (Fig. 3.8). For girders, the strength test was done right before the first experiment. For compressive cube strength tests, the speed of the actuator was 13.5 kN/sec and for the splitting tensile strength<sup>8</sup> tests, the speed was 1.1 kN/sec.

Since the experimental program started approximately three months after casting the deck slab and approximately nine months after casting the girders, a higher strength was used in the analysis calculations and comparison with the test results. An average of the mean strengths after 28 days till the last test was used (Fig. 3.6 and 3.7). For the deck and the transverse beams, the mean concrete compressive cylinder strength  $f_{cm}$  was taken as 65 MPa, the mean tensile strength  $f_{ctm}$  was taken as 5.41 MPa and the mean modulus of elasticity  $E_{cm}$  was calculated as 39 GPa (according to Model Code 2010 *fib* 2012). For the girders, the concrete compressive cylinder strength  $f_{cm}$  was taken as 75 MPa,  $f_{ctm}$  as 6.30 MPa and  $E_{cm}$  was 41GPa (Model Code 2010 *fib* 2012).

Table 3.4 Concrete properties of various components of the model bridge.

Component	Property	Value	Units
Deck slab (28 days) Maximum aggregate size = 20 mm	Mean compressive cube strength, $f_{cm,cube28}$	74.67	MPa
	Mean compressive cylinder strength, $f_{cm28}$	60	MPa
	Mean splitting tensile strength, $f_{csp28}$	5.40	MPa
	Modulus of elasticity, $E_{c28} - MC2010$	37.3	GPa
Transverse beams (28 days) Maximum aggregate size = 20 mm	Mean compressive cube strength, $f_{cm,cube28}$	71	MPa
	Mean compressive cylinder strength, $f_{cm28}$	57.5	MPa
	Mean value of axial tensile strength, $f_{ctm} - MC2010$	4.4	MPa
	Modulus of elasticity, $E_{c28} - MC2010$	37.18	GPa
Girders (273 days*)	Mean compressive cube strength, $f_{cm,cube}$	90	MPa
	Mean compressive cylinder strength, $f_{cm}$	75	MPa
	Mean splitting tensile strength, $f_{csp}$	6.30	MPa
	Modulus of elasticity, $E_c - MC2010$	40.26	GPa

\*The girders were made by Spanbeton. The material properties of the girders were measured in the laboratory after 273 days of casting and are considered as the mean strengths.

<sup>8</sup> The mean splitting tensile strength,  $f_{csp}$  has been taken equal to the mean tensile strength,  $f_{ctm}$  in this research. ( $f_{ctm} = A f_{csp}$ , where A = 1 in Model code 2010, section 5.1.5.1).

## Experimental Program – Design of the Test Setup

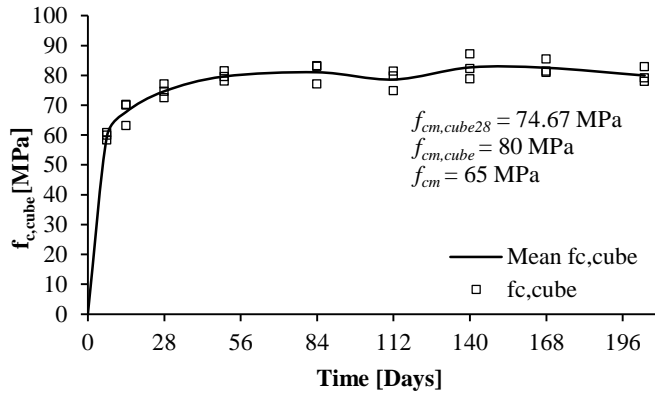


Fig. 3.6 Development of compressive cube strength of concrete in deck slab panels in time.

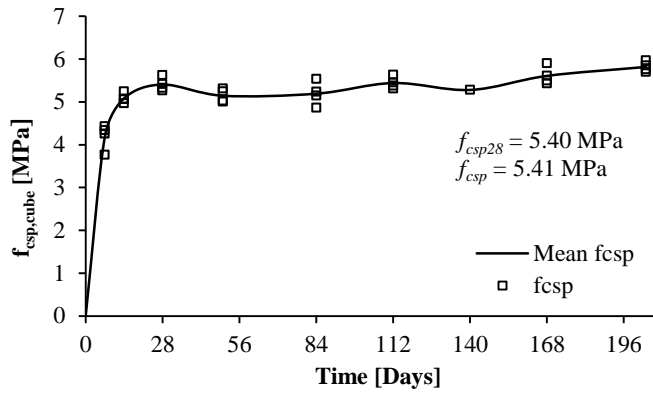


Fig. 3.7 Development of splitting tensile strength of concrete cubes in deck slab panels in time.

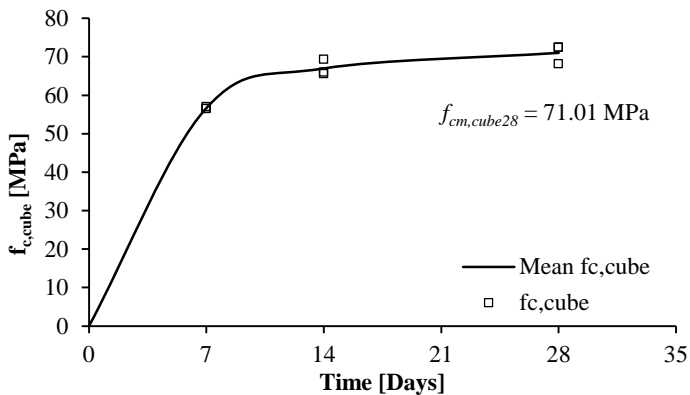


Fig. 3.8 Development of compressive cube strength of concrete in the transverse beams in time.

### 3.2.2 Prestressing and ordinary reinforcing steel

Two types of steel were used in the model bridge deck; Prestressing steel and ordinary reinforcement. The standard properties of the prestressing steel are given in Table 3.5.

Table 3.5 Standard prestressing steel properties used in the model bridge deck.

Component	Type	Property	Value	Units
Girders	Y1860S	Characteristic tensile strength, $f_{pk}$	1860	MPa
		Characteristic 0.1% proof stress, $f_{pk0.1}$	1640	MPa
		Modulus of elasticity, $E_p$	195000	MPa
Transverse beams and deck slab	Y1100H	Characteristic tensile strength, $f_{pk}$	1100	MPa
		Characteristic 0.1% proof stress, $f_{pk0.1}$	900	MPa
		Modulus of elasticity, $E_p$	205000	MPa

The girders had B500A steel for bars  $\leq 6$  mm  $\Phi$  and B500B steel for bars  $\geq 8$  mm  $\Phi$ . Table 3.6 shows the properties of the ordinary steel used in the model bridge deck slab and the transverse beams. Fig. 3.9 shows the results of the tensile strength tests carried out on the steel bar specimens according to Eurocode 2. The strain was measured by an extensometer attached to the test bar. The measuring length was 100 mm. The speed of the test was 0.01 mm/sec for specimen 1 and 0.05 mm/sec for specimen 2 and 3. The yield strength  $f_{sy}$  was defined as 0.2% proof stress and the tensile strength  $f_{su}$  was defined as the peak strength from the stress-strain curve. The modulus of elasticity  $E_s$  was computed from the slope of the curve between stress levels of 20% and 75% of the yield stress.

Table 3.6 Ordinary reinforcing steel properties used in the model bridge deck.

Component	Property	Value	Units
Deck slab and transverse beams	Mean yield strength, $f_{sy}$	525	MPa
	Mean ultimate tensile strength, $f_{su}$	580	MPa
	Modulus of elasticity, $E_s$	200000	MPa

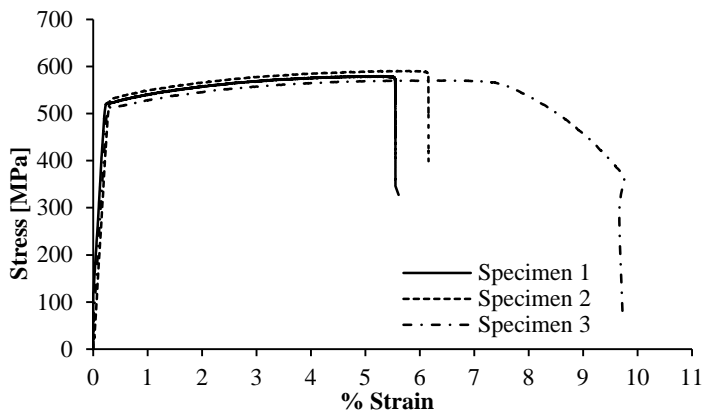


Fig. 3.9 Stress – Strain curves for steel specimens.

### 3.3 Construction of the model bridge deck in the laboratory

#### 3.3.1 Bridge deck

The girders of the model bridge deck were made by Spanbeton. The girders were transported to the laboratory approximately one month after casting. Fig. 3.10 shows the girders after placement in the laboratory. The bottom of the girders was positioned at an average height of 330 mm from the test floor. The c/c distance of the girders was 1800 mm c/c as scaled down from the real bridge dimensions.



(a)



(b)

## Experimental Program – Design of the Test Setup



(c)

*Fig. 3.10 Girders transported to the laboratory and placed in position: a) Top pictorial view; b) Temporary steel supports at each side of the girders to hold them in place; c) Girders positioned above the supports.*

The freedom of movement of the supports is depicted in Fig. 3.2. Generally, the support assembly consisted of 350×280×45 mm rubber bearing pads, 20 mm thick steel plates, a hinge and Teflon sheets, however, the freedom of movement in various directions was achieved by alternating the assembly and ending up in three different types of supports as shown in Fig. 3.11. The test report of the compression test carried out on the rubber bearings is given in the Stevin Report No. 25.5.13-06 (2013) and shows adequate compressive stiffness.



(a)



(b)



(c)

*Fig. 3.11 Supports of the girders: a) Fixed support; b) Free in two directions; c) Free in one direction. Refer to Fig. 3.2 for the location of these supports with regard to the girders.*

### 3.3.2 Transverse beams

#### Formwork

After the girders were supported and held in place, formwork (Fig. 3.12a) for the two transverse beams (810×350 mm) was put in position on each side of the deck (north and south). Ordinary reinforcement and plastic duct tubes for the prestressing bars were placed as shown in Fig. 3.12b. Rubber rings were put outside each duct opening to avoid passage of concrete inside. 350×100×15 mm steel anchor plates were provided for the prestressing bars on both sides of the two transverse beams as shown in Fig. 3.13.



(a)



(b)

Fig. 3.12 Transverse beam (North side): a) Formwork ready for casting; b) With reinforcement.



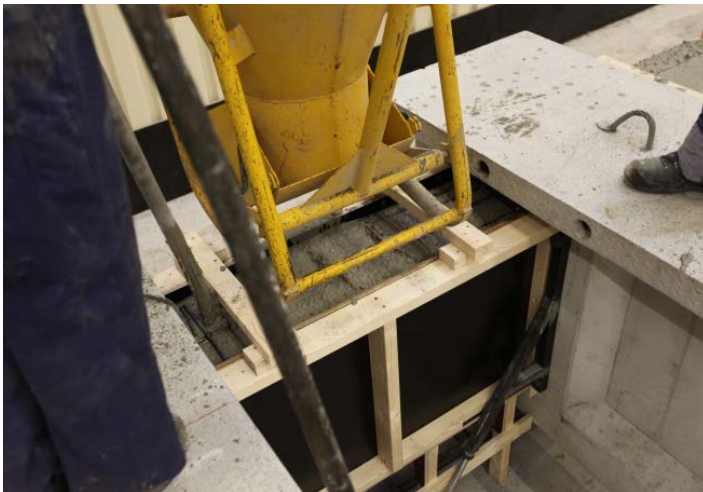
(a)

(b)

Fig. 3.13 Anchor plates for prestressing bars: (a) On active side; and (b) On passive side.

### Casting and curing

The transverse beams were covered with plastic sheets soon after casting (Fig. 3.14). The formwork was removed one week after casting of the concrete and the beams were prestressed to 1 MPa initially. Later it was increased to a level equal to that of the transverse prestressing of the deck slab.



(a)



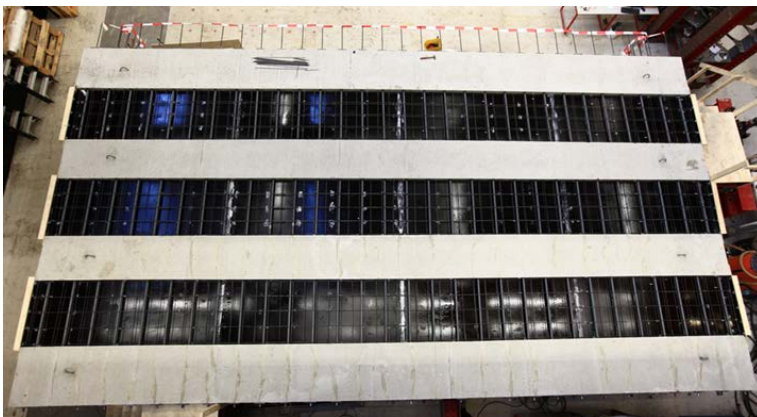
(b)

Fig. 3.14 The transverse beam (North side): a) Casting; b) Covered with plastic sheets.

### 3.3.3 Deck slab panels

#### Formwork

After casting the cross beams, the wooden formwork and the reinforcement for the deck slab panels were put in place as shown in the Fig. 3.15a. A 40 mm plastic tubing wound with a plastic wire was inserted in each duct and the prestressing bar was put inside it (Fig. 3.15b) and steel anchor plates were screwed on both sides of the deck along the exterior girder flanges (Fig. 3.15c). Wooden panels supported by wooden supports/planks were put in between the girders for casting of the concrete (Fig. 3.15d).



(a)

## Experimental Program – Design of the Test Setup

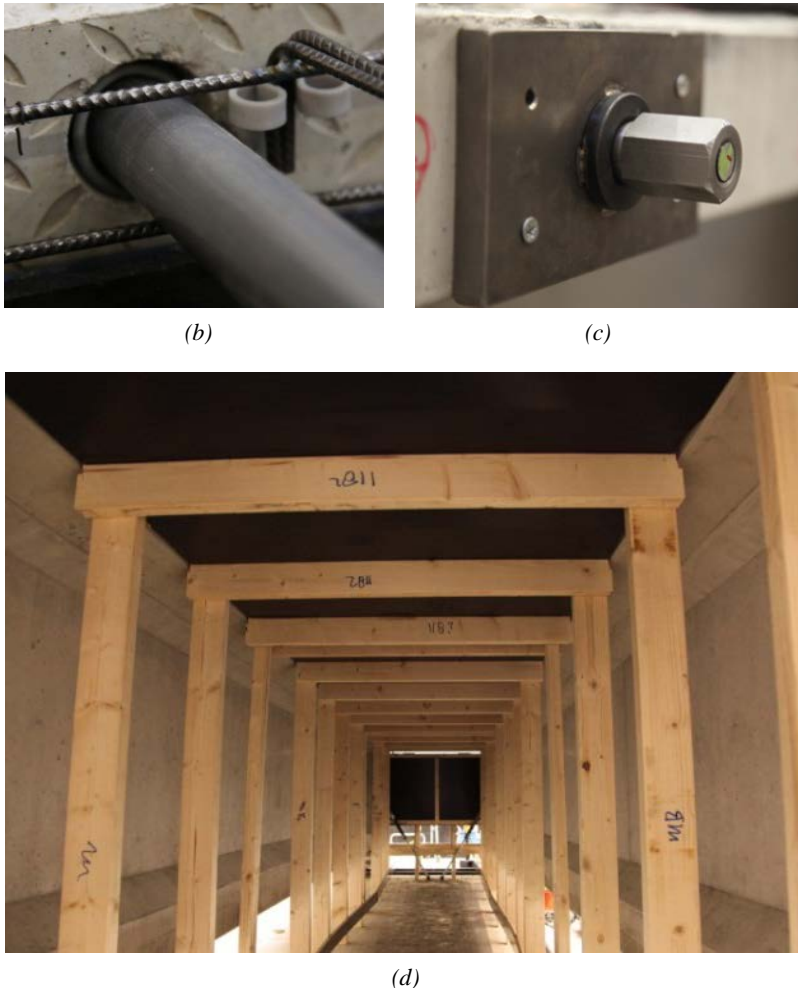


*Fig. 3.15 Deck slab: a) Top view of the deck slab panels ready for casting; b) Plastic tube inside the duct; c) Steel anchor plates; d) Bottom side of the deck slab panel showing the formwork.*

### **Casting and curing**

The concrete was cast as soon as the formwork was ready (Fig. 3.16b). The freshly cast concrete was covered by plastic sheets for 14 days. No grouting was done, hence the prestressing bars were unbonded.

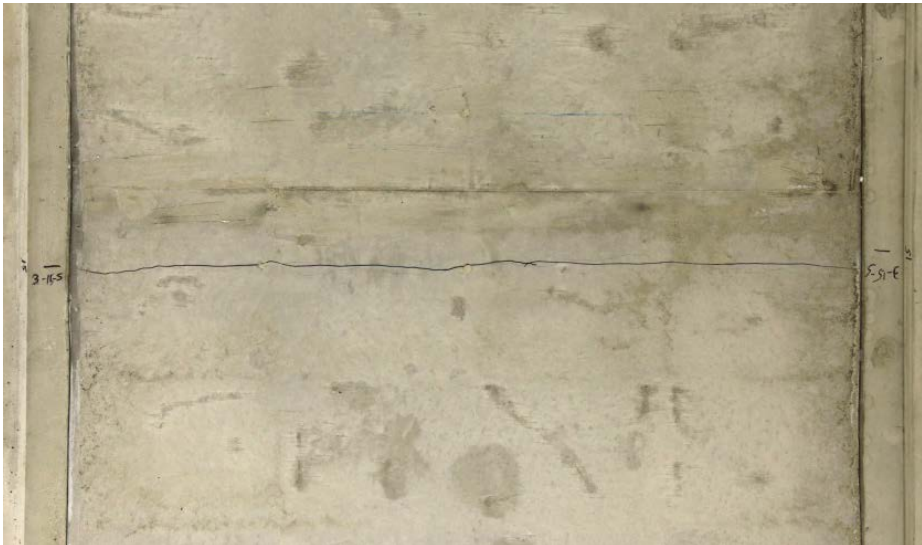
Although temperature and shrinkage reinforcement was provided in the bridge deck, soon after prestressing, shrinkage cracks appeared in the transverse direction along some of the duct lines and were observed and marked on both the top and bottom sides of the deck slab (Fig. 3.16a). The maximum crack width observed for the shrinkage cracks was less than 0.2

## Experimental Program – Design of the Test Setup

mm and therefore it was assumed that these cracks would not have an influence on the bearing capacity of the bridge deck later during the tests.



(a)



(b)

*Fig. 3.16 Deck slab: a) Casting of concrete; b) Shrinkage crack in the transverse direction.*

### 3.3.4 Post tensioning the model bridge deck

After 28 days, the formwork was removed and the transverse bars in the deck slab were post-tensioned according to the desired transverse prestressing level (2.5 MPa for initial tests). The prestressing level was monitored throughout the experimental phase to record any losses that would occur over the passage of time. Fig. 3.17 shows the model bridge deck after completion in the Stevin II laboratory.



*Fig. 3.17 Model bridge deck after completion.*

#### **Schedule and sequence**

One of the main reasons to keep the prestressing bars unbonded in the deck slab and the transverse beams was to be able to change the transverse prestressing level (TPL) during the experimentation. It was important to keep the prestressing level in the deck slab and the transverse beams as uniform as possible to avoid non-uniform stresses hence a particular sequence was followed to impart the prestressing equally and uniformly in the transverse direction along the length of the bridge deck.

The deck slab was prestressed first to a level of 2.5 MPa (TPL of initial tests), starting from the middle of the deck, post-tensioning alternating bars of the northern half of the deck and then switching to the southern half. After post-tensioning of alternating bars of the southern half, the remaining bars were also post-tensioned starting from the middle of the deck and



## 3.4 Experimental program and test setup

The experimental phase began as soon as the post-tensioning was completed in the bridge deck. The following sections explain the test setup in detail. Main components of the setup are the load assembly and the instrumentation.

### 3.4.1 Load assembly

Static tests were performed by using an electro-hydraulic actuator system. A typical arrangement of the load assembly is as shown in Fig. 3.19. A concentrated load simulating a wheel load was applied by the hydraulic actuator attached to an overhead reaction frame bolted to the test floor.



*Fig. 3.19 The typical load assembly.*

After each test, the test frame and the actuator were moved to the next load position. The applied load and the displacement were measured by the actuator through a built-in load cell with a capacity of 2000 kN and a built-in LVDT. In all the tests, the concentrated load was applied through a 200×200 mm, 8 mm thick rubber pad bonded to a 200×200×20 mm steel plate. The rubber pad was tested previously and its compressive stiffness was found to be satisfactory as shown in the detailed Stevin Report No. 25.5.13-06 (2013).

### Single and double loads

Two types of loads were applied to the system: a single load and a double load (Fig. 3.20). The double load was according to the Eurocode (NEN-EN 1991-2:2003) load configuration (Fig. 3.21) and consisted of two point loads placed at a distance of 0.6 m c/c, scaled down from 1.20 m c/c. An HEM-300 beam was used to transmit the load from the actuator to the

## Experimental Program – Design of the Test Setup

two loading plates. Both types of loads were applied at midspan and close to the girder flange-slab interface.

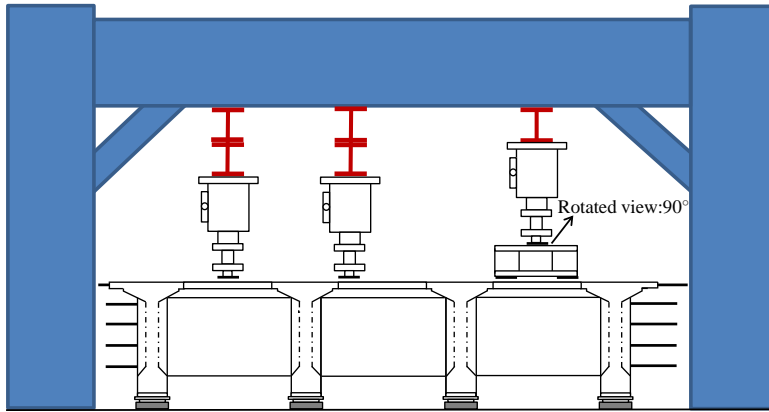


Fig. 3.20 Single and double loads (not drawn to scale).

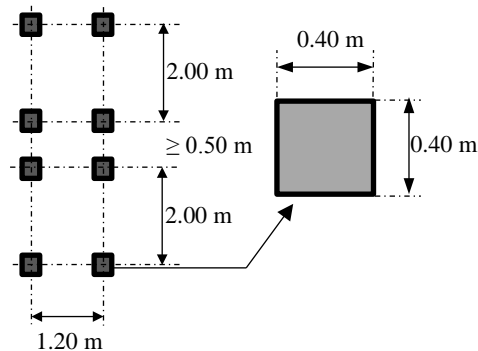


Fig. 3.21 Eurocode load configuration and wheel print (Load model 1, NEN-EN 1991-2:2003).

To refer to the load configuration and results of the test program the following abbreviations are used:

- Single point load acting at mid span of slab panel, P1M.
- Single point load acting close to the girder flange-slab interface/joint, P1J.
- Double point loads at 600 mm c/c acting at mid span of slab panel, P2M.
- Double point loads at 600 mm c/c acting close to the girder flange-slab interface/joint, P2J.
- Notations: M = Midspan, J = Joint/Interface, ST = Straight joint, SK = Skewed joint, AD = Above the duct, BD = In-between the ducts.

### 3.4.2 Instrumentation

The instrumentation of the test setup was done to make sure that all important parameters could be observed and the measurements could be used later in the analysis. Around 80 channels (0-79) of the data acquisition system were used for the measurements. The instrumentation varied slightly during the experimental phase but the generally used configuration of the channels is given in Table 3.8. The results obtained from the data acquisition system were immediately transferred to Microsoft Excel (2010) and later analyzed by MATLAB (2012) program.

Table 3.8 The general instrument measurements as recorded by the data acquisition system.

Instrument	Measurement	Instrument	Measurement
Actuator F	Applied Force*	Laser01	Deflection support 1
Actuator S	Displacement*	Laser02	Deflection support 2
LVDT01	Joint horizontal top	Laser03	Deflection support 3
LVDT02	Joint horizontal top	Laser04	Deflection support 4
LVDT03	Joint horizontal top	Laser05	Deflection support 5
LVDT04	Joint horizontal top	Laser06	Deflection support 6
LVDT05	Joint horizontal bottom	Laser07	Deflection support 7
LVDT06	Joint horizontal bottom	Laser08	Deflection support 8
LVDT07	Joint horizontal bottom	Laser09	Bending girder 1
LVDT08	Joint horizontal bottom	Laser10	Bending girder 2
LVDT09	Vertical Joint East	Laser11	Bending girder 3
LVDT10	Vertical Joint West	Laser12	Bending girder 4
LVDT11	Horizontal Deck East	Laser13	Deck vertical
LVDT12	Horizontal Deck West	Laser14	Deck vertical
LVDT13	Horizontal beam 4	Load Cell FR01-08	Reaction forces
LVDT14	Horizontal beam 4	Load Cell FP01-30	Prestress 01-30**
LVDT15	Deck vertical	Load Cell FP31-46	Prestress 31-46***
LVDT16	Deck vertical		

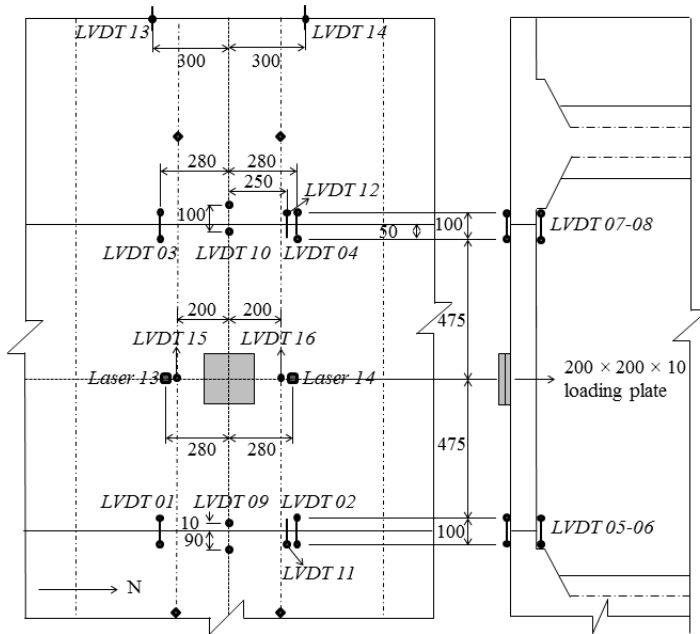
\* Hydraulic Actuator with built in LVDT.

\*\* Prestressing force in the deck slab bars.

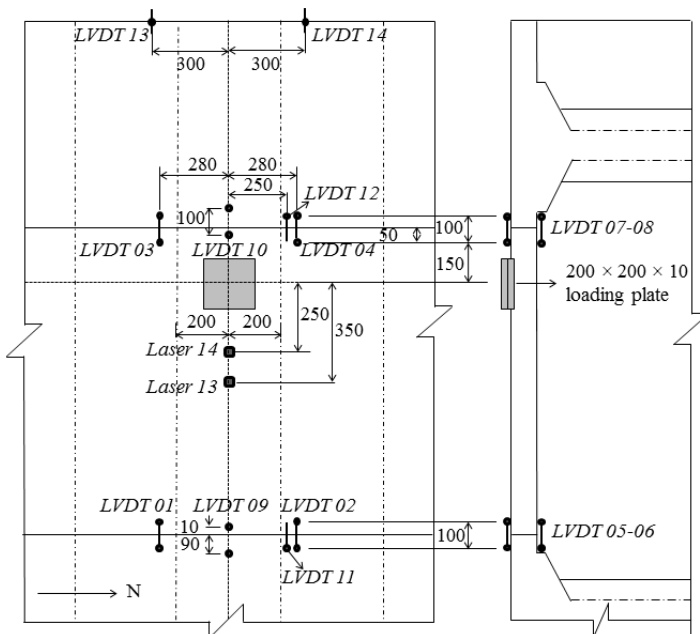
\*\*\* Prestressing force in the transverse beam bars.

Fig. 3.22 shows the instruments installed for the laboratory experiments. The position of the various instruments placed around the loading point depended on the type of the test being performed. Where the instrumentation was varied, this is mentioned in the respective test report in the Stevin Report No. 25.5.13-06 (2013).

## Experimental Program – Design of the Test Setup

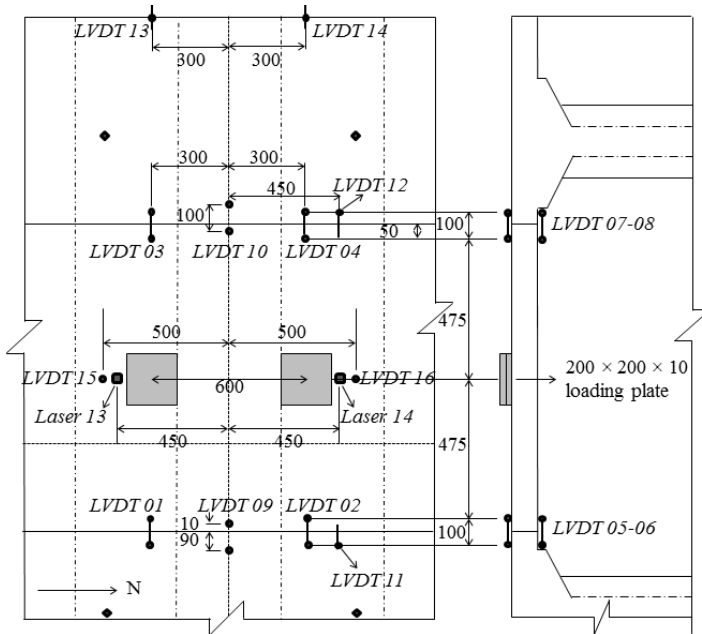


(a)

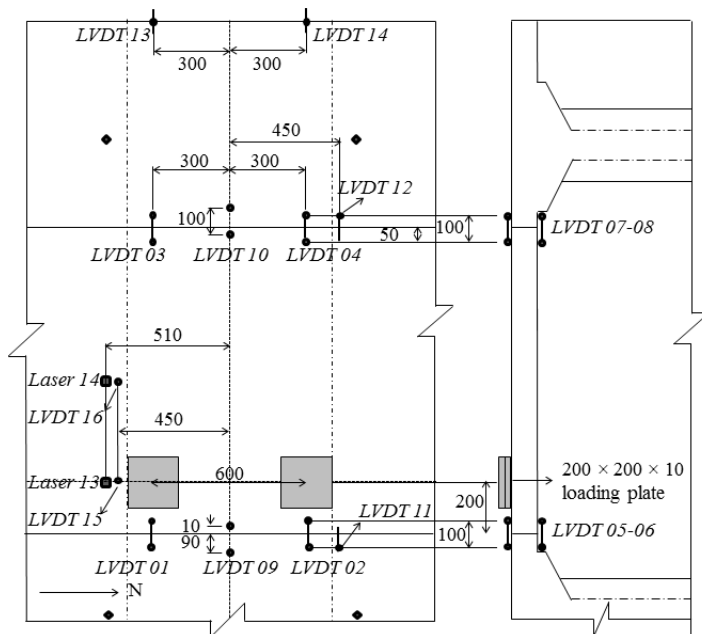


(b)

## Experimental Program – Design of the Test Setup



(c)

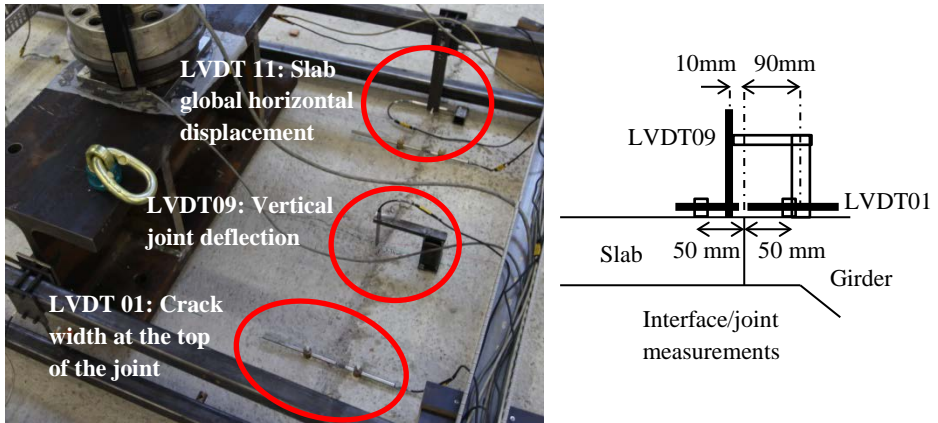


(d)

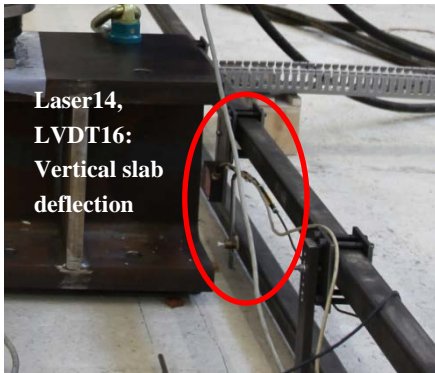
Fig. 3.22 Typical instrumentation of the top and the bottom side of the deck slab: a) P1M, single load at midspan; b) P1J, single load close to the interface; c) P2M, double load at midspan; d) P2J, double load close to the interface. Note: Figure is not drawn to scale. All dimensions are in mm.

### 3.4.3 Measurements

The measurements conducted by the various instruments in the experiments are shown in Fig. 3.23 and are explained in the following sections.



(a)



(b)



(c)



(d)

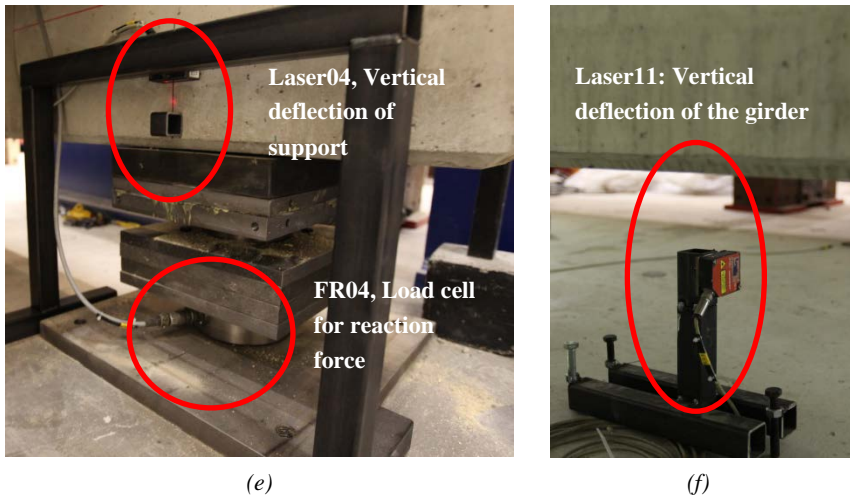


Fig. 3.23 Measurements conducted by various instruments: a) Slab global horizontal displacement, vertical joint deflection and crack width at the top of the deck slab; b) Midspan deflections; c) Horizontal displacement of the deck; d) Horizontal displacement (strain) at the bottom of the deck slab; e) Instrumentation for support; f) Vertical deflection of the girders.

## Applied load

The applied load was measured by a load cell attached to the hydraulic actuator (Fig. 3.19) and monitored by the data acquisition system. As explained before the vertical deflection under the load was also measured by the built-in LVDT.

## Midspan and interface deflections

The deflection measured by the actuator LVDT had errors arising from the deflections occurring globally in the test-setup. Therefore, it was deemed necessary to have an alternate arrangement as well to determine the deflections. Lasers 13-14 and LVDTs 15-16 were used at midspan (Fig. 3.23b) and also close to the interface when a single load or when a double load was applied at that respective position.

## Horizontal and vertical displacements

### Horizontal displacements

Reference is made to Fig. 3.23a. LVDTs 1-4 were used to measure the horizontal displacements of the slab-girder joint around the load position on the top side of the deck slab. This would lead to recording crack widths occurring on the top side at the joints. LVDTs 5-8 in Fig. 3.23d were used to measure the horizontal displacements of the slab-girder joint around the load position on the bottom side of the deck slab. This would lead to

## Experimental Program – Design of the Test Setup

recording the compressive strain occurring at the joint assuming that the strain remains constant within the measuring length of the LVDTs. LVDTs 11-12 in Fig. 3.23a were used to measure global horizontal displacements of the top side of the deck around the loading position near the slab-girder joint. *In some tests, lasers (15-16) were also used for this purpose.* LVDTs 13-14 were used to measure horizontal displacements of the exterior girder 4 flange right across the load position. *In some tests, lasers (17-18) were also used for this purpose* (Fig. 3.23c).

### Vertical displacements

Lasers 1-8 were used to measure vertical displacements of the supports of the four girders at each end (Fig. 3.23e). Lasers 9-12 were used to measure the vertical deflections of the girders across the load and sometimes at midspan (Fig. 3.23f). LVDTs 9-10 were used to measure the relative vertical deflections of the slab-girder joints across the single load or the midpoint of the double loads (Fig. 3.23a).

### **Support reactions and prestressing forces**

Reference is made to Fig. 3.23 (e). Load cells FR 1-8 were used to measure the vertical support reaction forces. Load cells FR 1-30 were used to measure the force in the prestressing bars in the deck slab bars and the load cells FP 31-46 were used to measure the forces in the prestressing bars in the two transverse beams.

### **Crack pattern**

A bright light source system was installed under the specimen. The cracks were marked manually and measured by a crack width card at various load intervals. A Canon EOS 5D Mark II camera was used to photograph the cracks.

## **3.5 Conclusions**

In this chapter, the design and construction of the 1:2 scaled model bridge has been briefly described and an overview of the experimental program and the test setup has been given in detail. For the individual test setup and instrumentation, reference is made to Stevin Report No. 25.5.13-06 (2013) by the author.

# **CHAPTER 4**

## **Experimental Results**

This chapter includes a summary of the results of the experimental program conducted on the 1:2 scaled bridge model constructed in the laboratory for the experimental part of this research. Typical test reports are also included.

## 4.1 Introduction

Previously, the design and construction of the experimental setup has been explained in detail. The actual testing program started 97 days after casting the deck slab panels. Nineteen static tests were performed in total to investigate the bearing capacity of the model bridge deck and the results are explained in the following sections.

### 4.1.1 Testing sequence

Table 4.1 gives the test configuration and sequence. Tests were performed at midspan (M) of the deck slab panel and close to the girder-flange-deck slab interface (J). A single load (P1M and P1J) and a double load (P2M and P2J) were applied. Both exterior (A and C) and interior (B) deck slab panels were tested at various positions along the length of the deck. Tests were mostly performed by placing the center of the loading plate in-between the transverse prestressing ducts (BD), however, a few tests were carried out with the load just above a duct (AD). The size of the loading plate was 200×200 mm in all the tests except in test BB19 where a 115×150 mm loading plate was used. The transverse prestressing level (TPL) used was 2.5, 1.25 and 0.5 MPa. The test positions are shown in Fig. 4.1 and the numbers are marked according to the sequence of the tests performed. Refer to the section 3.2.1 for the development of the concrete strength with respect to the time.

Table 4.1 Test configuration and test sequence.

#	Test	Test date	Panel	Offset from north end of the deck	Load type	TPL	Joint	Designation
		dd/mm/yy		[mm]	[kN]	[MPa]		
1	BB1	5/2/13	C-Midspan	800	Single (BD)	2.5	Straight	C-P1M-ST
2	BB2	8/2/13	A-Midspan	800	Single (BD)	2.5	Skewed	A-P1M-SK
3	BB3	14/2/13	A-Interface	2400	Single (BD)	2.5	Skewed	A-P1J-SK
4	BB4	19/2/13	C-Interface	2400	Single (BD)	2.5	Straight	C-P1J-ST
5	BB5	25/2/13	C-Midspan	3100	Double (BD)	2.5	Straight	C-P2M-ST
6	BB6	5/3/13	A-Interface	3100	Double (BD)	2.5	Skewed	A-P2J-SK
7	BB7	8/3/13	C-Midspan	5400	Single (BD)	2.5	Straight	C-P1M-ST
8	BB8	14/3/13	C-Midspan	11200	Single (BD)	1.25	Straight	C-P1M-ST
9	BB9	18/3/13	A-Midspan	11200	Single (BD)	1.25	Skewed	A-P1M-SK
10	BB10	22/3/13	A-Interface	9600	Single (BD)	1.25	Skewed	A-P1J-SK
11	BB11	27/3/13	C-Midspan	9600	Double (BD)	1.25	Straight	C-P2M-ST
12	BB12	5/4/13	A-Interface	8200	Double (BD)	1.25	Skewed	A-P2J-SK
13	BB13	10/4/13	C-Midspan	8200	Single (AD)	1.25	Straight	C-P1M-ST
14	BB14	15/4/13	C-Interface	6600	Single (AD)	1.25	Straight	A-P1J-ST
15	BB15	17/4/13	A-Midspan	6600	Single (AD)	1.25	Skewed	A-P1M-SK
16	BB16	6/5/13	B-Midspan	6600	Double (BD)	2.5	Skewed	B-P2M-SK
17	BB19*	12/6/13	B-Midspan	3600	Single (BD)	2.5	Skewed	B-P1M-SK <sup>a</sup>
18	BB21	26/6/13	B-Midspan	800	Single (BD)	0.5	Skewed	B-P1M-SK
19	BB22	3/7/13	B-Midspan	5000	Single (BD)	0.5	Skewed	B-P1M-SK

\* Size of the loading plate = 115×150 mm.

## Experimental Results

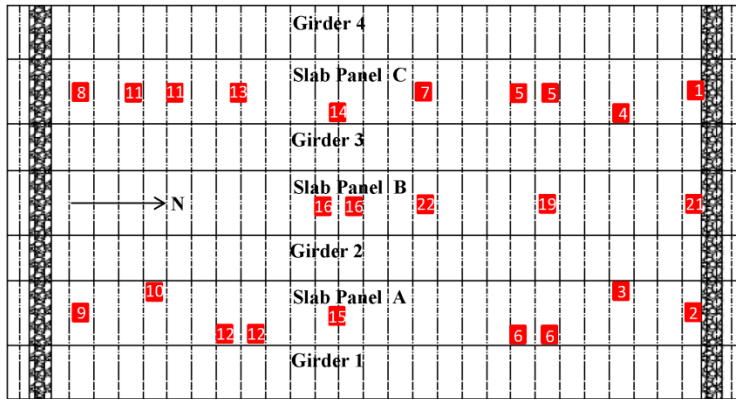


Fig. 4.1 Deck slab load positions highlighted. Duct positions are also labelled.

## 4.2 Description of typical tests

Individual test reports were made for each experiment conducted in the laboratory. A slide show with the cracking pattern being developed during the loading history was also prepared in Microsoft Powerpoint (2012) for each test. Here, four typical test are reported to give a general idea how the tests were performed. The remaining test reports are presented in detail by the author in the Stevin Report No. 25.5.13-06 (2013). The tests presented are BB10, BB15, BB16 and BB6.

### 4.2.1 Important test parameters

- **BB15:** Single load acting at midspan of the deck slab panel A and performed above the duct. TPL is 1.25 MPa.
- **BB10:** Single load acting close to the girder 2 flange - deck slab A interface (200 mm c/c) and performed in-between the ducts. TPL is 1.25 MPa.
- **BB16:** Double load acting at midspan of the deck slab panel B and performed in-between the ducts. TPL is 2.5 MPa.
- **BB6:** Double load acting close to the girder 1 flange - deck slab A interface (200 mm c/c) and performed in-between the ducts. TPL is 2.5 MPa.

### 4.2.2 Load application

In all the tests, the load was applied in increments @ 1 kN/sec. Generally a 25 kN increment was applied in the single load tests and a 50 kN in double load tests. Close to the expected failure, the actuator was switched to displacement control at 0.01 mm/sec till failure. Fig. 4.2 shows the individual load setups for the selected test cases.

## Experimental Results

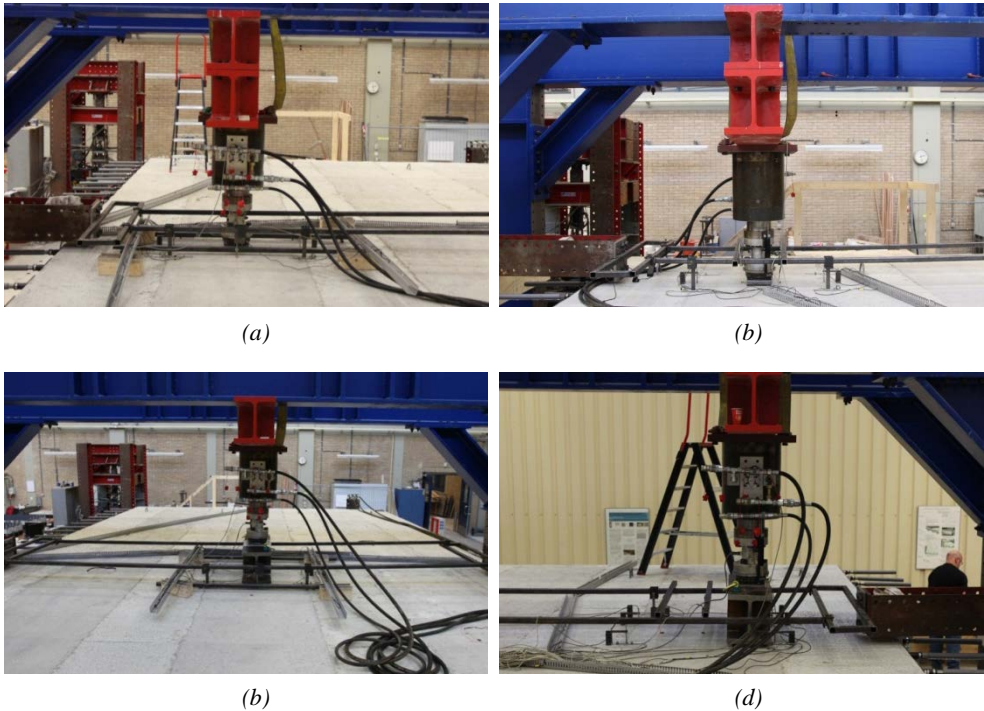
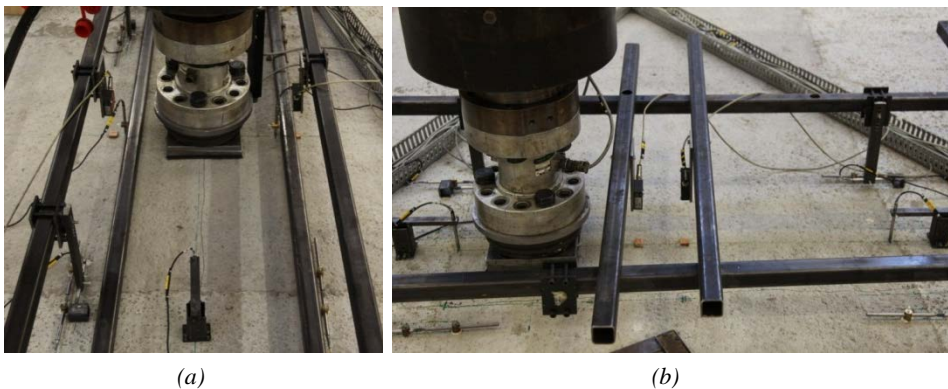


Fig. 4.2 Load setup: a) BB15 (P1M); b) BB10 (P1J); c) BB16 (P2M); d) BB6 (P2J).

### 4.2.3 Instrumentation

Fig. 4.3 shows the instrumentation used on the top side of the deck slab panel for the selected test cases. Section 3.4.2 explains the instrumentation in detail and gives the function of various instruments used.



## Experimental Results



Fig. 4.3 Instrumentation of the top side of the deck slab: a) BB15 (P1M); b) BB10 (P1J); c) BB16 (P2M); d) BB6 (P2J).

### 4.2.4 Test observations

Typical test observations are shown in Table 4.2 for selected test cases.

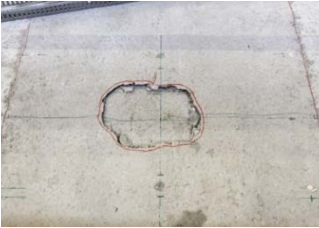
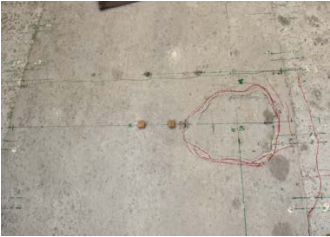
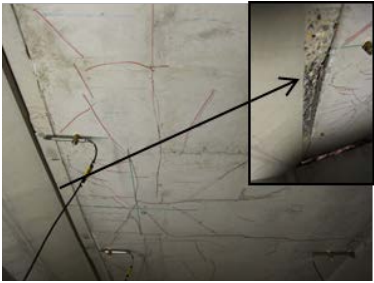
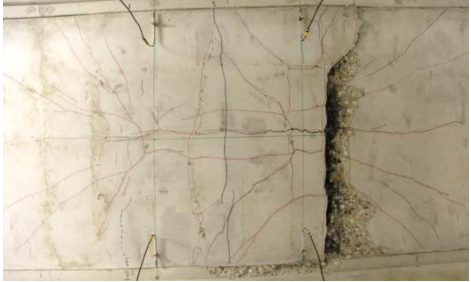
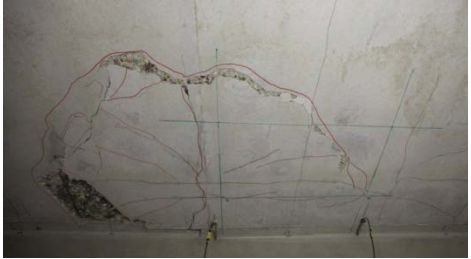
- Failure always occurred by punching, either by brittle punching (stiff load-deflection response) or by flexural punching (ductile load-deflection response).
- The concrete plug was pushed through the deck slab in a sudden and explosive manner. The part remained attached to the deck itself because of the reinforcement present as well as the joint with the interface.
- A square hole was left on the top of the slab having a size slightly larger than the loading plate.
- An increase in the prestressing force in the deck slab bars surrounding the loading point was observed for flexural punching failures in Test BB15 and BB16. For brittle punching failures in Test BB10 and BB6, there was a negligible increase in the prestressing force.

Note: Most of the single load tests at the midspan (P1M) showed brittle punching failures with negligible increase in the prestressing force. Only exceptions to this were the tests done above a transverse prestressing duct (BB15 and BB13) and tests done with a very low level of transverse prestressing (0.5 MPa). These tests showed a significant increase in the prestressing forces and failed in flexural punching shear (ductile load-deflection behavior). Hwang et al. (2010) have also reported a change in the failure mode from brittle punching of a fully prestressed deck slab to flexural punching when the prestressing level was changed to 0 MPa in the same deck. In the present experiments, flexural punching failures (with large increase in the prestressing forces of the surrounding bars) were also observed in the double load tests done at midspan in the current tests. All single and double load tests carried out close to the interface (P1J and P2J respectively) showed brittle punching failures.

### 4.2.5 Cracking pattern

The cracking pattern observed for the selected test cases is shown in Table 4.2. The development of cracks for individual test cases is discussed in detail in section 4.3.

Table 4.2 Punching shear failures for the selected test cases.

Test	Top side of the deck slab	Bottom side of the deck slab
BB15 ↓ N		
BB10 ↓ N		
BB16 → N		
BB6 ← N		

## 4.2.6 Test results

### Load – Deflection behavior

Fig. 4.4 shows the load – deflection behavior of the deck slab panel for the selected test cases. The net deflection has been obtained by subtracting the error arising from the deflections of the adjacent supports and girders from the gross average deflection of laser 13 & 14. In test BB15, failure occurred at 359.7 kN under a deflection of 13.96 mm. LVDT 15 & 16 went out of range after achieving 10 mm deflection. In test BB10, the maximum net deflection of the laser 14 (placed transversely at 250 mm from the loading plate) was 3.99 mm at the peak load of 340.3 kN. For BB 16, the maximum average deflection of laser 13 & 14 (placed longitudinally next to the loading plates) was 9.97 mm at the peak load of 553.4 kN. For BB6, the ultimate load was 576.82 and the deflection of laser 13 at the slab midspan was 5.90 mm.

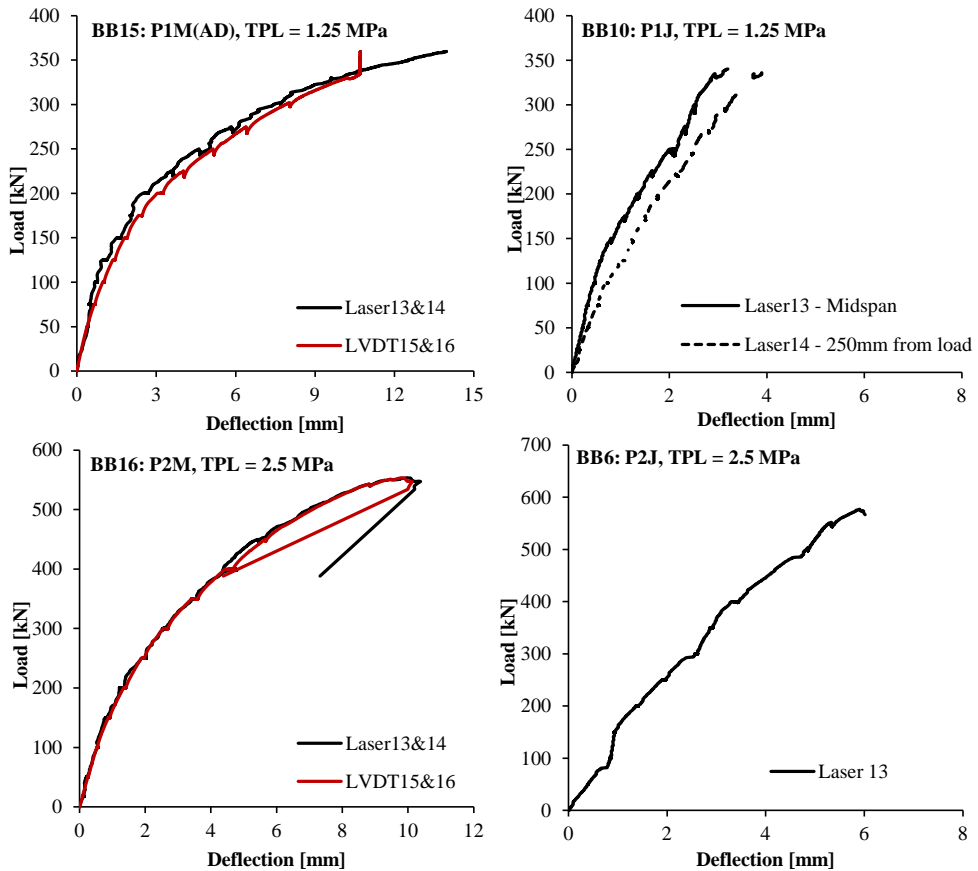


Fig. 4.4 Load – deflection response of the deck slab for selected test cases.

**Load – Crack width at the top of the deck slab panel near the interface**

Fig. 4.5 shows increasing crack widths at the top of the slab-girder joint under an increasing load. The crack width corresponds to LVDT 1 and 2 at the eastern end and LVDT 3 and 4 at the western end of the top of the deck slab. BB15 developed a maximum crack width of 2.57 mm at the peak load. A crack width of 0.38 mm at the peak load was observed for BB10. In test BB16, a maximum crack width of 1.56 mm was observed at the peak load and in test BB6, loaded close to the eastern side of the deck slab panel, LVDT 1 and 2 showed a maximum crack width of 0.74 mm and LVDT 3 and 4 showed a maximum crack width of 0.40 mm at the peak load.

*Note: In test BB10, LVDT 3 at the south-west corner showed different behavior as compared to the other LVDTs which was probably due to the initiation of a shear crack at the girder flange, however, failure still occurred in the span of the slab (the concrete cover to the girder flange stirrups at that location was found to be very small).*

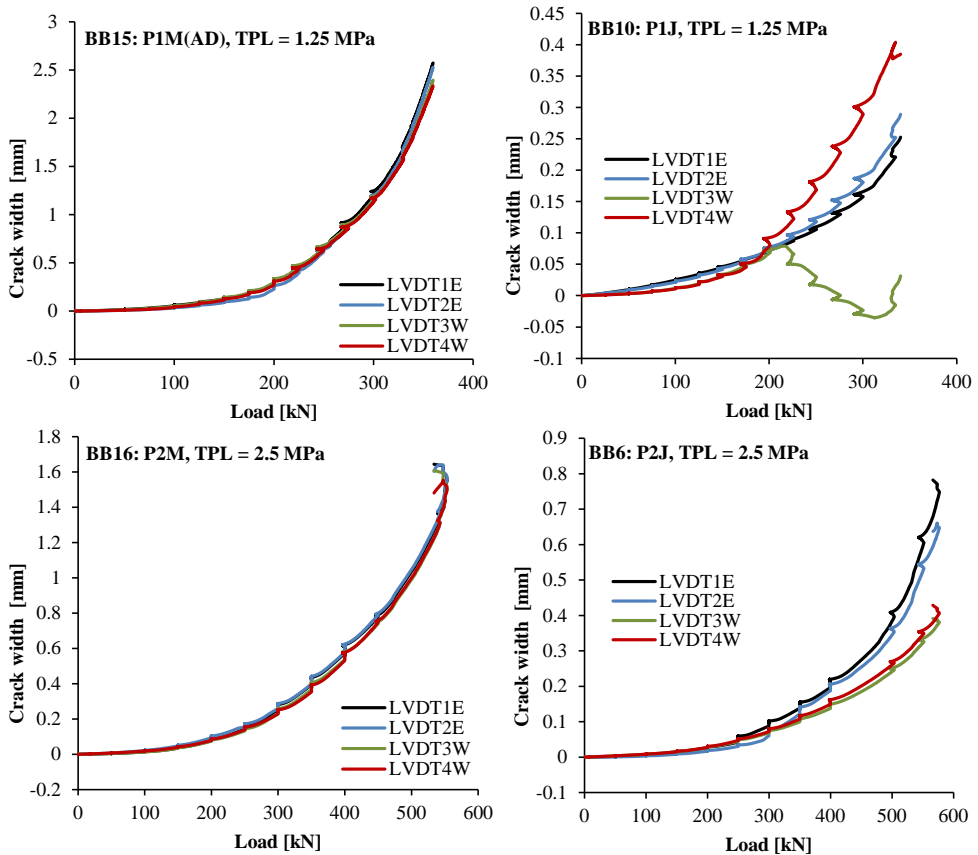


Fig. 4.5 Crack width at the top of the deck slab panel near the interface for selected test cases.

**Load – Strain at the bottom of the deck slab near the interface**

Fig. 4.6 shows increasing compressive displacements under an increasing load. Under the vertical loads, LVDT 5 and 6 at the eastern end and LVDT 7 and 8 at the western end of the bottom side of the deck slab showed that the bottom corners of the deck slab were under compression. The measuring length of the LVDT's was 100 mm giving an average compressive strain assuming that this strain remains constant over the measuring length. In test BB15, the maximum compressive displacement was 0.589 mm, giving a maximum strain of 0.00589 ( $0.589/100 = 0.00589$ ). Similarly, the maximum compressive strain for test BB10, BB16 and BB6 can be calculated as 0.00195, 0.00264 and 0.0027 respectively.

*Note: LVDT 7 and 8 in test BB15, LVDT 5 in test BB16 and LVDT 6 in test BB6 were disturbed close to failure. In test BB10, LVDT 7 at the south west corner showed a different behavior as compared to rest of the LVDTs which was probably due the initiation of a shear crack at the girder flange. This is also depicted by LVDT 3 at the top of the deck slab (Fig. 4.5).*

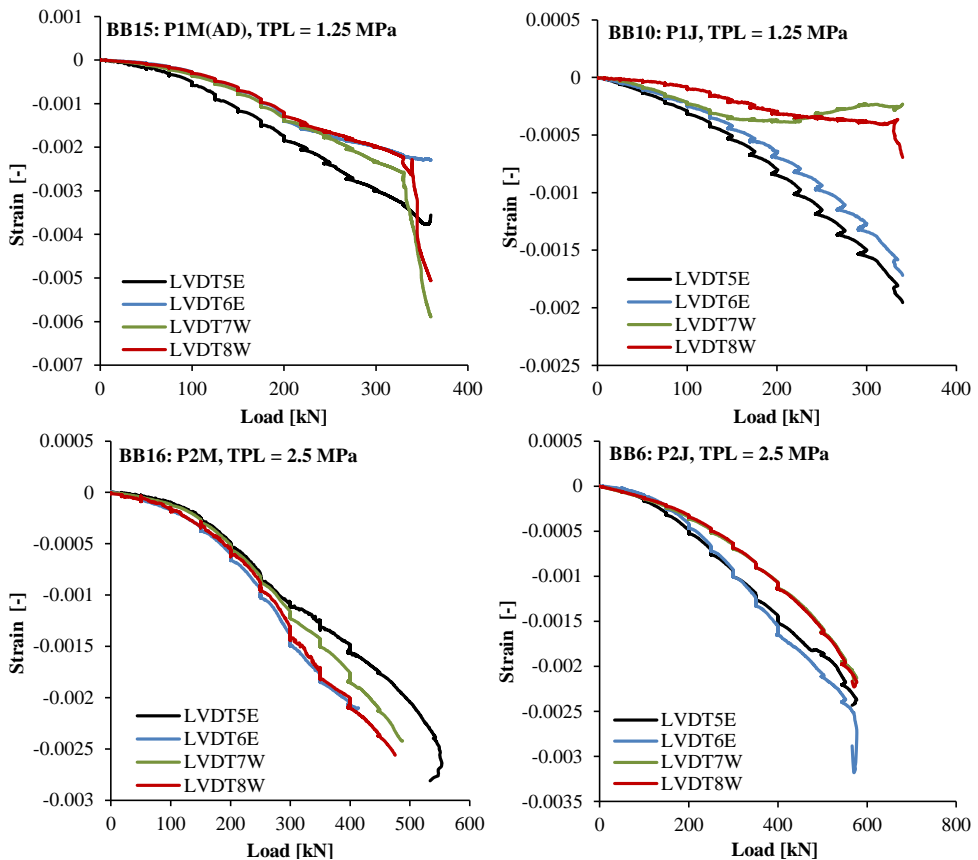


Fig. 4.6 Strain at the bottom of the deck slab near the interface for selected test cases.

### Load – Global horizontal displacement

Fig. 4.7 shows the transverse displacements of the deck slab by LVDT 11 in the eastern direction and LVDT 12 in the western direction. For test BB15, the horizontal displacement at the peak was 2.71 mm outwards (positive) in the eastern direction. In the western direction, the horizontal displacement at the peak load was 0.02 mm outwards (positive). In test BB10, the horizontal displacement occurred first in the inwards direction (negative) but at peak load, it changed to 0.144 mm outwards (positive). In the eastern direction, an outward displacement was observed with a maximum value of 0.14 mm at the peak load. In test BB16, the horizontal displacement at the peak load was 0.49 mm outwards in the eastern direction and 0.48 mm outwards in the western direction. Similarly, in test BB6, the horizontal displacement at the peak load was 0.16 mm inwards in the eastern direction and 1.87 mm outwards (measured by lasers) in the western direction. It was observed that generally the rate of change of horizontal displacements increased after the initial cracking of the slab.

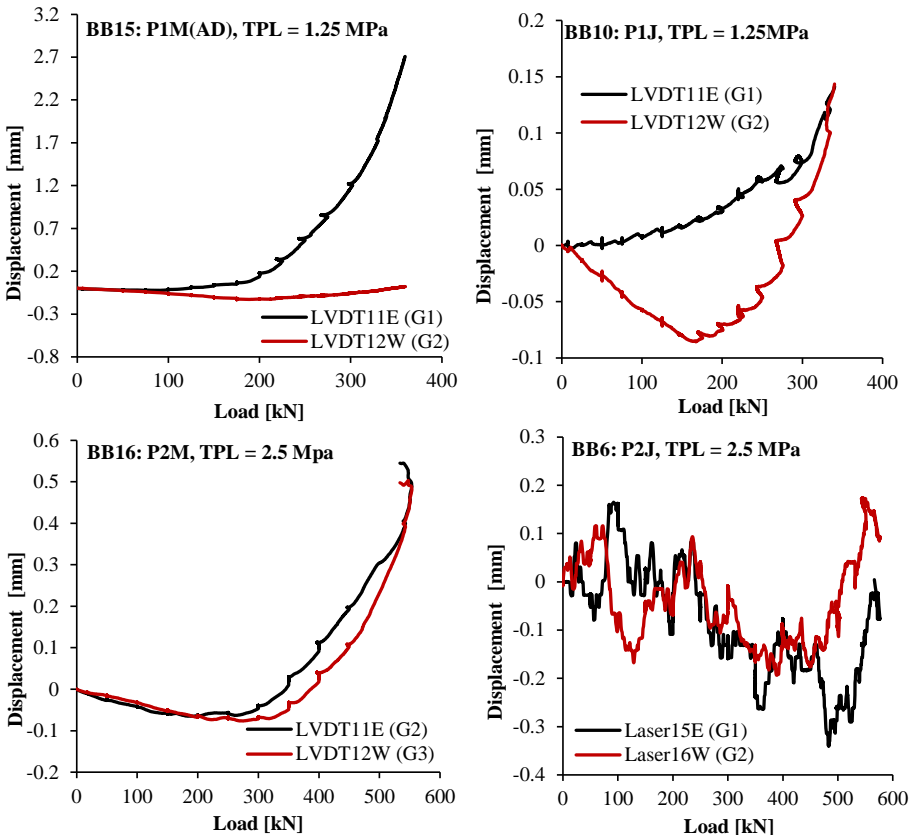


Fig. 4.7 Slab global horizontal displacements in the transverse direction for selected test cases.

**Load – Relative vertical deflection of the slab-girder joint**

Fig. 4.8 shows relative vertical deflections of the slab-girder joint measured by LVDT 9 at the eastern edge and LVDT 10 at the western edge. Test BB15 showed a maximum deflection of 1.90 mm of the eastern joint and 1.34 mm of the western joint at the peak load. In test BB10, the maximum deflection of the eastern joint was 0.123 mm and that of the western joint was 0.30 mm which later reduced to 0.243 mm at the peak load. In test BB16, at the eastern side, a maximum deflection of 1.05 mm and at the western side, a maximum deflection of 0.918 mm was observed at the peak load. In BB6, LVDT 9 and 10 at the eastern side showed a maximum deflection of 1.19 mm at the peak load and LVDT 11 and 12 at the western side showed a maximum deflection of 2.27 mm at the peak load.

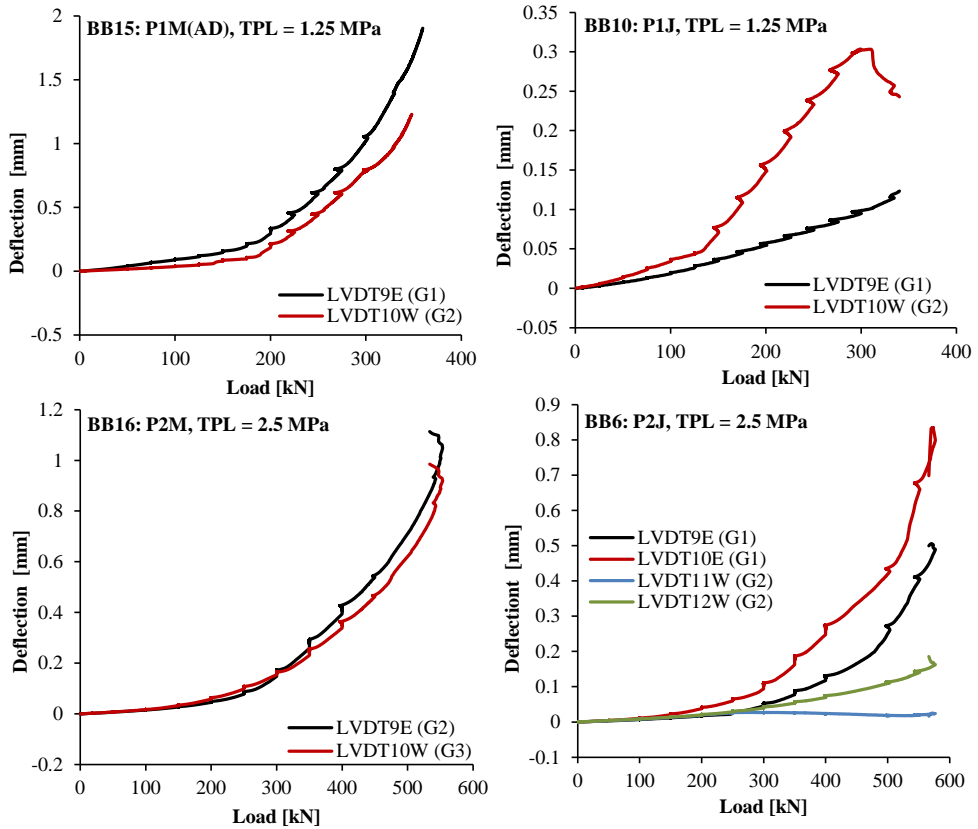


Fig. 4.8 Relative vertical deflections of the deck slab-girder flange interface/joint for selected test cases.

## Experimental Results

### Load – Prestressing force in the surrounding bars

The prestressing forces in the bars surrounding the loading point and in the transverse beams were closely monitored during the experiments. In test BB15, failing in flexural punching, the load was placed above FP14 which showed a maximum increase of 30% in the prestressing force. In test BB10 that failed in brittle punching, FP07 showed an increase of 3.6% which is small enough to be considered negligible. Test BB 16, which had double loads at midspan and failed by flexural punching, showed a considerable increase in the prestressing force in bars close to the loading points. A 103.8% increase in force was reported for FP15. Less than 2% increase in the prestressing force was observed in test BB6 failing by brittle punching.

### Load – Reactions at supports

The reaction forces at the ultimate load for the selected test cases are shown in Table 4.3. A maximum error of 9% is observed for test BB16.

Table 4.3 Reactions at supports for the selected test cases at the ultimate load.

Test	Load	FR01	FR02	FR03	FR04	FR05	FR06	FR07	FR08	Sum FR	Error
	kN	kN	kN	kN	kN	kN	kN	kN	kN	kN	%
BB15	-359.68	-92.31	-93.23	-16.54	10.32	-56.70	-83.64	-9.02	7.93	-333.17	7.37
BB10	-340.3	-95.38	-145.27	-37.82	10.02	-11.33	-31.81	-7.07	1.34	-317.32	6.75
BB16	-553.4	-26.6	-113.8	-136.8	-14.1	-8.4	-109.0	-79.9	-16.3	-504.8	8.8
BB6	-576.82	-88.27	-69.24	-2.88	10.68	-239.55	-168.07	-4.87	16.95	-545.26	5.47

### Presence of lateral restraint

The displacement or strain at the bottom of a restrained deck slab is smaller than that of an unrestrained slab, if all other parameters remain the same. In order to determine if sufficient lateral restraint was present in the current tests, a quick calculation is performed for the case of a single load at midspan, BB15, comparing the measured displacement at the bottom of the deck slab with that of an idealized-unrestrained slab. Using simple geometrical rules, with a midspan deflection of 13.96 mm and the deck slab span of 1050 mm, the unrestrained or simply supported end conditions give a bottom compressive displacement of 1.32 mm whereas the bottom compressive displacement measured in the test was 0.589 mm, showing that lateral restraint was present in the bridge deck model.

## 4.3 Summary and discussion of test results

Previously, experimental results of four selected test cases were described in detail. Here, the test results of all the experiments are summarized and discussed. The Stevin Report No.

## Experimental Results

25.5.13-06 (2013) includes the detailed results with the graphical representation of each parameter, and is referred for better understanding of the following sections. These tests are classified in Table 4.4 based upon their type and parameters and are discussed in the following order depending upon the group they fall in.

- Single load tests done at midspan: BB1, 2, 7, 19, 8, 9, 13, 15, 19, 21 & 22.
- Single load tests close to the interface (girder flange-slab panel): BB3, 4, 10 & 14.
- Double load tests done at midspan: BB5, 11 & 16.
- Double load tests done close to the interface (girder flange-slab panel): BB6 & 12.

Table 4.4 Classification of the test results.

Ultimate failure loads based on geometrical classification								TPL
Single				Double				
Midspan		Joint/Interface		Midspan		Joint/Interface		
Test	Failure load	Test	Failure load	Test	Failure load	Test	Failure load	MPa
	kN		kN		kN		kN	
BB1 (ST)	348.7	BB3 (SK)	441.6	BB5 (ST)	490.4	BB6 (SK)	576.8	2.5
BB2 (SK)	321.4	BB4 (ST)	472.3	-	-	-	-	
BB7 (ST)	345.9	-	-	-	-	-	-	
BB19* (SK)	317.8	-	-	-	-	-	-	
BB8 (ST)	284.5	BB10 (SK)	340.3	BB11 (ST)	377.9	BB12 (SK)	373.7	1.25
BB9 (SK)	258.2	BB14 (ST, AD)	295.9	BB16 (SK)	553.4	-	-	
BB13 (ST, AD)	322.9	-	-	-	-	-	-	
BB15 (SK, AD)	359.7	-	-	-	-	-	-	
BB21 (SK)	243.8	-	-	-	-	-	-	0.5
BB22 (SK)	257.5	-	-	-	-	-	-	

\* 115×150 mm loading plate.

Notations used in the following sections: M = Midspan, ST = Straight joint, SK = Skewed joint, J = Joint/Interface, AD = Above the duct, BD = In-between the ducts, TPL = Transverse prestressing level, FMODE = Failure mode, BP = Brittle punching, FP = Flexural punching.  $P_{CRi,T}$  = Test initial flexural cracking load (hairline),  $P_{CR0.1,T}$  = Test initial flexural cracking load (0.1 mm wide crack),  $P_T$  = Test failure load (ultimate/peak),  $S_T$  = Test ultimate deflection under the load (next to the load in some cases),  $S_{MT}$  = Test ultimate deflection at midspan of the deck slab panel ( $S_T = S_{MT}$  when the load is placed at midspan),  $S_{T,325}$  = Test ultimate deflection at 325 mm from the load in the transverse direction,  $W_{CR,E}$  = Crack width at the top east of the deck slab panel,  $W_{CR,W}$  = Crack width at the top west of the deck slab panel,  $\varepsilon_{C,E}$  = Compressive strain at the bottom east of the deck slab panel,  $\varepsilon_{C,W}$  = Compressive strain at the bottom west of the deck slab panel,  $\varepsilon_{avg}$  = Average compressive strain at the bottom of the deck slab panel,  $\Delta_{H,E}$  = Global horizontal displacement on the east side of the deck slab panel,  $\Delta_{H,W}$  = Global horizontal displacement on the west side of the deck slab panel,  $\Delta_{V,E}$  = Relative vertical deflection on the east side of

## Experimental Results

the deck slab panel,  $\Delta_{V,W}$  = Relative vertical deflection of the west side of the deck slab panel. Any other notation used is defined within the text.

### 4.3.1 Tests with a single load at midspan

Ten tests were performed with a single concentrated load acting at the midspan of a deck slab panel. The panel had either a straight or a skewed joint/interface with the adjacent girder flanges on either side. The test results are summarized and discussed below.

#### Failure mode and cracking pattern

Table 4.5 summarizes the cracking loads ( $P_{CRi,T}$  and  $P_{CR0.1,T}$ ) and the failure loads ( $P_T$ ) of all the single load tests conducted at midspan. The failure mode (FMODE) is also given. The initial cracking load  $P_{CRi,T}$  is characterized by hairline cracks and the cracking load  $P_{CR0.1,T}$  is defined as the load at which the crack width becomes 0.1 mm (clear visibility).

The following observations were made about the test results:

- All the tests failed in punching shear. The top of the loading plate punched through the deck slab pushing out a conical plug of concrete at the bottom.
- Failure always occurred at midspan and the joint/interface (whether straight or skewed) proved to have a sufficient bearing capacity to withstand the applied load.
- The tests carried out with a transverse prestressing level of 1.25 and 2.5 MPa and with the load in between the ducts showed failure in brittle punching (BP) with no significant increase in the prestressing forces and the tests carried out with 0.5 MPa or with the load above the ducts showed failure in flexural punching (FP) with a significant increase of the prestressing force.
- Initially small cracks in the longitudinal or transverse direction developed under the loading point at the bottom of the deck slab with radial cracks appearing soon after them. With increasing load levels, the cracks widened and propagated further and the radial cracks developed into a full fan-like pattern. In most of the tests, circumferential cracks appeared close to failure but were not always documented as observations were stopped due to safety reasons close to expected failure.
- In most of the tests, the first hairline cracks appeared at about 20% of the ultimate load with a visible crack of 0.1mm developing at 35-50% of the ultimate load. The higher the prestressing level, the higher was the cracking load.
- Test BB13 showed cracking earlier than the other tests with a similar TPL (1.25MPa) possibly because it was the 2<sup>nd</sup> last test done on that panel (C) and a lot of damage was already present close to the loading position.

## Experimental Results

Table 4.5 Cracking load, failure load and deflection and failure mode.

#	Test	Designation	TPL	$P_{CR1,T}$	$P_{CR0.1,T}$ (0.1 mm)	$S_T$	$P_T$	FMODE
			[MPa]	[kN]	[kN]	[mm]	[kN]	
1.	BB1	C-P1M-ST	2.5	75	150	5.8	348.7	BP
2.	BB2	A-P1M-SK	2.5	75	150	4.92	321.4	BP
3.	BB7	C-P1M-ST	2.5	75	125	5.77	345.9	BP
4.	BB19	B-P1M-SK	2.5	75	125	4.15	317.8	BP
5.	BB8	C-P1M-ST	1.25	50	100	5.25	284.5	BP
6.	BB9	A-P1M-SK	1.25	50	100	5.00	258.2	BP
7.	BB13	C-P1M-ST	1.25	25	75	13.88	322.9	FP
8.	BB15	A-P1M-SK	1.25	50	125	13.96	359.7	FP
9.	BB21	B-P1M-SK	0.5	50	100	9.46	243.8	FP
10.	BB22	B-P1M-SK	0.5	25	75	9.09	257.5	FP

### Load – Deflection behavior

Table 4.5 (in the previous section) shows the failure loads  $P_T$  and the corresponding deflections  $S_T$  of the single load tests performed at midspan. The following observations were made:

- The test results show that the ultimate bearing capacity increased with the level of transverse prestressing. The load-deflection behavior was also much stiffer for higher prestressing levels.
- The panels with straight joints showed a higher capacity than the panels with the skewed joints although the joint/interface was not governing. However, an exception to this is test BB13 which was performed on the slab panel C having straight edges but showed a lower capacity as compared to a similar test BB15 which was performed on the slab panel A having skewed edges. It is to be noted that prior to performing test BB13, the slab panel C had already been excessively damaged due to previous tests conducted on it and therefore the capacity could have been affected by the close proximity of previous cracks.
- The load deflection curves of all the tests showing failure in brittle punching display an abrupt failure, whereas tests failing in flexural punching show a plateau providing a warning before failure.
- The test BB15 (1.25 MPa TPL) with the load above the duct showed a higher capacity if compared with similar tests. However BB13 did not show as much increase in the bearing capacity as BB15 did. It is suspected that since this test was performed on a panel that was already damaged before, the capacity was affected by this factor.
- For all brittle punching failures, the deflection remained of the same order and the TPL did not significantly influence the ultimate midspan deflections of the deck slab panel. This is similar to the observations made by He (1992).

## Experimental Results

- Higher deflections were observed in the tests showing flexural punching as compared to the tests showing brittle punching. This correlates well with the increased rotations and flexural action of the deck slab.
- Tests with a TPL of 0.5 MPa showed failure in flexural punching at higher loads than expected owing to a large increase of the force in the prestressing bars. A maximum increase in the prestressing force was observed, hence the rotations and deflections were higher than measured in the tests with a TPL of 1.25 MPa showing failure in flexural punching.

### Load – Crack width at the top and strain at the bottom of the deck slab panel near the interface

Table 4.6 shows the crack width at the top side ( $W_{CR,E}$  on the east side and  $W_{CR,W}$  on the west side) and the strains at the bottom side ( $\epsilon_{C,E}$  on the east side and  $\epsilon_{C,W}$  on the west side) of the deck slab panel near the interface. An average strain  $\epsilon_{avg}$  at the bottom side is also calculated.

Table 4.6 Crack widths at top and strains at bottom of the deck slab panel near the interface.

#	Test	Designation	TPL	$S_T$	$W_{CR,E}$	$W_{CR,W}$	$\epsilon_{C,E}$	$\epsilon_{C,W}$	$\epsilon_{avg}$
			[MPa]	[mm]	[mm]	[mm]	100 mm control length		
1.	BB1	C-P1M-ST	2.5	5.8	0.767	0.76	0.0028	0.0032	0.003
2.	BB2	A-P1M-SK	2.5	4.92	0.56	0.65	0.0025	0.0017	0.0021
3.	BB7	C-P1M-ST	2.5	5.77	0.685	0.6	0.0019	0.0033	0.0026
4.	BB19	B-P1M-SK	2.5	4.15	0.54	0.485	0.0015	0.0018	0.0017
5.	BB8	C-P1M-ST	1.25	5.25	0.774	0.791	0.0011	0.0017	0.0014
6.	BB9	A-P1M-SK	1.25	5.00	0.772	0.775	0.0030	0.0015	0.0023
7.	BB13	C-P1M-ST	1.25	13.88	2.29	2.34	0.0067	0.0062	0.0064
8.	BB15	A-P1M-SK	1.25	13.96	2.545	2.36	0.0029	0.0055	0.0042
9.	BB21	A-P1M-SK	0.5	9.46	1.97	1.79	0.0019	0.0029	0.0024
10.	BB22	A-P1M-SK	0.5	9.09	1.49	1.56	0.0018	0.0019	0.0018

Note: Data from the LVDTs that were damaged or not working properly has not been considered.

The following observations were made about the test results:

- When a single load was applied at midspan of a deck slab panel, the top side of the deck slab panel near the interface (joints) showed tensile stresses (cracking) while the bottom side of the deck slab panel near the interface (joints) showed compressive strains.
- Tests that showed failure in flexural punching (BB13, 15, 21 & 22) had a higher midspan deflection  $S_T$  than the tests that showed failure in brittle punching. Therefore, the crack widths recorded at the top of the joints for the flexural punching tests were much larger than those of brittle punching tests.

## Experimental Results

- The observed crack widths were  $< 1$  mm for brittle punching tests and  $\geq 1.5$  mm for flexural punching tests at the onset of failure.
- The crack widths at the top of the joints seemed to have no relation with the level of transverse prestressing for tests failing in brittle punching. For the tests failing in flexural punching, the higher TPL gave rise to a higher midspan deflection (as shown in the previous section) leading to larger crack widths.
- The compressive strains recorded at the bottom of the joints of the deck slab followed a similar pattern like the crack widths at the top of the joints, i.e. larger strains in the flexural punching tests than in the brittle punching ones.
- The TPL seemed to have no effect on the strains in tests with failure in brittle punching. For tests failing in flexural punching, a higher TPL led to increased compressive strains at the bottom.

### Load – Global horizontal displacement

The global horizontal displacements ( $\Delta_{H,E}$  on the east side and  $\Delta_{H,W}$  on the west side) of the deck slab panel are displayed in Table 4.7. It was observed that the horizontal displacements occurred only after the initial cracking of the slab. The displacements seem to be dependent on the location of the panel with regard to the overall bridge deck (Fig. 4.1). For tests conducted on an interior panel (test BB19), the horizontal displacements on both sides were comparable. However, for the tests done on an exterior panel, larger displacements were observed on that respective side. For instance, test BB1 showed a larger horizontal displacement on the western side of the panel and this test was done on the western exterior panel. Similarly, test BB2 showed a larger horizontal displacement on the eastern side of the panel and this test was done on the eastern exterior panel. This can be explained by considering that a greater area was available on the inner side of the exterior panel to resist the horizontal displacements than on the outer side.

Table 4.7 Global horizontal displacement of the deck slab panel (- inwards,+ outwards).

#	Test	Designation	Panel location	TPL	$\Delta_{H,E}$	$\Delta_{H,W}$
				[MPa]	[mm]	[mm]
1.	BB1	C-P1M-ST	C = West exterior	2.5	-0.49	1.226
2.	BB2	A-P1M-SK	A = East exterior	2.5	0.88	-0.052
3.	BB7	C-P1M-ST	C = West exterior	2.5	-0.167	0.47
4.	BB19	B-P1M-SK	B = Interior	2.5	0.025	0.16
5.	BB8	C-P1M-ST	C = West exterior	1.25	-0.0014	0.728
6.	BB9	A-P1M-SK	A = East exterior	1.25	0.735	0.0126
7.	BB13	C-P1M-ST	C = West exterior	1.25	0.082	2.28
8.	BB15	A-P1M-SK	A = East exterior	1.25	2.71	0.021
9.	BB21	B-P1M-SK	B = Interior	0.5	1.19	1.28
10.	BB22	B-P1M-SK	B = Interior	0.5	0.76	0.99

## Experimental Results

### Load – Relative vertical deflection of the slab-girder joint

Table 4.8 shows relative vertical deflections of the slab-girder joint on either side of the loaded deck slab panel ( $\Delta_{V,E}$  on the east side and  $\Delta_{V,W}$  on the west side). It can be observed that the vertical deflections of the joints remained small ( $< 1\text{mm}$ ) for all the tests failing in brittle punching. However, for tests with flexural punching failure, the vertical deflections of the joints were  $\geq 1\text{mm}$ .

Table 4.8 Relative vertical deflections of the slab-girder joint.

#	Test	Designation	TPL	$\Delta_{V,E}$	$\Delta_{V,W}$
			[MPa]	[mm]	[mm]
1.	BB1	C-P1M-ST	2.5	0.844	0.98
2.	BB2	A-P1M-SK	2.5	0.75	0.74
3.	BB7	C-P1M-ST	2.5	0.487	0.258
4.	BB19	B-P1M-SK	2.5	0.418	0.414
5.	BB8	C-P1M-ST	1.25	0.55	0.85
6.	BB9	A-P1M-SK	1.25	0.357	0.813
7.	BB13	C-P1M-ST	1.25	1.45	1.78
8.	BB15	A-P1M-SK	1.25	1.903	1.338
9.	BB21	B-P1M-SK	0.5	1.535	1.57
10.	BB22	B-P1M-SK	0.5	1.1	1.07

### Load – Prestressing force in the surrounding bars and reactions at the supports

Table 4.9 shows the prestressing forces and the distribution of the load as reaction forces at the supports.

Table 4.9 Prestressing force in the surrounding bars and reactions at the supports (N=North, S=South).

#	Test	Designation	TPL	FMODE	Maximum increase in the prestress	Bars with increase in prestress force		Difference in load and sum of reactions	
						Slab	Xbeam	First load step	Peak load
			[MPa]		[%]			[%]	[%]
1.	BB1	C-P1M-ST	2.5	BP	-	-	-	29.24	14.07
2.	BB2	A-P1M-SK	2.5	BP	-	-	-	29.86	9.77
3.	BB7	C-P1M-ST	2.5	BP	-	-	-	20.3	10.82
4.	BB19	B-P1M-SK	2.5	BP	-	-	-	16.26	13.8
5.	BB8	C-P1M-ST	1.25	BP	7.63	FP1-7	S	13.11	5.79
6.	BB9	A-P1M-SK	1.25	BP	5.46	FP1-6	S	5.81	5.99
7.	BB13	C-P1M-ST	1.25	FP	26.19	FP4-17	-	14.51	9.38
8.	BB15	A-P1M-SK	1.25	FP	30.58	FP8-21	-	16.79	7.37
9.	BB21	B-P1M-SK	0.5	FP	45	FP15-30	N	20.28	13.96
10.	BB22	B-P1M-SK	0.5	FP	57.34	FP5-27	N & S	18.92	12.1

## Experimental Results

For tests with brittle punching failure, hardly any change in the prestressing force of the bars surrounding the loading point was observed except for BB8 and 9 which had a lower TPL than BB1, 2, 7 and 19. For tests failing in flexural punching, a much higher increase in the prestressing forces is observed with a maximum increase for tests with the lowest TPL of 0.5 MPa.

The accuracy of the sum of the reaction forces as recorded by the load cells seemed to improve with the increasing load. Also, the southern side load cells showed more accurate measurements than the northern side load cells. A lesser difference is observed for tests with the load closer to the southern side of the deck as a larger percentage of the load was distributed to that side reducing the overall error.

### 4.3.2 Tests with a single load close to the interface

Four tests were performed with a single concentrated load acting close to the interface of a deck slab panel. The panel was provided with either a straight or a skewed joint/interface with the adjacent girder flanges on either side. In the test BB3 and 4, the center of the loading plate was placed at 110 mm from the girder flange-deck slab interface. The test results showed a very high bearing capacity because of the close proximity with the girders with a higher concrete strength ( $f_{cm} = 75$  MPa) as compared to the deck slab ( $f_{cm} = 65$  MPa). In the remaining tests, the distance of the loading plate to the interface was 200 mm c/c. The test results are summarized and discussed below.

#### Failure mode and cracking pattern

Table 4.10 summarizes the cracking ( $P_{CRi,T}$  and  $P_{CR0.1,T}$ ) and failure loads ( $P_T$ ) of all the tests with a single load close to the interface. The failure mode (FMODE) is also given. The initial cracking load  $P_{CRi,T}$  is characterized by hairline cracks and the cracking load  $P_{CR0.1,T}$  is defined as the load at which the crack width becomes 0.1 mm (clear visibility).

- All the tests failed in brittle punching (BP) shear. The top of the loading plate punched through the deck slab pushing out a conical plug of concrete at the bottom.
- Failure always occurred in the span of the slab panel and the joint/interface (whether straight or skewed) proved to have sufficient bearing capacity to withstand the applied load.
- Initially small cracks in the longitudinal or transverse direction developed under the loading point at the bottom of the deck slab with radial cracks appearing soon after them. With increasing load levels, the cracks widened and propagated further

## Experimental Results

and the radial cracks developed into a full fan-like pattern. The cracks were clustered more towards the area of load application. The crack width remained small as compared to the midspan tests. No circumferential cracks were observed.

- In most of the tests, the first hairline cracks appeared at about 10-20% of the ultimate load with a visible crack of 0.1mm developing at about 30-40% of the ultimate load.
- The higher the prestressing level, the higher was the cracking load.

Table 4.10 Cracking load, failure load and deflection and failure mode.

#	Test	Designation	TPL	$P_{CRi,T}$	$P_{CR0.1,T}$ (0.1 mm)	Deflection		$P_T$	FMODE
						$S_{MT}$	$S_T$		
			[MPa]	[kN]	[kN]	[mm]	[mm]	[kN]	
1.	BB3	A-PIJ-SK	2.5	75	175	5.13	6.35	441.6	BP
2.	BB4	C-PIJ-ST	2.5	100	175	5.78	7.06	472.3	BP
3.	BB10	A-PIJ-SK	1.25	25	100	3.21	3.99	340.3	BP
4.	BB14	A-PIJ-ST	1.25	25	125	3.91	4.75	295.9	BP

### Load – Deflection behavior

Table 4.10 (previous section) shows the failure loads  $P_T$  and the corresponding deflections  $S_{MT}$  (at midspan) and  $S_T$  (under or next to the load) of the single load tests performed close to the interface. The following observations were made about the test results.

- Generally speaking the ultimate bearing capacity increased with the level of transverse prestressing. The load-deflection behavior was also much stiffer for higher prestressing levels.
- The panels with straight joints showed a higher capacity than the panel with the skewed joints although the joint/interface was not governing.
- The load deflection profiles of all the tests with loads close to the interface show abrupt brittle failure.
- The test BB14 (with 1.25 MPa TPL) performed with the load directly above the prestressing duct showed a lower capacity than expected when compared with similar tests, possibly because this test was the last one done on that slab panel (C) and like test BB13 (discussed in section 4.3.1), the capacity was probably affected by the previous damage of the slab.
- The deflection seemed to be influenced by the transverse prestressing level unlike observed in the brittle punching failure tests at the midspan. However, the effect was not significant since the failure load was also proportionally higher for a higher TPL.

## Experimental Results

- The deflection directly under the load close to the interface was higher than the deflection recorded at the midspan.

### Load – Crack width at the top and strain at the bottom of the deck slab panel near the interface

Table 4.11 shows the crack width at the top side ( $W_{CR,E}$  on the east side and  $W_{CR,W}$  on the west side) and the strains at the bottom side ( $\varepsilon_{C,E}$  on the east side and  $\varepsilon_{C,W}$  on the west side) of the deck slab panel. The following observations were made about the test results:

- When a single load was applied close to the interface of a deck slab panel, the top side of the deck slab panel near the interface (joints) showed tensile stresses (cracking) while the bottom side of the deck slab panel near the interface (joints) showed compressive strains.
- The crack width recorded at the top of the joints on either side ( $W_{CR,E}$  and  $W_{CR,W}$ ) remained small ( $< 1$  mm).
- Generally, larger crack widths and higher compressive strains were observed for the joint opposite to the one being loaded except for BB14.

Table 4.11 Crack widths at top and strains at bottom of the deck slab panel near the interface.

#	Test	Designation	TPL	Load position	$W_{CR,E}$	$W_{CR,W}$	$\varepsilon_{C,E}$	$\varepsilon_{C,W}$
			[MPa]		[mm]	[mm]	100 mm control length	
1.	BB3	A-P1J-SK	2.5	West joint	0.12	0.06	0.0009	0.0001
2.	BB4	C-P1J-ST	2.5	East joint	0.0625	0.128	0.0002	0.0011
3.	BB10	A-P1J-SK	1.25	West joint	0.271	0.208	0.0018	0.0005
4.	BB14	A-P1J-ST	1.25	East joint	0.639	0.376	0.0011	0.0030

### Load – Global horizontal displacement

The global horizontal displacements ( $\Delta_{H,E}$  on the east side and  $\Delta_{H,W}$  on the west side) of the deck slab panel are displayed in Table 4.12.

Table 4.12 Global horizontal displacement of the deck slab panel (- inwards, + outwards).

#	Test	Designation	Panel location	Load position	TPL	$\Delta_{H,E}$	$\Delta_{H,W}$
					[MPa]	[mm]	[mm]
1.	BB3	A-P1J-SK	A = East exterior	West joint	2.5	0.13	-0.74
2.	BB4	C-P1J-ST	C = West exterior	East joint	2.5	-	-
3.	BB10	A-P1J-SK	A = East exterior	West joint	1.25	0.141	0.144*
4.	BB14	A-P1J-ST	A = East exterior	East joint	1.25	0.0365	0.313

\* Change from inwards displacement (-0.085mm) to outwards (+0.144 ) close to failure .

Note: Data from the lasers that were damaged or not working properly has not been considered.

## Experimental Results

It was observed that the horizontal displacements occurred only after the initial cracking of the slab. A larger displacement occurred towards the joint opposite to the load in test BB3 and 14. The displacements seemed to be dependent more on the joint being loaded than the location of the panel with regard to the overall bridge deck (refer to Fig. 4.1) as compared to the midspan tests where only the panel location mattered. An exception to this is test BB-10 which was also performed close to the interface but showed outwards displacement on both sides of the panel. From the load – displacement profile given in Fig. 4.7, it is clear that initially the displacement was inwards but then moved outwards as that side of the girder flange sheared off due to smaller concrete cover available (see the cracking pattern of BB10 in Table 4.2).

### Load – Relative vertical deflection of the slab-girder joint

Table 4.13 shows the relative vertical deflections of the slab-girder joint on either side of the loaded deck slab panel ( $\Delta_{V,E}$  on the east side and  $\Delta_{V,W}$  on the west side). It can be observed that the vertical deflections of both the joints were < 1mm for all the tests done close to the interface. This is similar to the tests with a single load at midspan that failed in brittle punching shear.

Table 4.13 Relative vertical deflections of the slab-girder joint.

#	Test	Designation	TPL	Load position	$\Delta_{V,E}$	$\Delta_{V,W}$
			[MPa]		[mm]	[mm]
1.	BB3	A-P1J-SK	2.5	West joint	0.16	0.14
2.	BB4	C-P1J-ST	2.5	East joint	0.24	0.26
3.	BB10	A-P1J-SK	1.25	West joint	0.126	0.243
4.	BB14	A-P1J-ST	1.25	East joint	0.867	-

Note: Data from the LVDTs that were damaged or not working properly has not been considered.

### Load – Prestressing force in the surrounding bars and reactions at the supports

Table 4.14 shows the prestressing forces and the distribution of the load as reaction forces at the supports. Since the tests failed in brittle punching, hardly any change in the prestressing force of the bars surrounding the loading point is observed except for tests done with a lower TPL of 1.25 MPa and that too is not significant.

The accuracy of the sum of the reaction forces as recorded by the load cells seemed to improve with the increasing load. Also, the southern side load cells showed more accurate measurements than the northern side load cells. A smaller difference is observed for BB10 performed closer to the southern side of the deck as a higher percentage of the load was distributed to that side reducing the overall error.

## Experimental Results

Table 4.14 Prestressing force in the surrounding bars and reactions at the supports.

#	Test	Designation	TPL	Maximum increase in the prestress	Bars with increase in prestress force		Difference in load and sum of reactions	
					Slab	Xbeam	First load step	Peak load
			[MPa]	[%]			[%]	[%]
1.	BB3	A-PIJ-SK	2.5	-	-	-	19.72	9.31
2.	BB4	C-PIJ-ST	2.5	-	-	-	25.3	11.44
3.	BB10	A-PIJ-SK	1.25	3.59	FP6-9	-	8.01	6.84
4.	BB14	A-PIJ-ST	1.25	4.67	FP12-17	-	17.69	9.58

### 4.3.3 Tests with a double load at midspan

Three tests were performed with a double concentrated load acting at midspan of the deck slab panel. The test results are summarized and discussed below.

#### Failure mode and cracking pattern

Table 4.15 summarizes the cracking ( $P_{CRi,T}$  and  $P_{CR0.1,T}$ ) and failure loads ( $P_T$ ) of all the double load tests performed at midspan. The failure mode (FMODE) is also given. The initial cracking load  $P_{CRi,T}$  is characterized by hairline cracks and the cracking load  $P_{CR0.1,T}$  is defined as the load at which the crack width becomes 0.1 mm (clear visibility).

The following observations were made:

- All the tests showed failure in flexural punching (FP) shear. BB16 showed a more brittle behavior than BB5 and 11. One of the loading plates on the top side of the deck slab punched through and generated a typical punching cone at the bottom along with circumferential cracks. In the other two tests, large rotations occurred close to failure and the load did not increase further.
- Failure always occurred in the span of the slab panel and the joint/interface (straight or skewed) proved to have a sufficient bearing capacity.
- Initially small cracks in the longitudinal or transverse direction developed at the loading points at the bottom of the slab with radial cracks appearing soon after them. With increasing load levels, the longitudinal cracks under the loading points joined together and widened to a large extent. Also, the radial cracks developed into a full fan-like pattern at each loading point.
- Although the current double load tests were carried out with two point load acting at 600 mm c/c and not “one rectangular load”, but the failure mode and the cracking pattern observed are in good correlation with those observed in the tests of Zheng et al. (2010) where the ratio between the sides of the loaded area (plate) was large and flexural behavior was observed. The final failure was by punching

## Experimental Results

similar to the current tests. The ASCE-ACI Task Committee (1974) also noted from slab-column tests that if the length of the perimeter of the loaded area is kept constant and the ratio of the longer side to the shorter side is increased, the shear strength is governed by one-way bending action.

- The higher the prestressing level, the higher was the cracking load. Generally, the first hairline cracks appeared at about 10-30% of the ultimate load with a visible crack of 0.1mm developing at about 30-40% of the ultimate load.

Table 4.15 Cracking load, failure load and deflection and failure mode.

#	Test	Designation	TPL	$P_{CRi,T}$	$P_{CR0.1,T}$ (0.1 mm)	Deflection		$P_T$	FMODE
						$S_{MT}$	$S_{T,325}$		
			[MPa]	[kN]	[kN]	[mm]	[mm]	[kN]	
1.	BB5	C-P2M-ST	2.5	150	200	-	7.65	490.4	FP
2.	BB16	B-P2M-SK	2.5	150	200	9.97	-	553.4	FP
3.	BB11	C-P2M-ST	1.25	50	125	11.82	7.11	377.9	FP

### Load – Deflection behavior

Table 4.15 (previous section) shows the failure loads  $P_T$  and the corresponding deflections  $S_{MT}$  (at midspan) and  $S_{T,325}$  (at 325 mm in the transverse direction) of the double load tests performed at midspan. The following observations were made about the test results.

- The ultimate bearing capacity increased with the level of transverse prestressing.
- The panels with skewed joints showed a higher capacity than the panel with the straight joints although the joint/interface was not governing. This is in sharp contrast to the single load tests done at midspan with failure in brittle punching but correlates well with the single load tests with failure in flexural punching.
- The load-deflection profiles of the double load tests carried out at the midspan show a plateau providing a warning before failure (flexural action).
- For test BB11 with a TPL of 1.25 MPa, larger deflections along with a larger increase in the prestressing force close to failure were observed than for tests BB5 and BB16 with a TPL of 2.5 MPa.

### Load – Crack width at the top and strain at the bottom of the deck slab panel near the interface

Table 4.16 shows the crack width at the top side ( $W_{CR,E}$  on the east side and  $W_{CR,W}$  on the west side) and the strains at the bottom side ( $\epsilon_{C,E}$  on the east side and  $\epsilon_{C,W}$  on the west side) of the deck slab panel. An average strain  $\epsilon_{avg}$  at the bottom side is also calculated. The following observations were made about the test results:

## Experimental Results

- When a double load was applied at midspan of a deck slab panel, the top side of the deck slab panel near the interface (joints) showed tensile stresses (cracking) while the bottom side of the deck slab panel near the interface (joints) showed compressive strains.
- The crack width recorded at the top of the joints on either side of the deck slab panel (east and west) was  $\geq 1.5$  mm.
- The crack widths of the top of the joints were larger for tests BB5 and BB11 and showed a greater flexural action as compared to test BB16.
- The compressive strain recorded at the bottom of the joints of the deck slab followed a similar pattern like the crack widths at the top of the joints. For a similar TPL, BB5 showed larger compressive strains than BB16 owing to a larger flexural action in the former than in the latter.

Table 4.16 Crack widths at top and strains at bottom of the deck slab panel near the interface.

#	Test	Designation	TPL	$W_{CR,E}$	$W_{CR,W}$	$\epsilon_{C,E}$	$\epsilon_{C,W}$	$\epsilon_{avg}$
			[MPa]	[mm]	[mm]	100 mm control length		
1.	BB5	C-P2M-ST	2.5	2.315	2.5	0.0065	0.0034	0.00495
2.	BB16	B-P2M-SK	2.5	1.55	1.495	0.0024	0.0025	0.00245
3.	BB11	C-P2M-ST	1.25	2.475	2.595	0.0022	0.0028	0.0025

### Load – Global horizontal displacement

The global horizontal displacements ( $\Delta_{H,E}$  on the east side and  $\Delta_{H,W}$  on the west side) of the deck slab panel are displayed in Table 4.17. It was observed that the horizontal displacements occurred only after the initial cracking of the slab. The displacements seem to be dependent on the location of the panel with regard to the overall bridge deck (refer to Fig. 4.1). For tests done on an interior panel, the horizontal displacements on both sides were comparable. However, for tests done on an exterior panel, larger displacements were observed on the outer side, possibly because a greater area was available on the inner side of the exterior panel to resist the slab horizontal displacements than on the outer side.

Table 4.17 Global horizontal displacement of the deck slab panel (- inwards, + outwards).

#	Test	Designation	Panel location	TPL	$\Delta_{H,E}$	$\Delta_{H,W}$
				[MPa]	[mm]	[mm]
1.	BB5	C-P2M-ST	C = West exterior	2.5	-0.16	1.87
2.	BB16	B-P2M-SK	B = Interior	2.5	0.49	0.48
3.	BB11	C-P2M-ST	C = West exterior	1.25	0.16	2.8

### Load – Relative vertical deflection of the slab-girder joint

Table 4.18 shows relative vertical deflections of the slab-girder joint on either side of the loaded deck slab panel ( $\Delta_{V,E}$  on the east side and  $\Delta_{V,W}$  on the west side). The vertical

## Experimental Results

deflections of the joints were  $\geq 1$  mm for all the tests, similar to the single load tests failing in flexure.

Table 4.18 Relative vertical deflections of the slab-girder joint.

#	Test	Designation	TPL	$\Delta_{v,E}$	$\Delta_{v,W}$
			[MPa]	[mm]	[mm]
1.	BB-5	C-P2M-ST	2.5	1.175	1.86
2.	BB-16	B-P2M-SK	2.5	1.05	0.918
3.	BB-11	C-P2M-ST	1.25	1.12	1.49

### Load – Prestressing force in the surrounding bars and reactions at the supports

Table 4.19 shows the prestressing forces and the distribution of the load as reaction forces at the supports. In test BB16, a smaller increase in the prestressing force of the bars surrounding the loading point was observed than in the tests BB5 and 11. A maximum increase was observed for BB5 that had a TPL of 1.25 MPa.

Table 4.19 Prestressing force in the surrounding bars and reactions at the supports.

#	Test	Designation	TPL	Maximum increase in the prestress	Bars with increase in prestress force		Difference in load and sum of reactions	
					Slab	Xbeam	First load step	Peak load
			[MPa]	[%]			[%]	[%]
1.	BB5	C-P2M-ST	2.5	12.64	18-26	-	20.7	11.13
2.	BB16	B-P2M-SK	2.5	6.23	FP8-20	-	13.1	8.8
3.	BB11	C-P2M-ST	1.25	39.76	FP2-14	South	13.31	6.16

The accuracy of the sum of the reaction forces as recorded by the load cells seemed to improve with the increasing load. Also, the southern side load cells showed more accurate measurements than the northern side load cells. A smaller difference is observed for the tests performed closer to the southern side of the deck as a higher percentage of the load was distributed to that side reducing the overall error.

### 4.3.4 Tests with a double load close to the interface

Two tests were performed with a double load acting close to the interface of a deck slab panel. The center of the loading plate was placed at 200 mm from the girder flange-deck slab interface. The test results are summarized and discussed below.

#### Failure mode and cracking pattern

Table 4.20 summarizes the cracking ( $P_{CRi,T}$  and  $P_{CR0.1,T}$ ) and failure loads ( $P_T$ ) of all the double load tests done close to the interface. The failure mode (FMODE) is also given. The

## Experimental Results

initial cracking load  $P_{CRI,T}$  is characterized by hairline cracks and the cracking load  $P_{CR0.1,T}$  is defined as the load at which the crack width becomes 0.1 mm (clear visibility).

The following observations were made about the test results.

- All the tests failed in brittle punching (BP) shear. One of the loading plates punched through the deck slab pushing out a conical plug of concrete at the bottom. In both the tests BB6 and 12, the side that punched through was the one closer to a previously damaged deck slab portion.
- Failure always occurred in the span of the slab panel and the joint/interface (whether straight or skewed) proved to have a sufficient bearing capacity to withstand the applied load.
- Initially small cracks in the longitudinal or transverse direction developed under the loading points at the bottom of the deck slab with radial cracks appearing soon after them. With increasing load levels, the longitudinal cracks joined together and propagated further and the radial cracks developed into a full fan-like pattern.
- The cracks were clustered more towards the area of load application
- A circumferential crack was observed in test BB6.
- Crack width remained small as compared to the double load midspan tests.
- The first hairline cracks appeared at about 25-30% of the ultimate load with a visible crack of 0.1mm developing at about 40-50% of the ultimate load.
- The higher the prestressing level, the higher was the cracking load.

Table 4.20 Cracking load, failure load and deflection and failure mode.

#	Test	Designation	TPL	$P_{CRI,T}$	$P_{CR0.1,T}$ (0.1 mm)	Deflection		$P_T$	FMODE
						$S_{MT}$	$S_T$		
			MPa	kN	kN	mm	mm	kN	
1.	BB6	A-P2J-SK	2.5	150	250	5.9	-	576.8	BP
2.	BB12	A-P2J-SK	1.25	100	175	2.6	3.53	373.7	BP

### Load – Deflection behavior

Table 4.20 (in the previous section) shows the failure loads  $P_T$  and the corresponding deflections  $S_{MT}$  (at midspan) and  $S_T$  (under or next to the load) of the double load tests performed close to the interface. The following observations were made about the test results.

- The ultimate bearing capacity increased with the level of transverse prestressing.
- The load deflection profiles for the tests done close to the interface show abrupt brittle failure.

## Experimental Results

- The deflection directly under the load close to the interface was higher than the deflection recorded at the midspan.
- The test BB12 failed at a load lower than expected. Similar test with a single load (BB10) had failed at 340 kN but BB12 failed at only 373.7 kN despite being a double load.

### Load – Crack width at the top and strain at the bottom of the deck slab panel near the interface

Table 4.21 shows the crack width at the top side ( $W_{CR,E}$  on the east side and  $W_{CR,W}$  on the west side) and the strains at the bottom side ( $\epsilon_{C,E}$  on the east side and  $\epsilon_{C,W}$  on the west side) of the deck slab panel.

Table 4.21 Crack widths at top and strains at bottom of the deck slab panel near the interface.

#	Test	Designation	TPL	Load position	$W_{CR,E}$	$W_{CR,W}$	$\epsilon_{C,E}$	$\epsilon_{C,W}$
			[MPa]		[mm]	[mm]	100 mm control length	
1.	BB6	A-P2J-SK	2.5	East joint	0.696	0.39	0.0025	0.0022
2.	BB12	A-P2J-SK	1.25	East joint	0.575	0.33	0.0009	0.0016

Note: Data from the LVDTs that were damaged or not working properly has not been considered.

The following observations were made about the test results:

- When a double load was applied close to the interface of a deck slab panel, the top side of the deck slab panel near the interface (joints) showed tensile stresses (cracking) while the bottom side of the deck slab panel near the interface (joints) showed compressive strains.
- The maximum crack width recorded at the top of the joints on either side of the deck slab panel (east and west) was < 1 mm.
- For BB6, larger crack widths and higher compressive strains were observed for the joint opposite to the one being loaded (similar to a single load close to the interface) except for BB12.

### Load – Global horizontal displacement

The global horizontal displacements ( $\Delta_{H,E}$  on the east side and  $\Delta_{H,W}$  on the west side) of the deck slab panel are displayed in Table 4.22. The test results are too few to be conclusive about the pattern of the displacements, however, it was observed the displacements occurred only after the initial cracking of the slab.

## Experimental Results

Table 4.22 Global horizontal displacement of the deck slab panel (- inwards, + outwards).

#	Test	Designation	TPL	Load position	Panel location	$\Delta_{H,E}$	$\Delta_{H,W}$
			[MPa]			[mm]	[mm]
1.	BB6	A-P2J-SK	2.5	East joint	A: East exterior	-0.076	0.163
2.	BB12	A-P2J-SK	1.25	East joint	A: East exterior	0.35	-0.24

### Load – Relative vertical deflection of the slab-girder joint

Table 4.23 shows relative vertical deflections of the slab-girder joint on either side of the loaded deck slab panel ( $\Delta_{V,E}$  on the east side and  $\Delta_{V,W}$  on the west side). The vertical deflections of both joints were < 1mm for all the tests with loads close to the interface.

Table 4.23 Relative vertical deflections of the slab-girder joint (+ downwards, - upwards).

#	Test	Designation	TPL	Load position	$\Delta_{V,E}$	$\Delta_{V,W}$
			[MPa]		[mm]	[mm]
1.	BB6	A-P2J-SK	2.5	East joint	0.64	0.09
2.	BB12	A-P2J-SK	1.25	East joint	0.48	-

Note: Data from the LVDTs that were not working properly has not been considered.

### Load – Prestressing force in the surrounding bars and reactions at the supports

Table 4.24 shows the prestressing forces and the distribution of the load as reaction forces at the supports. Since the tests failed in brittle punching, hardly any change in the prestressing force of the bars surrounding the loading point is observed except for the tests done with a lower TPL of 1.25 MPa and that too is not as significant as for those in the double load flexural punching tests discussed in the previous section.

The accuracy of the sum of the reaction forces as recorded by the load cells seemed to improve with the increasing load. Also, the southern side load cells showed more accurate measurements than the northern side load cells. A lesser difference is observed for BB12 performed closer to the southern side of the deck than BB6, as a greater percentage of the load was distributed to that side reducing the overall error.

Table 4.24 Prestressing force in the surrounding bars and reactions at the supports.

#	Test	Designation	TPL	Maximum increase in the prestress	Bars with increase in prestress force		Difference in load and sum of reactions	
					Slab	Xbeam	First load step	Peak load
			[MPa]	[%]			[%]	[%]
1.	BB6	A-P2J-SK	2.5	-	-	-	19.57	5.47
2.	BB12	A-P2J-SK	1.25	6.07	FP8-12	-	10.7	6.52

## 4.4 Conclusions

Some important conclusions derived from the test results are as follows:

- Punching failure occurred in the span of the slab when a load was applied to the concrete deck regardless of the number of loads applied or position of the load. The interface between the girders and the deck slab remained unimpaired.
- Two types of punching failure modes were observed. For single loads at midspan and close to the interface, and for double loads acting close to the interface, brittle punching failure was observed. Exceptions to this were single loads applied above a duct or when the transverse prestressing level was too low, i.e. 0.5 MPa. In these cases, a flexural punching failure was observed with large increase in the prestressing force of the bars surrounding the loading point, or in the transverse beam bars in some cases. Such flexural action was also found in the double load tests at midspan. Apart from the large increase in the prestressing forces, a single longitudinal crack ran through the midspan area connecting the two loading points and kept widening close to failure. Final failure occurred, however, by punching.
- The top edges side of the deck slab showed tensile stressed (cracking) and the bottom edges showed compressive strains. The cracking at top and strains at the bottom were of a larger magnitude in the flexural punching cases than in the brittle punching cases.
- Small vertical movements of the deck slab were found with regard to the girders and combined with the cracking behavior of the top side and compressive strains on the bottom side led to small rotations at the edges.
- Sufficient lateral restraint was observed in the tests when the measured bottom compressive displacements were compared with those of simply supported, unrestrained boundary conditions.

The results are further analyzed in the next chapter where the experimental parametric study is carried out.

# **CHAPTER 5**

## **Experimental Parametric Study**

In the previous chapter, the experimental results of nineteen tests carried out on a 1:2 scale model of a bridge deck have been presented. This chapter describes a parametric study carried out by analyzing the test results.

## 5.1 Introduction

In this chapter, the test results presented in chapter 4 are analyzed by carrying out a parametric study and studying the influence of each parameter on the punching shear capacity or on the overall behavior of the transversely prestressed bridge deck. First the parameters will be introduced and explained how they are dealt with in the experimental program and then the relevant experimental observations will be discussed. Comparison with similar observations from the literature will also be made.

## 5.2 Important experimental parameters

The main parameters to be investigated experimentally were:

- Transverse prestressing level.
- Position of the load with regard to the transverse slab panel span: Midspan or close to the girder flange-slab interface.
- Position of the load with regard to the ducts: Above or in-between the ducts.
- Position of the load with regard to the whole deck: Interior or exterior slab panels.
- Inclination of the girder flange-deck slab panel joint: Straight or skewed.
- Position of the load with regard to the longitudinal span.
- Number of loads: Single or double loads.
- Size of the loading area (wheel print/loading plate).
- Influence of previous damage to the deck slab panel.

The general notations used in this chapter are as follows: TPL = Transverse prestressing level, P1M = Single point load acting at midspan of the deck slab panel, P1J = Single point load acting close to the girder flange-slab interface/joint, P2M = Double point loads at midspan of the deck slab panel, P2J = Double point loads acting close to the girder flange-slab interface/joint, ST = Straight joint, SK = Skewed joint, AD = Above the duct and BD = In-between the ducts. Any other notation used is explained within the text.

## 5.3 Results of parametric analysis

### 5.3.1 Transverse Prestressing Level

In a real bridge, a TPL of 2.5 MPa is usually present but tests with 1.25 MPa were done to simulate the condition of a fractured bar and also to study the influence of different levels of transverse prestressing. The main transverse prestressing levels investigated were: 1.25

and 2.5 MPa. A TPL of 0.5 MPa was also applied but such a low level of prestressing (that too with unbonded tendons) is realistically not present in a deck slab. Either bridge decks are carried out in reinforced concrete or in fully prestressed concrete. In the latter case, the level of TPL is usually higher than 0.5 MPa. Here, the assumption was that the very low TPL of 0.5 MPa in the deck was almost equivalent to a reinforced concrete deck since the (actual) ordinary reinforcement ratio was low. It also served as a control deck for the research. It was expected that the level of transverse prestressing would affect all aspects of deck slab behavior including the cracking loads, the deflections and the ultimate failure loads. Section 4.3 showed that the cracking loads are higher for a higher transverse prestressing level proving that an improvement in serviceability limit state can be made if TPL is increased. Increasing the TPL also increased the punching shear capacity. Similar experimental observations were made by Poston (1988), Moll (1984), He (1992) and Semelawy (2007) on prestressed concrete decks.

In the following sections, the influence of the transverse prestressing level on the ultimate load is studied based on type of the load for a better understanding and clarity.

### **Single load tests: Position at midspan or close to the joint/interface**

Fig. 5.1 shows the ultimate loads when a single load was applied at midspan or close to the support/interface with respect to the transverse prestressing levels.

It can be seen clearly that an increase of the transverse prestressing level has a positive influence on the ultimate bearing capacity (punching shear). Even with the lowest TPL of 0.5 MPa, sufficient strength exists in the slab as flexural action takes over the brittle behavior in punching. It can also be observed that a much higher capacity was found if the load was applied close to the interface, if all other parameters remained the same (TPL, position of the load with regard to the ducts etc.). Particularly, tests done with 2.5 MPa show a larger difference in the capacity when tested at the midspan and close to the interface, whereas, for 1.25 MPa, the difference between the two types of the tests is far less. This can be explained by considering the position of the load applied close to the interface. For 2.5 MPa tests, the loads were applied closer to the adjacent girder, at 110 mm from the joint, whereas, for 1.25 MPa tests, the loads were applied at 200 mm. Similar observations were made in the experimental program carried out at Queen's university, Ontario, Canada (Savides 1989, He 1992). Higher TPLs were found to increase the punching shear capacity when a single load was applied at a 1/4.04 scale model of a transversely prestressed concrete deck. A linear relationship was found between the punching shear capacity and the transverse prestressing level with a 53 kN failure load for a

## Experimental Parametric Study

TPL of 1.84 MPa to 88 kN for a level of 4.37 MPa. Marshe and Green (1999) reported even higher capacities for a similar model but prestressed with CFRP (carbon fiber reinforced polymer) tendons. Hassan et al. (2001) observed a linear increase in the cracking loads and Hwang et al. (2010) reported a linear increase in the punching shear capacity with an increasing prestressing level.

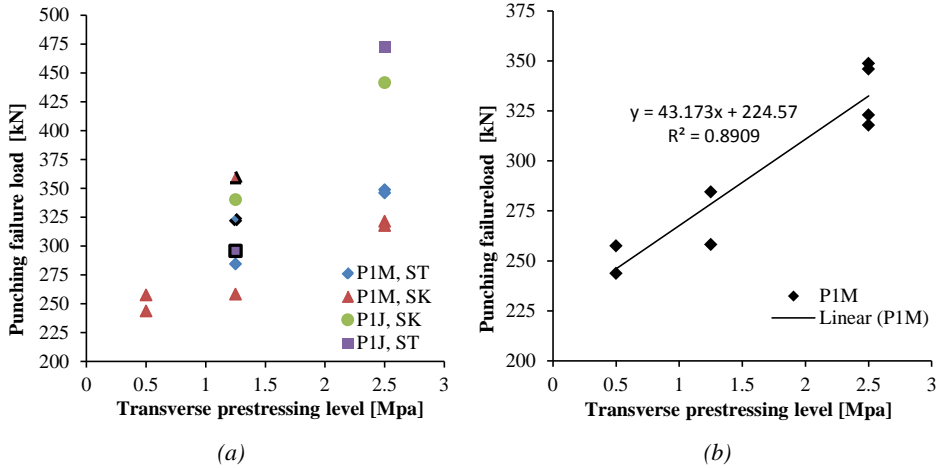


Fig. 5.1 Influence of TPL on the ultimate bearing capacity when a single load acts on the deck slab. The three tests that were performed above the ducts are bounded black: a) P1M and PIJ; b) Linearity of punching capacity with regard to the TPL.

### Double load tests: Position at midspan or close to the joint/interface

Fig. 5.2 shows the ultimate loads when a double load was applied at midspan or close to the interface with respect to the transverse prestressing level.

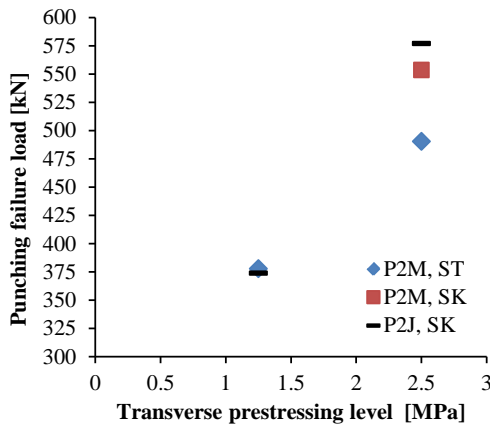


Fig. 5.2 Influence of TPL on the ultimate bearing capacity when a double load acts on the deck slab.

## Conclusion

The transverse prestressing level has a positive effect on the cracking loads and the punching shear capacity. Regardless of the failure mode; flexural punching or brittle punching, position of the load, type of the load and the geometry of the deck slab, the tests with a higher TPL failed at a higher load. To develop a more clear relationship between TPL and the punching shear capacity the levels of transverse prestressing should be increased keeping all other parameters constant. Since it is not possible experimentally, a numerical approach will be used in the succeeding chapters.

### 5.3.2 Position of the load with regard to the transverse slab panel span

The objective of studying the influence of the position of the load with regard to the transverse slab panel span was to study the failure mode as well as the effect on the bearing strength if the load was to be applied at midspan or when moved close to the girder flange – slab interface (Fig. 5.3). Even if the joint remained unimpaired when the slab was loaded at midspan or when load was applied close to a straight joint, it is quite possible that when the load was applied close to a skewed joint, it would become critical.

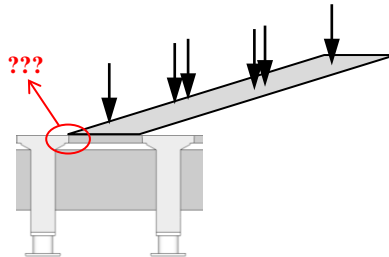


Fig. 5.3 Loads applied at midspan and close to the interface.

With regard to failure, the test results show that for both single and double loads, failure always occurred in the span of the slab and the joint/interface remained unimpaired regardless of the position of the load. This phenomenon can be explained by the fact that the concrete strength of the girders was much higher ( $f_{cm} = 75$  MPa) compared to the concrete strength of the slab panels ( $f_{cm} = 65$  MPa), see section 3.2.1. Consequently, when the load was applied close to the interface, punching failure could never occur along the side having the interface before the failure in the concrete panel itself (along the other three sides). The influence of the position of the load on the bearing capacity with regard to the transverse slab span is further explained for single and double loads in the following sections.

**Single load tests: Position at midspan or close to the joint/interface**

Fig. 5.4 shows the ultimate bearing capacity when a single load acts at midspan and close to the joint/interface. The results have been categorized depending on the level of the transverse prestressing present.

For the tests with 2.5 MPa TPL, it can be concluded that the deck slab showed a higher bearing capacity when loaded close to the joint. The close proximity of the stiff girders contributed more to the load carrying capacity than when the deck was loaded at midspan. For the tests with 1.25 MPa TPL, there were some variations in the test parameters. Some tests carried out at the midspan with the load directly above the ducts (BB13 and 15) gave a higher capacity than the tests carried out at the midspan and load positioned in-between the ducts. However, test BB14 showed comparatively lower capacity despite being loaded above the duct and close to the joint probably because this test was the last test to be performed on the previously damaged slab panel C affecting the deck slab capacity.

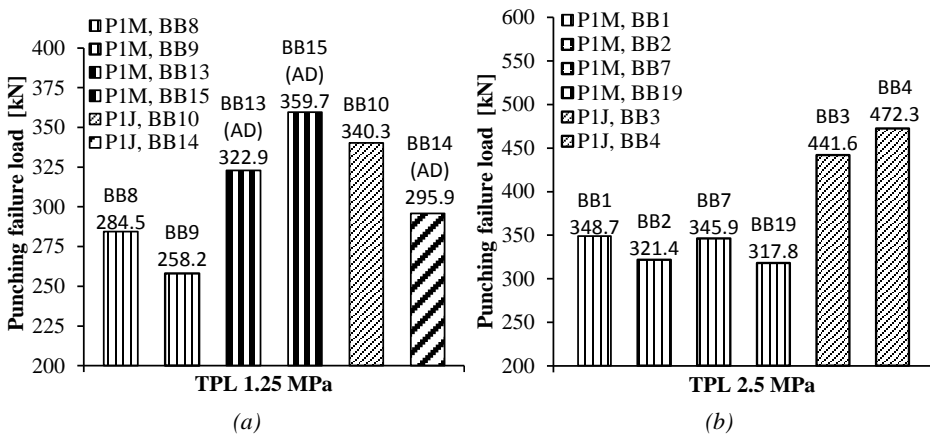


Fig. 5.4 Influence of the load position on the ultimate bearing capacity when a single load acts on the deck slab (P1M and P1J): a) When the TPL is 1.25 MPa; b) When the TPL is 2.5 MPa.

**Double load tests: Position at midspan or close to the joint/interface**

Fig. 5.5 shows the ultimate bearing capacity when a double load acts at midspan and close to the joint/interface. The results have been categorized by the level of transverse prestressing present in the deck slab, however, another important factor to be considered here is the mode of failure. All double load tests close to the interface showed brittle punching whereas the midspan tests showed flexural punching. For 2.5 MPa, the tests with loads at interface, failing in brittle punching, showed the highest capacity but for 1.25 MPa, the tests at midspan, failing in flexural punching, showed the highest capacity. However,

even in the 2.5 MPa tests, the difference in the capacity when loads were at midspan or when they were close to the interface was not high. The single load tests showed a much higher capacity when the load was applied at the interface. The reason the P2M tests show more or less similar results with the P2J tests, could be the flexural action in the former (explained in section 4.3.3) enhancing the bearing capacity which is not present in the typical P1M brittle punching failures .

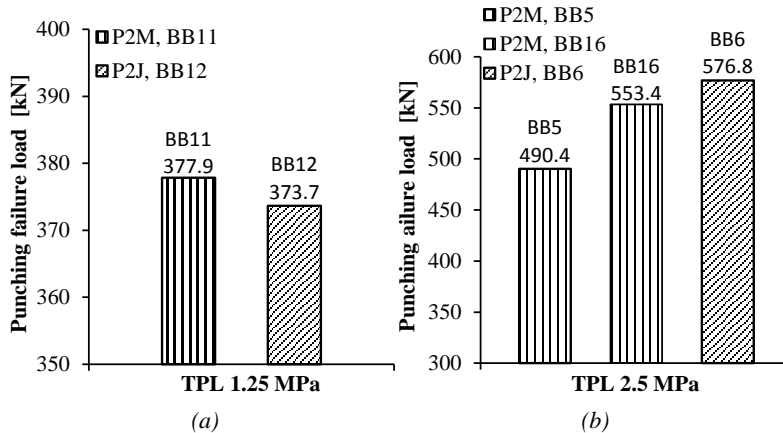


Fig. 5.5 Influence of the load position on the ultimate bearing capacity when a double load acts on the deck slab (P2M and P2J): a) When the TPL is 1.25 MPa; b) When the TPL is 2.5 MPa.

## Conclusion

It can be concluded that for single loads, the tests with the load close to the interface showed a higher ultimate bearing capacity than the tests with the load at midspan. Both types of tests showed failure in brittle punching. However, in the double load tests at midspan, the mode of failure played an important role. The flexural action in the double load midspan tests enhanced the capacity to almost to the level of the brittle punching failure of the double load interface tests. Had the failure mode been similar, the capacity of tests done at the interface would have been higher than at midspan as observed in the single load tests. Such flexural punching failures are also observed elsewhere (Zheng et al. 2010) due to a large ratio between the sides of the loading plate.

### 5.3.3 Position of the load with regard to the prestressing ducts: In-between or above the ducts

Since the deck was prestressed in the transverse direction at 400 mm c/c, the load had to be applied either in-between two prestressing ducts/bars or directly above a duct/bar. Hence,

the position of the load with regard to the prestressing duct/bar was considered an important parameter.

Fig. 5.6 shows the comparison between the tests carried out with the load in-between the prestressing ducts and directly above the ducts (for 1.25 MPa). It can be observed that when the load was applied above a duct, the deck slab failed at higher loads possibly because loading above a duct can distribute the load to two adjacent duct-to-duct panels without any hindrance to the punching shear cone, whereas loading in-between the ducts can limit the load distribution to the area within one duct-to duct panel and the presence of ducts also hinders the punching shear inclined cracks. Previous research by He (1992) on a prestressed deck also indicated that loading above a prestressing wire influenced the load deflection behavior positively. This also gives an important conclusion:

*“The deck slab shows a higher capacity when loaded directly above a prestressing duct. Since most of the tests were performed with loads in-between the prestressing ducts, the results of this experimental program represent a lower bound of the bearing capacity.”*

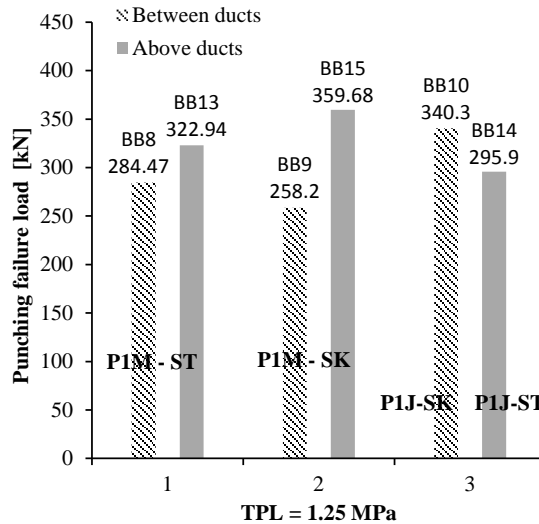


Fig. 5.6 Influence of the load position with regard to the prestressing ducts on the ultimate bearing capacity.

### 5.3.4 Position of the load with regard to the whole deck: Interior or exterior slab panels

For the development of compressive membrane action, a sufficient surrounding area should be available to provide the necessary restraint. In this investigation, the lateral restraint

would come from the adjacent girders and surrounding slab area. Hence the position of the load with regard to the slab panel position (interior or exterior) was considered an important parameter.

Fig. 5.7 shows the effect of the load position with regard to the location of the slab panels on the bearing capacity. The tests done on the interior panels are shown in bold. All the tests shown used for the comparison have similar TPL and are carried out with a load at midspan. No interface tests were conducted in the interior panel. It can be observed that the location of the load with regard to the panels; exterior or interior, had no significant effect on the bearing capacity when single loads were applied on the deck but there was some influence on the bearing capacity in case of double loads. Since there is no clear relationship between the capacity of interior and exterior deck slab panels for the analyzed load cases, this factor is considered not to have a significant influence. In the present study, most of the tests for 1.25 and 2.5 MPa were performed on the exterior panels so the results can be considered to provide a lower bound for the bearing capacity. Also, it seems from the test results that a sufficient area of concrete was available around the loading position (slab and adjacent girder flanges) for the development of compressive membrane forces for both interior and exterior panels.

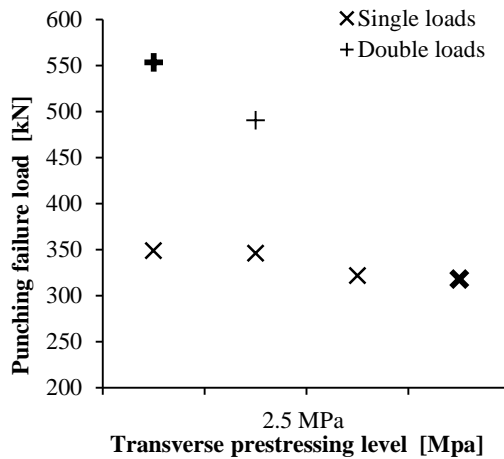


Fig. 5.7 Influence of loading the exterior or interior panels on the ultimate bearing capacity. The tests done on the interior panels are shown in bold.

### 5.3.5 Position of the load with regard to the longitudinal span

Since the transverse beams were provided near the ends of the deck, more restraint was expected near the edges providing extra stiffness to the nearby portion of the deck slab and therefore the longitudinal position of the load along the bridge deck could affect the bearing

strength. The test results show that there was no effect of the longitudinal position of the load on the ultimate bearing capacity. For instance, BB1 was tested with the load close to the north end of the deck provided with a transverse beam and it failed at 348.7 kN, whereas test BB7 was carried out at 5200 mm from the north end of the deck and it failed at 345.9 kN. The load-deflection behavior of the two tests was also similar (Stevin Report No. 25.5.13-06 2013).

### 5.3.6 Inclination of the girder flange-deck slab panel joint: Straight or skewed

The inclination of the joint between the girder and the deck slab panel was an important parameter in this research. In the real bridge, the joints were either straight (at right angle to the plane of the slab) or skewed at an angle. Hence, it was interesting to see what effect would skewness (Fig. 5.8) have on the bearing strength and whether the joint had sufficient strength to withstand the applied load regardless of the position of the load.

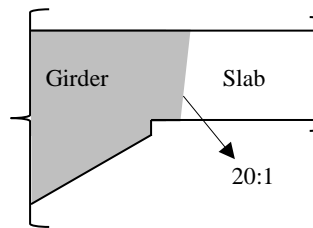


*Fig. 5.8 Skewed joint of the girder flange with slope of 100mm vertical: 5 mm horizontal.*

The role of the inclination of the girder flange-deck slab panel joint/interface is described for single and double loads.

#### **Single load tests: Position at midspan or close to the joint/interface**

Fig. 5.9 shows the influence of the inclination of the joint when a single load was applied at the midspan or close to the interface. Although the interface/joint was not critical or governing the failure, the test results have shown a higher capacity for the tests performed on slab panels with straight edges than the ones with skewed edges. The only tests that do not fall in this category are test BB13 and 14. These tests were performed on the panel C with straight joints but gave a lower capacity than similar tests done on panel A and B with skewed joints. It is to be noted that both of these were the last tests to be performed on the panel C that had been substantially damaged due to previous tests and this probably had a negative effect on the ultimate capacity.

## Experimental Parametric Study

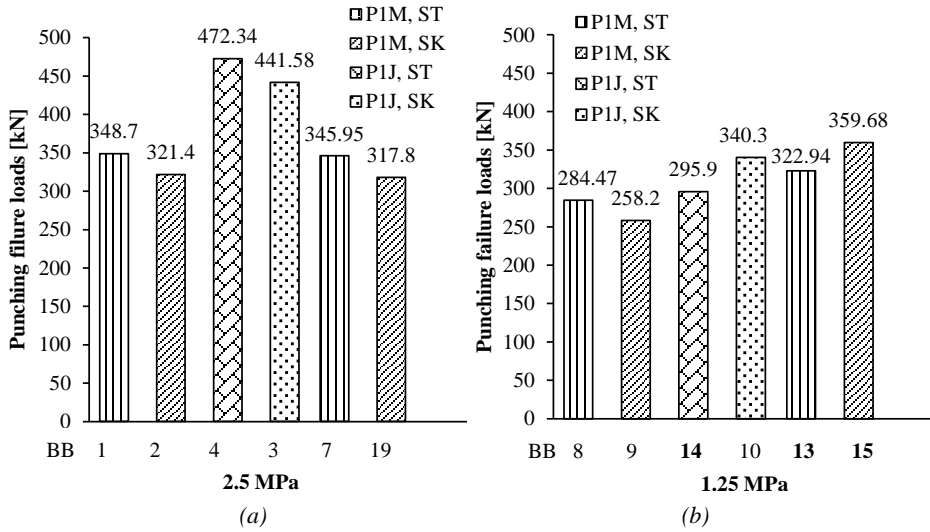


Fig. 5.9 Influence of the inclination of the joint on the ultimate bearing capacity when a single load acts on the deck slab (P1M and P1J): a) when TPL is 2.5 MPa; b) when TPL is 1.25 MPa.

### Double load tests: Position at midspan or close to the joint/interface

Fig. 5.10 shows no significant effect on the bearing capacity when a double load was applied at the skewed edged or straight edged panel for 1.25 MPa.

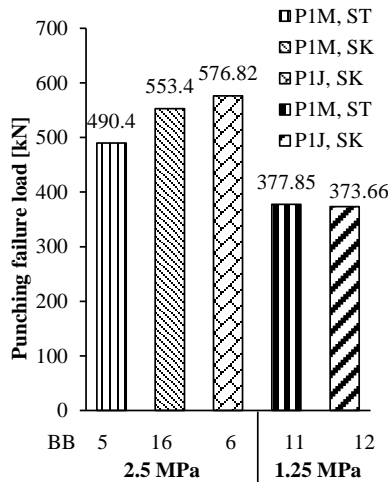


Fig. 5.10 Influence of the inclination of the joint on the ultimate bearing capacity when a double load acts on the deck slab (P2M and P2J).

BB5 (straight edged panel) showed a lower capacity than BB16 (skewed edged panel) although both were performed at midspan for a TPL of 2.5 MPa but with the difference of the panel position with regard to the overall bridge deck. If for double loads, the interior

panel is assumed to have more capacity (section 5.3.4), then this influence further becomes negligible considering that the interior panel was provided with skewed edges. It can be argued that the tests done with loads close to the interface show a higher capacity for the TPL of 2.5 MPa but a similar trend cannot be seen for 1.25 MPa. It has already been explained previously that the P2J tests show a comparable capacity with the P2M test cases because of the flexural action that dominated the behavior in the latter.

## Conclusion

It can be concluded from the test results that the inclination of the joint had no clear effect on the ultimate bearing capacity of the deck slab. For single loads, generally a higher capacity was achieved for tests done on straight edged panels but this was opposite in the double load tests. Anyhow, no failure occurred at the joint/interface so this does not need to be considered a governing factor.

### 5.3.7 Number of loads: Single or double

Fig. 5.11 shows the influence of applying a single or a double load on the ultimate bearing capacity of the bridge deck. Regardless of the position of the load, at midspan or close to the interface, or the TPL, double loads give a higher capacity as compared to single loads.

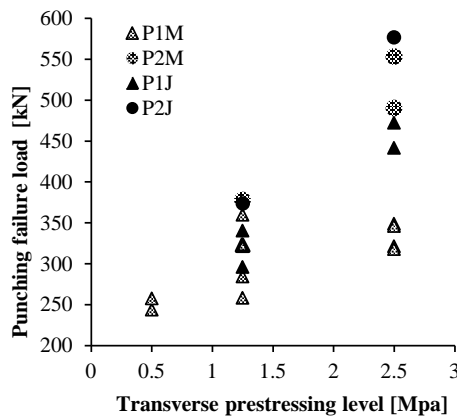


Fig. 5.11 Influence of applying a single or a double load on the ultimate bearing capacity.

However, the bearing capacity with double loads applied together (at 600 mm c/c) is less than double the bearing capacity of single loads. This could be because when two loads are applied close to each other, their stress fields overlap and a lesser volume of slab is available for stress distribution than when the loads are placed either as separate single loads or at larger distances and their individual stress fields do not overlap. A 20% reduction in the critical shear parameter is obtained when comparing the critical shear

parameters (calculated as per Eurocode 2, section 2.2.3) of double loads placed at 600 mm c/c with twice the critical shear parameter of a single load.

In UK HA BD81/02, the punching shear capacity  $P_{ps}$  is multiplied by a factor of 0.65 when a deck is subject to axle loading, either two wheels on one slab or two wheels on adjacent axles. The ultimate predicted wheel load,  $P_{pd}$  is taken as  $P_{pd} = 0.65P_{ps}$  as given in Eq. 2.13 in Chapter 2 ( $P_{pd}/P_{ps} = 0.65$ ).

Kirkpatrick et al. (1984) carried out tests on a 1/3<sup>rd</sup> scale M-beam bridge with a reinforced concrete deck slab and applied both single and double loads<sup>9</sup> at the midspan. For smaller span<sup>10</sup> deck slab panels, there was no difference between the capacities of the single and double loads. However, for larger span<sup>11</sup> deck slab panels, the capacities observed in the double load tests ranged between 0.65 and 0.72 times that of twice the capacities observed in single load tests ( $P_{double}/2P_{single} = 0.65-0.72$ ).

In the current study, the bearing capacities obtained by applying double loads at 600 mm c/c are 0.72 and 0.76 times that of twice the capacities for single loads with TPLs of 2.5 and 1.25 MPa, respectively ( $P_{double}/2P_{single} = 0.72-0.76$ ). Considering that the deck slab is transversely prestressed, the ratio of the capacity of single and double loads are comparable with those of Kirkpatrick et al. (1984).

### 5.3.8 Size of the loading plate

A smaller loading area is found to reduce the shear capacity in literature. The size of the loading plate was 200×200 mm in most of the experiments since the wheel print area in load model 1 of NEN-EN 1991-2 is 400×400 mm. For one test, the loading plate size was changed to Eurocode Super single wheel tire C, i.e. a rectangular tire print of 115×150 mm size (1:2 scale) having a smaller surface area as compared to the typical 200 mm square size (Fig. 5.12).



Fig. 5.12 Loading plates used in the tests.

<sup>9</sup> Equivalent to a wheel on each of the two axles of HB bogie (UK HA BD 37/01 2001) spaced at 1800 mm c/c (when scaled down to 1:3 gives 600 mm c/c).

<sup>10</sup> 500 mm c/c of supporting girders.

<sup>11</sup> 666 mm c/c of supporting girders.

## Experimental Parametric Study

Fig. 5.13 shows the effect of the size of the loading plate on the bearing capacity. It can be observed that although a lower ultimate load is achieved for 115×150 mm, the effect is not significant. This is further investigated numerically in Chapter 7 by using several sizes of loading areas.

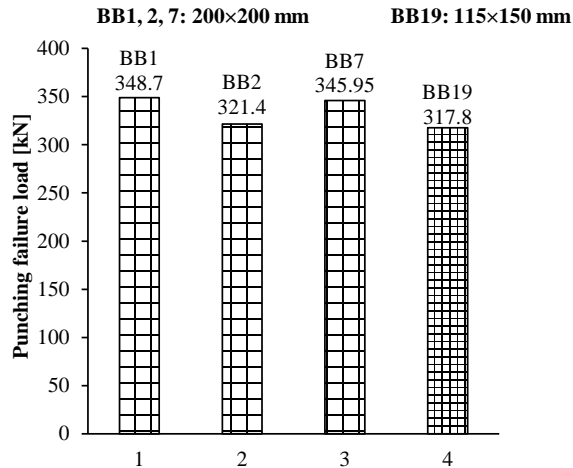


Fig. 5.13 Effect of the size of the loading plate on the ultimate bearing capacity.

### 5.3.9 Influence of previous damage to the deck slab panel

Tests BB12 conducted on slab panel A and BB13 and 14 conducted on slab panel C showed a lower than expected bearing capacity. These tests were the last ones to be carried on the respective deck slab panels leading to the conclusion that the damage to the deck slab due to previous tests and the close proximity of the position of these tests to the damaged area led to a reduced bearing capacity of the deck slab panel.

## 5.4 Summary and conclusions

The main results from the parametric study can be summarized as follows:

- The transverse prestressing level has a positive effect on the ultimate bearing capacity and the cracking loads are also higher for higher TPLs. Therefore, the behavior of a bridge deck with regard to both serviceability and ultimate limit states can be improved.
- For single loads acting close to the interface (P1J), a higher capacity was observed as compared to single loads at midspan of a deck slab panel (P1M). However, for double load tests at midspan (P2M), the flexural punching behavior increased the capacity almost to the level of double load interface tests (P2J).

## Experimental Parametric Study

- A higher punching shear capacity is observed when the deck slab is loaded directly above a prestressing duct.
- For single loads, no difference was observed between capacity of exterior and interior panels. For double loads, a higher capacity was observed. Since the number of tests performed on the interior panel is rather small, no clear relationship between the bearing capacity of interior and exterior deck slab panels for the analyzed load cases can be determined. The test results show that there was no effect of the longitudinal position of the load on the ultimate bearing capacity.
- The skewness of the joint is not critical in any of the tests and does not appear to have much influence on the punching shear capacity.
- Double loads give a higher capacity as compared to single loads regardless of the position of the load, at midspan or close to the interface, or the TPL.
- A factor of 0.7 can be used when deriving the bearing capacity of prestressed decks with double loads using twice the capacity of single loads, i.e.,  $P_{double} = 0.7 \times 2P_{single}$ , provided the loads comply with the Eurocode Load Model 1 (NEN-EN 1991-2:2003).

It can be concluded that there is a need to expand the parametric study to further investigate the influence of some important parameters, like the size of the loading plate, the relationship of the transverse prestressing level with the ultimate bearing capacity and the role of compressive membrane action, the influence of the panel position with regard to the overall deck (exterior or interior) etc. Also, the influence of a variation in material strength and the size effect need to be investigated as they could not be studied experimentally due to huge costs involved in construction of more specimens. Therefore, a finite element approach will be employed to study the in-depth behavior of the bridge deck model.

## Experimental Parametric Study

# **CHAPTER 6**

## **Numerical Model - Finite Element Analysis**

This chapter includes the description of a nonlinear finite element analysis of a 3D solid bridge model. Eight typical test cases from a total of 19 experiments have been simulated and the results are presented. A comparison with the experimental results has also been made and satisfactory results are obtained that validate the finite element model.

## **6.1 Introduction**

One of the main objectives of the numerical part of this research was to develop a finite element model that efficiently simulates the experimental behavior of the bridge tested in the laboratory. In this chapter, the load-deflection behavior, ultimate loads and mode of failure, the cracking pattern and cracking loads, stress distribution, and the compressive membrane action developed in the finite element bridge deck model are discussed. The results from the numerical investigation are later compared with the experimental results to validate the model. Such a numerical study will encourage engineers to use finite element analysis as a tool to analyze existing and new structures.

## **6.2 Finite Element Analysis**

This section introduces the software used for the finite element analysis and gives an overview of the bridge model.

### **6.2.1 TNO DIANA 9.4.4 finite element software**

Over the years finite element modeling of structures has proven to be an important analysis and design tool for engineers. In this research, an attempt has been made to construct and analyze the 1:2 scaled bridge model tested in the laboratory with the DIANA 9.4.4 software package. DIANA is a multi-purpose finite element program developed at the Department of Computational Mechanics at the TNO Building and Construction Research in the Netherlands and is being used by engineers all over the world. It is equipped with extensive material libraries and analysis procedures such as linear static, nonlinear, dynamic, Euler stability, potential flow, nonlinear dynamic analysis etc., and gives optimum solutions with the help of its powerful solvers.

The pre-/post processor used for the finite element model in this research is Midas FX+ (3.1.0) for DIANA. It has a graphical user interface which enables the user to build geometry of complex models, generate an appropriate mesh and assign basic material properties, boundary conditions and loads. The pre-neutral file is then exported to the DIANA mesh editor for assigning properties specific to the type of the analysis procedure being employed. The type of the analysis procedure commands are then checked and run via the command file. Once the analysis is complete, the post-neutral file is then imported by FX+ and the results are extracted in either tabular or any other post processing form (contour, vector etc.). The analysis results can also be expressed graphically within FX+ or can be exported to Microsoft Excel.

## 6.2.2 Overview of the bridge model

A 3D solid finite element bridge model, 2ELEM, was constructed in DIANA and two kinds of study were performed: a) Basic test case analysis; b) Parametric analysis.

### Basic test case analysis

The basic test cases include:

- Single point load acting at mid span of slab panel, P1M.
- Single point load acting close to the girder flange-slab interface/joint, P1J.
- Double point loads at 600 mm c/c acting at mid span of slab panel, P2M.
- Double point loads at 600 mm c/c acting close to the girder flange-slab interface/joint, P2J.
- Notations: M = Midspan, J = Joint/Interface.

Table 6.1 shows the test cases that have been simulated as part of the basic analysis. Four types of load cases have been analyzed for two levels of transverse prestressing (TPL).

Table 6.1 Test cases analyzed by DIANA.

#	Test Case	Transverse Prestressing Level (TPL)	
		1.25 MPa	2.5 MPa
1.	P1M	BB08, BB09	BB01, BB02, BB07
2.	P1J	BB10	BB03, BB04
3.	P2M	BB11	BB05, BB16
4.	P2J	BB12	BB06

### Parametric analysis

The parametric analysis is described in detail in the next chapter. Important parameters, the role of which has been investigated, are the transverse prestressing level, the type and the position of the load, the fracture energy, the concrete strength, the presence of ducts, the size factor etc. along with some finite element modeling parametric analyses like the mesh sensitivity, the step size and the nonlinear material model etc.

## 6.2.3 Modeling assumptions and limitations

A nonlinear analysis was performed for the deck slab panels, however, the girders and transverse beams were analyzed linearly (no reinforcement was provided) since it was known from the experiments that they do not show any nonlinear behavior. For cases where the load was applied very close to the interface (110 mm c/c distance between the loading

plate and the interface in tests BB3 and 4), the nearby flange of the loaded interface was analyzed nonlinearly since the linearity of the girders led to an unrealistic high capacity in such cases. The interface between the girder flange and the deck slab panel was not modeled since it was proven not to be critical experimentally and failure always occurred in the span of the slab. Only a limited central region of the bridge deck was constructed with a fine element mesh size and the remaining area of the deck slab and the girders was modeled with a coarse element mesh size. Ducts were only provided in the fine mesh zone of the bridge deck since only that portion was loaded locally and it was assumed that the remaining portion of the bridge deck without any ducts would not affect the load-deflection behavior or other characteristics like the cracking pattern etc. Providing a fine and coarse mesh combination of element size and limited number of ducts in the bridge deck led to a smaller number of elements and hence less computing time. The prestressing was applied as an external pressure on the bridge deck slab and the transverse beams. Section 6.4 details the setup of the finite element bridge model and further explains the aforementioned assumptions.

### **6.3 Modeling the material behavior**

Before modeling a structure in a finite element program, it is essential to understand its material behavior so that adequate constitutive relationships (stress-strain relations) can be applied to get reasonable results. The main material to be studied in this research is concrete with steel being a secondary material. In cases where failures are dominated by concrete, the material nonlinearity occurs either due to cracking of concrete in tension or plasticity of concrete in compression. A tensile failure is defined by major cracking and the loss of concrete tensile strength normal to the crack direction, whereas a compression failure is defined by the development of many small cracks (crushing) and the loss of concrete compressive strength.

The behavior of concrete becomes more complex when there are several components in a structure with varying strengths and subjected to different kinds of loading. The correct assessment of failure depends upon proper modeling of the constitutive behavior. In terms of finite element analysis, that means: *Proper selection of a material model that will explain the concrete stress-strain behavior till failure.* The more complicated a material model is, the larger the number of variables involved that should be based on material test results but can be selected based on approximations and engineering judgment.

### 6.3.1 Cracking model for concrete

DIANA offers a wide range of cracking models to simulate the constitutive behavior of concrete. A crack can be modeled as a discontinuity between adjacent elements, known as a discrete crack but this approach suffers from several drawbacks as pointed out by Rots (1989). Another way is to model a crack as a continuum, known as a “smeared” crack originally proposed by Rashid (1968). According to the smeared crack approach, the crack opening is smeared over the element and represented by means of crack strain (Fig 6.1) which is a function of the relative displacement of the crack surfaces and some length parameter over which this displacement is distributed known as the *crack band width* (Mosalam et al. 1997).

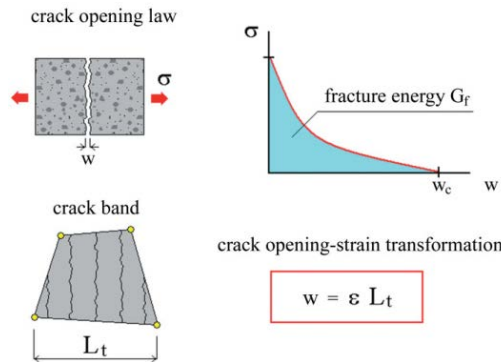


Fig. 6.1 Smeared crack model for tensile behavior of concrete (Strauss et al. 2003).

There are two common ways to model cracking in continua. Either by decomposing the strain into an “elastic strain and inelastic (crack) strain” or a “total strain” based approach. The former approach was introduced by Litton (1974) and has been used by a number of researchers (Bazant and Gambarova 1980, de Borst and Nauta 1985, Riggs and Powell 1986, Rots 1988). A decomposed strain model, such as multiple fixed crack, allows for elasticity or plasticity for the portion in between the cracks and a separate treatment of softening for the cracked portion and can also be combined with creep, shrinkage, temperature and maturity effects. Also, a combination of a multiple fixed crack model for tension and a plasticity model like Drucker-Prager in compression is possible. The basic parameters that need to be defined for cracking are the tension cut-off, tension softening and shear retention parameters. Rots (2002) points out that multiple fixed cracks are attractive from a physical and conceptual point of view but the algorithmic features are quite complex and may lead to numerical instability. Moreover, too many parameters have to be input in the model and no suitable criteria maybe available to select values for these functions.

On the other hand, the total strain crack model developed by Feenstra et al. (1998) is a rather simplified approach. Stresses are evaluated in the directions given by the crack directions and the tensile and compressive behavior of concrete is described by one stress-strain relationship, i.e. the phenomena of softening or stiffening in tension and the non-linear behavior and crushing in compression are combined. Therefore, the total strain crack model cannot be combined with other constitutive models (like plasticity models) which is in sharp contrast with multiple fixed crack model. Also, only orthogonal cracks can be modeled because the model uses stress-strain relations. The main advantage of the total strain cracking model is that a smaller number of parameters are involved, and since the model is expressed in terms of stress and strain relations, it is an easier choice for practicing engineers. The tension softening, compression behavior and shear behavior parameters define the cracking. Rots (2002) observes that the total strain crack model is attractive from an algorithmic point of view, is purely explicit and does not require internal iterations. The stress is directly computed from the strain after updating a number of internal state variables. Local convergence problems are also not present. Hence for modeling of cracking in this research, a total strain crack model is selected.

Two types of total strain crack models are available: *Fixed and Rotating crack models* that differ from each other in the post-cracking phase. According to the fixed crack model, the principal axes of orthotropy remain fixed in the post-cracking phase and shear retention parameters are required, whereas according to the rotating crack mode, the principal axes of orthotropy rotate coaxially with the principal strains during the crack propagation and an implicit shear term is used instead of defining the shear parameters separately. In this research, a rotating crack model is used since it provides less stress-locking and is ideal to deal with localized cracking as compared to a fixed crack model.

### **Rotating crack model**

The input for rotating crack model requires basic properties like the Young's modulus, Poisson's ratio, etc. and parameters defining tensile (cracking) and compressive (crushing) behavior.

#### Basic properties

DIANA can derive the basic properties like Young's modulus  $E$ , Poisson's ratio  $\nu$ , tensile strength  $f_t$ , Mode-I fracture energy  $G_f^I$  and compressive strength  $f_c$  from the Model Code 1990 regulations for a specific grade and aggregate size of concrete. Alternatively, basic properties can be used as input directly.

Tensile behavior

For the tensile behavior, one may choose a predefined function (Fig. 6.2) or customize it via a user-supplied subroutine. Depending upon the softening function chosen, the user has to select the input tensile parameters. For tensile softening, an exponential softening function, HORDYK (Cornelissen et al. 1986, Hordijk 1991) has been used in this research as recommended by RTD 1016 (2012).

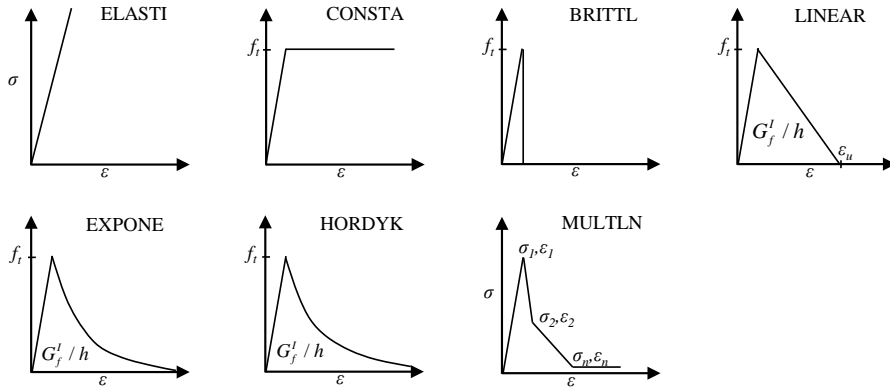


Fig. 6.2 Predefined tension softening for total strain crack model (DIANA 9.4.4 user’s manual 2012).

Compressive behavior

For the compressive behavior, one can either use a predefined function (Fig. 6.3) or customize the compressive behavior via a user-supplied subroutine. An elastic-perfectly plastic (ideal) function CONSTA was chosen for the modeling of the concrete compressive behavior. Other models have also been investigated in the parametric analysis in chapter 7.

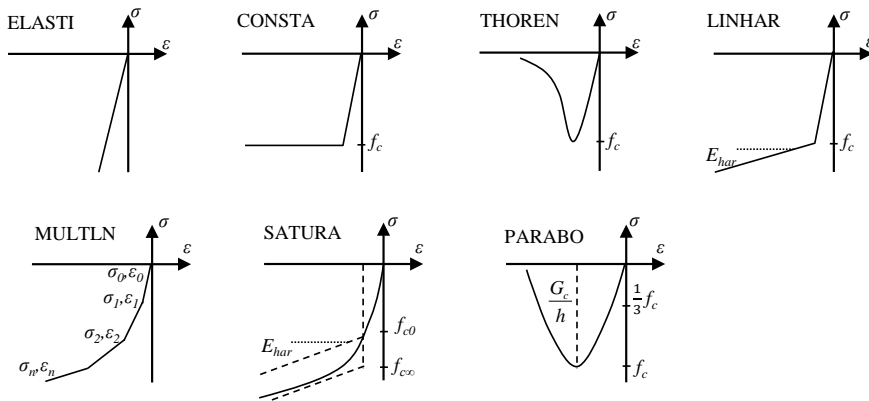


Fig. 6.3 Predefined compression behavior for total strain crack model (DIANA 9.4.4 user’s manual 2012).

### 6.3.2 Modeling of steel behavior

DIANA offers various material models for simulating the behavior of steel reinforcement. Generally a uniaxial stress-strain relationship assuming an elastic-perfectly plastic response (Fig. 6.4) for the steel is satisfactory for finite element analysis (Hon 2003). A von Mises yield criterion was used to model the reinforcement in the deck slab panels with a poisson's ratio of 0.3.

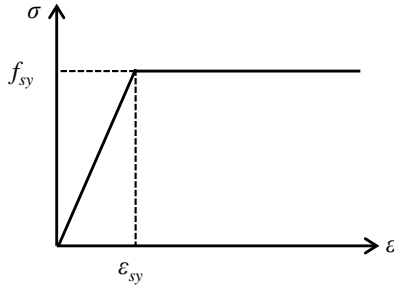


Fig. 6.4 An elastic-perfectly plastic stress-strain relationship for steel.

### 6.3.3 Material properties input

The basic properties used in the finite element model are given in Table 6.2. The concrete compressive and tensile strengths used as input in the finite element model are taken from the laboratory tests performed on cube specimens and converted to cylinder strengths. The basic material properties have been discussed in detail in section 3.2. Other than those, a typical value of 0.2 for Poisson's ratio is used. The fracture energy,  $G_f$ , defined as the amount of energy dissipated to create one unit area of crack, is calculated by using the Model Code (1993 and 2012). Both versions of the code differ drastically in their formulae for the calculation of the fracture energy. In Model Code 90 (1993), the fracture energy (Eq. 6.2) is a function of the maximum aggregate size ( $d_a$ ) and the concrete compressive strength ( $f_{cm}$ ).

$$G_f = G_{f0} \left( \frac{f_{cm}}{10} \right)^{0.7} \text{ Nmm / mm}^2 \quad (6.2)$$

where,

$$\begin{aligned} & 0.025 \quad \text{for } d_a = 8\text{mm} \\ G_{f0} = & 0.030 \quad \text{for } d_a = 16\text{mm} \\ & 0.058 \quad \text{for } d_a = 32\text{mm} \end{aligned}$$

In the Model Code 2010 (fib 2012), the fracture energy is a function of  $f_{cm}$  alone.

$$G_F = 0.073 f_{cm}^{0.18} \text{ Nmm} / \text{mm}^2 \quad (6.3)$$

Using MC90, for a mean compressive strength of 65 MPa and a maximum aggregate size of 20 mm (as used in the bridge deck model), the fracture energy is calculated as 0.135 N/mm while, using the MC2010 gives a value of 0.155 N/mm. An approximately average of the two values 0.15 N/mm has been used in the current finite element study for the nonlinear properties of the bridge deck slab.

Table 6.2 Material input data.

Material	Component	$f_{cm}$	$f_{ctm}$	$f_{sy}$	$E$	$\nu$	$G_f$
		[MPa]	[MPa]	[MPa]	[MPa]		[N/mm]
Concrete	Girders	75	6.31	-	41000	0.2	-
	Slab	65	5.41	-	39000	0.2	0.15
	Transverse beams	65	5.41	-	39000	0.2	-
Steel	Slab	-	-	525	200000	0.3	

## 6.4 Setup of the finite element model

In this section, the setup of the bridge model in DIANA is explained. Important considerations while modeling include the selection of the element type and mesh size, material properties, boundary constraints, loading and solution procedure. The general finite element 3D model of the bridge deck is shown in Fig. 6.5 and Fig. 6.6.

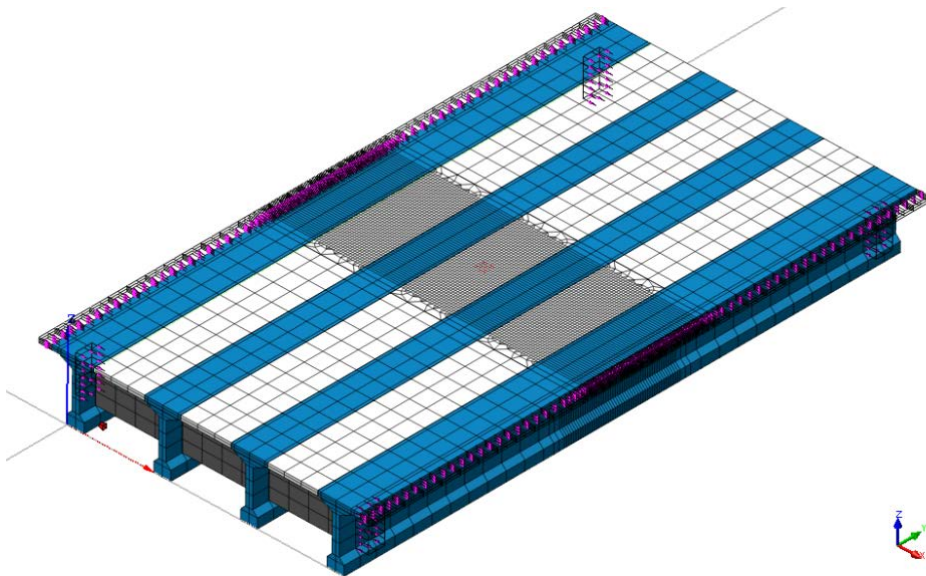


Fig. 6.5 3D solid finite element bridge model for the basic test case analysis.

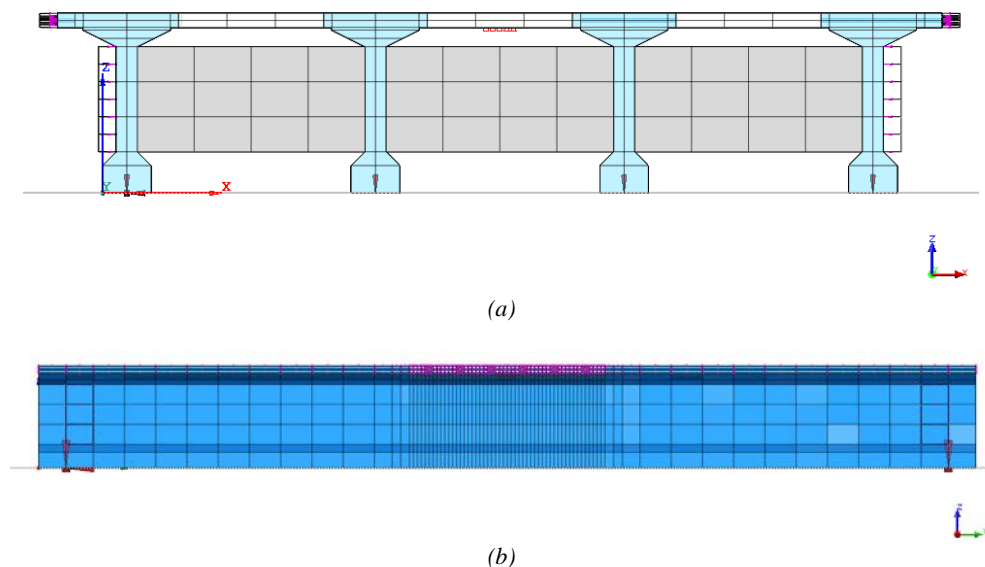


Fig. 6.6 The finite element bridge model for the basic test case analysis; a) The transverse cross-section; b) The longitudinal view.

## 6.4.1 Concrete: Element type and mesh

### Element type

DIANA offers a wide range of elements for structural modeling. The bridge model was constructed as a 3-D finite element model and solid elements were used for his purpose. Solid elements are general purpose elements but result in a large system of equations. For the same model and mesh size, 3D solid elements require quite a lot of computational time and storage memory as compared to 2D elements (plain stress/strain or shell elements etc.).

Solid elements have three important properties:

- The geometry of a solid element is defined in three directions.
- The stress situation is three dimensional.
- Arbitrary loading can be applied.

Following solid elements are used for modeling the bridge components:

- CHX60 – brick, 20 nodes
- CTP45 – wedge, 15 nodes

## Numerical Model – Finite Element Analysis

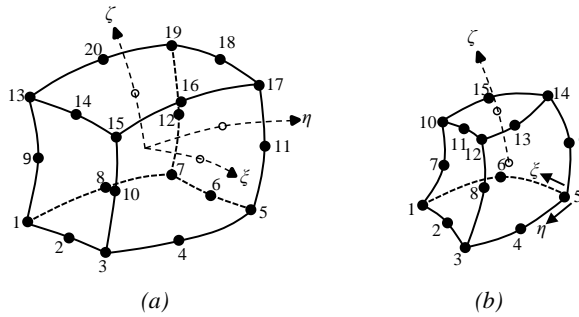


Fig. 6.7 Solid elements used in the model (adapted from DIANA user's manual 2012): a) CHX60 - brick, 20 nodes; b) CTP45 - wedge, 15 nodes.

The most commonly used element in the model is CHX60 (Fig. 6.7a) which is a 20 node, isoparametric, solid brick element based on quadratic interpolation and gauss integration. A  $3 \times 3 \times 3$  default integration scheme is used in the analysis. The other type of element used in the modeling is CTP45 (Fig. 6.7b) which is a 15 node, isoparametric solid wedge element based on quadratic interpolation and numerical integration. The default scheme of 4-point integration in the triangular domain and a 2-point integration in the  $\zeta$  direction is employed in the model.

### Mesh size

Fig. 6.8 shows the 2 ELEM finite element bridge model with two types of mesh; coarse and fine.

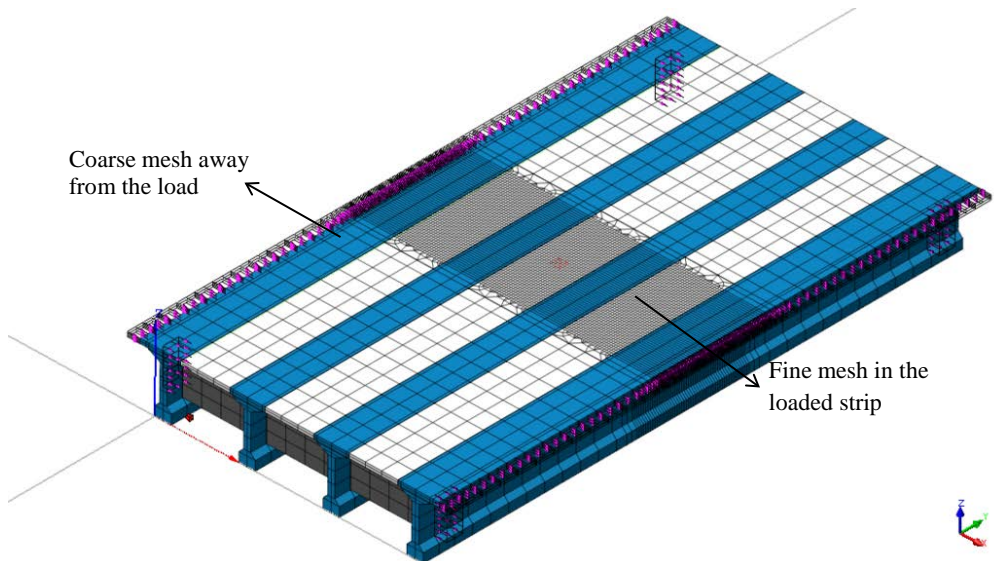


Fig. 6.8 Mesh size used in the 3D finite element bridge model.

Away from the loaded area, a coarse mesh was provided and close to the loading area, a fine mesh was provided for a strip of 2500 mm. A 50 mm element size was found to be the most appropriate after carrying out a mesh sensitivity analyses (section 7.3.1) and comparing the time elapsed for the simulation. An element size smaller than 50 mm increased the number of total elements to a large degree (more than 60 thousand) and hence enhanced the computational effort and storage requirements. The 2ELEM model shown in Fig. 6.8 has been used throughout the finite element study.

### Provision of transverse ducts in the model bridge deck

Fig. 6.9 shows the model bridge deck with the transverse ducts in the fine mesh area.

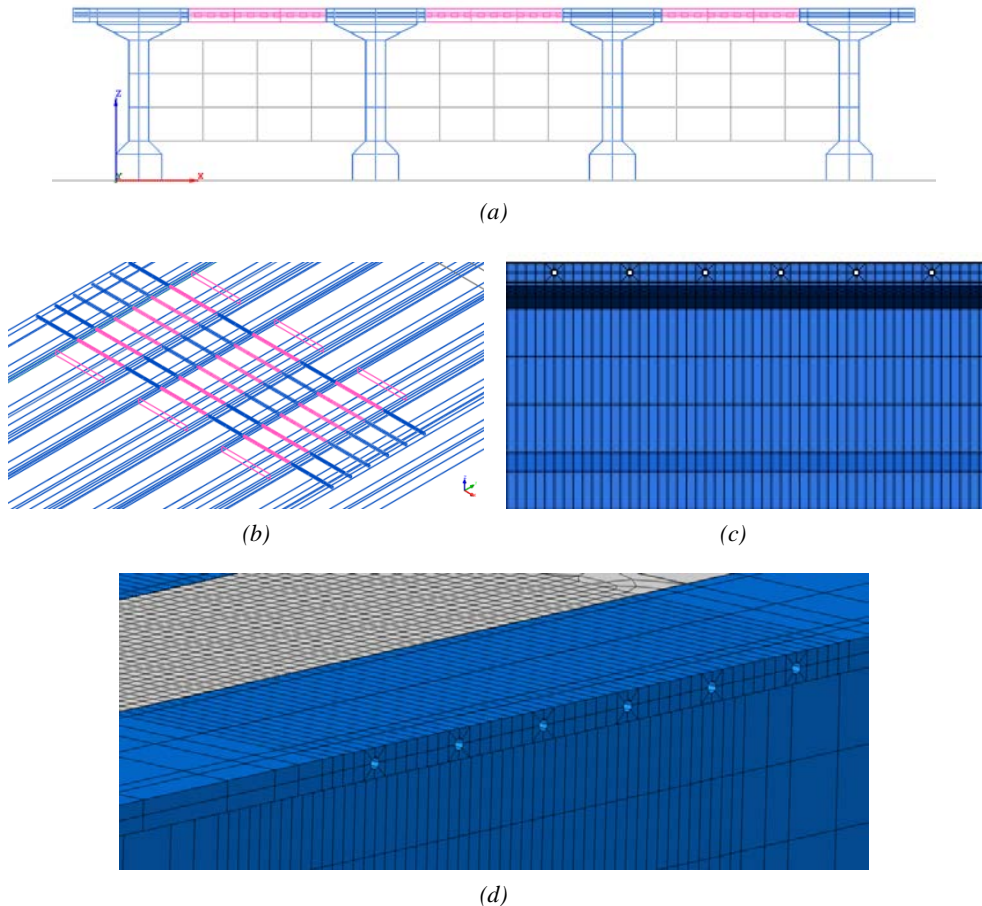


Fig. 6.9 Ducts in the bridge deck model: a) Cross section wire-frame view showing the transverse ducts in the girder flanges and the deck slab panels; b) 3D wire frame view of the transverse ducts; c) Longitudinal view of the fine mesh zone showing the ducts; d) 3D solid view of the fine mesh zone of the bridge model showing the ducts.

Six hollow ducts at 400 mm *c/c* were provided in the transverse direction of the bridge deck. Since the loads were always applied in the fine mesh zone and it was expected that the presence of the ducts would affect the bearing capacity of the bridge deck, the ducts were limited to this central region. The rest of the bridge deck did not have any ducts and it was assumed that this simplification would not affect the behavior of the loaded area. Provision of ducts in the loaded region also meant that the composed elements could not be provided in the transverse strips where the ducts were present.

### Composed elements for determination of compressive membrane forces

For extraction of element forces from solid elements, special composed elements were used in the model as shown in Fig. 6.10. The main application of composed elements is in the post processing of analysis results. They have no mechanical properties of their own.

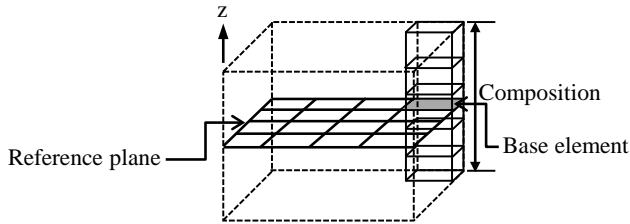


Fig. 6.10 Base elements in a structural composition (adapted from DIANA user's manual 2012).

DIANA 9.4.4 specifies a composed element via a base element and a composition of regular solid elements. The base element layer forms a reference plane for which the generalized moments and forces are calculated by integration in the local *z* direction over the elements in the composition of each base element. The selection of the type of base element depended on the type of the solid elements in the composition.

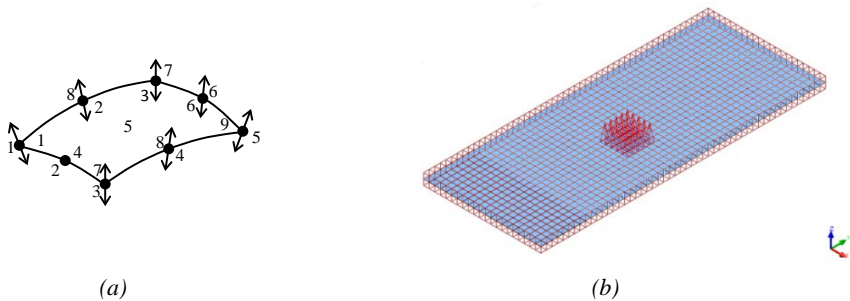


Fig. 6.11 Composed elements: a) CQ8CM base element for CHX60 brick (adapted from DIANA user's manual 2012); b) Base element layer provided within the solid element composition surrounding the loaded area in a typical slab.

The solid elements in the loaded area were CHX60 bricks, so for composed elements CQ8CM was used as recommended by DIANA user’s manual (2012). The CQ8CM element is an 8 node, quadrilateral curved base element and can only be provided where CHX60 elements are used in a composition (Fig. 6.11). The default integration scheme is 3×3 which matches that of CHX60 element. The thickness of the base element CQ8CM was given equal to the thickness of the structural composition, i.e. the thickness of the deck slab (100 mm).

Fig. 6.12 shows how the composed elements were provided in the finite element bridge model. Since these elements were used for the calculation of compressive membrane forces, they were only applied in the area of interest i.e. the loading area and its surroundings minus the area having ducts because composed elements can only be provided in structured meshes (DIANA user’s manual 2012).

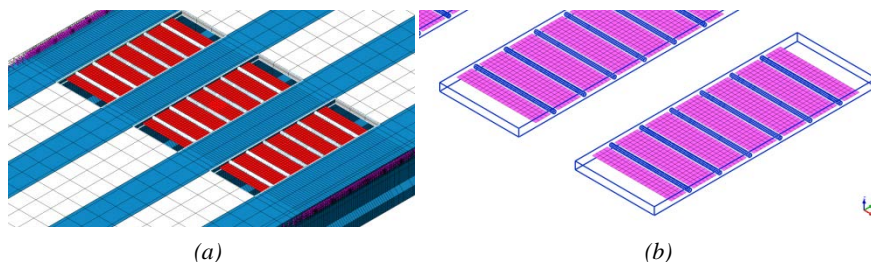


Fig. 6.12 Composed elements provided in the FE bridge model fine mesh strip: a) 3D view of the composed element layer (can be seen in red in the online version of this thesis) provided within the fine mesh area of the deck slab; b) 3D wire framing view of the composed elements in the fine mesh slab strips extracted from the bridge deck model.

## 6.4.2 Steel reinforcement

The steel reinforcement in the deck slab panels was modeled as a reinforcement grid embedded in the solid elements (Fig. 6.13). The embedded reinforcement grid adds stiffness to the finite element model without requiring any special interface modeling. No space is required by the embedded reinforcement in the *mother* structural elements.

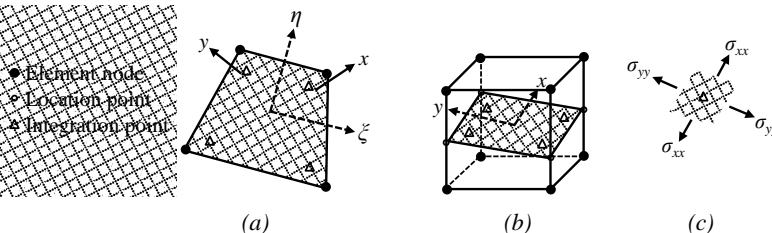


Fig. 6.13 Embedded grid reinforcement (adapted from DIANA 9.4.4 user’s manual 2012): a) Particle in 2D; b) Particle in solid; c) Stresses.

The reinforcement present in the model bridge deck was modeled with a horizontal grid ( $\rho_x$  and  $\rho_y$ ) having thickness in two directions at the top and the bottom of the deck slab and a vertical grid ( $\rho_z$ ) with thickness in one direction (Fig. 6.14). Basically the thickness of the reinforcing bars is smeared out per unit length of the embedded grid. The top and bottom horizontal grid consists of a thickness of 0.1413 mm ( $\Phi 6 @ 200$  mm c/c) and 0.113 mm ( $\Phi 6 @ 250$  mm c/c) in the x and y directions respectively. The vertical grid consists of a thickness of 0.1413 mm in the z direction ( $\Phi 6 @ 200$  mm c/c).

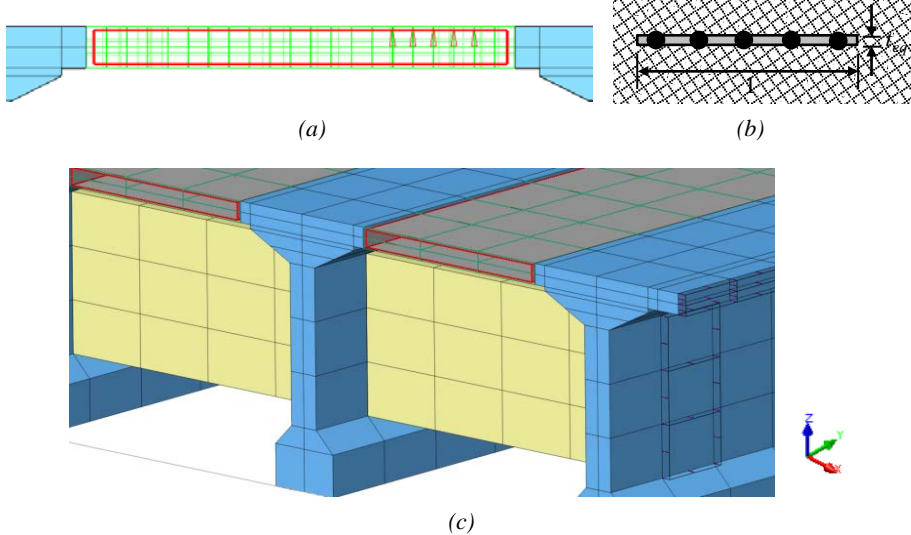


Fig. 6.14 Embedded grid reinforcement in the deck slab panel: a) Cross section of the reinforcement grid (in red) provided in the deck slab panels; b) Equivalent thickness of the grid (DIANA user's manual, 2013); c) 3D view of the reinforcement grid (in red) provided in the deck slab panels.

### 6.4.3 Material model input

The nonlinear material properties given to the model bridge deck slab are summarized in Table 6.3. For the girders and the transverse beams, only the basic material properties were used as input since they were generally limited to the linear range in the analysis (Table. 6.2).

Table 6.3 Nonlinear material properties input (material model) used for the model deck slab.

Component	Basic properties	Material model
	Refer to	
Girders & Transverse beams	Table 6.2	-
Slab	Table 6.2	Concrete: Total strain crack rotating model 1. CONSTA 2. HORDYK Steel: Von Mises plasticity; VMISES

### 6.4.4 Applied loads and support constraints

Fig. 6.15 shows the loading on the bridge deck and Fig. 6.16 shows the applied boundary constraints to the girders.

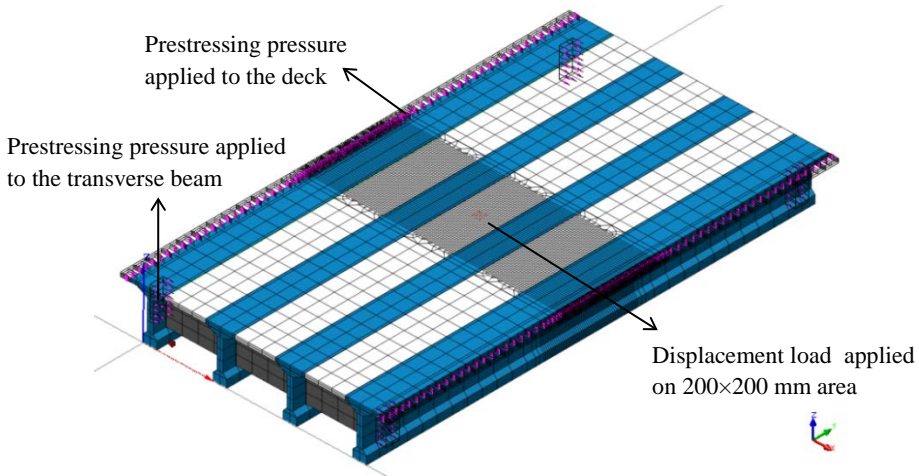


Fig. 6.15 Loading on the 3D bridge model.

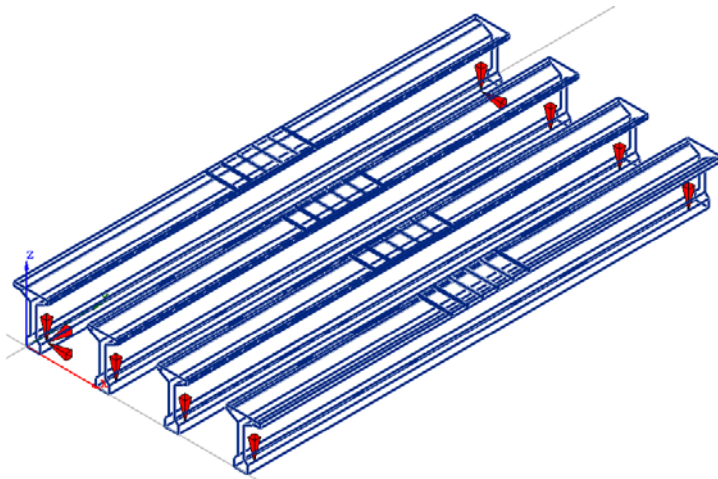


Fig. 6.16 Boundary constraints applied to the 3D bridge model (wire-framing view of the girders).

A displacement controlled load was applied over an area of 200x200 mm simulating the wheel print impression on the deck slab. Each node of all the elements falling under that area was given a specific incremental displacement. Because the prestressing bars were unbonded and generally the stress remained constant during the experiments, it was deemed reasonable to model the prestressing force as an external load or pressure whose magnitude equaled the required transverse prestressing level in the deck for a particular analysis.

### 6.4.5 Solution method

Both physical and geometrical nonlinearities were applied to the system. Composed elements were generated while giving the analysis commands. An incremental-iterative procedure was used for the nonlinear analysis. A displacement controlled incremental loading was applied and the Modified Newton Raphson method was used for the solution (Fig. 6.17). The advantage of using the Modified Newton Raphson method is that it is more stable and is able to converge in some cases where the Regular Newton Raphson fails. It only evaluates the stiffness relation at the start of the increment and the prediction is always based on a converged equilibrium state. Usually it requires a larger number of iterations but every iteration is faster than the Regular Newton Raphson. The prestressing load was applied to the bridge deck in a single step. After that the displacement load was applied with a step size of 0.1 mm unless the solution diverged, in which case the load step was reduced to 0.05 mm. Since the applied load was displacement controlled, the default force and energy based convergence criteria was employed, whichever was achieved first. The convergence tolerance for energy and force norms was set to 0.0001 and 0.01 respectively.

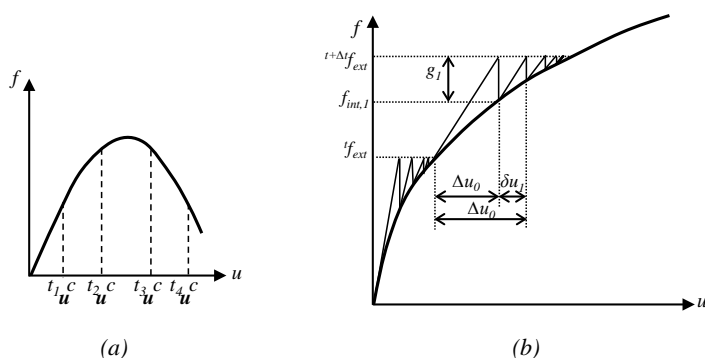


Fig. 6.17 Incremental iterative solution procedure: a) Incremental displacement control method; b) Modified Newton Raphson iteration method (adapted from DIANA user's manual 2012).

### 6.4.6 Special finite element bridge model with a nonlinear girder flange

As explained in section 6.2.3, for most cases the deck slab was analyzed nonlinearly while the girders and the transverse beams remained in the linear range. The only exceptions to this were the PIJ simulations in which the load was placed too close to the interface (test BB3 and 4 with load at 110 mm c/c). A special FE bridge model (Fig. 6.18) was developed in which the flange of the girder flange adjoining the loaded interface was analyzed as nonlinear. Similar nonlinear material model, as the one given to the deck slab panels, was assigned to the concrete material of the girder flange, i.e. a total strain crack rotating model (ROTAT) with HORDYK softening function in tension and CONSTA function in

compression. Table 6.4 shows the nonlinear material properties assigned to the concrete in the girder flange in this special finite element bridge model.

Table 6.4 Additional concrete properties used for the nonlinear girder flange model.

Material	Component	$f_{cm}$	$f_{ctm}$	$E_{cm}$	$\nu$	$G_f$
		[MPa]	[MPa]	[MPa]		[N/mm]
Concrete	Girders	75	6.31	41000	0.2	0.175

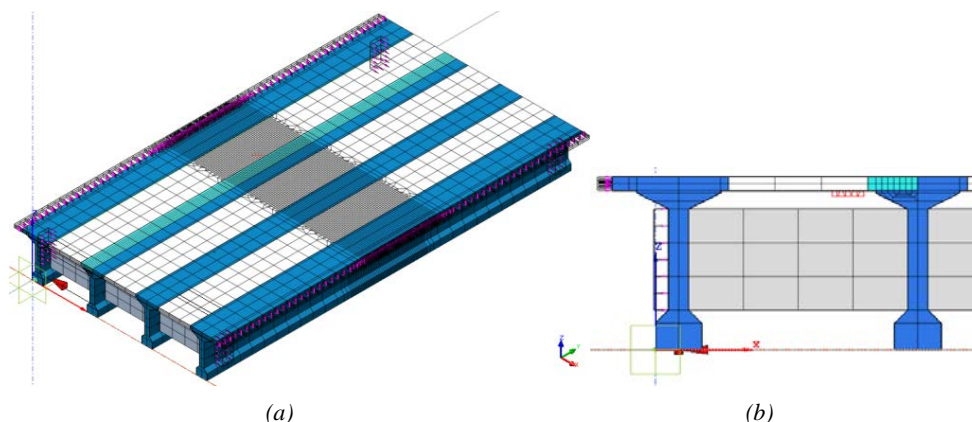


Fig. 6.18 3D solid finite element model with a nonlinear girder flange: a) 3D view; b) The cross-section of the bridge model showing load position with regard to the nonlinear girder flange.

## 6.5 Basic finite element analysis

This section describes the results of the basic finite element analysis simulating eight typical laboratory experiments carried out on the bridge model.

The notations used in the following sections are as follows: TPL = Transverse prestressing level, P1M = Single point load acting at midspan of the deck slab panel, P1J = Single point load acting close to the girder flange-slab interface/joint, P2M = Double point loads at the midspan of the deck slab panel, P2J = Double point loads acting close to the girder flange-slab interface/joint, ST = Straight joint, SK = Skewed joint, AD = Above the duct, BD = In-between the ducts.  $P_{FEA}$  = Finite element analysis ultimate load,  $S_{FEA}$  = Finite element analysis ultimate deflection,  $P_{CR,FEA}$  = Finite element analysis initial cracking load,  $P_T$  = Test ultimate load,  $P_{CR,T}$  = Test cracking load,  $P_{CRS,FEA}$  = FEA initial inclined shear cracking load, FMODE = Failure mode. Any other notation used is defined within the text.

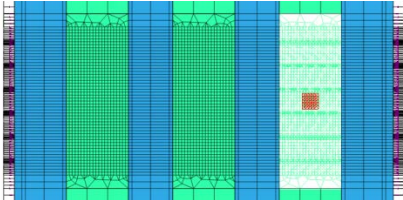
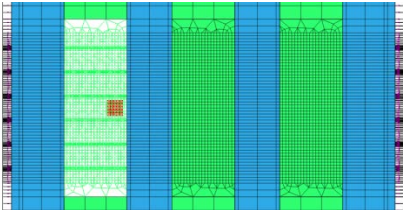
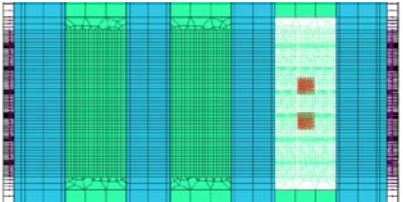
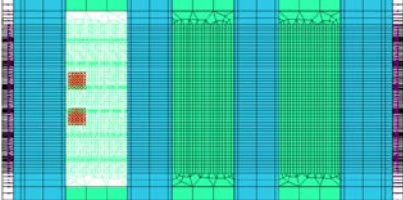
Table 6.5 and 6.6 show the test cases that were analyzed along with the loading geometry. The designation assigned to the test cases in Table 6.5 will be used throughout the discussion of the finite element results.

## Numerical Model – Finite Element Analysis

Table 6.5 Summary of the test cases analyzed.

No.	TPL [MPa]	Load type	Test position	Designation	Experiment
				Slab Panel-Load type and position	
1.	1.25	Single	Midspan (M)	A/C-P1M	BB8, BB9
2.	1.25	Single	Joint (J)	A/C-P1J	BB10
3.	1.25	Double	Midspan (M)	A/C-P2M	BB11
4.	1.25	Double	Joint (J)	A/C-P2J	BB12
5.	2.5	Single	Midspan (M)	A/C-P1M	BB1, BB2, BB7
6.	2.5	Single	Joint (J)	A/C-P1J	BB3, BB4
7.	2.5	Double	Midspan (M)	A/C-P2M	BB5, BB16
8.	2.5	Double	Joint (J)	A/C-P2J	BB6

Table 6.6 Loading applied to the bridge model for typical test cases.

No.	Load case	Displacement controlled load in plan
	Analyzed for both 1.25 and 2.5 MPa TPL	Shown as a square of 200 × 200 mm size
1.	P1M Load applied at the midspan of the deck slab panel.	
2.	P1J (linear flange model) for 1.25 MPa Load applied at 200 mm c/c from the deck slab – girder flange interface.  P1J (nonlinear flange model) for 2.5 MPa Load applied at 150 mm c/c from the deck slab – girder flange interface. The load could not be placed at 110 mm c/c like in the tests due to the mesh size.	
3.	P2M Load applied at the midspan of the deck slab panel.	
4.	P2J Load applied at 200 mm c/c from the deck slab – girder flange interface.	

### 6.5.1 Summary of analysis results

Just like the experimental results, the finite element results can also be distinguished based upon two modes of failure: Brittle punching (P1M, P1J and P2J) and flexural punching (P2M). The results are generally discussed based on either the mode of failure or the load type wherever it is necessary to do so. The important results of the basic analyses are summarized in Table 6.7.

Table 6.7 Summary of important analysis results.

No.	TPL	Designation	$P_{FEA}$	$S_{FEA}$	$P_{CR,FEA}$
	[MPa]		[kN]	[mm]	[kN]
1.	1.25	A/C-P1M	271.4	3.7	84.9
2.	1.25	A/C-P1J	300.7	2.6	83.7
3.	1.25	A/C-P2M	453.4	7.0	120.4
4.	1.25	A/C-P2J	454.9	5.0	116.4
5.	2.5	A/C-P1M	302.3	3.9	93.2
6.	2.5	A/C-P1J	429.9	5.05	107.1
7.	2.5	A/C-P2M	529.9	7.4	151.8
8.	2.5	A/C-P2J	537.1	5.2	165.2

### 6.5.2 Ultimate loads and mode of failure

The finite element and experimental ultimate loads with regard to the type of loading, position of the load and the transverse prestressing level (TPL) are collected in Fig. 6.19.

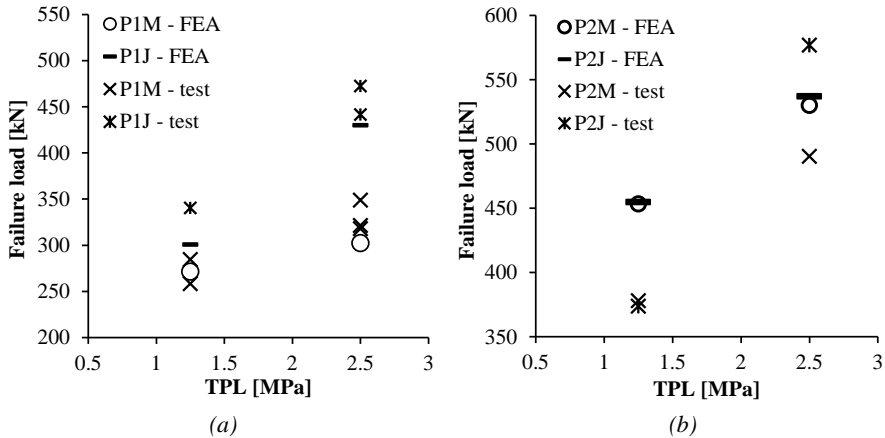


Fig. 6.19 Ultimate loads with regard to the transverse prestressing level obtained through basic finite element analyses: a) Single loads acting at midspan and close to the interface; b) Double loads acting at the midspan and close to the interface.

It can be observed from the numerical analysis that an increase of the transverse prestressing level has a positive influence on the ultimate bearing capacity and double loads gave a higher capacity as compared to single loads. All these FE simulations were

performed for the loads in-between the prestressing ducts (similar to the laboratory tests), hence the results represent a lower bound of the bearing capacity. Also, failure always occurred within the span of the slab in all the cases.

### Comparison with the experimental results

Table 6.8 compares the experimental and the finite element results.

Table 6.8 Comparison of finite element analyses and experimental ultimate loads.

Test BB.	TPL	Designation	$P_T$	$P_{FEA}$	Test FMODE	$P_T/P_{FEA}$
	[MPa]		[kN]	[mm]		
1.	2.5	C-P1M	348.7	302.3	Brittle punching	1.15
2.	2.5	A-P1M	321.4	302.3	Brittle punching	1.06
3.	2.5	A-P1J	441.6	429.9	Brittle punching	1.03
4.	2.5	C-P1J	472.3	429.9	Brittle punching	1.10
5.	2.5	C-P2M	490.4	529.9	Flexural punching	0.93
6.	2.5	A-P2J	576.8	537.0	Brittle punching	1.07
7.	2.5	C-P1M	345.9	302.3	Brittle punching	1.14
8.	1.25	C-P1M	284.5	271.4	Brittle punching	1.05
9	1.25	A-P1M	258.2	271.4	Brittle punching	0.95
10.	1.25	A-P1J	340.3	300.7	Brittle punching	1.13
11.	1.25	C-P2M	377.9	453.4	Flexural punching	0.83
12.	1.25	A-P2J	373.7	454.9	Brittle punching	0.82
				<b>Mean</b>		<b>1.02</b>
				<b>Standard deviation</b>		<b>0.11</b>
				<b>Coefficient of variation</b>		<b>0.11</b>

#### Brittle punching failure

When a single load was applied at the slab midspan (P1M) or when a single or double load was applied close to the interface (P1J and P2J respectively), brittle punching failure was observed in both the experiments and FE simulations. Generally the FEA results for brittle punching were conservative with the exception of the 1.25 MPa, P2J case where the test ultimate load (BB12) was found to be 0.82 times the FEA ultimate load. This test had failed at an unexpectedly lower load (section 4.3.4). For the 1.25 MPa, P1M case, the FE ultimate load lies within the experimental scatter (Fig. 6.19a) and for the rest of the single load cases, the finite element ultimate loads were well below the test values.

#### Flexural punching failure

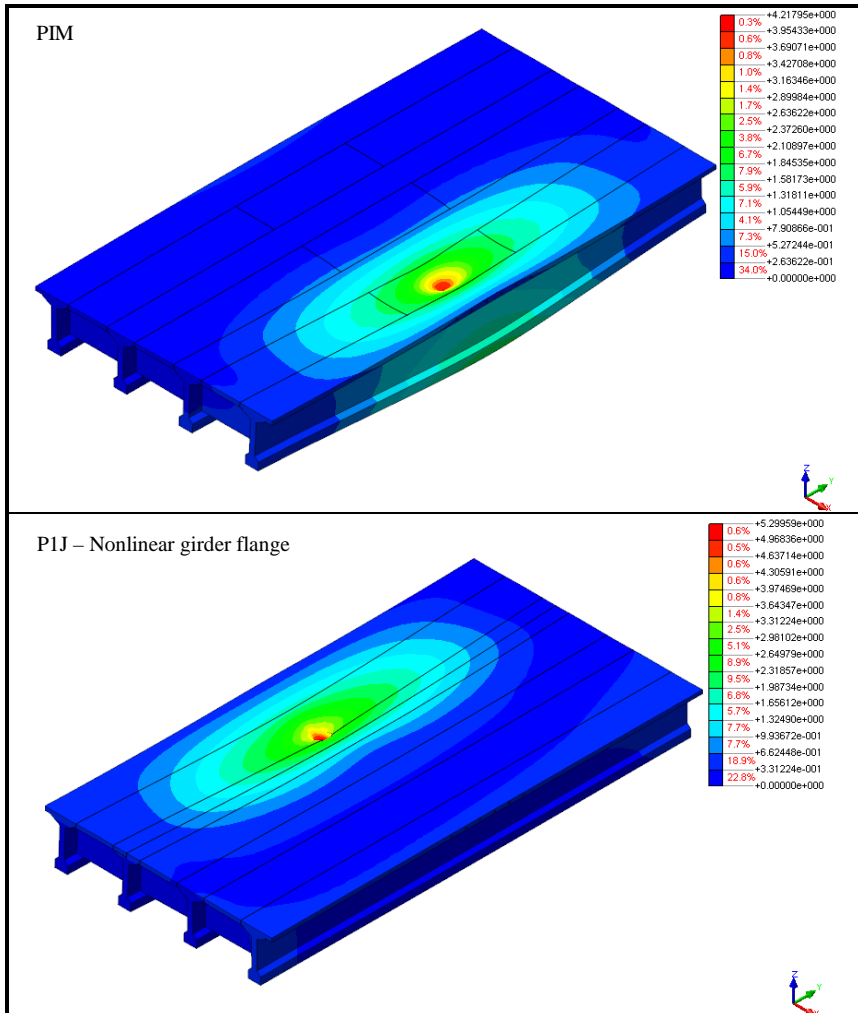
When a double load was applied at the slab midspan (P2M) flexural punching behavior was observed. Zheng et al. (2009) have reported such failures in their finite element study for cases where the ratio between the lengths in two directions of loaded area is large. In current experiments, such failures were associated with large rotations occurring during loading and the substantial widening of a single longitudinal crack when approaching

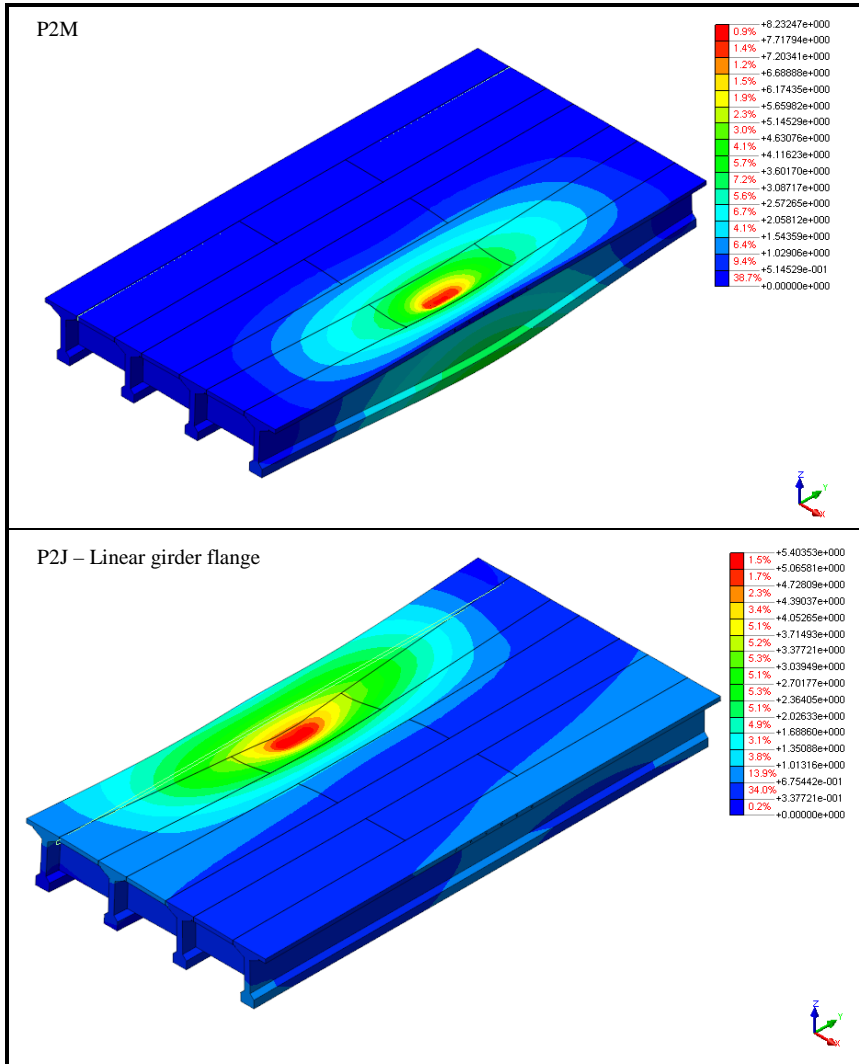
failure, while in the FEA, they were associated with a cracked longitudinal strip joining the two loading areas and more ductile behavior as compared to single load midspan cases (explained further in section 6.5.4). However, the final failure in both experiments and FEA still occurred according to the punching mode. The test ultimate loads for 1.25 MPa and 2.5 MPa (P2M) were 0.83 and 0.93 times the calculated FEA ultimate loads respectively.

### 6.5.3 Deflected shape at failure stage

The deflected shape of the FE bridge deck model for typical load cases: P1M, P1J, P2M and P2J (with TPL of 2.5 MPa) are shown in the Table 6.9.

Table 6.9 Deflected shape of the bridge deck for typical load cases.





### 6.5.4 Load – Deflection behavior

The load-deflection behavior of the finite element cases is discussed in this section and compared with the corresponding experimental behavior.

#### P1M: Single load acting at midspan of the deck slab panel

Fig. 6.20 shows the load-deflection behavior for the P1M case for two levels of transverse prestressing: 1.25 and 2.5 MPa. In both cases, the FE load – deflection behavior closely correlates with the experimental load – deflection behavior especially the initial stiffness.

It can be observed that the load increased linearly till the initial flexural cracking (84.9 kN for 1.25 MPa and 93.2 kN for 2.5 MPa). After that the curve goes into the nonlinear range. The first inclined shear crack was observed at 135.6 kN and 153.9 kN for 1.25 and 2.5 MPa respectively. After the detection of the inclined shear cracking, the load-deflection behavior in the FEA deviates slightly from the experimental observations showing a stiffer behavior in the FE simulations. As explained in the previous section, the mode of failure observed in the FE simulations was brittle punching, similar to experimental observations.

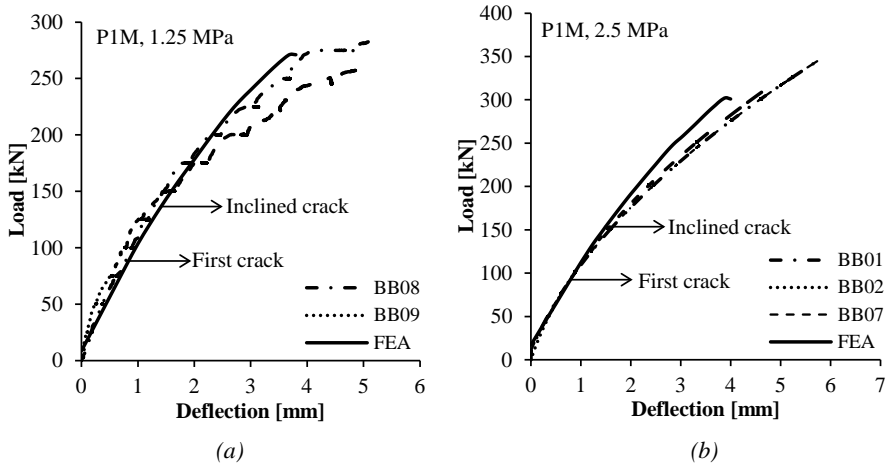


Fig. 6.20 Load-deflection behavior of P1M load case compared with the experimental curves: a) 1.25 MPa; b) 2.5 MPa.

### P1J: Single load acting close to the interface between the deck slab panel and the girder flange

Fig. 6.21 shows the load-deflection behavior for the P1J case. For 1.25 MPa, the displacement load was assigned at 200 mm c/c from the interface and for 2.5 MPa, it was assigned at 150 mm c/c from the interface. For the latter case, the nonlinear girder flange model was used for the analysis. In both simulations, the initial FE load – deflection behavior closely correlates with that of the experimental load – deflection behavior.

It can be observed that the load increased linearly till the initial flexural cracking (83.7 kN for 1.25 MPa and 107.1 kN for 2.5 MPa). After that the curve goes into the nonlinear phase. The first inclined shear crack was observed at 131.3 kN and 179.6 kN for 1.25 and 2.5 MPa respectively. After the detection of the inclined shear cracking, the load-deflection behavior in the FEA deviates from the experimental observations showing a stiffer behavior in the FE simulations. The mode of failure observed in the FEA simulations was *brittle punching*, similar to the experimental observations.

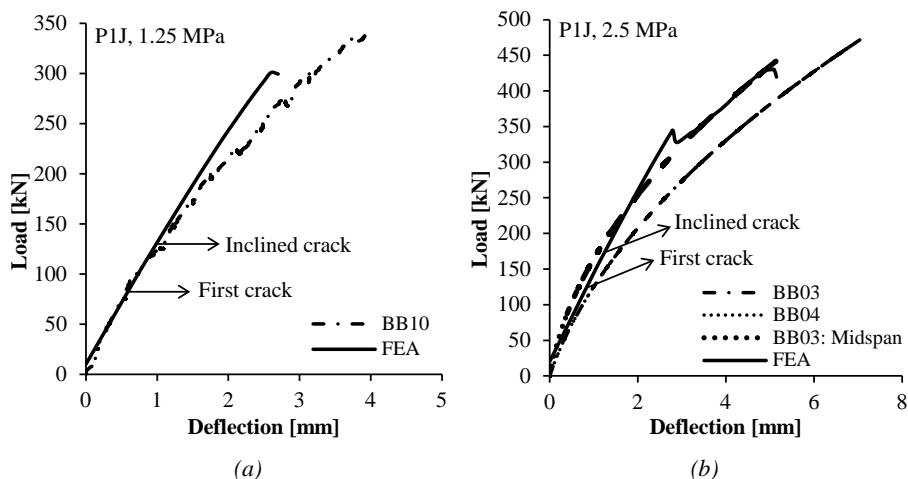


Fig. 6.21 Load-deflection behavior of PIJ load case compared with the experimental curves: a) 1.25 MPa; b) 2.5 MPa.

### P2M: Double loads at 600 mm c/c acting at mid span of the deck slab panel

Fig. 6.22 shows the load-deflection behavior for the P1M case. In both simulations, the initial FE load-deflection behavior closely correlates with that of the experimental load – deflection behavior.

It can be observed that the load increased linearly till the initial flexural cracking (120.4 kN for 1.25 MPa and 151.8 kN for 2.5 MPa). After that the curve goes into the nonlinear phase. The first inclined shear crack was observed at 180 kN and 212.2 kN for 1.25 and 2.5 MPa respectively. After the detection of the inclined shear cracking, the load-deflection behavior in the FEA deviates from the experimental observations showing a stiffer behavior in the FE simulations and failing at higher loads as compared to the experimental failure loads. The deflections in the FE and in the experiments are comparable except for BB 11 LVDTs<sup>12</sup> that were placed in the longitudinal direction. The reason behind such large deflections observed in that direction could be the development of the single longitudinal crack that kept widening near the failure stage. The lasers placed in the transverse direction in both test cases show similar values as the FE simulations. The mode of failure observed in the FEA simulations was *flexural punching* with large deflections (a ductile load-deflection response), similar to the finite element studies of others (Zheng et al. 2009).

<sup>12</sup> The LVDTs in BB11 were placed at 180 mm offset from each loading point in the outer direction. The lasers in BB11 and BB5 were placed at 325 mm offset from the loading points in the transverse direction.

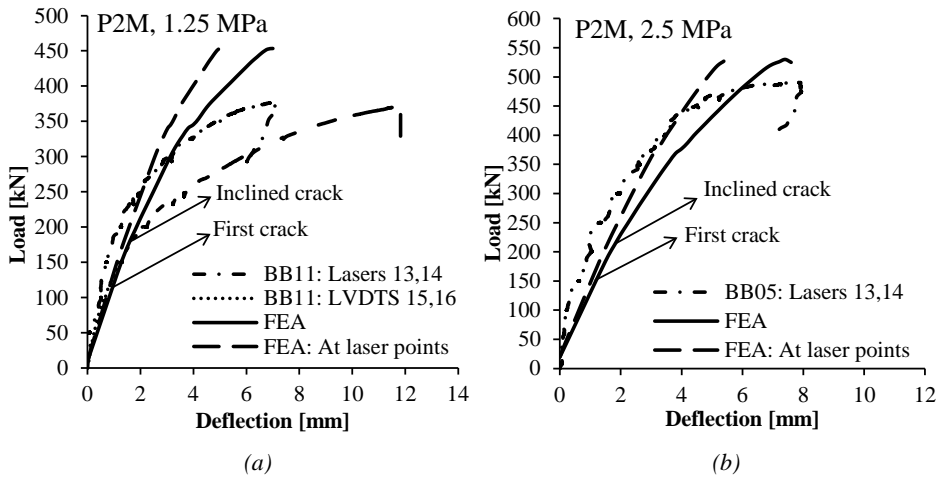


Fig. 6.22 Load-deflection behavior of P2M load case compared with the experimental curves: a) 1.25 MPa; b) 2.5 MPa.

**P2J: Double loads at 600 mm c/c acting close to the interface between the deck slab panel and the girder flange**

Fig. 6.23 shows the load-deflection behavior for the P1M case. In both simulations, the initial FE load – deflection behavior closely correlates with that of the experimental load – deflection behavior.

It can be observed that the load increased linearly till the initial flexural cracking (116.4 kN for 1.25 MPa and 165.2 kN for 2.5 MPa). After that the curve goes into the nonlinear phase. The first inclined shear crack was observed at 216.2 kN and 258.5 kN for 1.25 and 2.5 MPa respectively. Unlike the other test cases, after the detection of the inclined shear cracking, the load-deflection behavior of both FEA test cases correlates very well with the experimental observations. However, for 1.25 MPa, a higher ultimate load and deflection is observed and for 2.5 MPa, a lower ultimate load and deflection is observed as compared to the experimental values. The mode of failure observed in the FEA simulations was brittle punching, similar to the experimental observations.

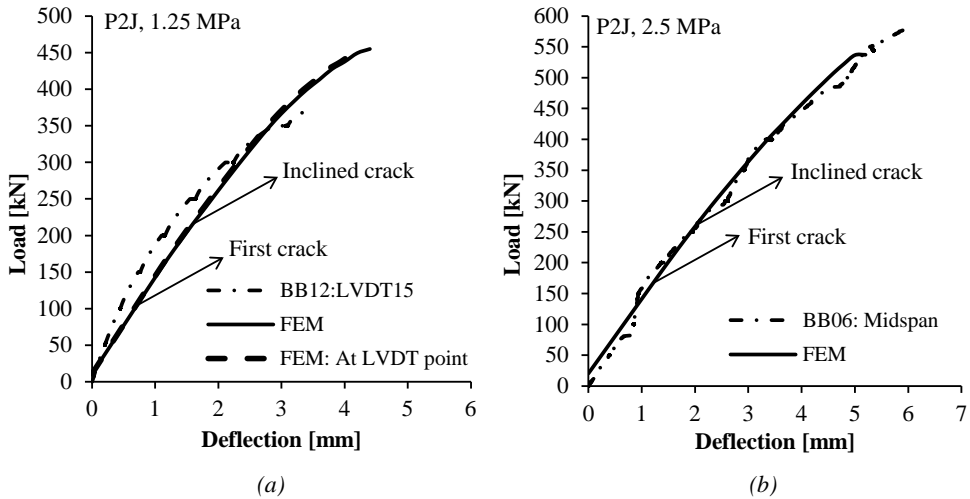


Fig. 6.23 Load–deflection behavior of PIM load case compared with the experimental curves: a) 1.25 MPa<sup>13</sup>; b) 2.5 MPa

### Conclusion

The overall load deflection behavior has been simulated reasonably well with the nonlinear finite element analyses. The initial stiffness observed in the load–deflection curves is comparable with the experimental results. After the initial cracking, the load-deflection response in the finite element simulations generally seems to be stiffer than the experimental observations leading to lower deflections. Such over-stiffness could be because of stress-locking in the smeared crack model (Rots et al. 1989) and is observed in the finite element study by other researchers as well (Hallgren 1996, Hon 2001, Zheng et al. 2009 etc.). However, stress-locking is more pronounced in a fixed crack model than in a rotating crack model which is currently employed in this research, hence this cannot be the sole reason. Another possible reason can be the fact that the interfaces were not modeled separately for the girder flange-deck slab connection and therefore, the crack at either side of the top of the deck slab panel that was experimentally observed could not be simulated discretely in the finite element analyses.

### 6.5.5 Cracking loads and cracking pattern

All the test cases showed a typical punching shear cracking pattern in the finite element analyses and the cracking loads showed good correlation with the experimental observations.

<sup>13</sup> In BB12, LVDT 15 was placed at 150 mm from the southern side loading point (Point 2) in the outer direction. In BB6, the laser was placed at midspan of the deck slab panel.

## Cracking loads

Table 6.10 shows the initial flexural and initial inclined shear cracking loads for the FE basic test cases and also compares the finite element initial cracking loads (flexural) with the experimental initial cracking loads.

Table 6.10 Comparison of FE and experimental cracking loads.

BB.	TPL	Designation	$P_T$	$P_{FEA}$	$P_{CR,T}$ (Initial hairline – 0.1mm wide)*	$P_{CR,FEA}$	$P_{CRS,FEA}$
	[MPa]		[kN]	[kN]	[kN]	[kN]	[kN]
1.	2.5	C-P1M	348.7	302.3	75-150	93.2	153.9
2.	2.5	A-P1M	321.4	302.3	75-150	93.2	153.9
3.	2.5	A-P1J	441.6	429.9	75-175	107.1	179.6
4.	2.5	C-P1J	472.3	429.9	100-175	107.1	179.6
5.	2.5	C-P2M	490.4	529.9	150-200	151.8	212.2
6.	2.5	A-P2J	576.8	537.0	150-250	165.2	258.5
7.	2.5	C-P1M	345.9	302.3	75-125	93.2	153.9
8.	1.25	C-P1M	284.5	271.4	50-100	84.9	135.6
9.	1.25	A-P1M	258.2	271.4	50-100	84.9	135.6
10.	1.25	A-P1J	340.3	300.7	25-100	83.7	131.3
11.	1.25	C-P2M	377.9	453.4	50-125	120.4	180.0
12.	125	A-P2J	373.7	454.9	100-175	116.4	216.2

\*The experimental cracking loads are characterized by hairline cracks and the cracking load defined at 0.1 mm wide cracks (first significant cracks).

The FEA cracking loads show good correlation with the experimentally observed values and fall somewhere between the initial hairline and 0.1 mm cracking loads. As expected, a higher TPL delayed cracking and double loads and loads close to the interface showed higher cracking loads as compared to the single loads and loads at the mid-span of the deck slab panel, respectively. It can be concluded that the higher the level of transverse prestressing, the higher will be the cracking loads, hence an improvement in serviceability can be achieved.

## Cracking pattern

Table 6.11 shows step by step the development of the cracking pattern ( $Eknn$ , normal crack strain) for a typical load case of a single load acting at midspan of the deck slab panel (P1M).

The general cracking pattern observed for a P1M case is as follows:

- After the application of few displacement load increments, initial tangential (flexural) cracks were observed at the bottom of the deck slab panel directly under the loading position (wheel print area).

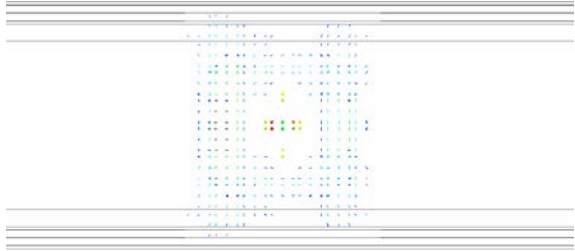
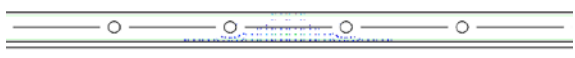
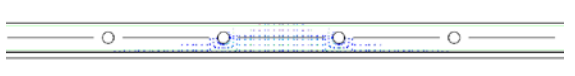
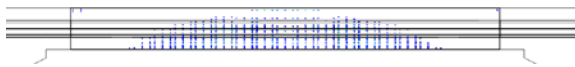
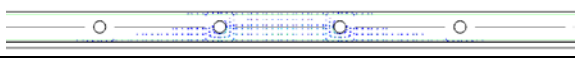
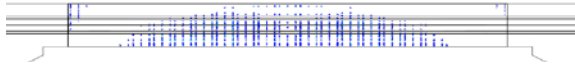
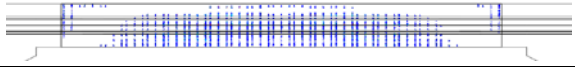
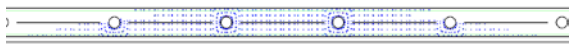
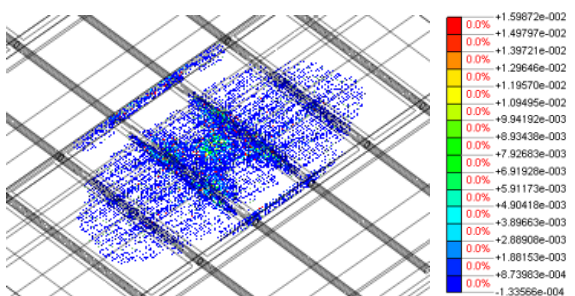
## Numerical Model – Finite Element Analysis

- The tangential flexural cracks propagated vertically upwards with simultaneous development of radial cracks from the corners of the wheel print area at the bottom of the deck slab panel.
- Initial inclined shear crack started forming close to the tip of a vertical flexural crack (tangential direction) approximately from the mid-depth of the deck slab panel.
- On further increments of the displacement-load, the radial and tangential (flexural and inclined shear) cracks propagated further and a lot of cracks accumulated around the ducts adjacent to the loading area.
- With further increments of the load, a clear punching cone started forming and almost all of the inclined and tangential cracking was concentrated within the punching cone. The radial cracks showed a fan-like pattern with long wings concentrating mostly within a span covering 4 ducts (4 ducts @ 400 mm c/c = 1200 mm).
- In the cross-section, the slope of the punching cone was approximately between 20-25 degrees for all test cases. In the longitudinal direction, the slope of the punching cone was between 10-15 degrees.
- At the failure stage, a clear punching cone was formed in either directions (transverse and longitudinal) with sort of circumferential (transverse) cracking encircling the ducts adjacent to the loading area.

*Table 6.11 Crack propagation and cracking pattern (Eknn) for P1M load case (2.5 MPa TPL).*

Position of cracks	Crack propagation and cracking pattern (Eknn) for P1M, 2.5 MPa TPL
TS, Load step 9 = Initial tangential (flexural) cracks .	
LV, Load step 9 = Initial tangential (flexural) cracks.	
BV, Load step 10 = Initial radial cracks at the corners of the loading area (wheel print) on the underside of the deck slab.	
TS, Load step 11 = Tangential cracks.	

## Numerical Model – Finite Element Analysis

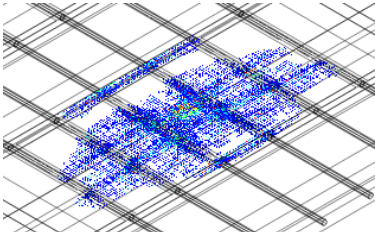
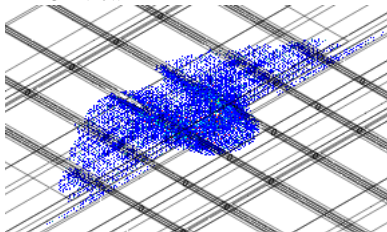
<p>BV, Load step 11= Radial cracks propagation from the corners of the loading area (wheel print) on the underside of the deck slab.</p>	
<p>TS, Load step 16 = Initial inclined shear cracks.</p>	
<p>LV, Load step 16 = Initial cracks around the ducts.</p>	
<p>TS, Load step 20 = Initiation of the punching cone.</p>	
<p>LV, Load step 20 = More cracking around the ducts.</p>	
<p>TS, Load step 25 = Development of the punching cone.</p>	
<p>LV, Load step 25 = Crack concentration around the ducts.</p>	
<p>TS, Load step 30 = Cracks at the joints on the top side.</p>	
<p>LV, Load step 30 = Cracks at the joints on the top side.</p>	
<p>TS, Load step 35 = Punching cone ~ 25 degrees slope</p>	
<p>LV, Load step 35 = Punching cone ~ 15 degrees slope</p>	
<p>TS, Failure: Load step 40 = Punching cone</p>	
<p>LV, Failure: Load step 40 = Cracks extending to 4 ducts</p>	
<p>Failure: Load step 40 = Punching shear failure (3D view)</p>	

Notations: TS = Transverse section, LV = Longitudinal view, BV = Bottom view of the deck slab.

## Numerical Model – Finite Element Analysis

Table 6.12a, b & 6.13 show a comparison of the experimental and finite element analyses cracking patterns for typical single and double load cases at the ultimate/failure stages respectively.

*Table 6.12a Comparison of experimental and FE cracking pattern at the failure/ultimate stage for typical single load cases (P1M and P1J).*

Single load at midspan, P1M – Typical case	Single load close to the interface – 2.5 MPa, P1J (110 mm from the interface and nonlinear flange in FEA)
<p>Test top view</p> 	<p>Test top view (BB3)</p> 
<p>Test bottom view</p> 	<p>Test bottom view (BB3)</p> 
<p>FEA 3D view</p> 	<p>FEA 3D view</p> 
<p>FEA sectional view</p> 	<p>FEA sectional view</p> 

Numerical Model – Finite Element Analysis

Table 6.12b Comparison of experimental and FE cracking pattern at the failure/ultimate stage for typical double load cases (P2M and P2J).

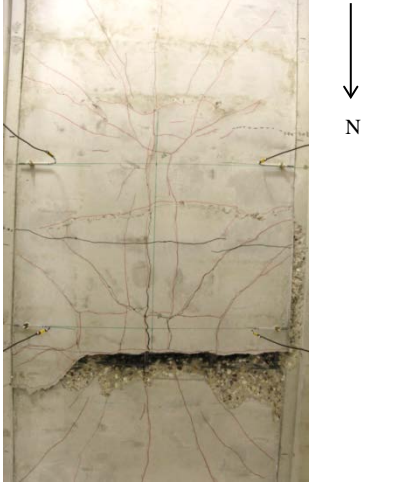
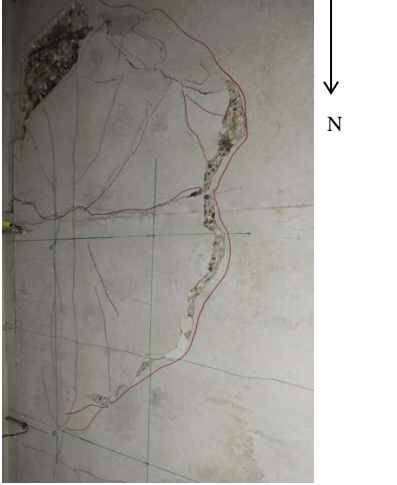
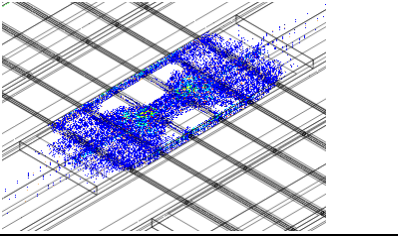
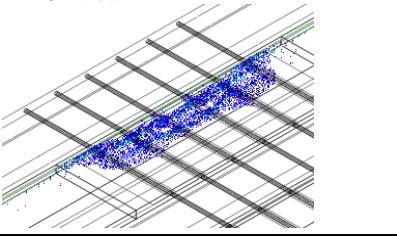
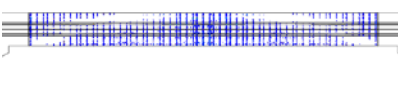
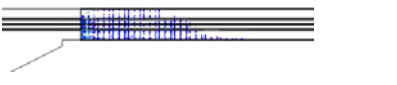
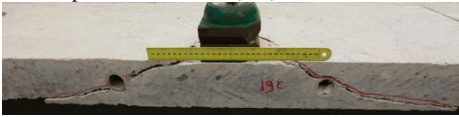
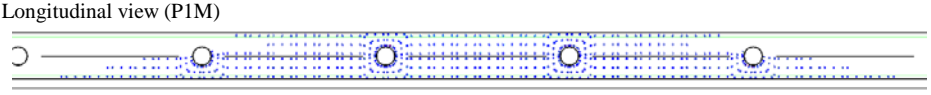
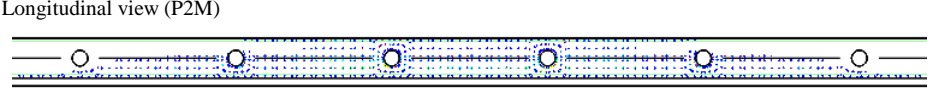
Double load at midspan – Typical case	Double load at 200 mm from the interface – Typical case
<p>Test top view</p> 	<p>Test top view</p> 
<p>Test bottom view</p> 	<p>Test bottom view</p> 
<p>FEA 3D view</p> 	<p>FEA 3D view</p> 
<p>FEA sectional view</p> 	<p>FEA sectional view</p> 

Table 6.13 Comparison of experimental sawed specimens after failure and FE cracking pattern at the failure/ultimate stage for typical load cases (P1M, P2M).

Single load at midspan, P1M – Typical test case	Double load at midspan, P2M – Typical test case
<p>Sawed specimen, east side (test)</p> 	<p>Sawed specimen, west side (test)</p> 
<p><b>FEA:</b> The cracking at the very top of the slab shown in the longitudinal view is due to the cross-sectional cracking at the top joint. Note that the cracking does not fully cover the second group of ducts in P1M case, after the immediate ones in both tests and FEA. The change of slope of the inclined crack due to the presence of ducts is also visible in both analyses.</p>	
<p>Longitudinal view (P1M)</p>  <p>Longitudinal view (P2M)</p> 	

For a single load acting close to the interface (P1J), the general cracking pattern remained the same as for the P1M case but instead of a symmetrical cracking pattern, the cracks were clustered more towards the interface. In the linear girder flange model analyses, the cracks remained within the span of the deck slab and in the nonlinear girder flange model analyses, some cracking was observed in the nonlinear flange area (in the experiments similar to P1J case, only surface spalling was observed at the interface). The punching cone was formed close to the interface at the ultimate stage but within the span of the slab.

For a double load acting at midspan of the deck slab panel (P2M), the crack development remained the same as for P1M case but occurred simultaneously at both loading points. In the experiments, a longitudinal crack was observed connecting both loading points and widened to a large degree close to failure. In the FEA, the longitudinal strip between the two loading points showed a band of cracking instead of a single longitudinal crack (smearing out effect). At the failure stage, symmetrical punching shear cracks were observed at both loading points.

For a double load acting close to the joint/interface (P2J), again the crack development remained the same as for the P1M or P1J case but happened simultaneously at both loading points. Also, instead of a symmetrical cracking pattern as for a P1M case, the cracks were clustered close to the interface (similar to P1J case) leading to punching cones at both loading points within the span of the slab.

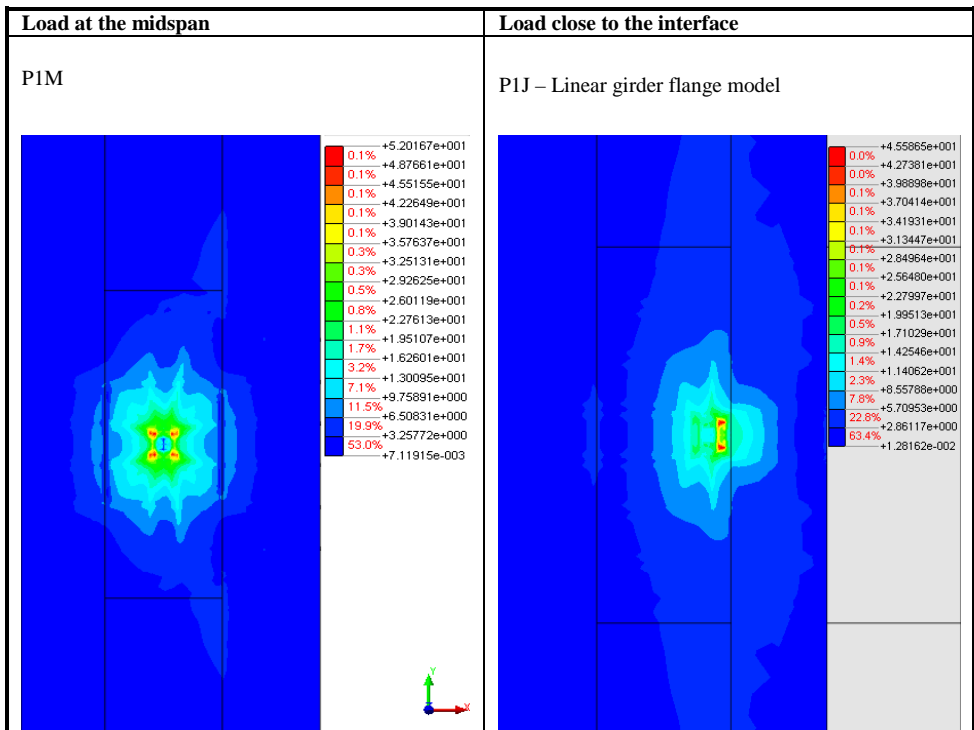
Conclusion

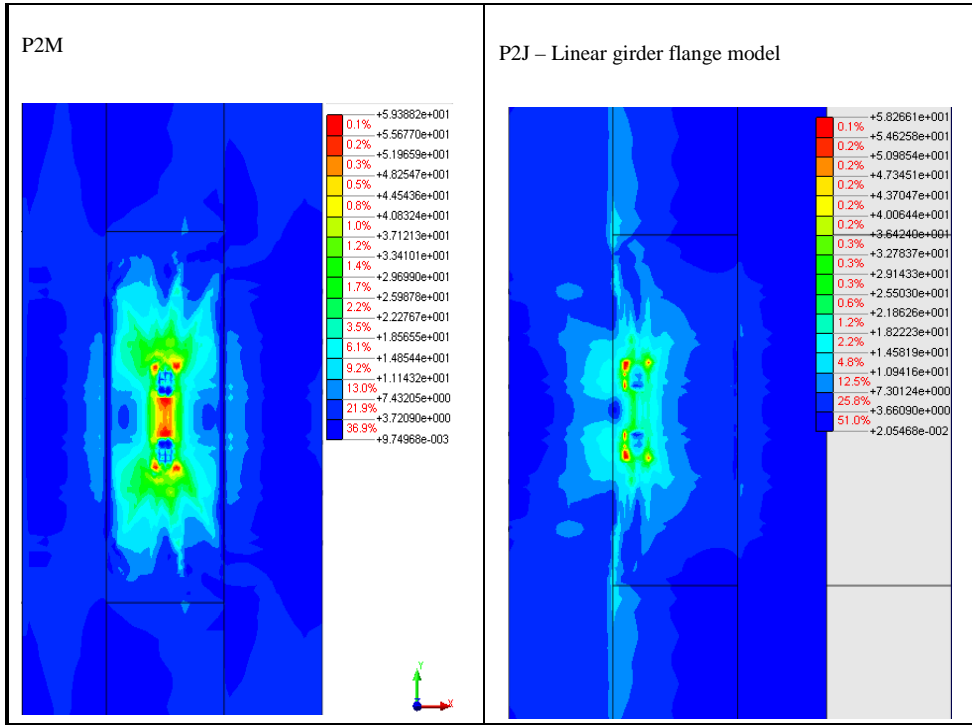
The crack propagation and resulting cracking pattern explained above closely matches with the experimental observations of the crack propagation and pattern explained in section 4.3. However, in most of the experiments, the circumferential cracks were formed outside the ducts adjacent to the loading area and in the FEA, cracking in the circumferential or the transverse direction was observed concentrated along the ducts adjacent to the loading area. No circumferential cracks were observed outside the adjacent ducts. Also, in double load cases, only one load side had punched through in the experiments, while, in the FEA, simultaneous punching of both loading points was observed.

**6.5.6 Von Mises stress distributions**

The von Mises stress distributions (gauss evaluation) on the top surface of the loaded deck slab panel at the ultimate load stage for typical load cases are shown in Table 6.14 below. The crack pattern shown in section 6.5.4 and the von Mises stress diagrams at the ultimate stage clearly suggest a punching shear failure for these load cases.

Table 6.14 Von Mises stress distributions for P1M and P1J load cases (TPL is 1.25 MPa for the stress distributions shown)





## 6.6 Compressive Membrane Action

### 6.6.1 Introduction

It has been established in literature that compressive membrane action enhances the punching shear capacity of a laterally restrained slab. In this research an attempt has been made to compute the compressive membrane forces and to determine the level of the membrane action developed for a particular transverse prestressing level. It is difficult, if not impossible, to theoretically predict the compressive membrane action that can be developed in a slab. This issue can be resolved by adopting a finite element approach rather than using cumbersome analytical methods. Keeping in mind that the deformation of a restrained slab is idealized as the rotation of two rigid bodies about the center and each end of the span giving rise to the arching force in the plane of the slab (Fig. 6.24), the edge displacements of the deck slab are shown in Fig. 6.26 and 6.27 and combined with the transverse stress distribution (section 6.6.3) and in-plane force distribution (section 6.6.4) is evidence of the development of compressive membrane action.

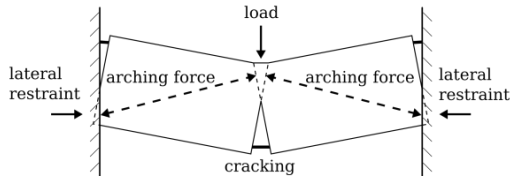


Fig. 6.24 The idealized model of a slab strip between two rigid supports and acted upon by a concentrated load (Mahdal 2013).

### 6.6.2 Horizontal edge displacements

In the literature, one of the conditions described for the development of CMA is that the lateral displacements increase at a greater rate after the initial cracking of the slab. To observe this behavior, the lateral displacements at the edges of the loaded deck slab panel at the top and bottom surfaces making up the edge rotations are computed by DIANA and are presented in this section. It is also shown how the horizontal lateral displacements increase rapidly after the initial cracking fulfilling one of the requirements of the development of CMA in the plane of the slab. The sign convention used in the finite element results is as shown in Fig. 6.25. Positive displacements show movement towards the western end of the deck. Negative displacements show movement towards the eastern edge of the deck.

Notations used in this section: ET = East side top edge, WT = West side top edge, EB = East side bottom edge, WB = West side bottom edge.

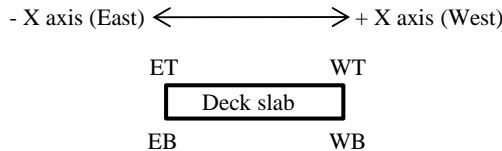


Fig. 6.25 Sign convention for lateral displacements in the FEA.

### General load - lateral displacement behavior

Fig. 6.26 shows the lateral displacements as a function of applied load for a P1M load case (Panel C) with a TPL of 2.5 MPa. In order to determine if sufficient lateral restraint was present in the current tests, a quick calculation is performed comparing the observed FEA displacement at the bottom of the deck slab with that of an idealized-unrestrained slab. Using simple geometrical rules, with a midspan deflection of 3.9 mm in this case (section 6.5.2), and the deck slab span of 1050 mm, the unrestrained or simply supported end conditions give a bottom compressive displacement of 0.37 mm whereas the maximum bottom compressive displacement observed in the FEA is 0.23 mm showing that lateral restraint was present in the bridge deck model.

## Numerical Model – Finite Element Analysis

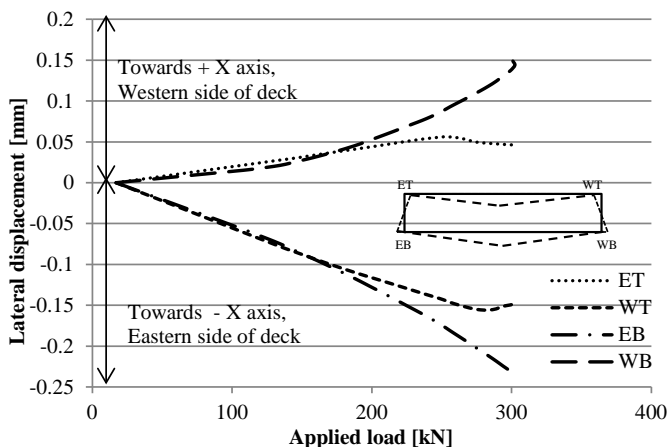


Fig. 6.26 Load - lateral displacements of the top and bottom edges on either side of the deck slab (PIM with a TPL of 2.5 MPa).

It can be observed that the top edges of the deck slab displaced *inwards* (showing tensile behavior) and the bottom edges of the deck slab displaced *outwards* (showing compressive behavior) similar to the structural configuration shown in the Fig. 6.24<sup>14</sup>. Gang et al. (2011) point out that due to the presence of lateral restraint, the tensile strain of the middle plane of the slab is restricted by the horizontal supports, the height of the compression zone is much larger than if no lateral restraint was present, and the movement of the neutral axis to the concrete compression face is restricted. It is worth noting that the lateral displacements for the bottom surface increased rapidly after the initial flexural cracking at about 93 kN. This correlates well with the findings of Liebenberg (1966), Fang (1985) and He (1992) that the horizontal lateral displacements occur only after the initial cracking if CMA is present. Also, both the top and bottom edges on either side of the deck slab displace by the same amount until the initial inclined shear crack at 154 kN and then the bottom displacements occur more rapidly than the top displacements. This is in agreement with the general punching shear concept that the slab portion outside the failure shear crack rotates as a rigid body (Kinnuen and Nylander 1960, Hallgren 1996). This also shows that the depth of the compression zone reduces at a much greater rate after the initiation of the inclined shear crack and punching shear failure occurs when the shear crack runs through the compression zone.

<sup>14</sup> The initial displacements due to the load step 1 of prestress have been subtracted from the overall displacements to make a better comparison with the experimental observations in section 4.3 (global horizontal displacements, crack width at top and compressive strains at bottom), where the LVDTs/Lasers start measuring from the vertical load application.

**Load – lateral displacements at the top and bottom edges at either side of the deck slab (edge rotations) for typical load cases (TPL = 1.25 MPa)**

Generally, the model bridge deck displaces more in the western direction probably due to fixed support being on the eastern side. Fig. 6.27 shows the load – lateral displacement behavior for load cases P1M, P1J, P2M and P2J with a TPL of 1.25 MPa.

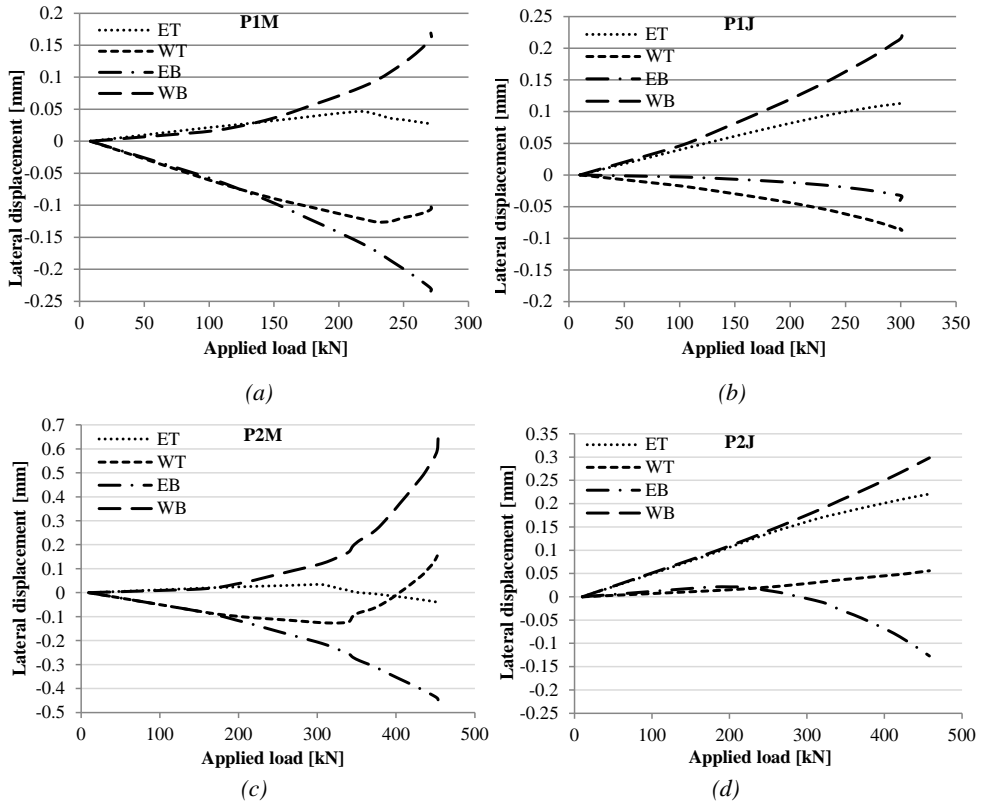


Fig. 6.27 Load – lateral displacements of the top and bottom edges on either side of the deck slab (TPL = 1.25 MPa): a) P1M; b) P1J (loaded close to the western side); c) P2M; d) P2J (loaded close to the eastern side).

For the P1M case, Fig. 6.27a, the lateral displacement profile remains the same as explained in the general description in the previous section. The displacements occur rapidly after the initial cracking at 85 kN on the bottom side of the deck slab and after the initial inclined shear crack at 135.6 kN, the bottom edges displace at a greater rate (maximum outwards displacement of 0.23 mm at the ultimate stage) as compared to the top edges (maximum inwards displacement of 0.126 mm at the ultimate stage). Also, a symmetrical displacement pattern is observed. The displacements on both sides at the bottom are comparable to each other and same is true for the top edge displacements.

For the P1J case, Fig. 6.27b, loaded close to the western side of the deck slab panel, the lateral displacements increase after the initial crack at 83.7 kN, but unlike a symmetrical displacement pattern of the two edges on either side, an unequal displacement pattern is observed on the bottom side. The bottom edge on the western side (WB) displaces by 0.218 mm in the outwards direction (+ X axis, towards west) and its counterpart (EB) displaces only by 0.04 mm in the outwards direction (- X axis, towards east) at the ultimate stage. This is because of the proximity of the loading to the western edge. The top edge on the eastern side (ET) displaces inwards by 0.11 mm (+ X axis, towards west) and the top edge on the western side displaces inwards by 0.09 mm (- X axis, towards east).

For the P2M case, Fig. 6.27c, large displacements on the bottom edges are observed as compared to the top edges. The rate of increase in the lateral displacements increases after the initial flexural cracking at 120.4 kN and especially after the initial inclined shear cracking at 180 kN. The bottom edges are seen to displace much more than the top edges once the inclined shear crack is initiated. This is also due to the large extent of longitudinal flexural cracking observed in the middle of the deck slab span (section 6.5.4) and therefore pushing the bottom edges of the deck slab portions (on either side of the longitudinal crack) outwards as shown in Fig. 6.24 with the difference that the longitudinal flexural cracking in the P2M load case is much more developed as compared to the P1M case leading to flexural punching in the former and brittle punching in the latter. The maximum bottom edge displacement (WB) is 0.65 mm in the outwards direction (WB, + X axis, towards west) and the top edge displacements are initially inwards but close to failure they also turn outwards owing to the large rotations, with a maximum value of 0.153 mm (WT, + X axis, towards west) at the ultimate stage.

For the P2J case, Fig. 6.27d, loaded close to the eastern side of the deck slab panel, the lateral displacements do not show a significant increase after the initial flexural crack at 116.4 kN but increase rapidly after the initial inclined shear crack at 216 kN especially on the loaded eastern bottom side (EB). Also, similar to the other load cases, the displacements at both sides remain equal until the origin of the inclined shear crack after which the bottom edges displace rapidly as compared to the top edges on both sides of the deck. Again, an unsymmetrical displacement pattern is observed like the P1J case. The top edge on the eastern side (ET) displaces inwards by 0.22 mm (+ X axis, towards west) and the top edge on the western side (WT) also displaces in the same direction by 0.05 mm (+ X axis, towards west) showing little displacement owing to the application of the double load on the opposite side of the deck (east). The bottom edge on the western side (WB) displaces by 0.29 mm in the outward direction (+ X axis, towards west) and its counterpart (EB)

displaces by 0.13 mm in the outwards direction (- X axis, towards east) at the ultimate stage.

### Conclusion

Generally, the horizontal lateral movements of the deck slab edges increased after the initial flexural cracking. The bottom edges displaced outwards even more rapidly after the initial inclined shear cracking leading to a net outwards in-plane expansion which correlates well with the general concept of compressive membrane action. With further increase in the applied load, the inclined shear cracking grew and the neutral axis kept on shifting upwards reducing the depth of the compression zone until the occurrence of punching shear failure.

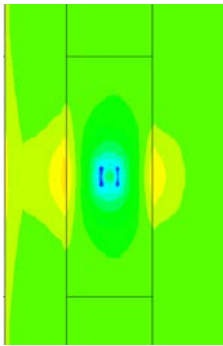
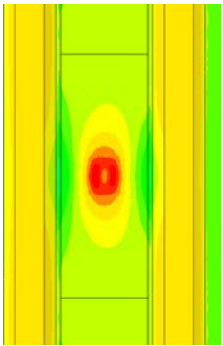
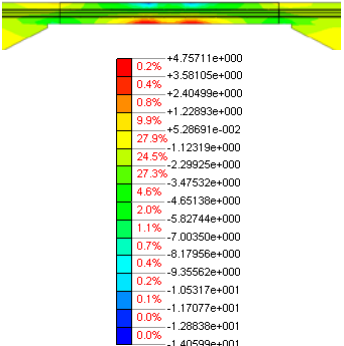
### 6.6.3 Transverse concrete stresses in the loaded deck slab panel

Since CMA develops in the plane of the slab, the transverse stress distribution is also an evidence of this phenomenon. The compressive arch of the membrane action, if it develops in the plane of a slab strip, will give rise to compressive stresses at the top side of the midspan and at the bottom side of the deck slab edges. A study of the transverse stress distribution will further reinforce the idea that sufficient compressive membrane action had developed in the finite element bridge deck model.

### General behavior of the deck slab under transverse stresses

The transverse stress distributions at various load steps for a typical load case of single load at the midspan of the deck slab panel, P1M (TPL = 2.5 MPa) and at the top and bottom surfaces as well as in the cross-section of the deck slab panel are shown in Table 6.15.

Table 6.15 Transverse stress distribution,  $S_{xx}$  for a typical P1M load case (TPL = 2.5 MPa).

Load step	Transverse stress, $S_{xx}$ in top view	Transverse stress, $S_{xx}$ in bottom view	Transverse stress, $S_{xx}$ in cross-section
Step 9 = 93 kN Initial flexural crack			

# Numerical Model – Finite Element Analysis

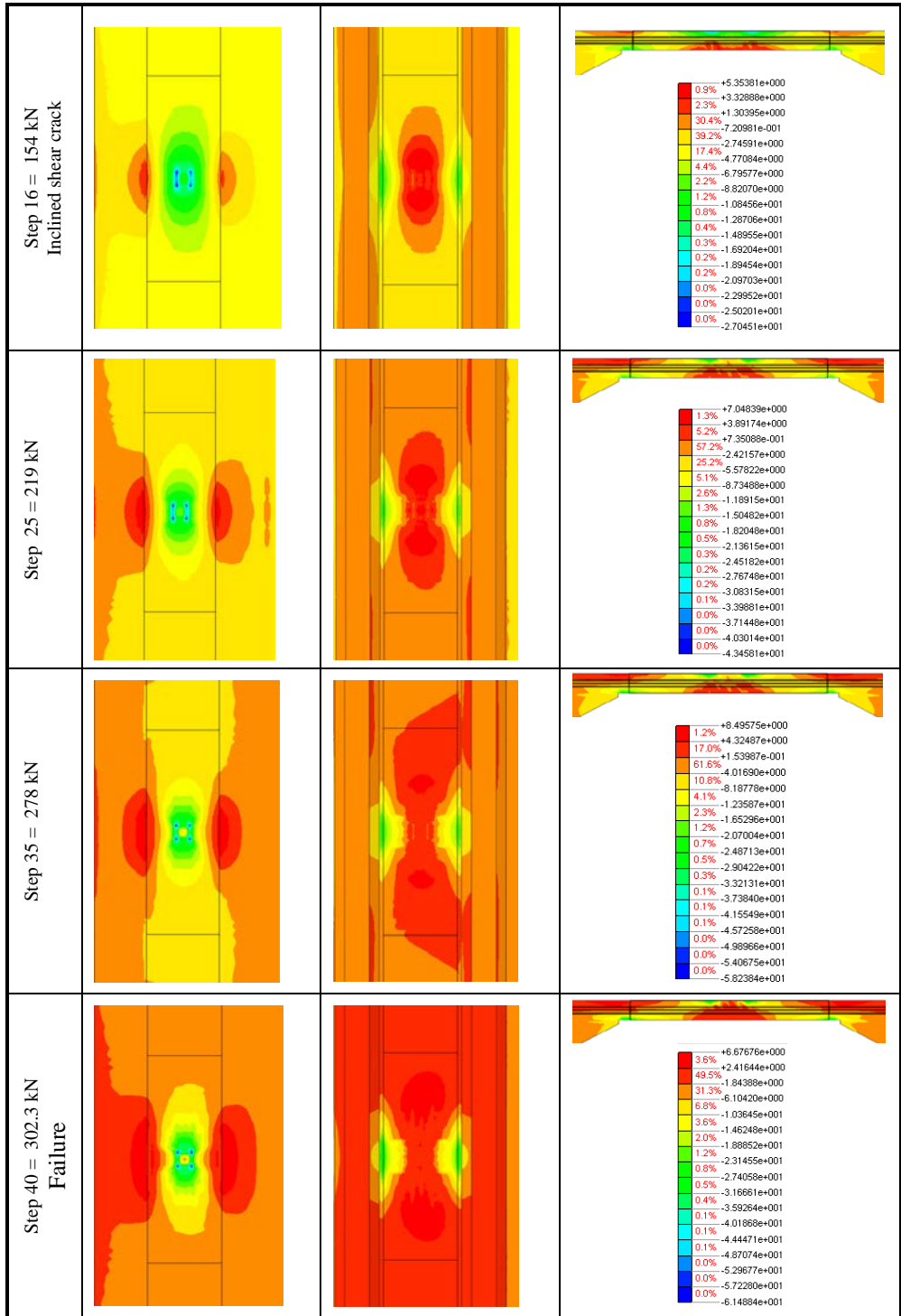


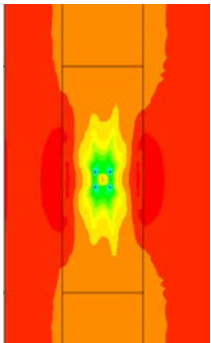
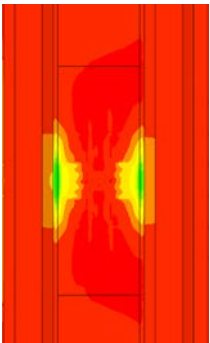
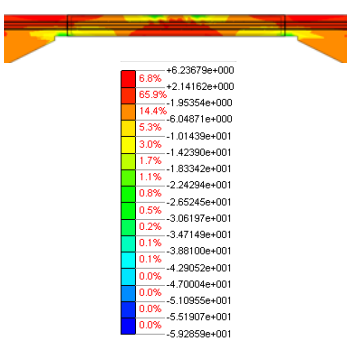
Table 6.15 demonstrates the development of transverse compressive stresses at the top surface at the loaded area and at the bottom surface of either edges of the deck slab panels (adjacent to the interface) giving rise to a compression arch in the plane of the deck slab panel which can also be observed in the cross-sectional stress distributions diagrams. As a result, tensile stresses are observed at the top surface of the deck slab panel edges and at the bottom surface of the midspan of the deck slab panel. The peak compressive stresses are observed just outside the loaded area (at the boundary) when the applied load reaches its ultimate value. In order to determine the magnitude of the membrane forces, these stresses can either be manually integrated over the depth or the built-in composed elements in DIANA can be used for this purpose.

**Transverse stresses in the deck slab panel for typical load cases (TPL = 1.25 MPa)**

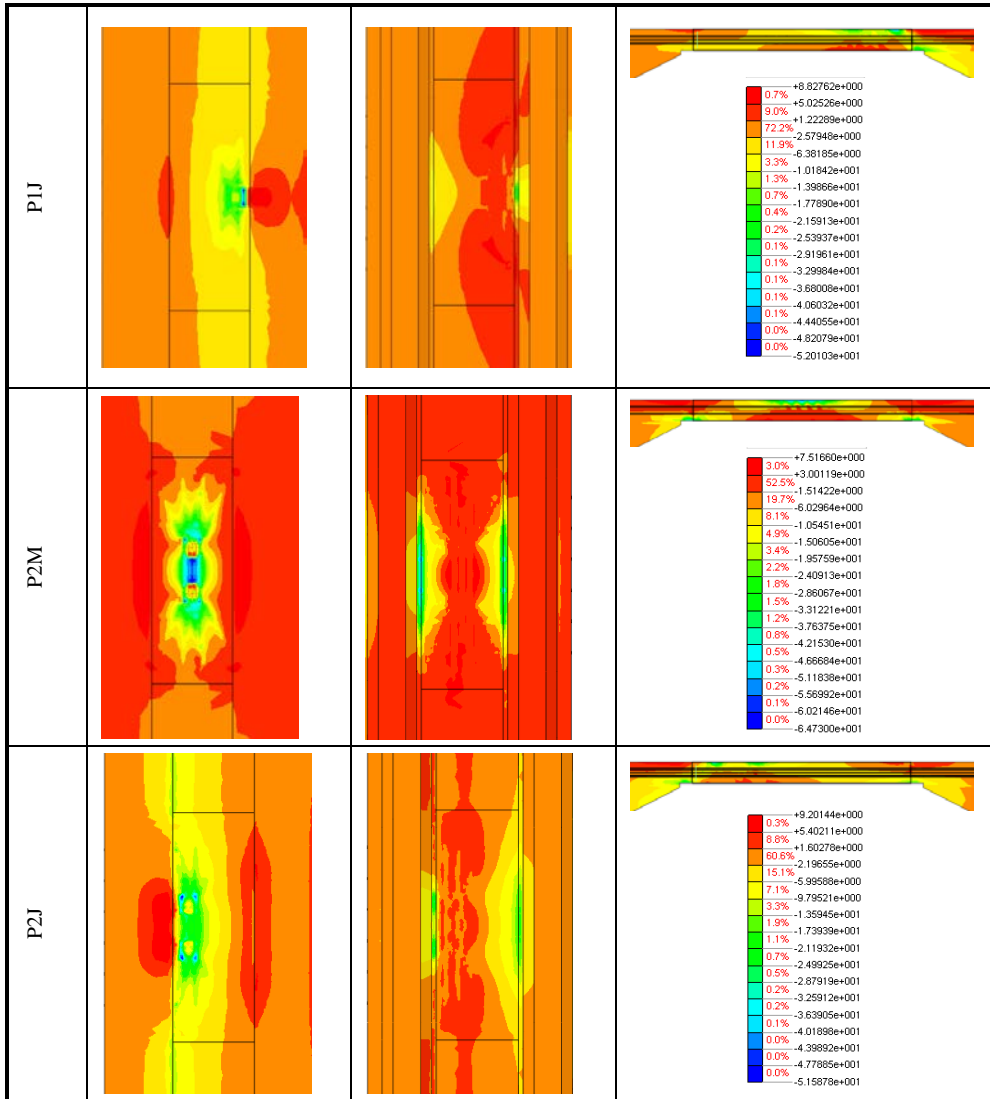
Table 6.16 shows the integration points transverse stress distributions at the ultimate stage for typical load cases: P1M, P1J, P2M and P2J with a TPL of 1.25 MPa.

For the typical load cases shown in Table 6.16, the compression dome can be clearly seen from the stress distribution diagrams. Infact, the compressive arch can not only be seen when the load is acting at midspan (P1M and P2M) but can also be observed when the load is acting close to the interface (P1J and P2J). It is also interesting to observe that in P2M case, the deck slab strip between the two loading areas has maximum compressive stresses on the top side of the deck slab showing a bending action which is in agreement with the experimental observations.

Table 6.16 Transverse stress distribution at ultimate/failure stage for typical load cases (TPL= 1.25 MPa)

Load step	Transverse stress, $S_{xx}$ in top view	Transverse stress, $S_{xx}$ in bottom view	Transverse stress, $S_{xx}$ in the cross-section view
P1M			

## Numerical Model – Finite Element Analysis



## Conclusion

A dome of concrete under compression that is typically associated with compressive membrane action can be seen from the stress distribution diagrams (Table 6.15 and 6.16,  $S_{xx}$  in top view). This is in good agreement with the finite element studies of other researchers (Graddy et al. 1995, Zheng et al. 2009). However, the difference herein lies in the type of stresses outside the compression dome. In reinforced concrete slabs, the area outside the dome shows tensile stresses, whereas, in prestressed concrete slabs, this area shows the initial prestressing stresses (compressive in nature) but its magnitude is definitely smaller

than that of the compressive membrane stresses developed during the loading history within the dome of compression as shown in Table 6.15. However, the presence of the compressive arch alone is not sufficient to prove that compressive membrane action had occurred in the plane of the slab. In the next section, the in-plane force distribution will be shown that is basically obtained by the integration of the transverse stresses through the depth (calculated automatically by the composed elements). For no compressive membrane action, any in-plane force, other than arising from the prestressing effect, will not occur and if compressive membrane action is present, there will be a normal compressive force in the cross-section of the slab.

#### **6.6.4 Development of in-plane forces with the applied load**

As explained in section 6.4.1, a layer of composed elements was provided at the mid depth of the loaded deck slab area (the fine mesh zone) to calculate the in-plane forces for the determination of the compressive membrane action (CMA). The procedure was repeated for all simulations, therefore, for each type of load case, not only the in-plane forces at the ultimate load were determined but their development with the loading history could be studied closely. Here, the in-plane forces are defined as the sum of the initial prestressing and the compressive membrane forces arising from the lateral restraint. Initially, the magnitude of the in-plane forces consists of only the prestressing forces and then it increases with the loading history due to the development of the compressive membrane forces arising from the lateral restraint. For zero compressive membrane action, the in-plane forces will be equal to the prestressing forces only.

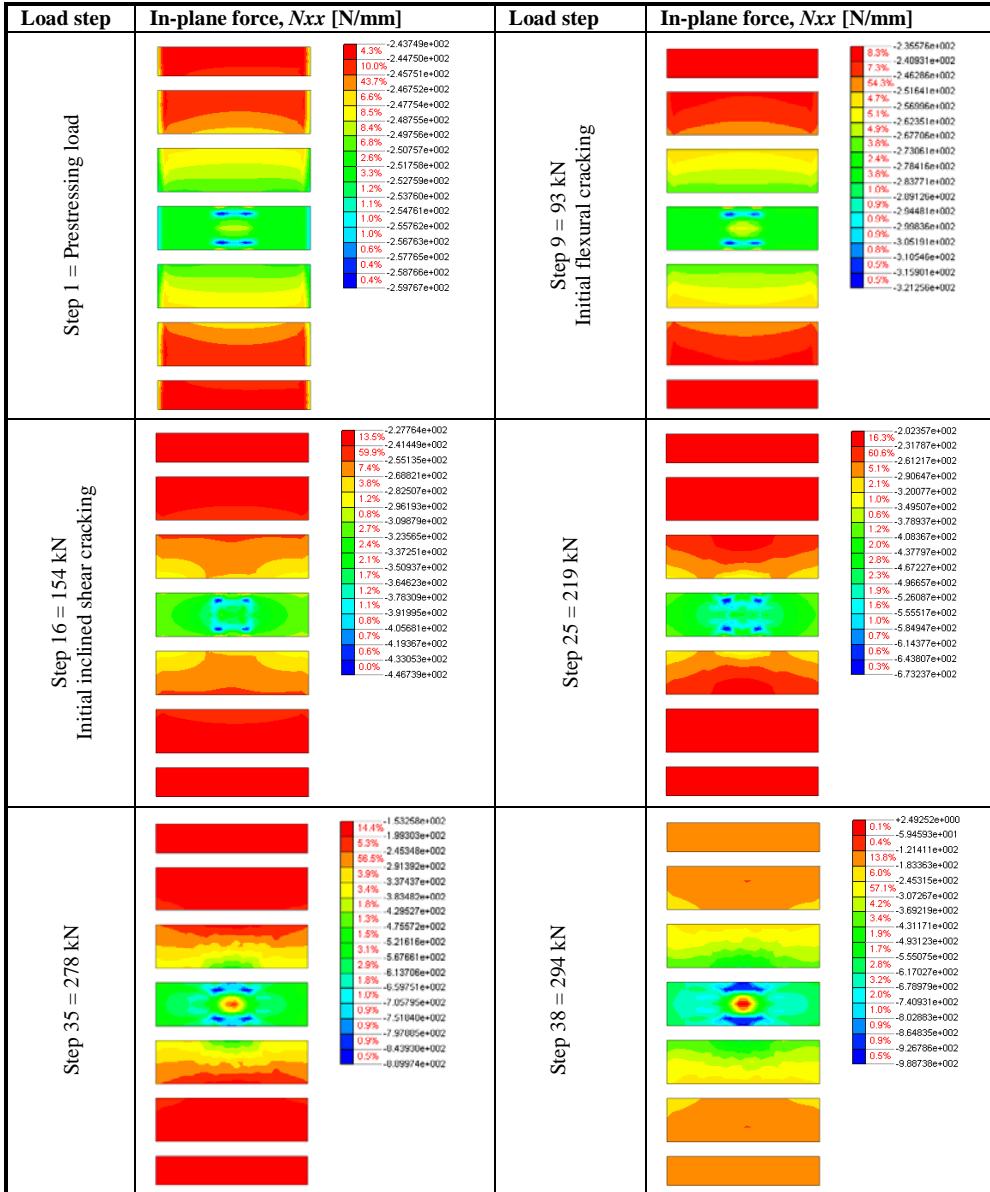
The main objective of this exercise was to develop a relationship between the transverse prestressing level (TPL), the applied load and the level of in-plane force developed for a particular load case. Since the basic analysis included only two levels of transverse prestressing, additional analyses were performed with 0.5 and 4.5 MPa to determine a valid relationship between the TPL and the CMA.

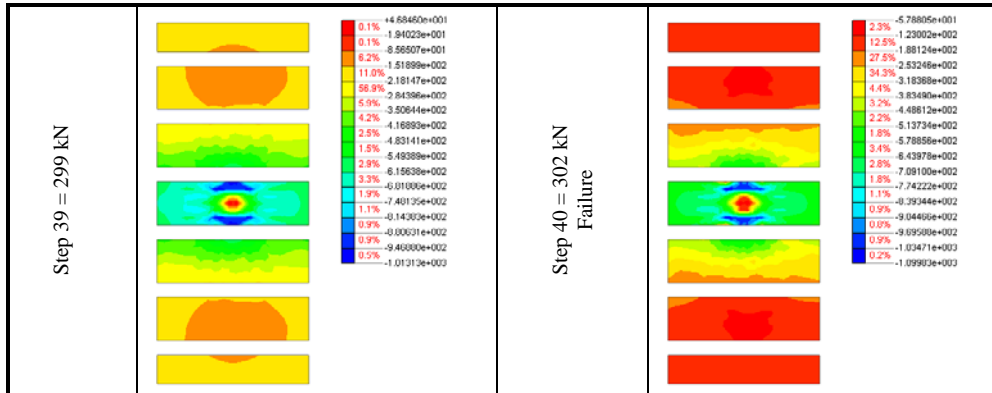
#### **In-plane force distribution in the transverse direction around the loaded area**

Table 6.17 shows the development of the in-plane distributed forces in the transverse direction ( $N_{xx}$ ) for a typical load case of a single load at the midspan of the deck slab panel (P1M) with regard to the applied load. The load case shown here has a transverse prestressing level of 2.5 MPa. It can be seen that the in-plane forces are compressive in nature around the loaded area.

## Numerical Model – Finite Element Analysis

Table 6.17 Top view of the in-plane force distribution ( $N_{xx}$ ) for a typical single load acting at midspan of the deck slab panel (P1M with a TPL of 2.5 MPa).





### In-plane force distribution over the width of the deck slab panel around the loading area

In Fig. 6.28, the *smoothed out dashed line* shows the in-plane force of the deck slab edge elements distributed over the width of the deck slab panel around the loading area for the load case P1M at the ultimate stage (a TPL of 2.5 MPa is considered for this example). The shape of the dashed curve shown holds true for all the P1M cases, regardless of the level of transverse prestressing but the magnitude of the peak of the distributed force depends on the prestressing level. For instance, considering that the fine mesh area is 2500 mm long, and the center of the load is at 1250 mm, the peak ordinate occurs right across the load and its magnitude depends on the transverse prestressing applied to the deck. Interestingly, this dashed curve intersects the initial transverse prestressing level at a width of 1200 mm (distance between three ducts at 400 mm c/c) and this distance remains the same for all the levels of transverse prestressing. This is the same width where maximum cracking is observed in the experiments and in the finite element analyses. Outside this width, the in-plane force first reduces and then increases back to the initial prestressing level. This phenomenon can be explained by the dome of compression associated with compressive membrane action having compressive stresses around the loading area and tensile stresses away from the loading area. However, as mentioned in section 6.6.3, instead of changing to tensile stresses outside this dome of compression as normally observed in reinforced concrete decks, in the prestressed deck finite element model, the stresses remain compressive with only a reduction in magnitude. For low levels of prestressing, tensile stresses are observed. For instance, a TPL of 0.5 MPa is low enough to show tensile stresses away from the compression dome.

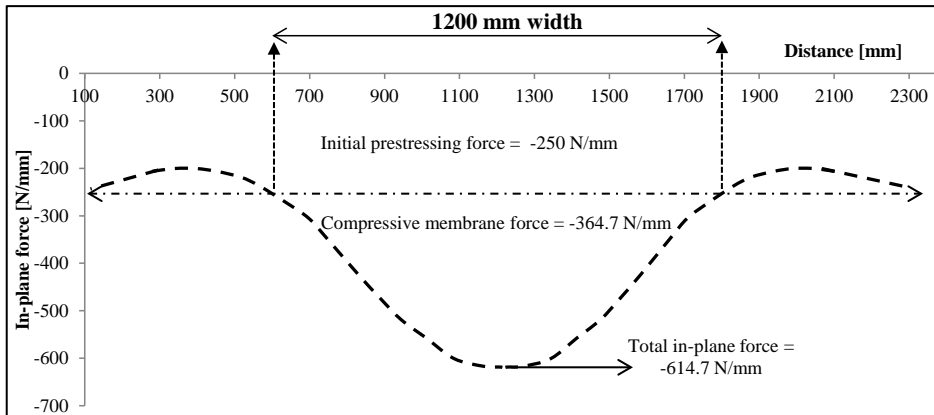


Fig. 6.28 In-plane force distributed over the width of the deck slab panel around the loading area (P1M with a TPL of 2.5 MPa).

### In-plane force with respect to the applied load for various levels of transverse prestressing

Fig. 6.29 shows the development of in-plane, compressive forces (in N/mm) in the deck slab edge elements (right across the loading center) with respect to the applied load for various levels of transverse prestressing. It can be observed that the in-plane force initiates with the level of prestressing applied to the bridge deck and remains almost unchanged until the initial cracking load is reached (for instance, 91.3 kN cracking load for a TPL of 2.5 MPa). At first it develops gradually but then increases rapidly with the increasing load until failure.

Fig. 6.30a shows the relationship between the distributed in-plane force (compressive in nature) and the failure load for various levels of transverse prestressing at the ultimate stage. It can be observed that the in-plane force increases with the increasing prestress and the relationship is almost linear. Interestingly, subtracting the initial prestressing force from the total in-plane force corresponding to that particular TPL gives a constant value of the compressive membrane force (CMF  $\approx$  370 N/mm) for the deck slab showing that CMF alone is independent of the transverse prestressing level. This implies that for a particular deck slab having a certain lateral stiffness, the compressive membrane action remains the same if all other parameters remain constant. This agrees well with the concept of compressive membrane action given in literature that the level of the CMA depends on the level of the external restraint available. In the present analysis, varying the transverse prestressing level affects the cracking loads and the failure loads but the compressive membrane action remains the same making CMA more of an inherent structural property. This is further proven in Fig. 6.30b that shows the relationship between the transverse

prestressing and the in-plane force (sum of the transverse prestressing force and the compressive membrane force) developed in the bridge deck. It can be concluded that regardless of the magnitude of the prestressing applied, a certain level of *default* compressive membrane force is developed in the plane of the deck slab due to the built-in restraint available in the form of edge supports (girders), diaphragms, surrounding slab area etc., if all other parameters remain the same (type of loading, concrete strength etc.).

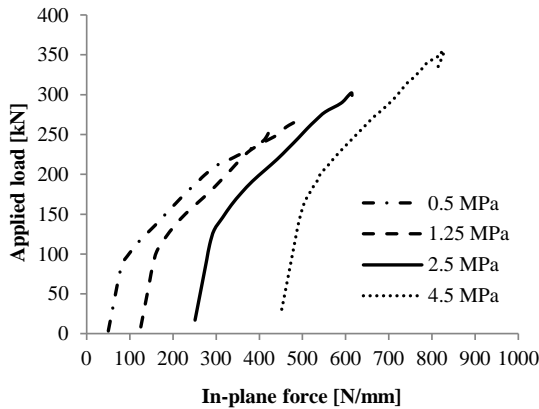


Fig. 6.29 Development of in-plane force (sum of the transverse prestressing force and the compressive membrane force) w.r.t the applied load for the load case PIM with various TPLs. Load case 1 was prestressing pressure. Load case 2 was displacement-controlled incremental load.

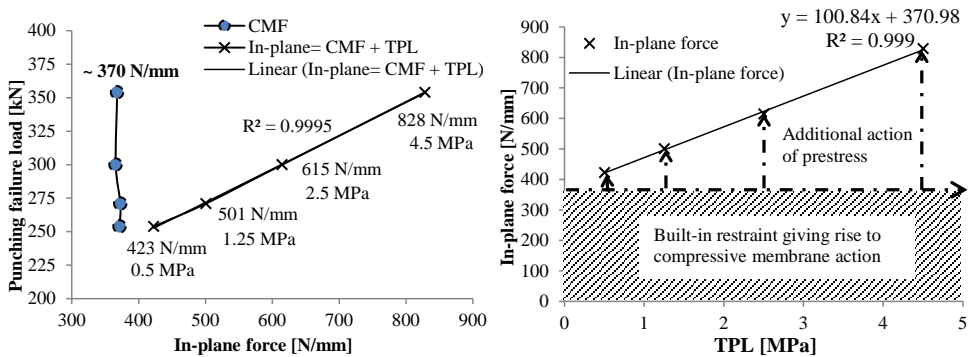


Fig. 6.30 Compressive membrane action: a) Relationship between the punching load and the in-plane force for various TPLs; b) In-plane forces due to the initial prestressing and due to the built-in restraint (compressive membrane force, CMF) in the model bridge deck slab.

## Conclusion

It can be concluded that a linear relationship exists between the punching shear capacity and the in-plane forces arising from the transverse prestressing and compressive membrane

action, where the prestressing is an external action and compressive membrane force is an inherent, internal structural property.

## 6.7 Summary and conclusions

A 3D, solid, 1:2 scaled model of a real bridge was developed in the finite element software DIANA and nonlinear analyses were performed to simulate the experiments done in the laboratory on the same prototype. A basic analysis comprising eight test cases was carried out and it was found that a nonlinear finite element study can simulate the actual structural behavior reasonably well. The results for overall load – deflection behavior, ultimate loads and mode of failure, cracking loads and cracking pattern, stress distribution and compressive membrane action were presented and discussed. The following important conclusions can be drawn from the finite element study:

- Punching shear failures can be well-predicted with nonlinear finite element analysis of 3D solid models. The use of composed elements can lead to the determination of in-plane forces as well as the level of compressive membrane action in a laterally restrained slab which were previously difficult to determine using analytical techniques.
- The mode of failure observed in the finite element model was punching shear similar to the experimental observations and the ultimate loads were also predicted well with a mean  $P_T/P_{FEA}$  (ratio of test failure load to finite element analysis failure load) of 1.02 with a standard deviation of 0.11.
- The initial cracking load for all the finite element test cases was found to be comparable to the experimental values. The cracking pattern was also simulated well.
- It was found that the level of transverse prestressing affects the cracking behavior. The higher the TPL, the higher was the initial cracking load.
- Substantial compressive membrane action was found to occur in the finite element model bridge deck and was established by the occurrence of horizontal lateral displacements after the initial cracking, the transverse stress distribution showing a compression dome in plan and a compressive arch in the cross-section, and the in-plane force distribution of the loaded area and its surroundings.
- The change in the mode of failure, from the theoretically predicted flexural failure to the numerically and experimentally observed punching shear, can be attributed to the compressive membrane action. This is in agreement with the findings of other researchers (Kirkpatrick et al. 1984, Batchelor 1990, Bakht and Jaeger 1992,

Mufti et al. 1993, Fang et al. 1994) that the governing mode of failure of restrained bridge slabs under wheel foot print is not flexure but punching shear.

- A certain amount of compressive membrane action (CMF  $\approx 370$  N/mm) was observed regardless of the magnitude of prestressing leading to the conclusion that a default compressive membrane action exists even for very low levels of prestressing and is dependent on the level of external restraint present.
- The in-plane, compressive forces were found to be a function of the transverse prestressing applied to the deck. The higher the TPL, the higher was the in-plane force. A linear relationship is found to exist between the level of in-plane compressive force and the punching shear load.
- The transverse prestressing along with the compressive membrane action positively affects the bearing capacity of the deck slab and the increase in the capacity with respect to the in-plane force is linear.

The 3D solid finite element model seems to be well calibrated as far as the comparison with the experimental results is concerned. In order to further validate the model, a detailed parametric study will be carried out in the next chapter.

# CHAPTER 7

## Numerical Parametric Study

Previously, a nonlinear finite element analysis of a 3D solid bridge model was described which efficiently simulated typical load cases from the laboratory experiments performed on the same prototype. In this chapter, a detailed parametric study will be carried out covering finite element modeling aspects as well as structural and geometrical variations.

## 7.1 Introduction

A reasonable finite element simulation requires in-depth knowledge of the structural and material behavior since certain assumptions or simplifications have to be made about the geometry and material models have to be selected for the analyses. Regardless of the results being comparable with the actual behavior, a parametric study should always be carried out to analyze the accuracy of the assumptions made and to evaluate the sensitivity of the material and structural parameters in order to validate the model. Therefore, apart from the basic analysis described in the previous chapter, a detailed parametric study has also been carried out to study the effect of different variables on the bearing capacity and is described in the following sections. An effort has been made to include all the experimental parameters discussed in Chapter 5 with the addition of several other aspects that could not be studied experimentally, for e.g. the variation in concrete strength, size of the ducts, higher transverse prestressing levels etc. Comparison with laboratory results is also made, where available.

## 7.2 Important numerical parameters

This section introduces the important parameters that were varied to analyze their effect on the bearing capacity. The 3D solid model bridge deck (2ELEM), its element type and mesh size, loading, material properties, convergence criteria and iteration scheme generally remain the same as in Chapter 6 except when any of these parameter is varied to study its influence on the bearing capacity. Two types of parametric study were carried out: a) Numerical modeling parametric study; b) Geometrical and material parametric study.

The following aspects of the numerical modeling were analyzed and results are presented:

- Mesh sensitivity and element size.
- Influence of the step size of the displacement load.
- Material models for concrete in compression.
- Comparison of the finite element modeling parameters used in this research with the recommendations of Rijkswaterstaat for finite element analysis of concrete structures (RTD 1016 2012).

The following aspects of the structural and loading geometry and material properties were analyzed and compared with the experimental results, where applicable:

- Transverse prestressing level (TPL).

- Position of the load with regard to the transverse deck slab span: Midspan or close to the interface.
- Position of the load with regard to the ducts: Above or in-between the ducts.
- Position of the load with regard to the whole bridge deck: Interior or exterior slab panels.
- Position of the load with regard to the longitudinal span.
- Number of loads: Single or double loads.
- Presence of previous damage to the deck slab panel.
- Size of the loading area (wheel print/loading plate).
- Presence of the ducts and size of the ducts.
- Fracture energy.
- Concrete strength.
- Size effect.

The general notations used in this chapter are as follows: TPL = Transverse prestressing level, FEA = Finite element analysis, FE = Finite element, P1M = Single point load acting the midspan of the deck slab panel, P1J = Single point load acting close to the girder flange-slab interface/joint, P2M = Double point loads at the midspan of the deck slab panel, P2J = Double point loads acting close to the girder flange-slab interface/joint, AD = Above the duct, BD = In-between the ducts, SLP = Small loading plate (115×150 mm),  $P_T$  = Test ultimate load,  $S_T$  = Test ultimate deflection,  $P_{FEA}$  = FEA ultimate load,  $S_{FEA}$  = FEA ultimate deflection, ECOV = Estimation of coefficient of variation of resistance method, GRF = Global resistance factor method, PSF = Partial safety factor method, ULS = Ultimate limit state. Any other notation used is defined within the text.

### 7.3 Numerical modeling parametric study

While constructing the 3D solid bridge model in DIANA, certain parameters were selected that could possibly have an influence on the outcome of the nonlinear finite element analyses. The following sections describe the parametric study carried out to check the influence of these parameters.

#### 7.3.1 Mesh sensitivity and element size

##### General

The finite element mesh size had to be selected carefully since the smeared cracking models are sensitive in that aspect. A fine mesh generally gives a lower bound,

conservative estimate of the capacity, whereas, a coarse mesh can lead to overestimation of the bearing capacity. In literature (Hallgren 1996, Hon 2003), the load-deflection response of a fine mesh is said to be stiffer as compared to a coarse mesh leading to brittle failures in reinforced concrete slabs.

### **Minimum and maximum element sizes**

There is no minimum element size requirement in the “Guidelines of nonlinear FEA of concrete structures” (RTD 1016 2012), however the maximum size is limited to ensure that no snap-back behavior occurs in the simulation. While a too coarse mesh may neither show smooth stress fields nor simulate the cracking behavior accurately (especially where the failure type is punching shear), a finer mesh size will have a higher number of elements in the constant stress zone and as a result more elements will show cracking behavior initially. This can lead to convergence issues in the simulation (RTD 1016 2012).

### **Practical aspects**

A practical aspect of the selection of the finite element mesh size is the computational time and storage requirements. The computational time shows approximately a quadratic increase with the number of elements and therefore requires greater storage space (RTD 2012). The type of the elements and mesh size were also restricted because of the provision of composed elements that require a structured mesh.

### **Mesh size selected for the 3D solid finite element bridge model**

Considering that a 3D solid bridge model had to be constructed and analyzed *nonlinearly*, an optimum solution was found by using two types of mesh in the bridge deck. A fine mesh zone with element size 50×50×50 mm was provided for a limited length of the bridge deck, around the loaded area, and a coarse mesh was provided away from the loaded area where it would cause no influence on the structural behavior (Fig. 6.9, Chapter 6).

### **Parametric analysis**

For the mesh sensitivity and element size parametric analysis, two other bridge deck models were constructed with a finer mesh in the fine mesh zone than the one used in the basic analysis. The main mesh refinement was made over the depth (thickness) of the bridge deck with the maximum element size limited to 50 mm because an element size larger than that in a total bridge deck thickness of 100 mm would have made the mesh too coarse leading to high inaccuracies in the analysis results. The refinement of the fine mesh

## Numerical Parametric Study

zone consequently decreased the element size of the girders but since the girders remained in the linear range, the reduced mesh size was assumed not to have an influence on the structural behavior and is not discussed here. The coarse mesh away from the loaded area remained the same.

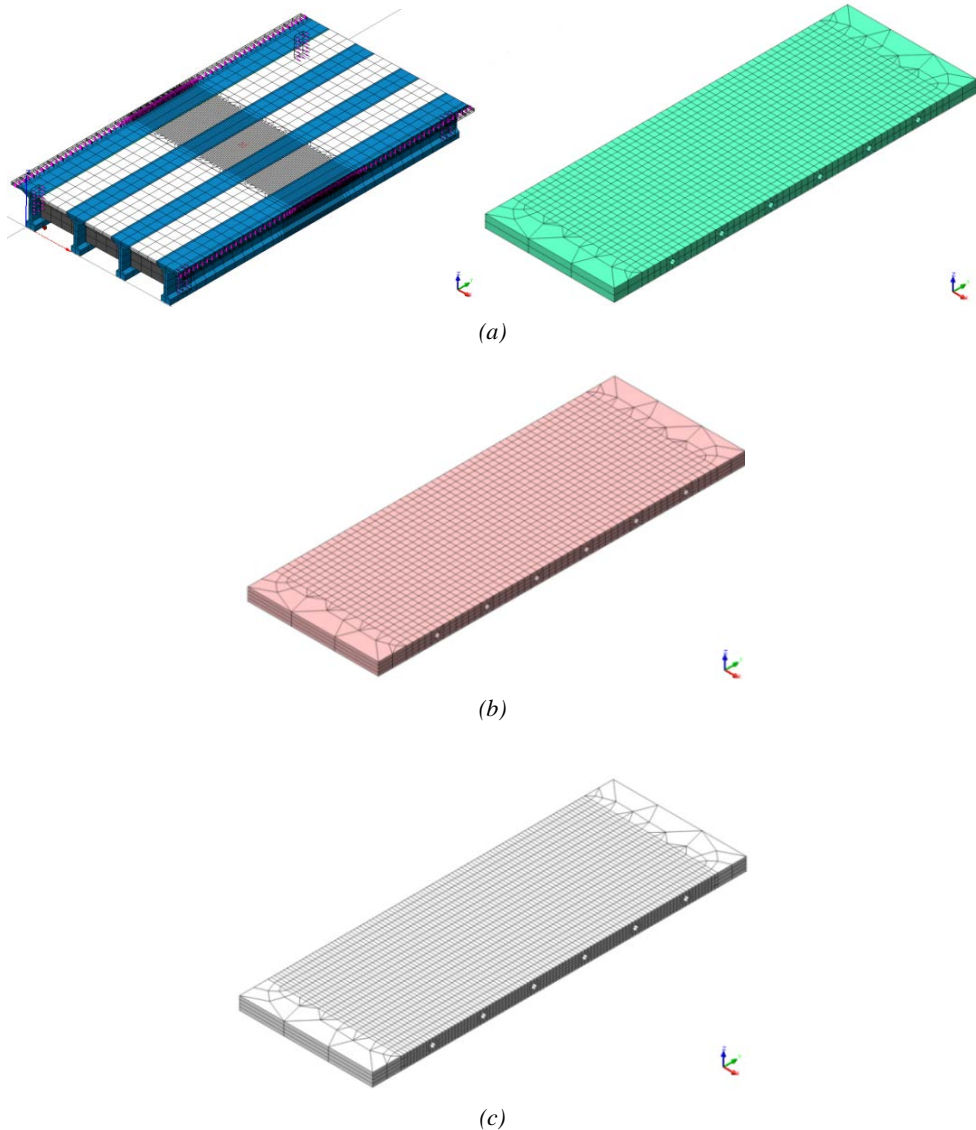


*Fig. 7.1 Finite element mesh sensitivity analysis: a) The original model, 2ELEM slab strip; b) 4ELEM slab strip; c) 6ELEM slab strip.*

Fig. 7.1 shows the fine mesh slab strip constructed for the parametric study: a) The original model with the fine mesh zone having two elements over the depth and a size of  $50 \times 50 \times 50$

## Numerical Parametric Study

mm (2ELEM); b) Four elements over the depth and an element size of 50×50×25 mm (4ELEM); c) Six elements over the depth and an element size of 50×25×16.67 mm (6ELEM).

Table 7.1 shows the ultimate loads and deflections of the three 3D FE bridge deck models with different mesh sizes (2 ELEM, 4ELEM and 6ELEM). Comparing the ultimate loads of the basic 2ELEM model ( $P_{BAS}$ ) with those of finer mesh models, 4ELEM and 6ELEM ( $P_{MOD}$ ) for a P1M load case; the ratio of  $P_{MOD}/P_{BAS}$  is 0.95 for a TPL of 0.5 MPa and CONSTA compression function, whereas, the ratio of  $P_{MOD}/P_{BAS}$  is 0.98 and 0.99 for a TPL of 2.5 MPa for CONSTA and THOREN compression functions respectively.

*Table 7.1 Comparison of ultimate loads and deflections for three models with different mesh size. Load case is P1M in all the simulations.*

Model	Nodes	Elements	Compression function	TPL	$P_{FEA}$	$S_{FEA}$	$P_{MOD}/P_{BAS}$
	#	#		[MPa]	[kN]	[mm]	
2ELEM	96081	19338	CONSTA	2.5	302.3	3.9	1
			THOREN	2.5	296.5	3.8	1
			PARABO	2.5	302.1	3.9	1
			CONSTA	0.5	253	3.7	1
4ELEM	139063	29262	CONSTA	0.5	241	3.25	0.95
6ELEM	275743	63804	CONSTA	2.5	295.6	3.9	0.98
6ELEM	275743	63804	THOREN	2.5	292	3.9	0.98

*Notations:  $P_{BAS}$  = Basic model used in the FEA (2ELEM),  $P_{MOD}$  = Ultimate load for a finer mesh.*

Fig. 7.2 compares the load-deflection behavior for the basic 2ELEM model and the finer mesh models, 4ELEM and 6ELEM. It seems that the sensitivity of mesh size reduces for higher transverse prestressing levels. The ultimate deflections for the 6ELEM simulations are also comparable with those of the basic 2ELEM model. The 4ELEM model for 0.5 MPa TPL is slightly more stiff than its 2ELEM model counterpart.

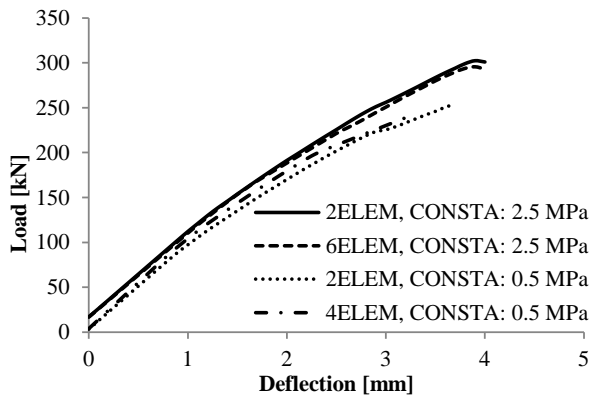


*Fig. 7.2 Comparison of 3D bridge deck models with different mesh sizes.*

## Numerical Parametric Study

Table 7.2 compares the model size (no. of nodes and elements) with the CPU, and I/O times as well as the FILOS file accesses for the three models: 2ELEM, 4ELEM and 6ELEM. It can be observed that the time required to run the simulations increases with the smaller mesh sizes and therefore greater space is needed for the storage of the output data.

*Table 7.2 Comparison of CPU time, I/O time and FILOS file accesses for three models with different mesh size\*. Load case is P1M in all the simulations.*

Model	Nodes	Elements	Material Model	TPL	CPU time	I/O time	FILOS file accesses
	#	#		[MPa]	[sec]	[sec]	#
2ELEM	96081	19338	CONSTA	2.5	5106	1414	66861575
			THOREN	2.5	4549	1407	60880174
			PARABO	2.5	4501	1256	61201319
			CONSTA	0.5	11718	4438	220213741
4ELEM	139063	29262	CONSTA	0.5	27429	10207	492045974
6ELEM	275743	63804	CONSTA	2.5	49825	24777	423343150
6ELEM	275743	63804	THOREN	2.5	49797	21449	372843409

*\*Refer to DIANA-9.4.4 user's manual (2012) for the description of the CPU time, I/O time and FILOS file accesses.*

### Conclusion

It has been demonstrated in chapter 6 that the basic 2ELEM model reasonably simulated the experimental results, including the initial stiffness, the overall load-deflection behavior and the cracking pattern, of typical test cases. Previous sections have shown that the ultimate loads predicted by the basic 2ELEM model were comparable with the finer mesh models and the time required for running a simulation was more practical as compared to the finer mesh sized models, therefore, the 2ELEM model mesh size was deemed reasonable for simulations throughout the finite element study. However, having a finer mesh model with a larger number of elements over the depth can be useful to closely monitor the development of the cracks and the movement of the neutral axis w.r.t the applied load.

### 7.3.2 Influence of the step size of the displacement load

For the incremental displacement-controlled load, a certain step size had to be selected for the finite element simulations. Fig. 7.3 shows the parametric study carried out with regard to the displacement load step size for a P1M load case with a TPL of 2.5 MPa. Three different step sizes were considered: 0.05, 0.1 and 0.2 mm. It can be observed that the load-deflection curves for the three step sizes simply overlap each other if all other parameters remain the same. No difference in the stiffness can be found except that because of the step

size, the cracking loads vary a little but the difference is insignificant. Post the peak load, the iterations of simulation with the smallest step size of 0.05 mm seem to converge rather easily than the larger step sizes that diverged soon after achieving the peak load.

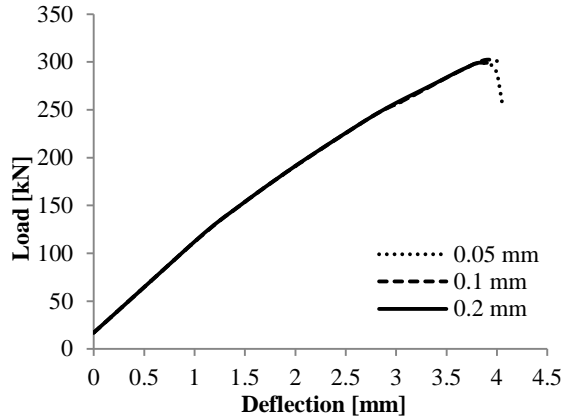


Fig. 7.3 Influence of the step size of the displacement-controlled load on the load-deflection behavior of a typical load case (PIM with a TPL of 2.5MPa).

Table 7.3 compares the CPU, and I/O times as well as the FILOS file accesses for 0.05, 0.1 and 0.2 mm step sizes of the displacement-controlled load. It can be observed that the smallest step sized simulation requires more time to run as compared to the larger step sizes and as a result needs larger storage space for the output results.

Table 7.3 Comparison of CPU time, I/O time and FILOS file accesses for different step sizes for the displacement-controlled load\*. Load case is PIM with a TPL of 2.5 MPa in all the simulations.

Model	Step size	CPU time	I/O time	FILOS file accesses
	[mm]	[sec]	[sec]	#
2ELEM	0.05	8075	2597	114961167
	0.1	5106	1414	66861575
	0.2	4065	1234	56136677

\*Refer to DIANA-9.4.4 user’s manual (2012) for the description of the CPU time, I/O time and FILOS file accesses.

## Conclusion

From the parametric study carried out regarding the step size of the displacement controlled load, a step size of 0.1 mm was deemed suitable for the finite element simulations of the 3D model bridge deck. However, wherever convergence seemed to be an issue, like close to the peak load, the step size was refined to 0.05 or sometimes even 0.025 mm to achieve convergence. In double load cases that showed higher ultimate loads, the initial step sizes were kept at 0.2 mm for a faster simulation run and were later refined to a smaller step size.

### 7.3.3 Material model for concrete in compression

There are several predefined compression functions available within the total strain crack model. In the present study, the function CONSTA was selected assuming an elastic-perfectly plastic behavior of concrete. However, as mentioned in the next section (7.3.4), the *Guidelines of nonlinear finite element analysis of concrete structures* (RTD 1016 2012) recommend the compression function PARABO, a formulation based on fracture energy, according to Feenstra (1993), a parabolic compression diagram with a compression fracture energy for concrete, for beams. Therefore, it was necessary to check the 3D finite element model for its sensitivity against the concrete compression functions. Another compression function, THOREN (Thorenfeldt et al. 1987) was also used in the parametric analysis. Refer to DIANA 9.4.4 user’s manual (2012) for the description of these compression functions. It can be observed that varying the concrete compression function does not have a significant influence for a typical load case (P1M with a TPL of 2.5 MPa) if all other parameters remain the same.

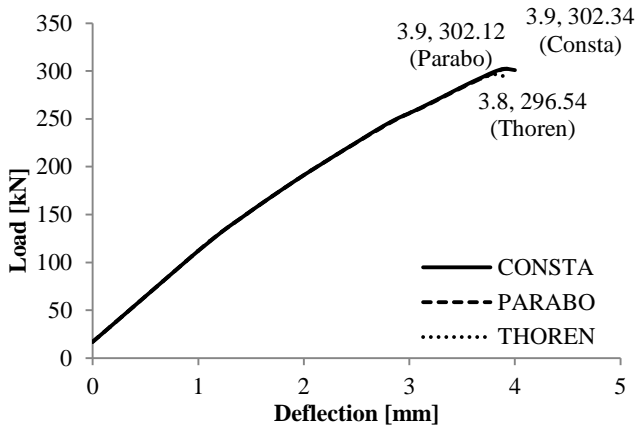


Fig. 7.4 Influence of various concrete compression functions on the load-deflection behavior of a typical load case (P1M with a TPL of 2.5 MPa). The concrete compression fracture energy  $G_c$  was taken equal to 37.5 N/mm (250 times the concrete tensile fracture energy  $G_f$  where  $G_f = 0.150$  N/mm as used in the basic analysis throughout the present study).

### Conclusion

An idealized, elastic-perfectly plastic behavior of concrete in compression (CONSTA function) was assumed in the present study. The purpose of the parametric analysis was to determine if changing the material model would have a significant effect on the results. Since the other functions showed comparable results, and the selected function CONSTA gave good correlation with the experimental observations as well, it was considered to suitably simulate the behavior of concrete in compression.

### 7.3.4 Comparison of the finite element modeling parameters in the present study with the recommendations of Rijkswaterstaat for nonlinear finite element analysis

The Ministry of Infrastructure and the Environment of the Netherlands, Rijkswaterstaat, recommends guidelines for the nonlinear finite element analysis of concrete structures. Although the guidelines focus on structures with beams as the main load carrying members, they can still be used as general recommendations for slabs. Table 7.4 enlists the guidelines given in RTD 1016 (2012) and compares with the parameters used in the present study. Any deviations from the guidelines are remarked upon or justified, wherever applicable.

Table 7.4 Comparison of the finite element nonlinear analysis parameters used in the present study with the guidelines set by Rijkswaterstaat (RTD 1016 2012).

Parameter	Recommendations by the guidelines (RTD 1016 2012)	Parameters used in the present study	Remarks
Units	Consistent	SI Units [N, mm]	Check.
Concrete Properties	MC90/MC2010. For ULS, characteristic, mean or design values should be used. <i>If using MC2010 for fracture energy, <math>G_f</math> a sensitivity study has to be carried out.</i>	Material properties (mean values) derived from laboratory tests or from EC2.	Check. Average of MC90/MC2010 used for $G_f$ . Sensitivity study has been carried out.
Steel properties	Manufacturer, original specifications or in-situ testing. MC90 or MC2010 can also be used.	Values derived from laboratory tests or EC2.	Check.
Concrete material model	A total strain-based rotating crack model.	Total strain rotating crack model.	Check.
	Poisson ratio (0.15) should be reduced. Else do an additional analysis with poisson ratio of 0.0.	Poisson ratio of 0.2 has been used.	An additional analysis with 0.0 value has been performed.
	Use a reduced E modulus (0.85E)	No reduction has been applied.	-
	Exponential softening diagram in tension, eg. Hordijk model.	Hordijk model (HORDYK).	Check.
	Parabolic diagram in compression. Else check ultimate compressive strains.	Elastic plastic model (CONSTA).	Performed check for compressive strains. They do not exceed 0.0035 for single loads. For double loads, < 0.8% volume is showing more than 0.0035 and localized at load point at ultimate stage.
	Tension-compression interaction. Difficult to model.	No softening model applied.	Not important for slabs.
	Compression-compression interaction does not need to be modelled.	Not modelled.	A conservative approach.
Equivalent length/ Crack bandwidth	Automatic determination by FE program.	Crack bandwidth by automatic determination.	Check.

## Numerical Parametric Study

Steel material model	Elasto-plastic material model with hardening ( $E_{har}$ ) for improved stability of the analysis.	Von Mises plasticity.	Plasticity used. No hardening modulus ( $E_{har}$ ) has been used.
Concrete-reinforcement interaction.	For bonded reinforcement: tension stiffening, Slip, Dowel action.	Embedded grid/ smeared cracking/ Hordijk softening used.	As per section 2.4.3.1 in the guidelines, it is a conservative approach to ignore and only consider energy dissipated in cracks.
Finite element	Quadratic interpolation	Quadratic interpolation	Check
	Preferably 20 node hexahedral in 3D.	CHX60 - brick	Check. Composed elements are also quadratic 2D.
		CTP45 - wedge	15 nodes to connect coarse mesh with fine mesh.
	Do not use flat shell elements if shear failure is expected.	Continuum elements used.	Check.
Numerical integration.	Full integration should be used.	Default gauss integration of $3 \times 3 \times 3$ is used.	Check.
	Embedded reinforcement is preferred. Same order of interpolation as concrete elements.	Embedded grid is used with same order.	Check.
Mesh	Regular mesh with less than 5% distorted elements.	Regular, structured mesh has been used.	Check.
Minimum element size	No limit. Determined by practical considerations.	Combination of coarse and fine mesh is used.	Computational time increases quadratically .
Maximum element size	Limited to ensure no snap-back occurs. $H_{eq} < E^*G/f_1^2$	$50 \times 50 \times 50$ mm.	Equivalent length, $H_{eq}=205$ mm. Maximum element edge length = $H_{eq}/2 = 100$ mm
	3D element for slabs ( $l/50, b/50, h/5$ )	$50 \times 50 \times 50$ mm.	A 240, 21, 20 mm element size is not feasible for the one-way spanning slab panel in the present study.
Existing cracks	Can be modelled by reducing tensile strength, E modulus, fracture energy.	Not modelled.	Shrinkage cracks ignored.
Loads	Dead load/permanent loads as initial load case. Displacement controlled load for stability.	Prestressing applied as initial load case. Displacement controlled load.	Check. Self-weight ignored.
Load increment	$0.5 \times$ first crack load	Displacement controlled.	Check. Cracking occurs after 5 steps atleast.
Equilibrium iteration	Newton Raphson with an arc length for stability.	Modified Newton Raphson.	No arc-length control. Peak load achieved by load step refinement.
Convergence	Iterations to be limited. Tolerance of convergence as per guidelines.	Iterations limited to 100 or 150. Tolerance of 0.01 for force and 0.0001 for energy.	Check.
ULS design	GFR/PSF/ECOV Mean properties (fictitious) to be used for GFR. Partial safety factors to be applied.	Actual mean material properties are used.	GFR method used with partial safety factors to calculate design values.

## Conclusion

Although the guidelines for the nonlinear finite element analysis set by RTD 1016 (2012) are applicable more on beams and the current study focuses on the nonlinear analysis of the deck slab, yet they have generally been followed and the deviations, if any, have been reasonably justified.

## 7.4 Geometrical and material parametric study

Several variations in the structural and loading geometry and material properties were made and nonlinear analyses performed to study their influence on the bearing (punching shear) capacity. Comparison with the experimental parametric analyses results is also made, where available.

### 7.4.1 Transverse prestressing level (TPL)

The transverse prestressing level was varied to study its effect on the punching shear capacity. A single load was applied at the midspan (P1M) and at 200 mm c/c with regard to the load center and the interface (P1J) and the TPL was varied between 0.5 to 4.5 MPa. Also a double load was applied at midspan (P2M) and at 200 mm c/c with regard to the load center and the interface (P2J) for 1.25 and 2.5 MPa. All the loads were acting on the exterior panels. All other parameters remained the same as in the basic analysis.

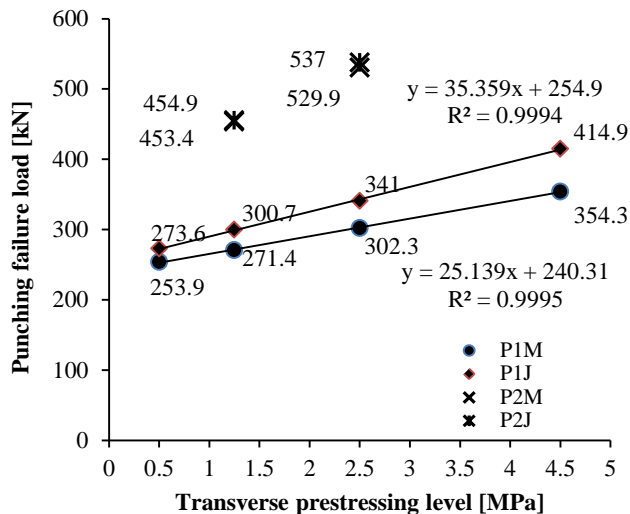


Fig. 7.5 Influence of the transverse prestressing level on the punching shear capacity.

Fig. 7.5 shows that increasing the TPL increases the punching shear capacity of the deck slab and the relationship is almost linear. Similar findings were made in the experimental parametric study (section 5.3.1). The load-deflection behavior shown in Fig. 7.6 depicts an increase in the stiffness for higher TPLs. From section 6.6, it is clear that increasing the TPL, leads to higher in-plane forces and sufficient membrane action exists even for a very low level of 0.5 MPa TPL. The cracking loads shown in Table 6.10 also indicate an increase in the initial cracking loads with higher TPLs. This leads to the conclusion that increasing the transverse prestressing level not only improves the ultimate state behavior but the serviceability state is also improved even when the prestressed deck slab is as thin as 100 mm like in the current study. This correlates well with the finite element studies of other researchers on thin prestressed decks (Poston 1988, Moll 1984, He 1992, Marshe 1997). The additional analysis carried out with 0.5 MPa, P1M load case has been compared with the test BB 21 and 22 in section 7.5.

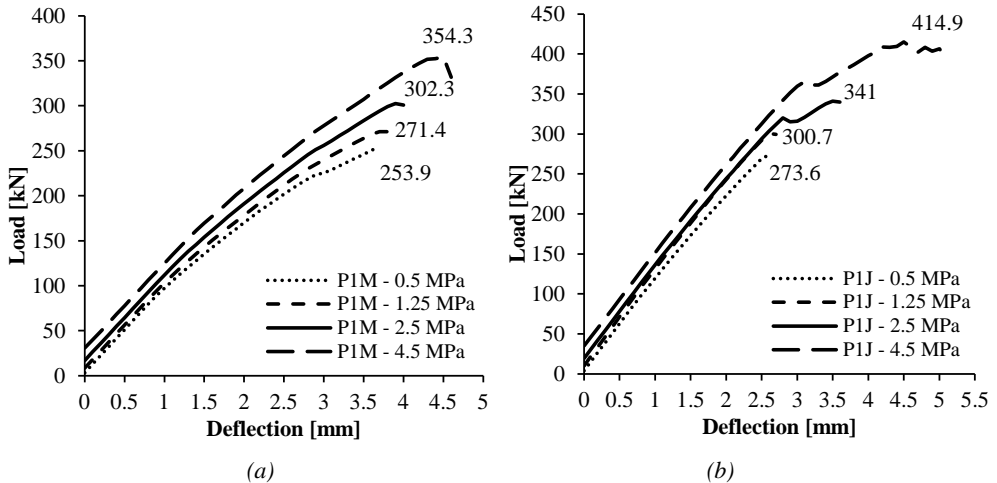


Fig. 7.6 Influence of the transverse prestressing level on the load-deflection behavior: a) Single load acting at midspan (P1M); b) Single load acting close to the interface (P1J).

It is also interesting to note that for a higher TPL (2.5 MPa and 4.5 MPa), when the load is applied close to the interface, the load-deflection curve shows a *snap-through* behavior which is not present when the TPL is low (0.5 MPa and 1.25 MPa). This could be because when the TPL is high and the load is applied close to the higher strength girder flange, after the first peak (also known as first limit point in literature), instead of achieving failure, the deck slab shows some residual capacity and achieves another equilibrium path. Basically a snap-through response combines softening (after the first limit point) with hardening (after the second limit point). The response branch between the two limit points is unstable owing to the negative stiffness. If in the present case, a larger step-size had been used, this snap-through behavior could not have been captured.

### 7.4.2 Position of the load with regard to the transverse deck slab span: Midspan or close to the interface

The position of the load with regard to the transverse slab span is studied in this section. Both single and double loads were applied at midspan of the deck slab and close to the girder flange-deck slab interface (200 mm c/c). Only an exterior panel was loaded.

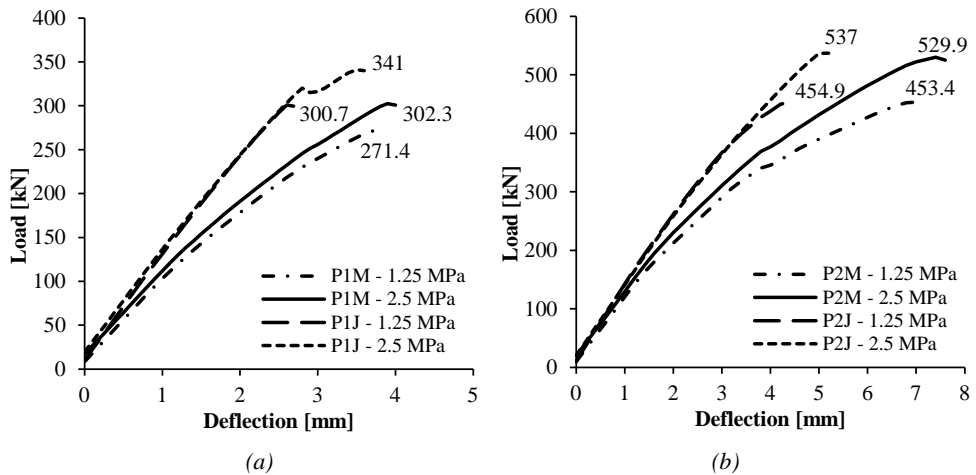


Fig. 7.7 Influence of the position of the load (midspan and close to the interface) on the load-deflection behavior for a TPL of 1.25 and 2.5 MPa: a) P1M and P1J; b) P2M and P2J.

Fig. 7.7 shows that a higher bearing capacity was achieved when a single load was applied close to the girder flange-deck slab interface (P1J) than at midspan of the deck slab panel (P1M) regardless of the level of transverse prestressing. This could be because in the P1J case, the higher concrete strength of the girders led to an increase in the stiffness resulting in higher ultimate loads with smaller deflections. Failure was brittle punching in both cases.

When a double load was applied at midspan (P2M) and close to the interface (P2J), almost no difference in the ultimate load was observed which is in sharp contrast to the single load case. However, the stiffness was higher and the deflections were smaller for the P2J case as compared to P2M, similar to the single load case. This can be explained by the fact that the double loads at midspan (P2M) showed flexural behavior leading to much larger deflections and also higher loads that may not have been achieved if brittle punching was governing. Failure always occurred in the span of the slab regardless of the position of the load which correlates with the experimental observations as well.

### 7.4.3 Position of the load with regard to the ducts: Above or in-between the ducts

Most of the finite element analyses were performed by loading in-between the ducts. Previous research by He (1992) on prestressed decks indicated that loading above a prestressing duct (having bonded tendons) could influence the load deflection behavior positively. Hence, the influence of the loading position with regard to the ducts was investigated numerically with loads applied on the exterior panels. A TPL of 1.25 MPa was applied. All other parameters remained the same as in the basic analysis.

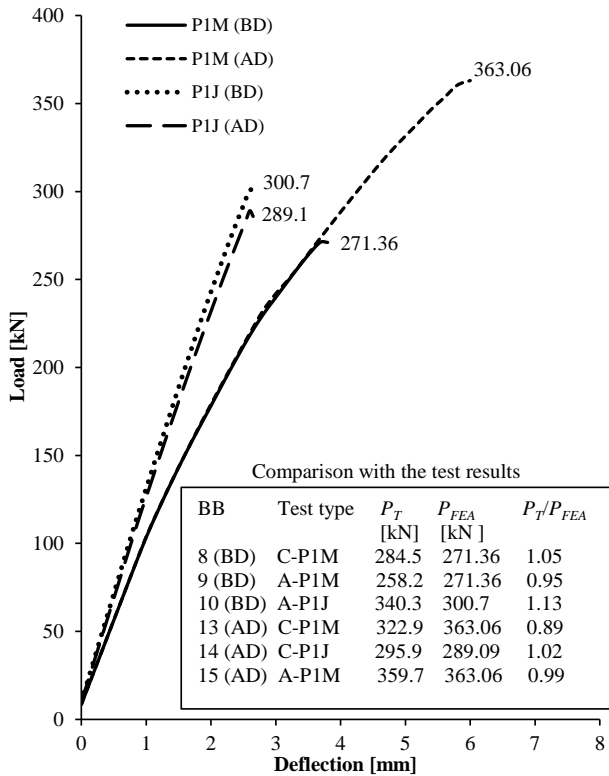


Fig. 7.8 Influence of the loading position with regard to the ducts on the load – deflection behavior (P1M and P1J applied with a TPL of 1.25 MPa for this analysis). BD and AD indicate in-between or above the ducts respectively. A and C in the test type indicate the exterior deck slab panels.

Fig. 7.8 shows that when the load was applied at the midspan and above a duct, the deck slab failed at a higher load and deflection compared to when the same load was applied in-between two ducts, however the stiffness remained the same. For loads close to the interface, no significant difference was found with loading above or in-between the ducts in

the load-deflection behavior. Experimentally, as discussed in section 5.3.3, similar result was obtained for the midspan test cases (BB13 and 15), i.e. a higher capacity was obtained when loaded above the ducts as compared to when loaded in-between the ducts (BB8 and 9). However, for the interface test BB14, a lower capacity was obtained when the deck slab panel was loaded above the duct than when loaded in-between the ducts (BB10). This discrepancy has already been explained in section 4.3.2, noting that the test BB14 was the last test performed on the slab panel C which was severely damaged by previous tests. The FEA simulation for this test did not include previous damage effects.

It can be concluded that the deck slab shows a higher capacity when loaded directly above a prestressing duct. As explained before in section 5.3.3, possible reason can be the distribution of maximum load to two adjacent duct-to-duct panels when the load acts above a duct, whereas, loading in-between the panels can limit the maximum load distribution to the area within one duct-to duct panel. This could also explain why no difference was found when the load was acting close to the interface, since in this case, the proximity of the girder played a major role in the bearing capacity rather than load position with respect to the ducts. It can also be concluded that the results of this research represent a lower bound of the bearing capacity since most of the analyses were performed in-between the prestressing ducts.

### **7.4.4 Position of the load with regard to the deck slab panels: Interior or exterior deck slab panels**

Fig. 7.9 shows the effect of loading the interior or the exterior deck slab panels for a particular load type. The TPL used for the analysis was 2.5 MPa. All other parameters remained the same as in the basic analysis.

Fig. 7.9a shows P1M and P1J with loads applied at the interior or exterior panels. It can be observed that for P1M, the interior and exterior deck slab capacities are almost equal whereas for P1J, the capacity of the interior panel is 1.09 times that of the exterior panel. Fig. 7.9b shows the case of the double load applied at interior and exterior panels (P2M load case). Both experimental and numerical capacities of the interior deck slab panel are 1.12 times that of the exterior deck slab panel. It can also be observed that the stiffness of the interior and exterior deck slab panels in all load cases is fairly comparable. Since there is no clear relationship between the capacity of interior and exterior deck slab panels for the analyzed load cases, this factor is considered not to have a significant influence. In the present study, the capacity of the exterior panels has mostly been considered which makes it a lower bound.

## Numerical Parametric Study

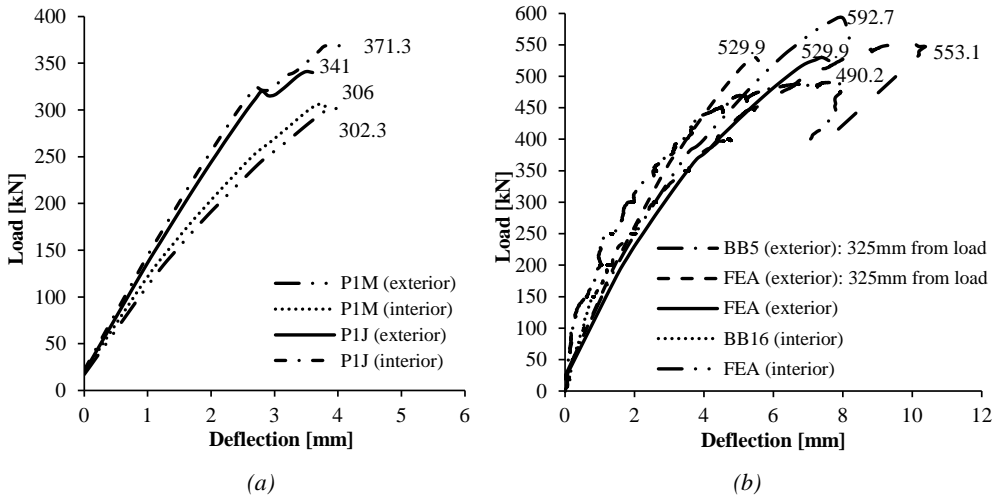


Fig. 7.9 Influence of loading interior and exterior slab panels (TPL 2.5 MPa): a) P1M and P1J; b) Comparison of FEA and test results for the load case P2M. The deflections were measured at a transverse distance of 325 mm from the double load centers in BB5 (Stevin Report No. 25.5.13-06).

### 7.4.5 Position of the load with regard to the longitudinal span

Fig. 7.10 shows the effect of the loading position with regard to the longitudinal deck span or its proximity with the transverse beams at the end for the load case P1M. Both experimental (BB1 and 7) and numerical results are presented. The TPL used for the analysis was 2.5 MPa. All other parameters remained the same as in the basic analysis.

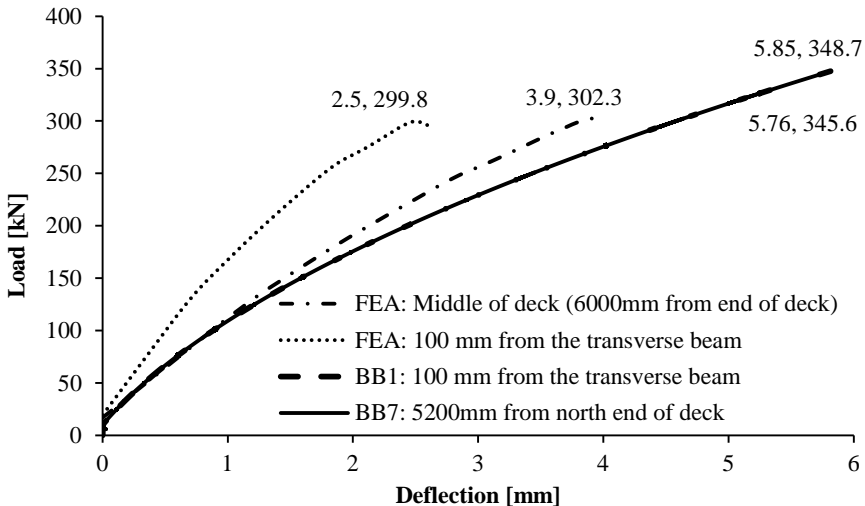


Fig. 7.10 Influence of the longitudinal position of the load and proximity with the transverse beam for P1M load case (TPL 2.5 MPa).

It can be observed that in the finite element analyses, there was almost no difference in the ultimate load, however, a much higher stiffness is observed when the load was placed close to the end transverse beam. As a result, the ultimate deflection is only 2.5 mm as compared to the ultimate deflection of 3.9 mm when the load was placed at the middle of the deck. This higher stiffness can result from the extra restraining action from the prestressed transverse beam. In contrast to the numerical results, no difference in the load-deflection behavior was found experimentally. A probable reason behind this discrepancy between the two results is the overall stiffer response (smaller deflections and displacements) of the finite element model as compared to the laboratory specimen even for the same load position. Therefore, moving the load close to the transverse beam pronounced this difference even more.

### 7.4.6 Number of loads: Single or double loads

Fig. 7.5 showed the influence of a single or a double load on the bearing capacity of the bridge deck. It can be observed that for both midspan and interface load cases, double loads show a higher bearing capacity as compared to single loads, if all other parameters remain the same. The influence of a single or double load on the load-deflection behavior is demonstrated in Fig. 7.11. Larger ultimate loads and ultimate deflections are observed for the double loads (P2M and P2J) as compared to the single load (P1M and P1J). The difference between  $P_{double}$  and  $2P_{single}$  probably exists because of the overlapping of the stress fields of the double loads placed close to each other and as a result a lesser punching shear capacity is obtained, as discussed before in section 5.3.7.

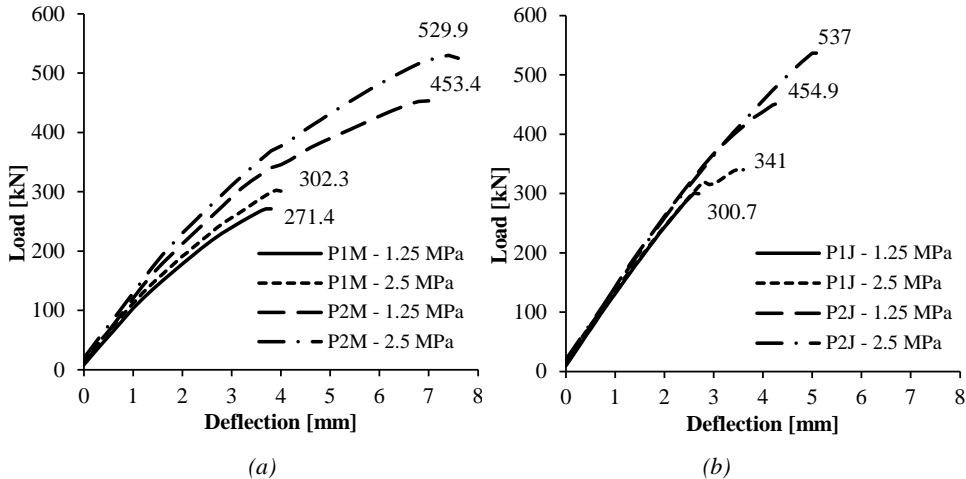


Fig. 7.11 Influence of applying single or double loads on the load – deflection behavior of the bridge deck (TPL = 1.25 and 2.5 MPa): a) P1M and P2M; b) P1J and P2J.

Experimentally, the bearing capacities obtained by applying double loads at the midspan were 0.72 and 0.76 times that of twice the capacities for single loads with TPLs of 2.5 and 1.25 MPa, respectively ( $P_{double}/2P_{single} = 0.72-0.76$ ). In the finite element analysis, the ratio  $P_{double}/2P_{single}$  is 0.88 and 0.84 for TPLs of 2.5 and 1.25 MPa, respectively. In section 5.4, a factor of 0.7 was recommended to be used when deriving the bearing capacity of prestressed decks with double loads using twice the capacity of single loads. From the results of FEA, it can be observed that the factor of 0.7 is on the conservative side.

### 7.4.7 Size of the loading area (wheel print/loading plate)

Fig. 7.12 shows the load-deflection behavior of the deck slab when the load is applied on a 125×150 mm loading area (18750 mm<sup>2</sup>). It is compared with BB19 which had a loading plate of size 115×150 mm (17250 mm<sup>2</sup>). The load case is P1M with the load applied on the interior deck slab panel B and having a TPL of 2.5 MPa. It can be observed that the load-deflection behavior of the FEA model is stiffer as compared to BB19, however, the ultimate loads show excellent agreement.

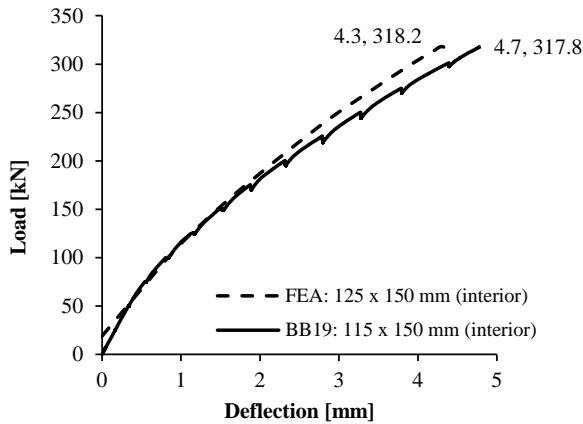


Fig. 7.12 Influence of the size of the loading area on the load – deflection behavior of the bridge deck (TPL = 2.5 MPa).

Table 7.5 shows the influence of the size of the loading plate with various lengths of the loading areas in the transverse direction. The longitudinal length remains the same. It can be observed that with an increasing transverse length, the ultimate capacity also increases. Similar findings have been reported by Regan (1982), Furuuch et al. (1998) and Lantsoght (2013). ASCE-ACI committee 426 (1974) reports an increase in the shear strength for decreasing  $c/d$  (column side length/effective depth) ratios. The higher shear capacity for an increasing loading area is attributed to an improved load redistribution. However, in the current study, the percentage increase in the ultimate capacity is relatively small as

compared to the large percentage increase in the length. This could be because the transverse span of the deck slab is only 1050 mm as compared to the length (12000 mm) and a change in the transverse length of the loading plate may not affect the capacity too much.

Table 7.5 Influence of increase in the transverse length of the loading area (wheel print).

Model	Dimensions of the loading plate, Length×Width	Area of the loading plate	Percentage increase in length w.r.t model 1	FEA ultimate load, $P_{FEA}$	Percentage increase in capacity w.r.t model 1
	[mm×mm]	[mm <sup>2</sup> ]	[%]	[kN]	[%]
1.	100×100	20000	-	285.25	-
2.	150×200	30000	50	299.3	4.92
3.	200×200	40000	100	302.3	5.97

### 7.4.8 Presence of previous damage to the deck slab panel

The influence of previous damage to the deck slab panel was studied numerically by using an approach inspired by He (1992). Some elements from a deck slab panel, which was in the transverse direction from the loaded panel, were removed and the bridge deck was analyzed. Then, more elements were taken out in the longitudinal direction from the loaded deck slab panel and the deck slab was analyzed again. The pattern in which the elements were removed symbolized, more or less, the typical punching shear failures. Results for a P1M load on an exterior panel with a TPL of 2.5 MPa are presented in Fig. 7.13.

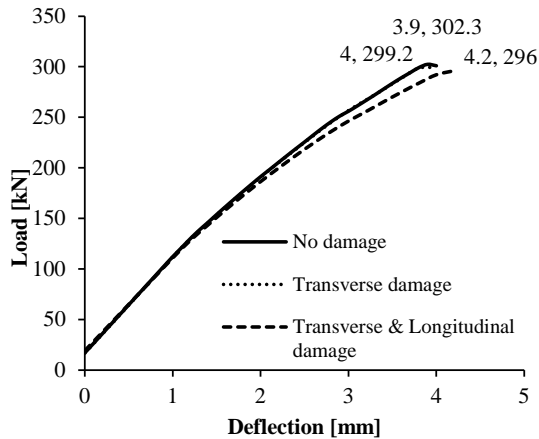


Fig. 7.13 Influence of previous damage on the load-deflection behavior of the deck slab (P1M with a TPL of 2.5 MPa).

It can be observed that the transverse damage to the deck slab did not significantly influence the load – deflection response or the ultimate capacity. The damage in the longitudinal direction lowered the stiffness after the initial cracking (93 kN) and also

showed a slight reduction in the bearing capacity that is still small enough to be ignored. This is in contrast to the experimental observations that show a significant reduction in the bearing capacity for test BB12 on slab panel A and tests BB13 and 14 on slab panel C. However, similar results are reported by He (1992) where the previous damage was found to be significant in the experiments while the finite element results did not show much influence. This could be because the modeling technique of the damaged panels did not fully simulate the actual damage exerted to the panels in the laboratory tests.

### 7.4.9 Presence of ducts and size of the ducts

The influence of the presence and the size of the ducts has been investigated by making 3D bridge finite element models with no ducts, 25 mm  $\Phi$  ducts and the basic 45 mm  $\Phi$  ducts (2ELEM) model and analyzing them nonlinearly. The mesh size, element type, loading, nonlinear analyses parameters and all other geometrical and material properties remained the same.

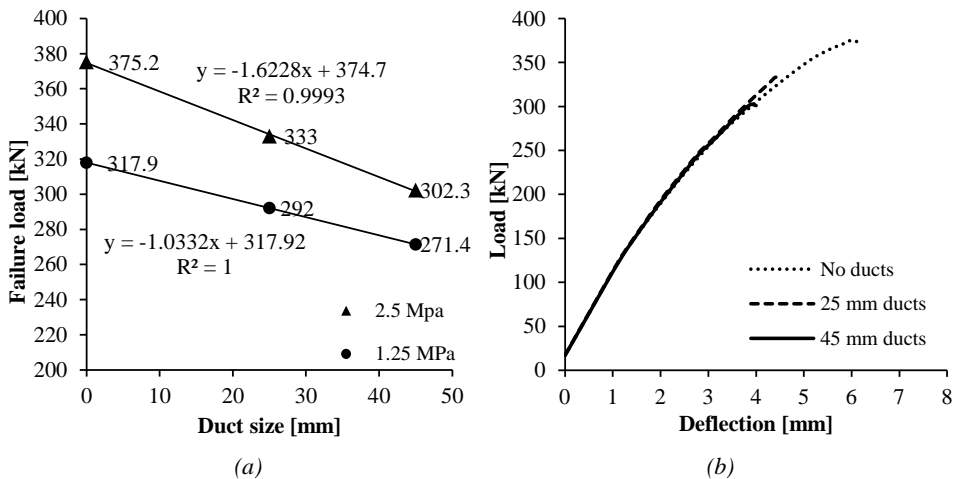


Fig. 7.14 Influence of ducts on the behavior of the deck slab (PIM load case: a) Ultimate bearing capacity for TPLs of 1.25 and 2.5 MPa; b) Load-deflection behavior for a TPL of 2.5 MPa.

Fig. 7.14a shows the influence of ducts on the ultimate load bearing capacity (punching shear capacity) for a load case of PIM on an exterior panel, with two levels of transverse prestressing: 1.25 and 2.5 MPa. It can be observed that the ultimate bearing capacity increases linearly for a reducing duct size, the highest being for no ducts in the decks as a larger volume of concrete is available for carrying the load. Also a larger rate of increase in capacity is observed for a higher level of transverse prestressing which could be because of a larger rate of increase of compressive membrane action being developed for a higher transverse prestressing level.

Fig. 7.14b shows the load-deflection behavior for a P1M load case with a TPL of 2.5 MPa. It can be seen that the stiffness remains the same for the three models, however, the ultimate load and the deformation capacity with reduction in the size of ducts (larger concrete volume) and is highest for the model with no ducts.

### 7.4.10 Fracture energy

Section 6.3.3 explains how a fracture energy ( $G_f$ ) of 0.15 N/mm was selected for the current finite element study for general analyses (based on MC90 and MC 2010). Therefore, it was deemed important to study the influence of  $G_f$  on the capacity of the deck slab since there is a difference between the theoretical determination of fracture energy by using Model Code 90 (1993) and Model Code 2010 (*fib* 2012). MC90 gives lower values while MC2010 gives much higher values of the fracture energy for the same concrete strength and aggregate size. Also, RTD 1016 (2012) suggests a sensitivity analyses for fracture energy in case MC2010 has been used to calculate its value for the nonlinear analyses. A third reason and probably the most important one for carrying out a parametric analyses for  $G_f$  is its large influence on the punching shear capacity reported in the literature. A higher value of  $G_f$  leads to a stable growth of cracks in the tensile chord increasing the height of the compression zone and ultimately increasing the punching shear capacity with more brittle failures (Ozbolt and Vocke, *fib* 2001).

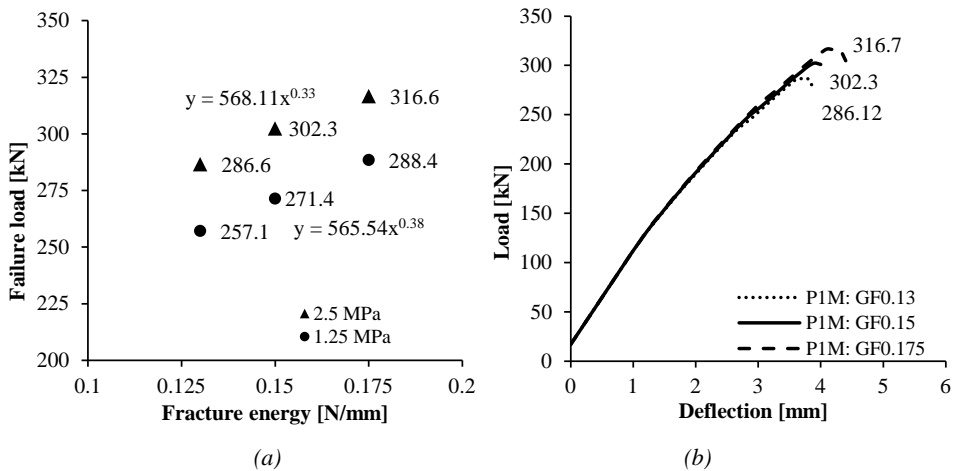


Fig. 7.15 Influence of the fracture energy on the behavior of the deck slab (P1M load case): a) Ultimate bearing capacity for a TPL of 1.25 and 2.5 MPa; b) Load-deflection behavior for 2.5 MPa.

The influence of  $G_f$  on the ultimate capacity of the model bridge deck was determined by carrying out analyses with 0.13 N/mm and 0.175 N/mm fracture energy along with the general value of 0.15 N/mm used in the present study. The load case applied was P1M on

an exterior panel and two levels of transverse prestressing were investigated (1.25 and 2.5 MPa). All other parameters remained the same as in the basic analyses. Fig. 7.15a shows a positive influence of the fracture energy on the ultimate capacity with the capacity being approximately a cube root function of the fracture energy which is similar to findings of Ozbolt and Vocke (*fib* 2001). Fig. 7.15b shows that although there is no difference in the stiffness of the deck slab for the three levels of  $G_f$  checked for the analysis (0.13, 0.15 and 0.175 N/mm), the deformation capacity of the deck slab increases with increasing fracture energy. As a result the ultimate bearing capacity (punching shear in this case) also increases which correlates well with the observations made by Hallgren (1996).

### 7.4.11 Concrete strength

It is generally accepted in literature that increasing the concrete strength improves the punching shear capacity although the contribution of compressive and tensile strength towards the capacity differs in magnitude. Here, the influence of the concrete strength was studied by varying the important material properties of the concrete like the compressive strength, the tensile strength and the fracture energy. A normal strength concrete (NSC) with a mean compressive cylinder strength ( $f_{cm}$ ) of 50 MPa, mean tensile strength ( $f_{ctm}$ ) of 4.5 MPa and a fracture energy ( $G_f$ ) of 0.13 N/mm and a high strength concrete, HSC1 (Hallgren 1996) with an  $f_{cm}$  of 91.3 MPa,  $f_{ctm}$  of 6.21 MPa and a  $G_f$  of 0.179 N/mm was used. The control analysis case (test) was the concrete strength used in the laboratory tests as well as in the basic finite element analyses. A single load was applied on an exterior panel in all cases with a TPL of 2.5 MPa. All other parameters remained the same as in the basic analyses.

Fig. 7.16 shows that the ultimate bearing capacity of the deck slab has a direct relation with the concrete strength. A higher concrete strength improves the punching shear capacity (Hallgren 1996, Edalatmanesh and Newhook 2012, Hassan et al. 2002) although the response is slightly stiffer after initial cracking and a more brittle behavior is observed (Fig. 7.16a, b). Fig. 7.16c, d show the punching capacity as a function of compression strength and tensile strength respectively for the three concrete types investigated (NSC, Test and HSC1). It can be observed that the tensile strength seems to influence the punching shear capacity by a much larger degree than the compressive strength (similar observations by Menetrey 1994) and although there is an increase in brittleness, it is not as high as reported in the literature. This could be because of the results being dependent on the overall concrete class. For instance, *increasing the tensile strength or the compressive strength alone may show a higher rate of increase of brittleness but if the fracture energy is also*

increasing proportionally, it may reduce the rate of increase of brittleness for that particular strength, since a higher fracture energy leads to a more ductile behavior.

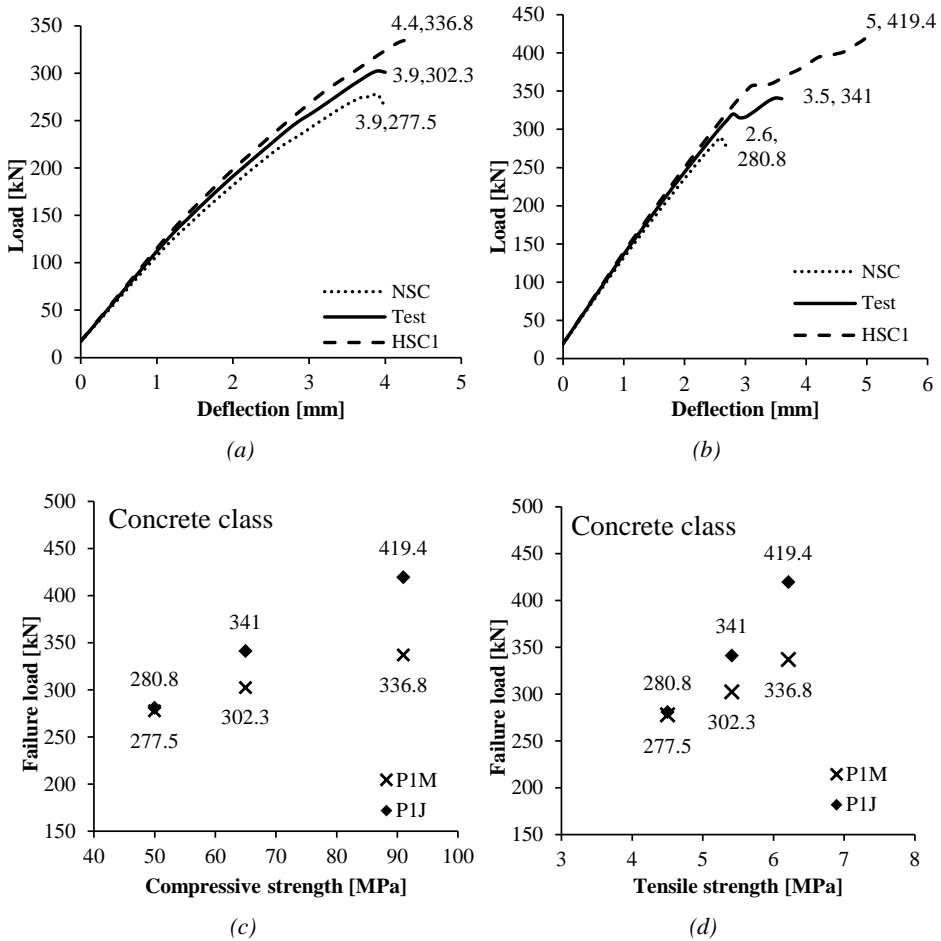


Fig. 7.16 Influence of the concrete strength on the behavior of the model bridge deck (TPL = 2.5MPa): a) Load-deflection behavior for P1M; b) Load-deflection behavior for P1J; c) Influence of the compressive strength on the ultimate capacity for P1M and P1J; d) Influence of the tensile strength on the ultimate capacity for P1M and P1J.

### 7.4.12 Size effect

Bazant and Cao (1987) state that the nominal strength decreases with an increase of the structural size. This phenomena is termed as *size effect* in literature. The size effect is an established phenomena for shear in beams and slabs (Elstner and Hognestad 1956, Kani 1967, Collins and Kuchma 1999, Hallgren 1996, Mitchell, Cook and Dilger 2005, Broms 2006, Birkle and Dilger 2008, Muttoni 2008). It is important to determine the size effect in

the current study since the experiments have been based on a 1:2 scaled model of a real bridge having a deck slab thickness of only 100 mm. In reality, the bridge deck is 200 mm thick and since the size effect is an established factor for punching shear, the results from the scaled model cannot simply be projected by using the geometrical scale factor only to obtain punching shear capacity for the real bridge. A structural size factor that takes into account the thickness of the deck slab has to be used to predict the ultimate loads for the real bridge. Experimentally, it is difficult to analyze a full scale bridge due to economic constraints but a finite element study can easily be carried out. Therefore, a numerical approach to determine the size effect was employed in the current study.

A 3D finite element real bridge model (RB4ELEM) was constructed in DIANA to study the size effect on the bearing capacity (Fig. 7.17). Section 3.1.1 gives an overview of the real bridge on which the prototype has been based for this study. The scale factors used to design the prototype have also been discussed in section 3.1.2. Not all components of the real bridge could be scaled down exactly to 1:2 due to design and construction limitations (for instance, the size of the girders or the ordinary reinforcement) but all the main components of the bridge like the deck slab, the duct spacing, the transverse prestressing level have been appropriately used.

The main features of the real bridge finite element model are mentioned below:

- The bridge model consists of four girders, three deck slab panels and two transverse beams. The girders and the transverse beams remain in the linear range while the deck slab is analyzed nonlinearly just like the model bridge deck.
- The girders are 3000 mm high with a web thickness of 200 mm. The top flange is 1500 mm and the bottom flange is 580 mm wide.
- Each deck slab is 2100 mm wide and 12000 mm long with a thickness of 200 mm.
- 400 mm wide transversely prestressed end transverse beams are present close to the supports.
- Four ducts of 50 mm diameter are modeled in the transverse direction in the deck slab at a spacing of 800 mm c/c.
- The top and bottom horizontal grid consists of a thickness of 0.25 mm and 0.2 mm in x and y directions respectively. The vertical grid consists of a thickness of 0.2 mm in the y direction.
- A similar transverse prestressing level is applied to the real bridge deck model (RB4ELEM) as in the scaled bridge deck model (2ELEM). The displacement load applied to the deck is spread over an area of 400×400 mm, similar to the wheel print area for a real case given for Load Model 1 in NEN:EN 1991-2:2003.

## Numerical Parametric Study

- The modeling technique, the mesh size, the element type, the material properties and the nonlinear analysis parameters remain the same as in the 2ELEM model. However, assuming that the real bridge has a larger aggregate size than the model bridge deck, a fracture energy of 0.175 N/mm has been used in the analyses. It is remarkable that for the scaled model with an aggregate size of 20 mm, the fracture energy calculated by MC90 (0.135 N/mm) is lower than the one by MC2010 (0.155 N/mm). But for the real bridge model, assuming an aggregate size of 32 mm, MC90 gives a higher value (0.21 N/mm) than MC2010 (0.155 N/mm), since the latter calculates a constant fracture energy for any aggregate size if the mean compressive strength of concrete remains the same.

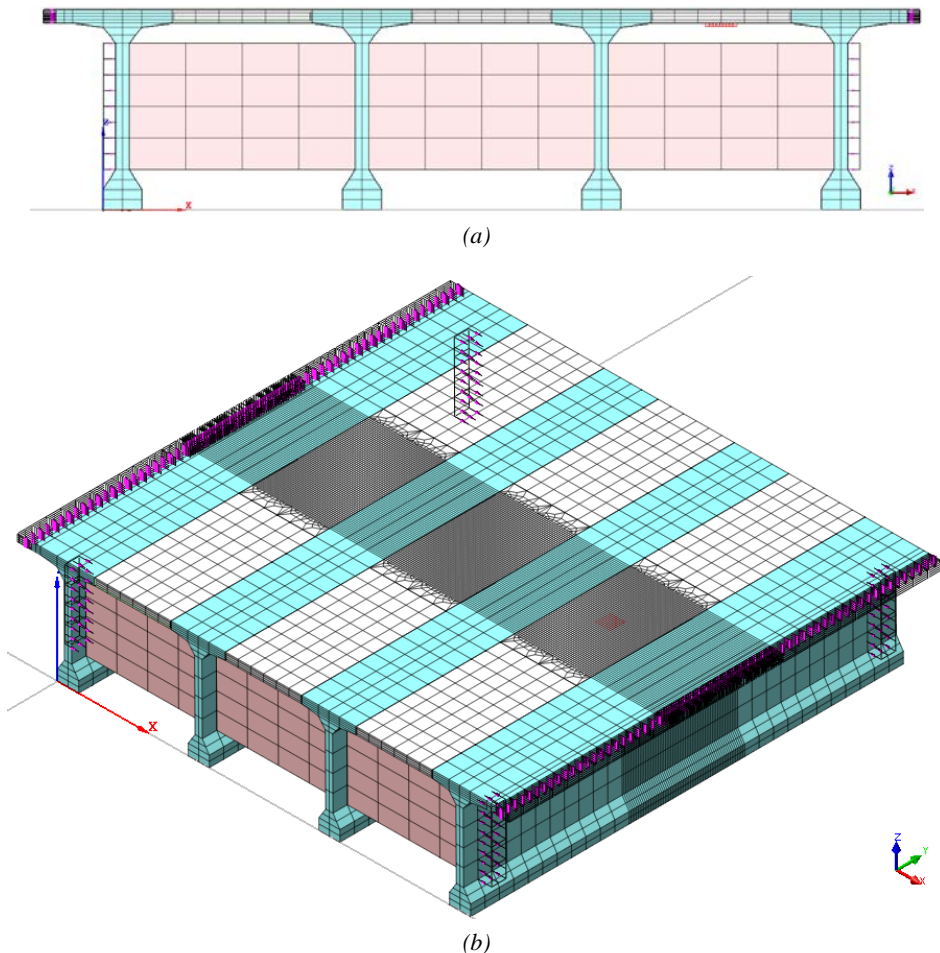


Fig. 7.17 The finite element real bridge model (RB4ELEM) loaded by transverse prestressing pressure and the displacement load on the exterior panel (PIM): a) The cross-section of the model; b) The 3D view of the model.

**Summary of analysis results for the RB4ELEM model**

A single load at midspan (P1M) of the exterior panel was applied to the real bridge model with the transverse prestressing levels of 0.5, 1.25 and 2.5 MPa and was analyzed nonlinearly. All other parameters remained the same. The main results are summarized in the Table 7.6. Fig. 7.18a shows the load-deflection behavior of RB4ELEM model and Fig. 7.18b shows the ultimate loads for the RB4ELEM and 2ELEM (25 mm and 45 mm  $\Phi$  ducts) models. The cracking pattern ( $E_{knn}$ , normal crack strain) close to the failure for P1M load case with a TPL of 2.5 MPa is shown in Fig. 7.19.

Table 7.6 Summary of analysis results for the RB4ELEM model.

Test RB.	TPL	$P_{FEA, RB}$	$S_{FEA, RB}$	$P_{CR, FEA}$	$P_{CRS, FEA}$	$N_{xx}$	FMODE
	[MPa]	[kN]	[mm]	[kN]	[kN]	[N/mm]	
1.	0.5	678.3	3.6	240	328.3	486	Brittle punching
2.	1.25	957.5	6.1	277	368.4	864	
3.	2.5	1228.8	7.6	295.3	397	1240	

Notations:  $P_{FEA, RB}$  = Real bridge FEA ultimate load,  $S_{FEA, RB}$  = Real bridge FEA ultimate deflection.  $P_{CR, FEA}$  = FEA initial cracking load,  $P_{CRS, FEA}$  = FEA Initial inclined shear cracking load,  $N_{xx}$  = In-plane force, FMODE = Failure mode.

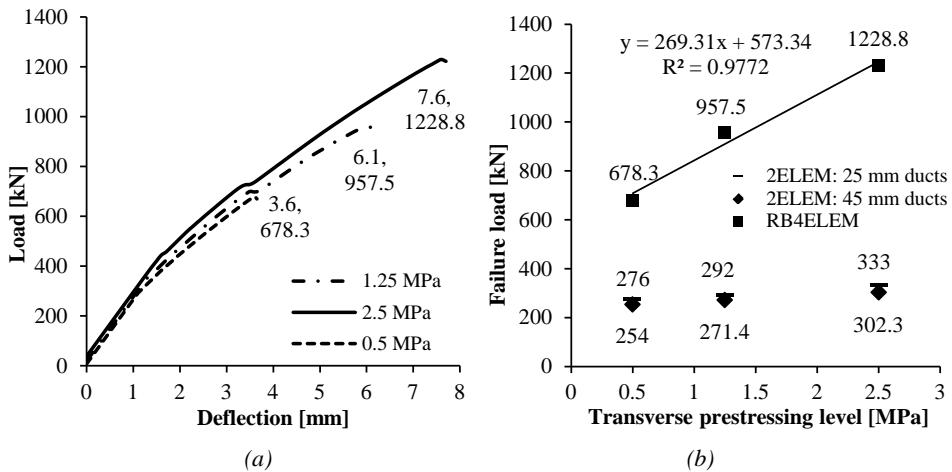


Fig. 7.18 Behavior of the real bridge 3D finite element model (RB4ELEM) for 1.25 and 2.5 MPa transverse prestressing levels and P1M load case: a) Load-deflection behavior; b) Ultimate loads.

Table 7.6 and Fig. 7.18 show that when a single load acts on the transversely prestressed real bridge deck model (RB4ELEM), punching shear failure occurs and a higher TPL leads to a higher punching shear capacity. The stiffness, the initial flexural cracking load and the initial inclined shear cracking load, and the in-plane force (sum of the transverse prestressing force and the compressive membrane force) are also improved by increasing the TPL. The typical radial and tangential cracking and a cone-like failure associated with the punching shear mode can be observed in Fig. 7.19.

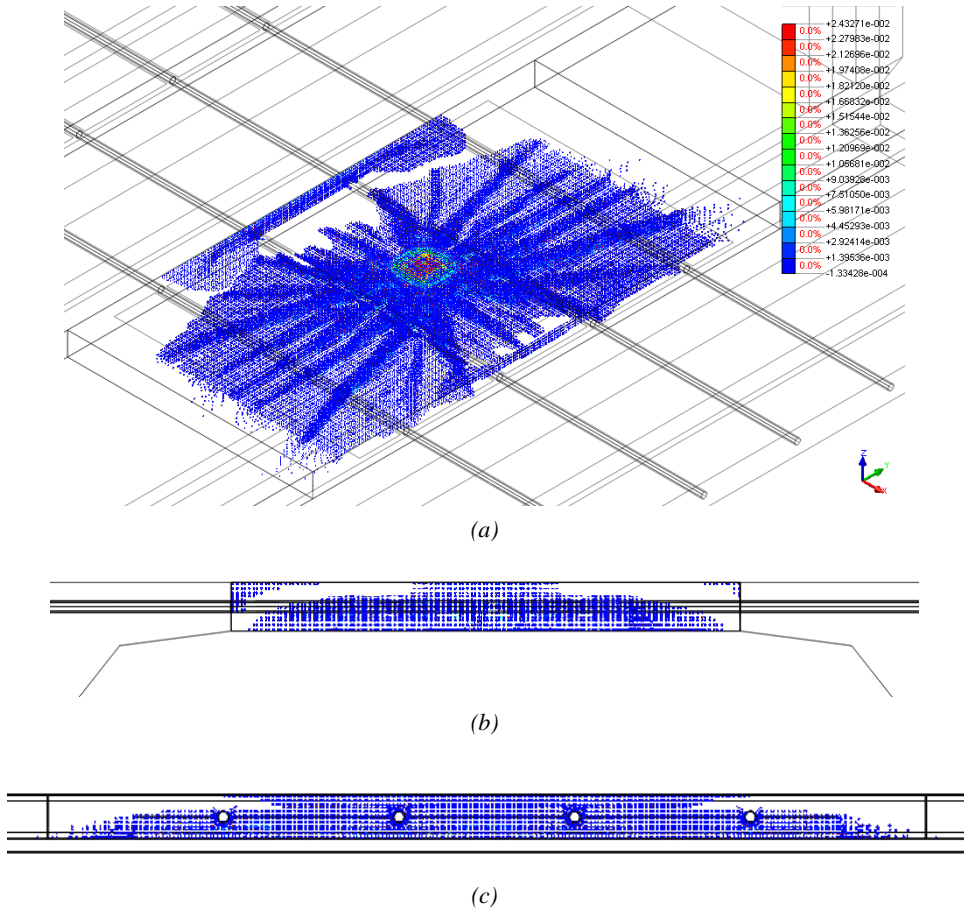


Fig. 7.19 The cracking pattern (normal crack strain) of the RB4ELEM model under a single load at the midspan and close to failure ( $TPL = 2.5 \text{ MPa}$ ): a) 3D view; b) Transverse cross-sectional view; c) Longitudinal side view.

### Calculation of the size factor

For the calculation of the size factor, the ultimate loads of the 2ELEM model and those of RB4ELEM model are compared. Since the RB4ELEM model had 50 mm  $\Phi$  ducts (size of the ducts in a real bridge), the 2ELEM model having 25 mm  $\Phi$  ducts (used for studying the influence of ducts on the bearing capacity in section 7.4.9) is also used for the calculation of the size factor. For the sake of comparison, results with 2ELEM basic model with 45 mm  $\Phi$  ducts are also presented.

Table 7.7 The size factor.

TPL	$P_{pr,FEA}$		$P_{FEA,RB}$	Size factor normalized for 200 mm thick slab	
	25 mm ducts	45 mm ducts	50 mm ducts	25 mm ducts	45 mm ducts
[MPa]	[kN]	[kN]	[kN]	$P_{pr,FEA}/P_{FEA,RB}$	$P_{pr,FEA}/P_{FEA,RB}$
0.5	1104	1016	678.3	1.63	1.5
1.25	1168	1086	957.5	1.22	1.13
2.5	1332	1209	1228.8	1.08	0.98

Notations:  $P_{pr,FEA}$  = finite element model bridge (2ELEM) projected ultimate load by force scale factor  $x^2 = 2^2$ ,  $P_{FEA,RB}$  = Real bridge FEA ultimate load.

Table 7.7 shows that the size factors for a level of 0.5, 1.25 and 2.5 MPa transverse prestressing considering the 2ELEM model with 25 mm and 45 mm  $\Phi$  ducts. It is interesting to note that the size factor seems to be dependent on the level of transverse prestressing and reduces for a higher TPL. Regan (1981) states that if the same concrete mix is used in the specimens of varying depth while the maximum aggregate size is scaled along with the depth, the size effect is somewhat reduced. In the current study, the same concrete strength but different fracture energies were used for the scaled 2ELEM and real bridge RB4ELEM models (considering a larger aggregate size for the RB4ELEM model than the 2ELEM model), therefore some effect of the size has already been considered. Smaller size factors are obtained when the projected capacity of 45 mm  $\Phi$  ducts 2ELEM model is compared with the real bridge capacity. This subject will be further elaborated in Chapter 8.

## 7.5 Summary and conclusions

A nonlinear, finite element parametric analysis was performed for a 3D, solid, 1:2 scaled model of a real bridge in the finite element software DIANA. Comparison with the experimental results was also made, where available. The following important conclusions can be drawn from the finite element investigation:

- The 2ELEM model mesh size is found to be most suitable for simulations throughout the finite element study because the ultimate loads and the load-deflection behavior are quite comparable with the finer mesh sized models (4ELEM and 6ELEM) with the 2ELEM model requiring far less time as compared to others for running a simulation.
- A step size of 0.1 mm is found to be reasonable for the finite element simulations of the 3D model bridge deck.
- The idealized, elastic-perfectly function, CONSTA, for concrete in compression shows comparable results with THOREN and PARABO and simulates the experimental cases reasonably well.

## Numerical Parametric Study

- The current finite element study generally follows the guidelines for nonlinear finite element analysis set by RTD 1016 (2012).
- An increase in the TPL linearly increases the punching shear capacity when loads are applied at midspan or at the interface. Cracking loads are also improved leading to the conclusion that the behavior in both the ultimate limit state and the serviceability limit state can be improved for thin deck slabs.
- Generally when the loads are applied close to the interface or above the ducts, a higher capacity is achieved as compared to when they are applied at the midspan or in-between the ducts. The load position on the exterior or the interior deck slab panels has a negligible influence on the punching shear capacity, although a slight increase in stiffness and capacity is observed for interior panels. Most of the finite element analyses have been performed with the load in-between the ducts and on exterior panels so that the calculations made and the results obtained can be considered to be on the conservative side.
- The double loads give a higher capacity as compared to the single loads for both deck slab midspan and close to girder flange-deck slab interface positions. A factor of 0.7 can be used conservatively when deriving the bearing capacity of prestressed decks with double loads using twice the capacity of single loads obtained experimentally or by finite element analysis ( $P_{double} = 0.7 \times 2P_{single}$ ), provided the loads comply with the Eurocode Load Model 1 (NEN-EN 1991-2:2003).
- Increasing the loading area by increasing the transverse length increases the punching shear capacity, however, for the model under study, the increase was small.
- The larger the ducts, the lower is the punching shear capacity because of the reduction in the cross-sectional area of the slab and in the volume of concrete.
- Increasing the fracture energy increases the deformation capacity of the deck slab as well as the ultimate loads. The value of fracture energy has to be selected carefully since MC 90 (1993) and MC2010 (*fib* 2012) show a considerable difference in its recommendation.
- A higher concrete strength leads to an improved behavior of the deck slab. The tensile strength of the concrete influences the punching shear capacity much more than the compressive strength.
- A thinner deck slab shows a higher punching shear capacity as compared to a thicker one provided that all other parameters remain the same. Therefore, for projecting the 1:2 scaled model numerical and experimental results to a real bridge, a structural size factor has to be applied. The size factor found in the current analysis varies with the TPL as well as the maximum aggregate size.

## Numerical Parametric Study

- The overall results of the basic analyses and the parametric analyses are summarized in the Table 7.8 and compared with the experimental results. The average ratio of  $P_T/P_{FEA}$  is 1, the standard deviation is 0.10 and the coefficient of variation is 10%. Generally, for single load tests, the finite element approach gives conservative results, while for double loads, the bearing capacities are over-estimated but within reasonable limits<sup>15</sup> as compared to the experimental results.

Table 7.8 Comparison of the finite element analyses ultimate loads with experimental results.

Test BB.	TPL [MPa]	Designation	$P_T$ [kN]	$P_{FEA}$ [kN]	$P_T/P_{FEA}$
1.	2.5	C-P1M	348.7	302.3	1.15
2.	2.5	A-P1M	321.4	302.3	1.06
3.	2.5	A-P1J	441.6	429.9	1.03
4.	2.5	C-P1J	472.3	429.9	1.10
5.	2.5	C-P2M	490.4	529.9	0.93
6.	2.5	A-P2J	576.8	537.0	1.07
7.	2.5	C-P1M	345.9	302.3	1.14
8.	1.25	C-P1M	284.5	271.4	1.05
9.	1.25	A-P1M	258.2	271.4	0.95
10.	1.25	A-P1J	340.3	300.7	1.13
11.	1.25	C-P2M	377.9	453.4	0.83
12.	1.25	A-P2J	373.7	454.9	0.82
13.	1.25	C-P1M (AD)	322.9	363.1	0.89
14.	1.25	A-P1M (AD)	295.9	294.0	1.01
15.	1.25	A-P1M (AD)	359.7	363.1	0.99
16.	2.5	B-P2M	553.4	592.7	0.93
19.	2.5	B-P1M (SLP)	317.8	306.0	1.04
21.	0.5	A-P1M	243.8	274.6	0.89
22.	0.5	A-P1M	257.5	274.6	0.94
			<b>Mean</b>		<b>1.00</b>
			<b>Standard deviation</b>		<b>0.10</b>
			<b>Coefficient of variation (COV)</b>		<b>0.10</b>

Notations: AD = Above the duct, BD = In-between the ducts, SLP = Small loading plate (115×150 mm),  $P_T$  = Test ultimate load and  $P_{FEA}$  = Finite element analysis (FEA) ultimate load.

<sup>15</sup> with the exception of test BB12 FE simulation which gave an error of 21% as compared to the experimental result but this test had failed at an unexpectedly lower load, see section 4.3.4 and 6.5.2.

## Numerical Parametric Study

# **CHAPTER 8**

## **Theoretical Analysis of Transversely Prestressed Deck Slabs**

Previously, results of experimental and numerical analyses of a 1:2 scaled bridge model regarding its punching shear capacity under various types of loading were described and compared. In this chapter, detailed theoretical analyses are carried out using various codes and punching shear theories including the Critical Shear Crack Theory leading to important conclusions.

## 8.1 Introduction

Generally there are two types of theoretical analyses approaches for punching shear; either by calculating shear stress at a particular critical perimeter around the loaded area (North American approach) or by mechanical models considering equilibrium of forces and defining certain failure criteria (European approach). Sieving out the current theories for those that consider compressive membrane action leaves us with only a handful of methods and further filtering for prestressed slabs leaves us with hardly any methods available. The test data available for punching shear tests on laterally restrained prestressed slabs is also less. At present, codes like Eurocode 2 (2005) and ACI 318 (2011) do not consider compressive membrane action in their capacity formulae for the punching shear capacity of prestressed slabs. However, there are some codes and methods that do allow taking account of the beneficial effects of CMA in punching shear analysis and design of slabs but for reinforced concrete only, like CHBDC: CAN/CSA-S6-06 (2006), the New Zealand (TNZAA 2003) code, UK HA BD81/02 (2002), Hewitt and Batchelor (1975) etc.

This chapter presents the results of calculations done for the bearing capacity of the model bridge deck. To make calculations for the punching shear capacity, existing codes that do not consider CMA, codes that do consider CMA and the critical shear crack theory, CSCT (Muttoni 2008) as given in the Model Code 2010 (2012) for prestressed slabs (Clément et al. 2013) will be used to calculate the bearing (punching shear) capacity of the 1:2 scaled model bridge deck slab and the real bridge deck slab under study. The size effect will also be considered in the calculations and design values for the bearing capacity using appropriate safety factors will be determined.

## 8.2 Existing codes and methods

### 8.2.1 Important parameters used in the calculations

Chapter 2 outlines the provisions of various codes and methods for the calculation of the punching shear capacity with or without considering the effect of compressive membrane action. Some of these methods apply for reinforced concrete only, therefore an equivalent steel reinforcement ratio (Eq. 8.1) approach by DIN 4227 (1978) is used to convert the prestressing steel ratio into an ordinary reinforcement steel ratio as used in the regular formulae for reinforced concrete. Stefanou (1993) regards the DIN 4227 approach suitable for unbonded tendons since it simply equates the prestressing forces in the tendons and the yield forces in the equivalent bar reinforcement. Rankin and Long (1987) and Rankin (1982) also recommend a similar approach.

## Theoretical Analysis of Transversely Prestressed Deck Slabs

$$\rho_{eq} = \frac{\rho_{ps} f_{pe}}{f_y} \quad (8.1)$$

where,  $\rho_{eq}$  is the equivalent reinforcement ratio,  $\rho_{ps}$  is the geometric ratio of the prestressed reinforcement,  $f_{pe}$  is the effective prestress of the tendons and  $f_y$  is the yield strength of the non-prestressed reinforcement.

Some important parameters used in the calculations done in this chapter are explained below. For the 1:2 scaled model bridge, this concerns:

- Longitudinal reinforcement = 6 mm  $\Phi$  bars @ 250 mm c/c
- Transverse reinforcement = 6 mm  $\Phi$  bars @ 200 mm c/c
- Average effective depth of deck slab as per EC2,  $d_{avg} = 87$  mm ( $d_l = 90$  mm,  $d_t = 84$  mm)
- Average steel reinforcement ratio calculated as per EC2,  $\rho_{avg} = \rho_l = 0.0019$
- Area of prestressing steel,  $A_p$  (177 mm<sup>2</sup>/bar @ 400 mm c/c) = 0.4425 mm<sup>2</sup>/mm

For the real bridge, assuming a 30 mm clear cover to the top and bottom reinforcement:

- Longitudinal reinforcement = 8 mm  $\Phi$  bars @ 250 mm c/c
- Transverse reinforcement = 8 mm  $\Phi$  bars @ 200 mm c/c
- Average effective depth of deck slab as per EC2,  $d_{avg} = 162$  mm ( $d_l = 166$  mm,  $d_t = 158$  mm)
- Average steel reinforcement ratio calculated as per EC2,  $\rho_{avg} = \rho_l = 0.0017$
- Area of prestressing steel,  $A_p$  (462 mm<sup>2</sup>/cable @ 800 mm c/c) = 0.5775 mm<sup>2</sup>/mm

The material properties used in the calculations are expressed in Table 8.1

*Table 8.1 Material properties for the model and real bridge deck slab.*

Material	Property	Value	Units
Concrete	Mean compressive cylinder strength, $f_{cm}$	65	MPa
	Mean splitting tensile strength, $f_{csp}$	5.41	MPa
	Modulus of elasticity, $E_{cm}$ - EC2	39	GPa
Prestressing steel	Characteristic tensile strength, $f_{pk}$	1100	MPa
	Characteristic 0.1% proof stress, $f_{p0.1k}$	900	MPa
	Modulus of elasticity, $E_p$	205	GPa
Ordinary steel	Mean yield strength, $f_{sy}$	525	MPa
	Mean ultimate tensile strength, $f_{su}$	580	MPa
	Modulus of elasticity, $E_s$	200	GPa

The general notations used in the following sections are as follows: TPL = Transverse prestressing level, FEA = Finite element analysis, P1M = Single point load acting the midspan of the deck slab panel, P1J = Single point load acting close to the girder flange-slab interface/joint, P2M = Double point loads at midspan of the deck slab panel, P2J = Double point loads acting close to the girder flange-slab interface/joint, AD = Above the duct, BD = In-between the ducts, SLP = Small loading plate (115×150 mm),  $P_T$  = Test ultimate load,  $S_T$  = Test ultimate deflection,  $P_{FEA}$  = FEA ultimate load,  $S_{FEA}$  = SEA ultimate deflection,  $P_{FP}$  = Flexural punching load. Any other notation used is defined within the text.

### 8.2.2 Model bridge analyses

#### Flexural capacity with compressive membrane action

It has already been described in the literature that the compressive membrane action enhances the bearing capacity of laterally restrained slabs above the capacity predicted by the traditional bending failure theories like the yield line theory. The reason that the failure mode in such cases changes to punching rather than flexure is that the increase in capacity in bending is larger than in punching, making punching shear more critical. Before calculating the punching capacity using various codes and methods, first it will be demonstrated why punching shear failure occurs rather than flexural failure when a concentrated load acts on a restrained slab. To demonstrate this analytically, the experimental punching failure loads are compared with the flexural bearing capacity of the deck slab considering compressive membrane action. No material factors have been used.

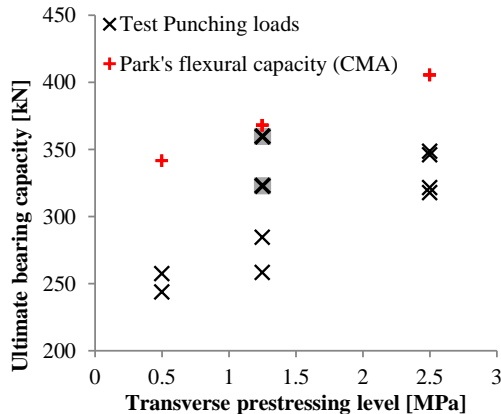


Fig. 8.1 Comparison of experimental punching shear capacity with Park and Gamble's (2000) flexural capacity by considering CMA for single loads acting at midspan of the deck slab panel. The highlighted data points are the tests done above a duct.

A method developed by Park and Gamble (2000) that considers CMA in laterally restrained reinforced concrete slabs is employed to calculate the flexural capacity (Fig. 8.1). The original theory was developed for uniformly distributed loads and has been modified for concentrated loads by Wei (2008), see Appendix C. Equivalent steel reinforcement ratio is used with various levels of transverse prestressing. It can be seen that the experimental loads never reach the capacity in flexure for any of the tests that failed in brittle punching. However, it is interesting to observe that the bearing capacity of the tests performed above a prestressing duct that failed in flexural punching (BB13 and 15) is comparable to the flexural capacity calculated by Park's theory. It can be concluded that although CMA enhances both punching shear and flexural capacity, it is the punching shear that becomes critical.

### Punching shear capacity without CMA

The punching shear capacity of single load tests with failure in brittle punching is calculated according to the background report 25.5-02-37-prENV 1992-1-1(2002) and ACI 318 (2011). The TPLs investigated are 0.5, 1.25 and 2.5 MPa. The mean material properties used are described in Table 8.1. No material factors have been used (Fig 8.2).

The background report 25.5-02-37-prENV 1992-1-1(2002) calculates the design punching shear capacity as:

$$v_{Rd,c} = C_{Rd,c} k (100 \rho_l f_{ck})^{1/3} + k_1 \sigma_{cp} \quad [SI Units : N, mm]$$

$$V_{r,EC2} = v_{rd,c} u d \quad [SI Units : N, mm] \quad (8.2)$$

where,  $C_{Rd,c} = 0.18 / \gamma_c$ , ( $\gamma_c = 1$  as no material factors are used) and  $k_1 = 0.08$ . On the basis of the background report, for further calculations, it is assumed that an average prediction is obtained by replacing  $C_{Rd,c}$  in Eq. 8.2 by 0.18. The remaining parameters remain the same as in section 2.2.3 or in NEN-EN 1992-1-1:2005.

The ACI 318 (2011) punching shear equation is:

$$V_{c,ACI} = (0.29 \sqrt{f_{cm}} + 0.3 \sigma_{cp}) b_0 d \quad [SI Units : N, mm] \quad (8.3)$$

where,  $0.9 \text{ MPa} \leq \sigma_{cp} \leq 3.5 \text{ MPa}$  (prestressing in each direction) and  $f_{cm} < 35 \text{ MPa}$ . The limitation on  $\sigma_{cp}$  has been ignored here. Calculations are done for both  $f_{cm} = 35 \text{ MPa}$  and  $65 \text{ MPa}$ . The remaining parameters are as defined in section 2.2.3 or in ACI 318 (2011).

## Theoretical Analysis of Transversely Prestressed Deck Slabs

Fig. 8.2 shows that the basic equations used for both codes underestimate the punching shear capacity of laterally restrained prestressed slabs. This lack of capacity is attributed to the ignorance of CMA that is present in such slabs. However, it can be observed that the capacity prediction for ACI 318,  $V_{r,ACI}$  (65 MPa), when the limit on  $f_{cm}$  is not followed is better, although still conservative for higher TPLs. For 0.5 MPa, it is comparable with the test results. A similar observation was made by He (1992) using ACI (1983), AASHTO (1987) and OHBDC (1983) code provisions for the punching shear capacity for prestressed decks for his 1/4.04 scaled models. He (1992) had followed the limitation on the concrete strength for ACI code and observed that the capacity was underestimated for all TPLs but using the corresponding AASHTO and OHBDC equations for punching shear with no limitations on concrete strength, it was found that the capacity of a non-prestressed deck slab was predicted quite well. Further discussion will be made in section 8.2.4.

Looking at the 25.5-02-37-prENV 1992-1-1 results, the results ( $V_{r,EC2}$ ) are conservative even for a very low level of 0.5 MPa TPL. It is obvious that the contribution of prestressing ( $\sigma_{cp}$ ) is low in both ACI 318 and the background report EC2.

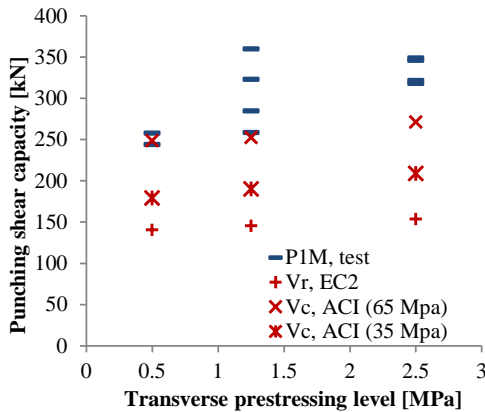


Fig. 8.2 Comparison of experimental punching shear capacity (PIM, test) with that of background report 25.5-02-37-prENV 1992-1-1:2002 ( $V_{r,EC2}$ ) and ACI 318 ( $V_{r,ACI}$ ).

### Background report 25.5-02-37 – prENV 1992-1-1:2002

The maximum punching shear capacity without compressive membrane action is calculated according to background report 25.5-02-37-prENV-1992-1-1:2002 for prestressed slabs (Eq. 8.2). According to the level II method (Eq. 8.4), a reliable design equation can be derived with:

$$B_{RD} = \mu_{BR} (1 - \alpha_{BR} \beta \delta_{BR}) \quad (8.4)$$

## Theoretical Analysis of Transversely Prestressed Deck Slabs

where,  $B_{RD}$  is the design value,  $\mu_{BR}$  = mean ratio  $V_{u,exp}/V_{u,calc}$  of test results,  $\alpha_{BR} = 0.8$ ,  $\beta = 3.8$  and  $\delta_{BR}$  is the coefficient of variation of the tests results which is equal to 0.128.

Fig. 8.3 shows the mean ratio  $V_{u,exp}/V_{u,calc}$  for the tests to be 2.32 as compared to 1.58 of the background report data. It is to be noted that the 5% fractile of the tests is comparable to the 95% fractile of the background report test data. Consequently, the increase in capacity is related to the phenomenon of CMA being developed in the experiments.

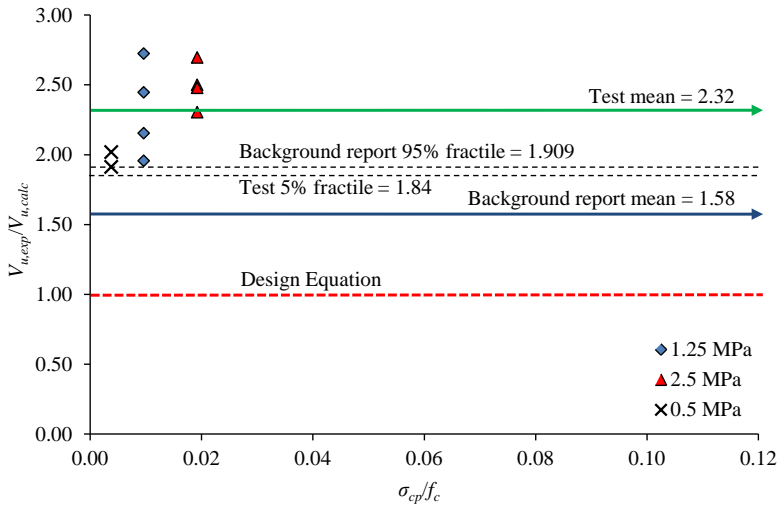


Fig. 8.3 Comparison of test results with punching shear equations according to the background report 25.5-02-37-prENV 1992-1-1:2002 (Equations from EN 1992-1-1 recalculated to mean values).

### Punching shear capacity with CMA

#### Single loads at midspan of the deck slab, P1M

The code provisions for UK BD81/02 have been outlined in Chapter 2. Fig. 8.4 shows the punching shear capacity for single loads acting at midspan of the deck slab panel calculated by UK BD81/02 ( $P_{p,BD81/02}$ ) considering compressive membrane action. No material factors have been used.

For a low TPL of 0.5 MPa, the code slightly overestimates the capacity since it is applicable for at least a 0.3% steel reinforcement ratio and  $\rho_{eq}$  (Eq. 8.1) for a TPL of 0.5 is even less than 0.2%. For more realistic TPLs in a prestressed deck (1.25 and 2.5 MPa), the code predicts a conservative punching capacity probably because it was developed for reinforced concrete only. It is worth noting that since UKBD81/02 does not consider the effect of steel reinforcement, it gives the same result for all TPLs.

## Theoretical Analysis of Transversely Prestressed Deck Slabs

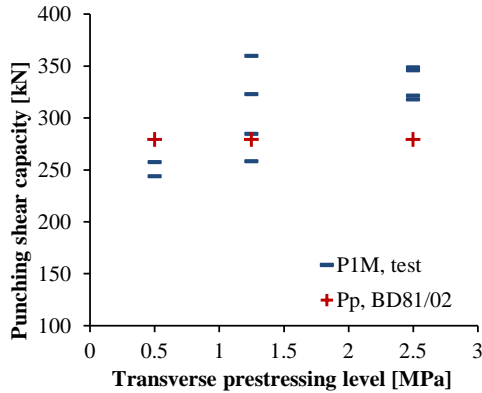


Fig. 8.4 Punching shear capacity calculated by UK BD81/02 ( $P_{p, BD81/02}$ ) considering CMA.

### Double loads at midspan of the deck slab panel, P2M

The flexural punching shear capacity considering CMA for double loads acting at midspan is calculated by assuming that the total flexural capacity is the sum of the arching moment capacity (Rankin and Long, 1997) and the bending moment capacity (BS5400). The effective width ( $b_{eff}$ ) is calculated by the formula given by Taylor et al (2002). The formula is modified to incorporate two point loads acting at 600 mm c/c and the overlapping effective width due to loads being close to each other is corrected by considering them as patch loads (similar to  $c_x$  and  $c_y$  of the patch loads by Zheng et al. 2010), see Fig. 8.5. Pucher charts (1964) have been used to find out the relationship between the bending moment,  $M$  and the load,  $P$ . An average moment factor for simply supported and fixed ended conditions was obtained from the Pucher charts giving  $P = 5.88M$ . The method outlined by Taylor et al (2002) gives a fairly good estimation of the failure loads when compared to those observed in tests (Table 8.2).

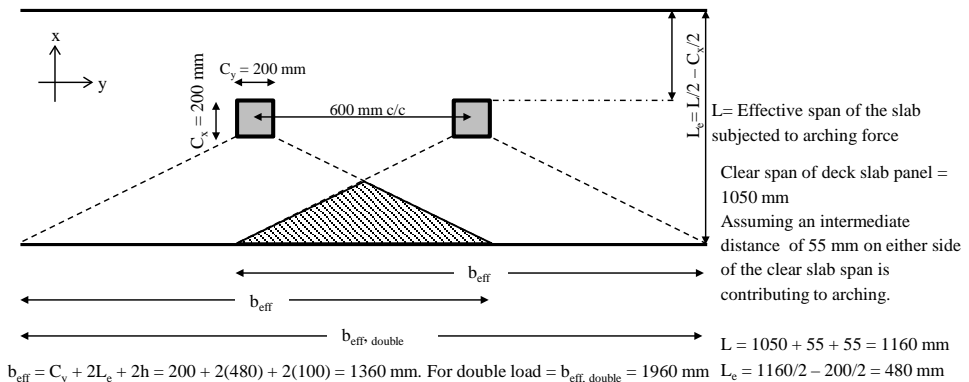


Fig. 8.5 Calculation of effective width for double loads (Taylor et al. 2002, Zheng et al. 2010). Figure not drawn to scale.

## Theoretical Analysis of Transversely Prestressed Deck Slabs

Table 8.2 Comparison of test and calculated capacity.

Test	TPL	Ultimate test load, $P_T$	Flexural Punching load, $P_{FP}$ ( $b_{eff} = 1960$ mm)	$P_T/P_{FP}$
	[MPa]	[kN]	[kN]	
BB11	1.25	377.9	412	0.92
BB05	2.5	490.4	533	1.04
BB16	2.5	553.4	533	0.92
			<b>Mean</b>	0.96
			<b>Standard deviation</b>	0.07
			<b>Coefficient of variation (COV)</b>	0.07

### 8.2.3 Real bridge analyses

The ultimate objective of carrying out this research study is to predict the capacity of transversely prestressed real bridge decks. Therefore, calculations using existing methods and codes are also made for a full scale bridge deck. Chapter 3 outlines the structural details of the Van Brienoord bridge on which the scaled model is based. The thickness of the deck is 200 mm and the clear span of the deck slab is 2100 mm. Other important parameters are described in section 8.2.1.

The background report 25.5-02-37-prENV-1992-1-1:2002, ACI 318 will be used to assess the capacity without considering CMA and UK HA BD81/02 and CHBDC will be used to make the assessment with CMA. The capacity evaluation provisions in section 14.14.1.3 of CHBDC are recommended for deck slabs with at least a 150 mm thickness. The design charts are also limited to a concrete cylinder strength  $f_c'$  of 40 MPa. Using the equivalent steel ratio method (Eq. 8.1), the code provisions are then applicable for prestressed deck slabs (post-tensioned, unbonded tendons) except for a very low level of TPL (0.5 MPa). Table 8.3 shows the punching shear capacity for the real bridge using the aforementioned codes. Mean material strengths are used with no material factors. The finite element analyses results presented in the previous chapter are considered as the bench mark here as direct experimental results are not available.

Table 8.2 Calculated punching shear capacity using various codes and finite element analyses.

#	TPL	$\rho_{eq}$	$V_{r,EC2}$		$V_{c,ACI}$		$P_{p,BD81/02}$	$R_{n,CHBDC}$	$P_{FEA,RB}$
	[MPa]	[%]	[kN]	[kN]	[kN]	[kN]	[kN]	[kN]	
			$k \leq 2$	$k > 2$	$f_{cm} = 35$ MPa	$f_{cm} = 65$ MPa		For $q, d_p = 100$ mm	
1	0.5*	0.19	484	510	652	879	1027	996	678
2	1.25	0.48	502	528	693	920	1027	1059	958
3	2.5	0.95	531	557	761	988	1027	1163	1229

Notations:  $V_{r,EC2}$  = Punching capacity from the background report EC2,  $V_{c,ACI}$  = Punching capacity from ACI 318,  $P_{p,BD81/02}$  = Punching capacity from UKBD81/02,  $R_{n,CHBDC}$  = Punching capacity from CHBDC,  $P_{FEA,RB}$  = Real bridge FEA ultimate load (punching capacity).

\* $\rho_{eq} < 0.2\%$ ,  $\sigma_{cp} < 0.9$ MPa.

Note: The highlighted values are the ones where the limit on minimum steel reinforcement ratio or the minimum prestress has been ignored.

### **Without CMA (for prestressed decks)**

#### The background report 25.5-02-37-prENV 1992-1-1 (2002)

It can be observed that the background report EC2 gives the lowest capacity out of all the methods. With an increasing transverse prestressing level, the difference with the finite element results grows. For 0.5 MPa, the punching shear capacity according to the FEA is 1.34 times that of the Eurocode 2, while for 1.25 and 2.5 MPa, it is 1.8 and 2.2 times that of the Eurocode 2, respectively. Calculations have been made by first keeping the limit on the size factor ( $k \leq 2$ ) in the first column and then ignoring the limit ( $k > 2$ ) in the second column. Slightly higher capacities are achieved when the limit on the size factor is ignored.

#### ACI 318 (2011)

The ACI 318 has limitations on  $\sigma_{cp}$  and  $f_{cm}$  and does not consider a size effect. In the first column the limitation on  $f_{cm}$  is followed and in the second it is ignored. The first column results are on the conservative side except for 0.5 MPa which compares well with the FEA result although for higher TPLs, the results are underestimated again. The second column results seem reasonable for 1.25 MPa but at the conservative side for 2.5 MPa. The increase in capacity that is seen in the second column is the result of ignoring the limit on  $f_{cm}$  rather than increasing the prestressing contribution. As a result, the punching shear capacity for 0.5 MPa is grossly overestimated.

### **With CMA (for reinforced concrete decks only)**

#### UK BD81/02 (2002)

The UK BD81/02 does not differentiate between the variation in the TPLs since it neither considers the actual steel reinforcement ratio in its capacity formula, nor was it developed for prestressed decks so that the TPL could not be input directly like in the EC2 or ACI 318 formulae. The results are approximately an average of the two TPLs FEA results.

#### CHBDC: CAN/CSA-S6-06 (2006)

This is the only code where the steel reinforcement ratio is required in the calculations directly, therefore, an equivalent steel area is used to calculate the reinforcement ratio and the effective depth is taken until the prestressed reinforcement (100 mm). The unfactored nominal resistance  $R_n$  is calculated through rating charts by multiplying the resistance for a certain thickness of the slab with correction factors for the concrete compressive strength  $f_{cm}$  and steel reinforcement ratio  $q$ . The capacity for 2.5 MPa is comparable with the FEA results. For 1.25 MPa, the code slightly over estimates the capacity and for 0.5 MPa, it

grossly overestimates like the other codes. The rating charts are not applicable for  $q$  less than 0.2% and an extrapolation leads to unsafe results. It is also to be noted that the wheel foot print considered in CHBDC is 600×250 mm making the wheel footprint area smaller than the one used in the finite element analysis (400×400 mm according to the load model 1 of the Eurocode).

### 8.2.4 Discussion

Current design codes' punching shear provisions are based on experimental studies involving slab-on-column specimens whose behavior is essentially different from that of bridge deck slabs under wheel loads. This ultimately means that the contribution of the prestressing considered in the code equation holds true for the overall in-plane forces arising from the lateral restraint (compressive membrane action) as well.

#### **Eurocode 2**

The results of the punching shear calculations by the background report EC2 are similar for both the model bridge and the real bridge decks. A factor of 0.08 for  $\sigma_{cp}$  is on the conservative side and the code also does not consider compressive membrane action. Not much difference between the capacity for the three levels of transverse prestressing is seen, again, due to the very small contribution of prestressing being considered. Also no difference in the size factor  $k$  is seen in the model and the real bridge punching capacities when the limit  $k \leq 2$  is observed (for both the model and real bridges  $k > 2$  so it is taken equal to 2) since EC2 only considers a size effect on slab effective depth of 200 mm and higher. EC2 also calculates the non-prestressed shear contribution of concrete far more conservatively than ACI 318.

#### **ACI 318**

##### Minimum prestressing level requirement

If a certain level of  $\sigma_{cp}$  is not present, the ACI 318 punching shear equation is not recommended. Ramos et al. (2011) observed a very low capacity for a zero MPa prestressing level for the unrestrained, reinforced concrete slab AR2 (2300×2300×100 mm) and recommended increasing the contribution of the first part of the Eq. 8.3 (that represents the non-prestressed slab) from 0.29 to 0.4 since the latter part of the equation made no influence for zero MPa prestress and zero boundary restraint in slab AR2. However, the slabs were only 100 mm thick and for larger thicknesses, the results could be overestimated. Such a result leads to the conclusion, that for no restraint present, the ACI equation limitation on  $\sigma_{cp}$  is valid since the original tests on which the equation is based had

no boundary restraints also. In the current study, sufficient lateral restraint (giving rise to in-plane membrane forces) is already present, hence the limit on  $\sigma_{cp}$  does not need to be followed. In fact the contribution of prestressing (or the in-plane forces) must be increased if enough lateral restraint is present in a slab system keeping all other limitations intact ( $f_{cm}$ ).

### Limitation on concrete compressive strength

He (1992) recommended no limit on the compressive strength and an increase in the coefficient for the prestress contribution from 0.3 to 0.8. However, the concrete compressive strength of his tested specimens was below 50 MPa and the deck slabs were only 47 mm thick. In the current study, for the model bridge deck of 100 mm thickness, ignoring the  $f_{cm}$  limit of 35 MPa produced good agreement for 0.5 MPa TPL and improved the results for higher TPLs. But in the real bridge deck of 200 mm thickness, when the limit on the concrete strength was ignored, the capacity for 0.5 MPa was grossly overestimated. Therefore, until more results are available with high concrete strengths and a size factor is introduced for thicker slabs, the limit on  $f_{cm}$  seems reasonable.

### **UKBD81/02**

The UK BD81/02 code overestimates the capacity for 0.5 MPa for both the model bridge (Fig. 8.4) and the real bridge decks since  $\rho_{eq}$  is far below 0.3% (limited in code but not in actual provisions). Since the code does not recognize any difference in the level of actual reinforcement, the results become conservative for higher levels of transverse prestressing. As mentioned before, the code is for reinforced concrete only.

### **CHBDC**

The CHBDC code limits the depth to 150 mm, hence no calculations were made for the model bridge. For the real bridge, the results are conservative for 2.5 MPa as compared to the FEA results but for 1.25 MPa, the capacity is slightly overestimated.

### **Conclusion**

As expected, EC2 and ACI give conservative results since they do not consider CMA. UKBD81/02 and CHBDC overestimate the capacity for 1.25 MPa and are conservative for 2.5 MPa, however, they are not developed for prestressed decks. It is also worth mentioning that the FEA results for the real bridge may very well be conservative themselves compared to the actual capacity since the model FEA results are also conservative for single loads as compared to the experimental results (Table 7.8).

Recommendation

If enough lateral restraint is present in the slab system, an increase in the contribution of the in-plane forces towards the punching shear strength should be made. In ACI 318 (2011), no minimum limit on  $\sigma_{cp}$  is required for restrained slabs. If more than 35 MPa  $f_{cm}$  has to be used, then a size effect should also be introduced in the equation for thicker slabs to obtain reasonable results for both high and low levels of TPLs. The numerical results in section 7.4.12 show that the size effect varies with the TPL. A higher size factor was obtained for a lower TPL.

Using  $k_l = 0.7$  in EC2 and  $0.7\sigma_{cp}$  in ACI 318 punching shear equations (Eq. 8.2 and 8.3 respectively), the following results are obtained. Note that EC2 uses a cube root and ACI uses a square root expression for  $f_{cm}$ . It can be concluded that increasing the contribution of the in-plane forces improves the results of the codes.

Table 8.3 Punching shear capacity with  $0.7\sigma_{cp}$  in code equations.

#	TPL [MPa]	$V_{r,EC2}(f_{cm} = 65 \text{ MPa})$		$V_{c,ACI}(f_{cm} = 35 \text{ MPa})$		$P_{FEA,RB}$
		Model bridge	Real bridge	Model bridge	Real bridge	Real bridge
1.	0.5*	169	575	201	689	678
2.	1.25	209	730	246	784	958
3.	2.5	284	987	321	944	1229

Notations:  $V_{r,EC2}$  = Punching capacity from the background report EC2,  $V_{c,ACI}$  = Punching capacity from ACI 318 and  $P_{FEA,RB}$  = Real bridge FEA ultimate load (punching capacity).

\* $\rho_{eq} < 0.2\%$ ,  $\sigma_{cp} < 0.9 \text{ MPa}$ .

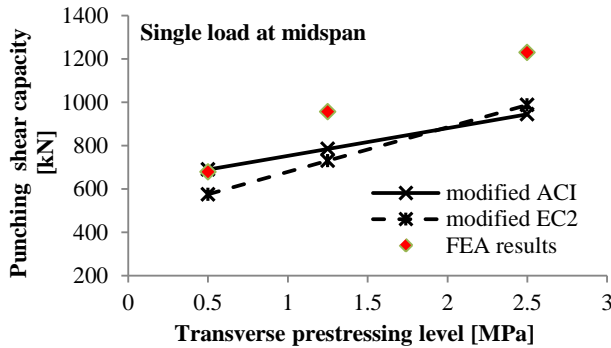


Fig. 8.6 Punching shear capacity of real bridge with  $0.7\sigma_{cp}$  in code equations.

### 8.3 The Critical Shear Crack Theory (CSCT)

It is clear from the previous sections that currently no code analysis or design method is fully suitable for the prediction of the punching shear capacity of prestressed slabs

considering compressive membrane action and there is a dire need to develop a method for such cases. Considerable saving in cost can be made if the beneficial effect of compressive membrane action can be used in the analysis of old structures and design of new ones.

In this section an attempt will be made to apply the Critical Shear Crack Theory, CSCT, (Muttoni 2008, Clément et al. 2013) on the transversely prestressed bridge deck under study using the Levels of Approximation approach (Muttoni and Fernández Ruiz 2012a, 2012b). Provisions from the Model Code 2010 (*fib* 2012) regarding punching shear in slabs using CSCT will be used in combination with numerically found in-plane forces comprising compressive membrane action (section 6.6).

### 8.3.1 MC2010 punching shear provisions for prestressed slabs

The fundamental mechanical model of the CSCT that provides the basics of MC2010 provisions for punching shear in reinforced concrete slabs has been described in chapter 2. The relevant provisions for punching shear in prestressed slabs (without shear reinforcement) according to MC2010 are explained below.

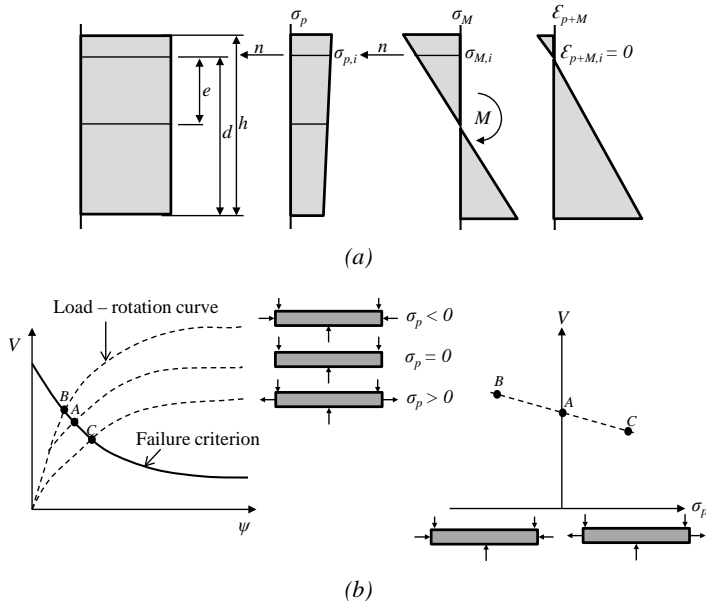


Fig. 8.7 The Critical Shear Crack Theory: a) Section subject to in-plane normal force, state of associated stress, state of stress due to decompression moment, and resulting state of strain (from left to right); b) Influence of an in-plane force ( $\sigma_p$ ) on the punching shear capacity,  $V$  (Clément et al. 2013).

### Failure criterion

According to the CSCT, the width of the critical shear crack can be correlated to the product of the rotation and the flexural effective depth of the slab ( $w \propto \psi d$ ), see Fig. 8.7a. In MC2010, the design shear resistance attributed to the concrete is:

$$V_{Rd,c} = k_{\psi} \frac{\sqrt{f_{ck}}}{\gamma_c} b_0 d_v \quad [SI \text{ Units : } N, mm] \quad (8.5)$$

where,  $b_0$  is the length of the control perimeter at  $d_v/2$  of the edge of the supported area,  $d_v$  is the shear-resisting effective depth of the member (accounting for supported area penetration, MC2010),  $f_{ck}$  is the characteristic compressive cylinder strength of the concrete,  $\gamma_c$  is the partial safety factor for concrete and  $k_{\psi}$  is the rotation parameter depending on the opening and the roughness of the cracks (Muttoni et al. 2013):

$$k_{\psi} = \frac{1}{1.5 + 0.9k_{dg}\psi d} \leq 0.6 \quad (8.6)$$

where,  $d$  is the (flexural) effective depth for the x and y-directions (in mm). When the maximum size of the aggregate,  $d_g$ , is not less than 16 mm,  $k_{dg}$  in Eq. 8.6 can be taken as  $k_{dg} = 1.0$ . If concrete with a maximum aggregate size smaller than  $d_g = 16$  mm is used, the value of  $k_{dg}$  can be calculated as:  $32 / (16 + d_g) \geq 0.75$ .

### Load-rotation relationship of the prestressed slab

The rotation at failure ( $\psi$  in Eq. 8.6) can be evaluated by using the Levels-of-Approximation (LoA) approach. In the Model Code 2010, the influence of *prestressing* (Fig. 8.7b) on punching shear strength is explored at the LoA II and III (typical LoA to be used for structures where punching shear strength is governing). No calculations are made at LoA I for prestressed slabs. In LoA IV, the rotation  $\psi$  can be calculated on the basis of a nonlinear flexural analysis of the structure and accounting for cracking, tension-stiffening effects, yielding of the reinforcement and any other nonlinear effect relevant for providing an accurate assessment of the structural bearing capacity (*fib* 2012).

#### Level of approximation II

For prestressed slabs, the rotation can be calculated as:

$$\psi = 1.5 \frac{r_s}{d} \frac{f_{yd}}{E_s} \left( \frac{m_{sd} - m_{pd}}{m_{Rd} - m_{pd}} \right)^{1.5} \quad (8.7)$$

where,  $r_s$  refers to the distance from the axis of the column to the line of contra-flexure of the bending moments. The value of  $r_s$  can be approximated as  $0.22L_x$  ( $r_{sx}$ ) or  $0.22L_y$  ( $r_{sy}$ ) for the x and y directions, respectively, for regular flat slabs where the ratio of the spans ( $L_x/L_y$ ) is between 0.5 and 2.0.  $f_{yd}$  is the design yield strength of the flexural reinforcement.  $E_s$  is the modulus of elasticity of flexural steel.  $m_{sd}$  is the average design moment per unit length for the calculation of the flexural reinforcement in the support strip.  $m_{Rd}$  is the average design flexural strength per unit length in the support strip which can be calculated by assuming that both flexural and prestressing reinforcement are yielding at failure.  $m_{Pd}$  denotes the average decompression moment over the width of the support strip due to prestressing. The width of the support strip is to be taken as  $b_s = 1.5\sqrt{r_{sx} \cdot r_{sy}}$  but should be less than or equal to the minimum span in x or y-directions ( $L_{min}$ ). Constrained forces and moments and losses due to shrinkage, creep and relaxation need to be taken into account.

### Level of approximation III

This Level of Approximation is recommended for irregular slabs or for flat slabs where the ratio of the span lengths ( $L_x/L_y$ ) is not between 0.5-2.0. The coefficient 1.5 in Eq. 8.7 can be replaced by 1.2 if a linear-elastic flexural analysis is carried out to determine  $r_s$  and  $m_{sd}$ .

### **8.3.2 Application of CSCT to the research problem**

The current research problem is the assessment of the bearing (punching shear) capacity of transversely prestressed concrete decks. For the calculations, mean values of material strengths will be used with no material factors. For openings and inserts, the basic control perimeter is recommended to be reduced (*fib* 2012) but the presence of ducts in the current problem has been ignored while calculating  $b_0$ . A MATLAB program (Appendix C) has been developed to make the iterative calculations and plot the load-rotation curves against the failure criterion for the model bridge deck. The possibility of flexural failure has been ruled out of the iterative procedure, since no such failure was observed in the tests or the FEA. Tests done above the ducts and the control tests with 0.5 MPa TPL have not been considered. The following sections explain the application of the CSCT in the present research.

### **The failure criterion**

Eq. 8.8 gives the failure criterion of the Critical Shear Crack Theory. This equation does not involve any material factors and is based on mean strengths.

$$\frac{V_R}{b_0 d_v \sqrt{f_{cm}}} = \frac{3/4}{1 + 15 \frac{\psi d}{d_{g0} + d_g}} \quad [SI \text{ Units : } N, mm] \quad (8.8)$$

where,  $V_R$  is the shear strength,  $b_0$  is the length of the control perimeter at  $d_v/2$  of the edge of the supported area,  $d_v$  is the shear-resisting effective depth of the member,  $f_{cm}$  is the mean compressive strength of the concrete,  $\psi$  is the rotation and is calculated depending on the required LoA,  $d$  is the flexural effective depth of the member,  $d_{g0}$  is the maximum aggregate size and  $d_g$  is the reference aggregate size equal to 16 mm.

### Verification of the failure criterion

The failure criterion (Eq. 8.8) is verified by plotting the experimental results based on actual, measured rotations and the punching loads. The rotations are calculated using the deflections from the experiments as shown in Fig. 8.8. The deflections from the actuator are used for this purpose since the LVDTs and Lasers were placed at various locations around the load and not directly at the loading point (Section 3.4). It is assumed that no rotation occurs at the deck slab panel edges and uniform vertical deflection  $\delta_v$  occurs under the steel loading plate due to the punching load  $V$ . The rotation  $\psi$  of the deck slab can be calculated from the geometry of the deflected structure, where  $r_c$  is half the transverse length of the loading plate (100 mm),  $r_w$  is half the transverse span of the deck slab panel (525 mm). The flexural effective depth (from top of the slab till the level of the bottom tensile steel reinforcement) is taken equal to the shear resisting effective depth ( $d = d_v = 87$  mm).

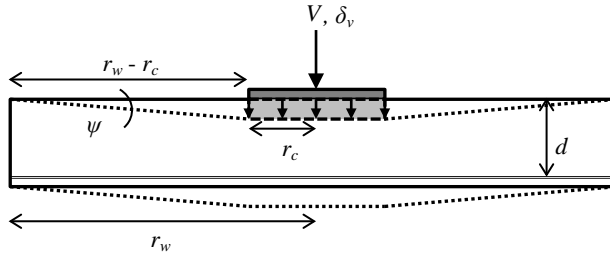


Fig. 8.8 Calculation of rotations for the model bridge deck slab panel.

### Assessment of the punching shear capacity using CSCT

For the assessment of the punching shear capacity, an iterative procedure needs to be carried out to find the intersection point of the failure criterion and the load-rotation curve of the slab representing the available punching shear strength and the shear force for a given rotation, respectively. Instead of using the traditional LoA approach, a different

criterion will be introduced to calculate the capacity of the model bridge deck. The following general equation will be used to calculate the rotations.

$$\psi = 1.5 \frac{r_s}{d} \frac{f_{sy}}{E_s} \left( \frac{m_s - m_p}{m_R - m_p} \right)^{1.5} \quad (8.9)$$

In Eq. 8.9,  $m_s \approx V/8$ , for inner columns without unbalanced moments (Muttoni 2008, Clément et al. 2013),  $m_R = \rho f_{sy} d^2 (1 - 0.5\rho f_{sy}/f_{cm})$  and  $m_p = n (h/2 - d/3 + e)$ . Here,  $V$  is the acting shear force,  $\rho$  is the steel reinforcement ratio,  $f_{sy}$  is the yield strength of the steel,  $f_{cm}$  is the mean compressive cylinder strength of concrete,  $n$  is the normal force per unit length,  $h$  is the depth of the slab,  $d$  is the effective depth and  $e$  is the eccentricity of the normal force from the center of gravity of the section. As a sign convention, the decompression moment is considered positive when it leads to compressive stresses on the top side of the slab (Clément et al. 2013). For the current case, no eccentricity exists since the prestressing bars are applied at mid-depth.  $\rho_{ps}$  (geometric prestressing steel ratio) and  $f_{pe}$  (effective prestress) representing an equivalent steel will be used in place of  $\rho$  and  $f_{sy}$ , respectively, to determine the flexural strength of the deck slab panel with unbonded transversely prestressed bars. Similar to the verification procedure, the flexural effective depth of the section will be taken equal to the shear resisting effective depth in the assessment calculations ( $d = d_v = 87\text{mm}$ ).

#### Elementary Level of Approximation

The load-rotation relationship will be established using the transverse prestressing force as the normal force  $n$ . This will serve as a lower bound for the ultimate capacity (Fig. 8.9).

#### Advanced Level of Approximation

The load-rotation relationship will be established using the overall in-plane force (sum of transverse prestressing force and compressive membrane force) as the normal force  $n$ , found from the nonlinear analyses of the 3D solid, finite element model bridge in Chapter 6 and 7 ( $N_{xx}$  from composed elements). This will serve as the upper bound of the ultimate capacity and compressive membrane action will automatically be incorporated in the load-rotation relationship (Fig. 8.9).

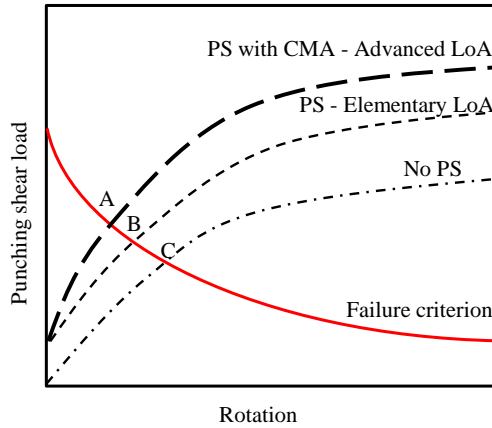


Fig. 8.9 The Level of Approximation (LoA) approach for the analysis of the transversely prestressed deck slab (PS = Prestressing, CMA = Compressive membrane action). The elementary LoA giving punching shear load B and the advanced LoA giving punching shear load A. For no prestressing, the failure load is C.

### 8.3.3 Verification of the failure criterion

In this section, the failure criterion of the critical shear crack theory will be verified for the current test results. It should be noted that the concrete strength of the girders ( $f_{cm} = 75$  MPa) is higher than that of the deck slab panels ( $f_{cm} = 65$  MPa) which means that a higher bearing capacity exists when the deck slab is loaded close to the interface but this effect has been ignored in the calculations. Also, tests done above the ducts and the control tests with 0.5 MPa TPL have not been considered. Fig. 8.10 shows the critical shear perimeters being considered. For single loads, Model Code 2010 considers the critical shear perimeter at half the effective depth from the face of the loaded area. For the double load cases, the perimeters of the two loaded areas are combined according to the stress distributions shown in section 6.5.6 and 6.6.3.

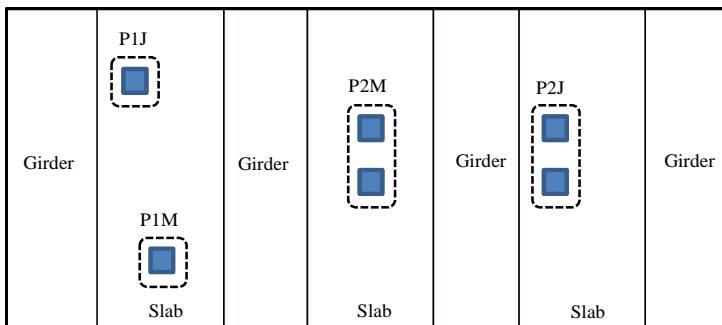


Fig. 8.10 Determination of critical shear perimeter for various load cases at a distance  $d/2$  from the face of the loaded area (fib 2012).

## Theoretical Analysis of Transversely Prestressed Deck Slabs

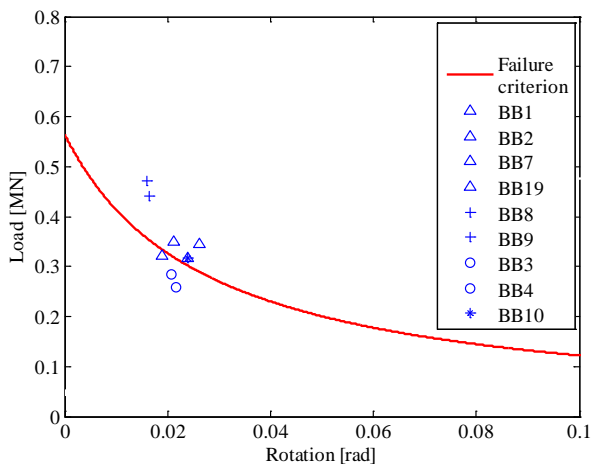
Table 8.4 shows the input of the MATLAB program related to the experimental cases.

Table 8.4 Experimental punching loads and corresponding rotations to verify the failure criterion.

Test BB.	TPL	Designation	Test ultimate load, $P_T$	Test ultimate rotation, $\psi_T$	Miscellaneous
	[MPa]	Load type	[kN]	[radians]	
1.	2.5	P1M	348.7	0.0212	$f_{cm} = 65\text{MPa}$ $E_s = 200\text{ GPa}$ $d_g = 20\text{mm}$ $B = 1050\text{ mm}$ $b_c = 200\text{ mm}$ $c_c = 200\text{ mm}$ for single loads and $800\text{ mm}$ for double loads $d = 87\text{ mm}$
2.	2.5	P1M	321.4	0.019	
3.	2.5	P1J	441.6	0.0164	
4.	2.5	P1J	472.3	0.016	
5.	2.5	P2M	490.4	0.0394	
6.	2.5	P2J	576.8	0.0244	
7.	2.5	P1M	345.9	0.0263	
8.	1.25	P1M	284.5	0.0208	
9.	1.25	P1M	258.2	0.0216	
10.	1.25	P1J	340.3	0.0166	
11.	1.25	P2M	377.9	0.041	
12.	1.25	P2J	373.7	0.015	
16.	2.5	P2M	553.4	0.0329	
19.	2.5	P1M (SLP)	317.8	0.0239	

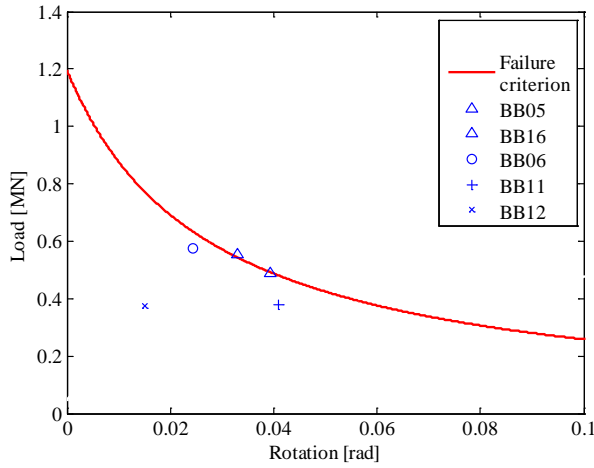
Notations: SLP= Small loading plate ( $115 \times 150\text{ mm}$ ),  $f_{cm}$  = Mean compressive cylinder strength of concrete,  $E_s$  = Young's modulus of steel,  $d_g$  = Maximum size of the aggregate,  $B$  = Transverse span of the slab,  $b_c$  = Transverse length of the loaded area,  $c_c$  = Longitudinal length of the loaded area,  $h$  = overall/total depth of the slab,  $d$  = effective depth of the slab.

The experimental punching loads and the corresponding rotations are plotted with respect to the failure criterion for all the load cases in Fig. 8.11a, b. In Fig. 8.11c, the test data is plotted with respect to the failure criterion normalized at both axes to account for the support size/loaded area, concrete compressive strength, depth of the member and aggregate size.

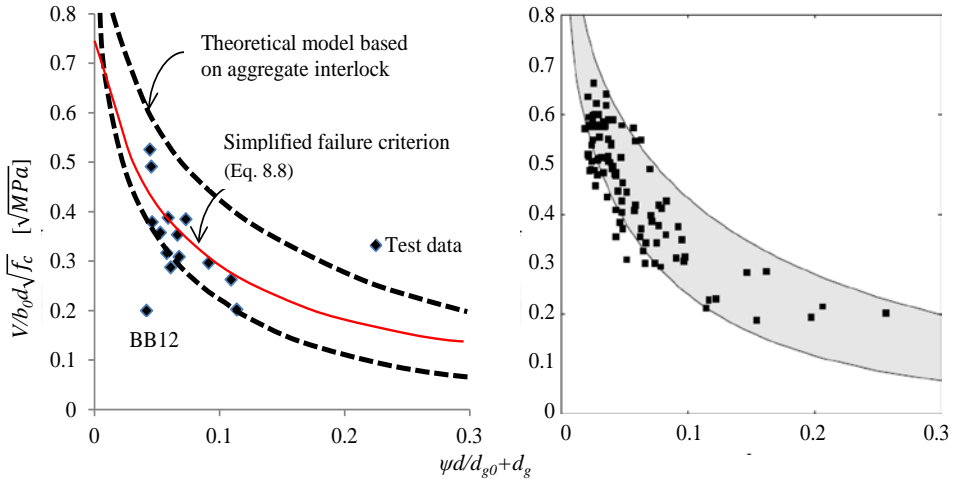


(a)

## Theoretical Analysis of Transversely Prestressed Deck Slabs



(b)



(c)

Fig. 8.11 Verification of the failure criterion w.r.t the experimental results: a) Single loads (P1M and P1J); b) Double loads (P2M and P2J); c) Comparison of CSCT normalized extreme parameters (from Guidotti 2010, Muttoni and Fernández Ruiz 2010) with the present test data (19 tests).

A good correlation is observed between the load cases and the CSCT punching failure criterion in general. BB3 and 4 were tested very close (110 mm) to the high strength girder, hence they seem to be above the failure criterion drawn for the lower deck slab concrete strength in Fig. 8.11a. But when the failure criterion is normalized with respect to the concrete strength and other parameters in Fig. 8.11c, BB3 and 4 data points fall closer to the simplified failure criterion of Eq. 8.8 and within the scatter of the extreme parameter failure envelopes (reproduced according to Guidotti 2010 and Muttoni and Fernández Ruiz

2010). For double loads, the test BB12 lies out of the failure envelope (Fig. 8.11b, c). This is probably because in the experiments, BB12 had failed at a much lower load than expected. The single load case BB10 tested close to the interface with a TPL of 1.25 MPa failed at 340.3 kN, while BB12, despite being a double load tested at the interface with the same TPL failed at only 373.7 kN (section 4.3.4). Similar discrepancy between BB12 FEA bearing capacity and the test bearing capacity was observed in section 6.5.2 and Table 7.8.

## Conclusion

It can be concluded that the test data generally falls within the narrow band of the failure envelope developed from a wide range of data from literature (Muttoni 2008), verifying the failure criterion for the current research experimental set of data.

### 8.3.4 Assessment of the punching shear capacity for the experimental load cases using the proposed LoA approach

For the assessment of the ultimate bearing (punching shear) capacity, Eq. 8.8 and 8.9 are solved iteratively with the help of a MATLAB program (Appendix C). The input is shown in the Table 8.5. The procedure has already been explained in section 8.3.2.

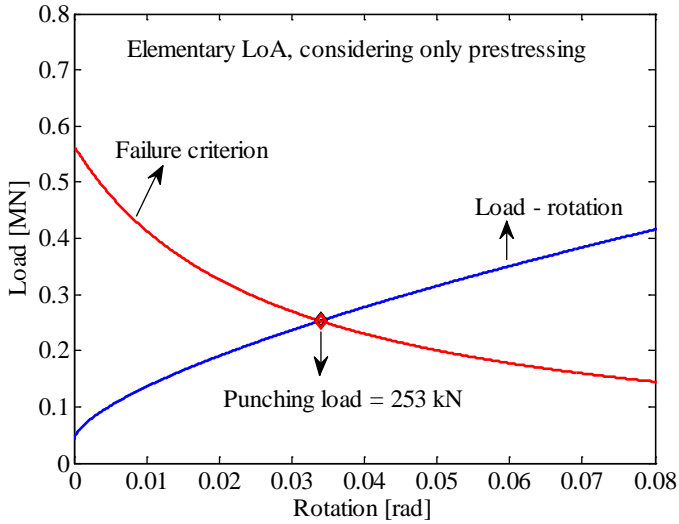
Table 8.5 Input for the MATLAB program to estimate the ultimate capacity using CSCT.

Test BB.	TPL	Designation	Normal force, n	Miscellaneous
	[MPa]	Panel - Load type	[N/mm]	
1.	2.5	C-P1M	615	$f_{cm} = 65\text{MPa}$ $E_s = 200\text{ GPa}$ $d_g = 20\text{ mm}$ $B = 1050\text{ mm}$ $b_c = 200\text{ mm}$ $c_c = 200\text{ mm}$ for single loads and $800\text{ mm}$ for double loads $d = 87\text{ mm}$  From FEA: $r_s = 250\text{ mm}$ ( $\approx B/4$ , assuming maximum rotations occur in the transverse direction). $n$ = depends on TPL and CMA, found from FEA ( $N_{xT}$ of composed elements).
2.	2.5	A-P1M	615	
3.	2.5	A-P1J	1668*	
4.	2.5	C-P1J	1668*	
5.	2.5	C-P2M	678	
6.	2.5	A-P2J	681	
7.	2.5	C-P1M	615	
8.	1.25	C-P1M	501	
9.	1.25	A-P1M	501	
10.	1.25	A-P1J	614	
11.	1.25	C-P2M	555	
12.	1.25	A-P2J	556	
16.	2.5	B-P2M	867	
19.	2.5	B-P1M (SLP)	708	

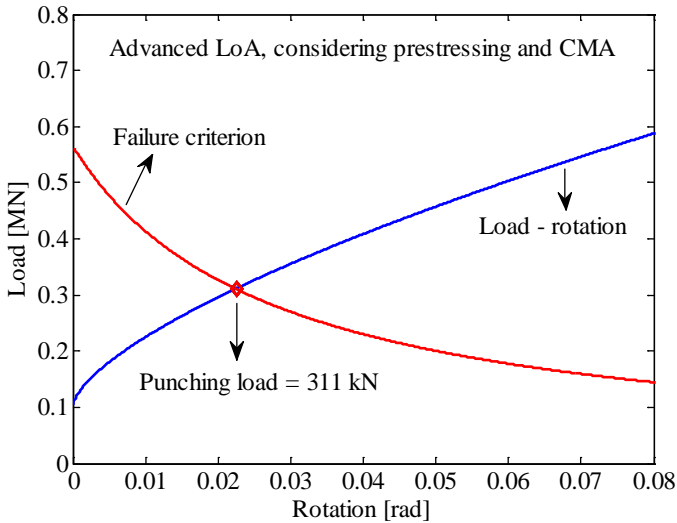
\*The center of the loaded area was too close to the girder flange-deck slab interface in the FEA (150 mm), hence these cases show very high in-plane forces.

Fig. 8.12a shows typical the load-rotation behavior for a single load at the midspan (P1M) with a TPL of 2.5 MPa at an elementary LoA and Fig. 8.12b shows the same load case but for an advanced LoA. The failure criterion remains the same for both cases but the load-rotation behavior changes due to a different contribution of the in-plane forces arising either

from only prestressing, or from prestressing and compressive membrane action. Smaller rotation and consequently a higher punching load is obtained when considering compressive membrane action in the load-rotation behavior. A sample calculation is given in Appendix C.



(a)



(b)

Fig. 8.12 Graphical representation of the CSCT LoA approach for PIM load case: a) Elementary LoA with only prestressing forces; b) Advanced LoA with prestressing and compressive membrane forces.

### 8.3.5 Comparison of the theoretical, experimental and FEA punching loads

A comparison is drawn between the punching shear capacity obtained theoretically from the critical shear crack model and the results of the experimental and finite element analysis, see Table 8.6. A coefficient of variation of 11% and 9% is obtained when the experimental and the FEA punching loads are compared with the advanced LoA results, respectively.

Table 8.6 Comparison of the CSCT punching loads with the experimental and FEA results.

Test BB.	TPL	Designation	$P_T$	$P_{FEA}$	$P_{CSE}$	$P_{CSA}$	$P_T/P_{FEA}$	$P_T/P_{CSA}$	$P_{FEA}/P_{CSA}$
	[MPa]		[kN]	[kN]	[kN]	[kN]			
1.	2.5	C-P1M	348.7	302.3	253	311	1.15	1.12	0.97
2.	2.5	A-P1M	321.4	302.3	253	311	1.06	1.03	0.97
3.	2.5	A-P1J	441.6	429.9	253	422.4	1.03	1.05	1.02
4.	2.5	C-P1J	472.3	429.9	253	422.4	1.10	1.12	1.02
5.	2.5	C-P2M	490.4	529.9	362.2	453.3	0.93	1.08	1.17
6.	2.5	A-P2J	576.8	537.0	362.2	482.3	1.07	1.20	1.11
7.	2.5	C-P1M	345.9	302.3	253	311	1.14	1.11	0.97
8.	1.25	C-P1M	284.5	271.4	220.2	295	1.05	0.96	0.92
9	1.25	A-P1M	258.2	271.4	220.2	295	0.95	0.87	0.92
10.	1.25	A-P1J	340.3	300.7	220.2	310.9	1.13	1.09	0.97
11.	1.25	C-P2M	377.9	453.4	314.7	431.3	0.83	0.88	1.05
12.	1.25	A-P2J	373.7	454.9	314.7	432.1	0.82	0.86	1.05
16.	2.5	B-P2M	553.4	592.7	362.2	482.3	0.93	1.15	1.23
19.	2.5	B-P1M	317.8	306.0	220.9	281.9	1.04	1.13	1.09
			<b>Mean</b>				<b>1.02</b>	<b>1.05</b>	<b>1.03</b>
			<b>Standard deviation</b>				<b>0.11</b>	<b>0.11</b>	<b>0.09</b>
			<b>Coefficient of variation</b>				<b>0.11</b>	<b>0.11</b>	<b>0.09</b>

Notations:  $P_{FEA}$  = Finite element ultimate load,  $P_{CSE}$  = CSCT elementary LoA ultimate punching load,  $P_{CSA}$  = CSCT advanced LoA ultimate punching load.

### 8.3.6 Application of the proposed LoA approach using CSCT on test results from past literature

The elementary and advanced LoA approach for the CSCT have been applied on restrained, prestressed deck slabs or slabs from the literature. Where lateral restraint is low, the calculation is done on the elementary level only.

Fig. 8.13 shows the theory applied on 8 experimental studies, comprising 56 tests that are similar in nature with the current experiments. All the tests cases cover transversely prestressed slabs (unbonded, bonded or external) and showed evidence of compressive membrane action arising either from the lateral restraints provided by the supports or external prestressing. The details of the investigated cases are given in Appendix D. The in-

plane forces used in the calculations were either obtained experimentally or by FEA in these studies (Graddy et al. 1995), or have been assumed proportionally based on the in-plane forces obtained in the FEA of the current model under study. For instance, for tests done by Savides (1989), He (1992) and Marshe (1997) on a 1/4.04 scaled model with a 43 mm thick deck slab, 50% of the normal forces obtained by the FEA of the 1:2 scaled model bridge deck of the current study have been assumed to be developed. The assumption is valid since sufficient CMA was witnessed in the tests done by He (1992) and others. It can be observed that a coefficient of variation of 10% was obtained when the punching loads calculated by CSCT were compared with the experimental results.

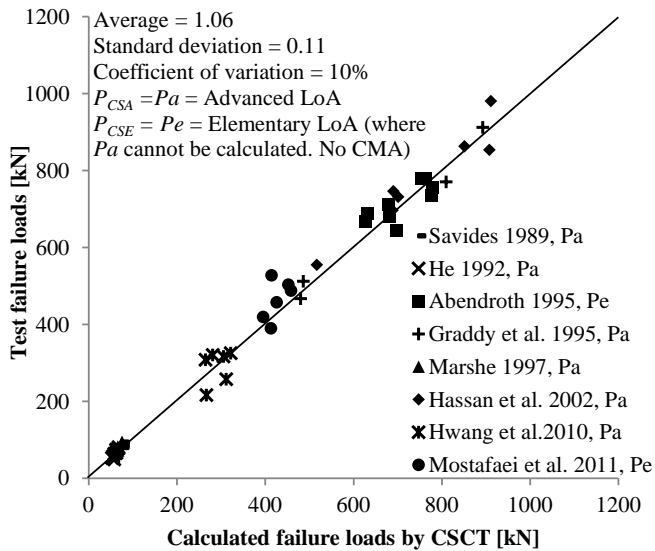


Fig. 8.13 Application of the proposed LoA approach using CSCT on test results from past literature.

### 8.3.7 Ultimate bearing capacity of the real bridge by CSCT

The ultimate capacity of the real, full scale bridge can be estimated by the CSCT in a similar way as for the scaled model bridge. The input to the MATLAB code is given in Table 8.7.

In order to calculate the size effect, the results of CSCT regarding the model bridge are projected using the force scale factor ( $x^2=2^2$ , section 3.1.2) to obtain the real bridge capacity as shown in Table 8.8. The size factors calculated from the FEA model bridge results (section 7.4.12) are also given.

## Theoretical Analysis of Transversely Prestressed Deck Slabs

Table 8.7 Input for the MATLAB code for the real bridge calculations by CSCT.

#	TPL	Designation	Normal force, $n$
	[MPa]	Load type	[N/mm]
1.	1.25	P1M	864
2.	2.5	P1M	1240
$f_{cm} = 65 \text{ MPa}$ , $E_s = 200 \text{ GPa}$ , $d_g = 32 \text{ mm}$ $d = 162 \text{ mm}$ , $B = 2100 \text{ mm}$ , $b_c = 400 \text{ mm}$ $c_c = 400 \text{ mm}$			
<i>From FEA:</i> $r_s = 525 \text{ mm}$ ( $\approx B/4$ , assuming maximum rotations occur in the transverse direction), $n$ depends on TPL and CMA.			

It can be observed from Table 8.8 that when comparing the projected CSCT model bridge results with the actual calculated CSCT capacity of the real bridge, the size factor is approximately equal to 1 (in sharp contrast to FEA results where a size effect is observed). Keeping in mind that the model bridge is not exactly 1:2 scale model because of certain construction limitations, the negligible difference in the projected model bridge capacity and the actual real bridge capacity shows that the size effect has already been considered quite realistically in the critical shear crack theory. Eq. 8.8 shows that the size effect has been introduced in the CSCT by multiplying the slab rotation  $\psi$  by its thickness  $d$  which cancels out when the  $\psi$  of the Eq. 8.9 is put into Eq. 8.8. Muttoni (2008) concludes that the reduction of the strength for size effect is not a function of the slab thickness but rather of the span, represented by the radius  $r_s$  defined earlier in section 8.3.1. Therefore, for further calculations based on CSCT, no size factor is required. However, for calculations based on FEA, considering that the maximum average size factor obtained from the FEA is 1.15, a factor of 1.2 is selected conservatively and is also used for the model bridge experimental results. It should be noted that Mitchel et al. (2005) show a size factor of 1.2 for an effective depth of 100 mm when the shape of the size effect expressions from various design codes are normalized to give a size factor of 1 for an average effective depth of 200 mm (Appendix C).

Table 8.8 Ultimate bearing capacity of the real bridge calculated by the CSCT and the size factor.

TPL	$P_{pr,CSE}$	$P_{pr,CSA}$	$P_{CSE,RB}$	$P_{CSA,RB}$	Size factor FEA		Size factor CSCT	
	Scale factor, $x = 2^2$	Scale factor, $x = 2^2$			25mm ducts	45mm ducts	$P_{pr,CSE}/P_{CSE,RB}$	$P_{pr,CSA}/P_{CSA,RB}$
[MPa]	[kN]	[kN]	[kN]	[kN]				
1.25	881	1180	879	1128	1.22	1.13	1.00	1.04
2.5	1012	1244	1005	1228	1.08	0.98	1.00	1.01
			<b>Average</b>		<b>1.15</b>	<b>1.1</b>	<b><math>\approx 1</math></b>	

Notations:  $P_{pr,CSE}$  = Projected CSCT elementary LoA ultimate punching load for the real bridge,  $P_{pr,CSA}$  = Projected CSCT advanced LoA ultimate punching load for the real bridge,  $P_{CSE,RB}$  = CSCT elementary LoA ultimate punching load for the real bridge,  $P_{CSA,RB}$  = CSCT advanced LoA ultimate punching load for the real bridge.

### 8.3.8 Conclusion

The theoretical analyses based on the CSCT shows that the mechanical model satisfies the experimental results fairly well. A different level of approximation has been used and is found to give satisfactory results. The model also seems to simulate the size effect properly in its equations.

## 8.4 Real bridge ultimate bearing capacity

One of the main objectives of this research study is to arrive at the ultimate bearing capacity of the real (full scale) bridge. While the numerical results of the analyses carried out on the real bridge can be used directly to evaluate the capacity (7.4.12) after applying the necessary safety factors, the experimental results, based on the 1:2 scaled model of the real bridge, still need to be projected to obtain the capacity of the full scale bridge. As mentioned in section 3.1.2 and section 7.4.12, apart from the linear scale factor (1:2), a size factor needs to be introduced before the results can be compared with the expected design wheel load to determine if the real bridge has sufficient capacity or not. In this section, the numerical and experimental results will be projected using all safety factors and compared with the design wheel loads to assess if the real structure is able to carry the modern traffic loads. Both the numerical analyses results of the 1:2 scaled model (2ELEM) and the real bridge model (RB4ELEM) will be used. In order to keep similarity between the experimental and numerical results, the 2ELEM model with 45 mm ducts will be used here. This will be a lower bound of the capacity obtained via the numerical analyses. Realistically, the 2ELEM 25 mm  $\Phi$  ducts model is the 1:2 scaled model for RBELEM 50 mm  $\Phi$  ducts model. Also results with 0.5 MPa have not been considered since they were performed only as control cases and such a low level of TPL does not exist in the type of the bridge under study. Analyses with wheel print above the ducts have also been disregarded although they give a higher capacity.

### 8.4.1 The Global Safety format and model uncertainty

The Model Code 2010 (*fib* 2012) has introduced numerical analyses as a tool for the design of structures but in order to make use of this, adequate model validation and safety requirements need to be met. Cervenka (2013) compares in detail various methods of global safety assessment found in the MC2010; the Global Resistance Factor Method (GRF), full probabilistic analysis, Estimation of Coefficient of Variation of Resistance Method (ECOV) and Partial Safety Factors (PSFs). Generally, the global resistance factor (GRF) is considered the most promising format to be used for concrete structures since it is easy to use with an adequate safety margin. The nonlinear analysis is performed using mean values

for the material characteristics and geometrical properties. The ultimate limit state verification requires a comparison of design resistance and design loads expected on the structure. The design equation is:

$$F_d < R_d \quad (8.10)$$

where,  $F_d$  is the design action and  $R_d$  is the design resistance. Both the action and resistance have individual safety margins incorporated into them (Cervenka 2013). The safety margin for the resistance part can be expressed as:

$$R_d = \frac{R_m}{\gamma_{GL}} \quad (8.11)$$

The calculated resistance  $R_m$ , using mean values for the material strengths, is divided by a global resistance factor,  $\gamma_{GL}$ , to obtain the design value for the structural resistance  $R_d$ . The guidelines for the nonlinear finite element analysis of concrete structures (RTD 1016 2012) give  $\gamma_{GL} = 1.2 \times 1.06 = 1.27$ , where  $\gamma_{GL}$  is the product of the safety and the model coefficients. However, the mean resistance in the Model Code 2010 (*fib* 2012) and in RTD 1016 (2012) is based on fictitious values ( $f_{cm} \approx 0.85 f_{ck}$ ) and not the actual mean strengths. In the present study, since the actual mean strengths are used, therefore,  $\gamma_{GL}$  is further divided by 0.85 to obtain a factor of 1.5 ( $\gamma_{GL} = 1.27/0.85 = 1.5$ ). The design load  $F_d$  is obtained by multiplying the characteristic load with a partial factor  $\gamma_Q$ . The characteristic wheel load,  $Q_k$  according to the Load Model 1 of EC2<sup>16</sup> is 150 kN for a single wheel (300 kN for a double load) and 300 kN for an axle. Hence the actions part of the Eq. 8.10 can be rewritten as:

$$F_d = \gamma_Q Q_k \quad (8.12)$$

The Ministry of Infrastructure and the Environment in the Netherlands, Rijkswaterstaat, allows a partial factor for traffic actions  $\gamma_Q$  of 1.25 for existing bridges built before 2012 in RBK Table 2.1 (RTD 1006 2013) but a partial factor of 1.5 according to NEN-EN 1990+A1+A1/C2:2011/NB:2011 (Table NB.13-A2.4(B), CC3) for new bridges is used here conservatively.

## 8.4.2 Factor of safety

In this section, the factor of safety of the model bridge and the real bridge against the design wheel load of the Eurocode 2 will be evaluated as per Eq. 8.10, 8.11 and 8.12.

---

<sup>16</sup> The ultimate distributed load is not taken into account. Also, the Load Model 2 of EC2 is not being considered, as the wheel footprint of only Load Model 1 was used in all the analyses.

### Using the 1:2 scaled model bridge deck analyses results

There are two approaches by which factor of safety can be calculated from the results of 1:2 scaled model bridge deck analyses. The first approach is to use the actual results as the resistance of the model bridge deck, calculate the design resistance and compare it with the *scaled down* Eurocode design wheel load. The factor of safety thus obtained will be applicable for the model bridge deck. The second approach is to *scale up* (or to project) the actual results by using the scale and size factors to get the resistance of the real bridge, calculate the design resistance and compare it with the Eurocode design wheel load. The factor of safety thus obtained will be applicable for the real bridge.

#### Using actual analyses results in a calculated factor of safety for the model bridge deck

Table 8.9 Calculation of the factor of safety for the model bridge deck using the actual analyses results.

BB	TPL	$P_T$	$P_{FEA}$	$P_{CSA}$	$R_{md,T}$	$R_{md,FEA}$	$R_{md,CSA}$	Test FOS	FEA FOS	CSCT FOS
					$P_T/\gamma_T$	$P_{FEA}/\gamma_{GL}$		$R_{md,T}/F_{md}$	$R_{md,FEA}/F_{md}$	$R_{md,CSA}/F_{md}$
	[MPa]	[kN]	[kN]	[kN]	[kN]	[kN]	[kN]			
1.	2.5	348.7	302.3	311	232	202	234	4.13	3.58	4.16
2.	2.5	321.4	302.3	311	214	202	234	3.81	3.58	4.16
3.	2.5	441.6	429.9	422.4	294	287	325	5.23	5.10	5.78
4.	2.5	472.3	429.9	422.4	315	287	325	5.60	5.10	5.78
5.	2.5	490.4	529.9	453.3	327	353	346	2.91	3.14	3.08
6.	2.5	576.8	537.0	482.3	385	358	346	3.42	3.18	3.08
7.	2.5	345.9	302.3	311	231	202	234	4.10	3.58	4.16
8.	1.25	284.5	271.4	295.7	190	181	222	3.37	3.22	3.95
9	1.25	258.2	271.4	295.7	172	181	222	3.06	3.22	3.95
10.	1.25	340.3	300.7	310.9	227	200	234	4.03	3.56	4.16
11.	1.25	377.9	453.4	431.3	252	302	329	2.24	2.69	2.92
12.	1.25	373.7	454.9	432.1	249	303	329	2.21	2.70	2.92
16.	2.5	553.4	592.7	482.3	369	395	369	3.28	3.51	3.28
19.	2.5	317.8	306.0	281.9	212	204	208	3.77	3.63	3.70
					<b>Average factor of safety</b>			<b>3.65</b>	<b>3.56</b>	<b>3.93</b>

The resistance  $R_m$  is taken equal to the ultimate (punching) loads from the tests, the finite element results and the critical shear crack theory results at an advanced LoA ( $P_T$ ,  $P_{FEA}$  and  $P_{CSA}$  respectively) from the analyses of the 1:2 scaled bridge model. The test design resistance  $R_{md,T}$  is calculated by applying Level II method<sup>17</sup> (Eq. 8.4) on the test ultimate load  $P_T$  ( $\gamma_T = \mu_{RD} / B_{RD} = 1.5$ ). The FEA design resistance  $R_{md,FEA}$  is obtained by dividing  $P_{FEA}$  by  $\gamma_{GL}$  (1.5). Design resistance using CSCT<sup>18</sup>  $R_{md,CSA}$  is calculated for the model bridge deck at an advanced LoA with the appropriate material and safety factors. The scaled down

<sup>17</sup>  $B_{RD} = \mu_{RD}(1 - \alpha_{BR}\beta\delta_{BR})$ , where  $\alpha_{BR} = 0.8$ ,  $\beta = 3.8$  and  $\delta_{BR} = 0.11$ , see Table 8.6. Therefore,  $\gamma_T = \mu_{RD} / B_{RD} = 1.5$ .

<sup>18</sup> Refer to the recommendations for practice in Chapter 9.

## Theoretical Analysis of Transversely Prestressed Deck Slabs

design wheel load  $F_{md}$  is obtained by multiplying the characteristic load  $Q_K$  with a partial factor  $\gamma_Q$  (1.5) and dividing by the force scale factor ( $x^2 = 2^2$ ). The factor of safety (FOS) is obtained by dividing the design loads with the design resistance.

### Using projected analyses results in a calculated factor of safety for the real bridge deck

Table 8.10 Calculation of the factor of safety for the real bridge using the projected model bridge analyses results.

BB.	TPL	$P_{pr,T}$	$P_{pr,FEA}$	$R_{d,T}$	$R_{d,FEA}$	$R_{d,CSA}$	Test FOS	FEA FOS	CSCT FOS
		$P_T \times 2^2/1.2$	$P_{FEA} \times 2^2/1.2$	$P_{pr,T}/\gamma_T$	$P_{FEA}/\gamma_{GL'}$	$R_{md,CSA}^* \times 2^2/1.2$	$R_{d,T}/F_d$	$R_{d,FEA}/F_d$	$R_{d,CSA}/F_d$
	[MPa]	[kN]	[kN]	[kN]	[kN]	[kN]			
1.	2.5	1162	1008	775	793	780	3.44	2.99	3.47
2.	2.5	1071	1008	714	793	780	3.17	2.99	3.47
3.	2.5	1472	1433	981	1128	1083	4.36	4.25	4.81
4.	2.5	1574	1433	1050	1128	1083	4.66	4.25	4.81
5.	2.5	1635	1766	1090	1391	1153	2.42	2.62	2.56
6.	2.5	1923	1790	1282	1409	1153	2.85	2.65	2.56
7.	2.5	1153	1008	769	793	780	3.42	2.99	3.47
8.	1.25	948	905	632	712	740	2.81	2.68	3.29
9	1.25	861	905	574	712	740	2.55	2.68	3.29
10.	1.25	1134	1002	756	789	780	3.36	2.97	3.47
11.	1.25	1260	1511	840	1190	1097	1.87	2.24	2.44
12.	1.25	1246	1516	830	1194	1097	1.85	2.25	2.44
16.	2.5	1845	1976	1230	1556	1230	2.73	2.93	2.73
19.	2.5	1059	1020	706	803	693	3.14	3.02	3.08
				<b>Average factor of safety</b>			<b>3.05</b>	<b>2.96</b>	<b>3.28</b>

\*  $R_{md,CSA}$  is taken from Table 8.9 and projected by using scale and size factors to get the design resistance  $R_{d,CSA}$ . There is no need to apply any safety factors since they have already been considered in  $R_{md,CSA}$ .

The resistance  $R_m$  is taken equal to the projected ultimate (punching) loads from the tests and the finite element results ( $P_{pr,T}$  and  $P_{pr,FEA}$ , respectively) that are derived from the experimental and the FEA results of the 1:2 scaled bridge model using the scale and size factors, as shown in Table 8.10. The test design resistance  $R_{d,T}$  is calculated by applying Level II method<sup>19</sup> (Eq. 8.4) on the projected test results,  $P_{pr,T}$  ( $\gamma_T = \mu_{RD} / B_{RD} = 1.5$ ). The FEA design resistance  $R_{d,FEA}$  is obtained by dividing  $P_{pr,FEA}$  by  $\gamma_{GL'}$  (1.5). Design strength using CSCT<sup>20</sup> calculated for the model bridge deck at an advanced LoA ( $R_{md,CSA}$  in Table 8.9) is projected to give design strength of the real bridge,  $R_{d,CSA}$  using the scale and size factors. The factor of safety (FOS) is obtained by dividing the design loads with the design resistance.

<sup>19</sup>  $B_{RD} = \mu_{RD}(1 - \alpha_{BR}\beta\delta_{BR})$ , where  $\alpha_{BR} = 0.8$ ,  $\beta = 3.8$  and  $\delta_{BR} = 0.11$ , see Table 8.6. Therefore,  $\gamma_T = \mu_{RD} / B_{RD} = 1.5$ .

<sup>20</sup> Refer to the recommendations for practice in Chapter 9.

### Using the real bridge deck analyses results

A similar calculation is made for the real bridge (using actual dimensions) from the FEA (section 7.4.12) and the CSCT (section 8.3.7).  $P_{CSA, RB}$  and  $P_{FEA, RB}$  will be taken as  $R_m$ , the resistance obtained from the CSCT (advanced LoA) and the FEA. Since these are *direct* analyses results and no projection from the model bridge involving scale factors is made, therefore, no size factor is employed. Muttoni (2008) and Table 8.8 show that the size effect (that reduces the capacity as the thickness increases) is already included in the CSCT. The FEA design resistance  $R_{d, FEA}$  is obtained by dividing  $P_{FEA, RB}$  by  $\gamma_{GL'}$  (1.5).  $P_{CSA, RB}$  is recalculated using Eq. 8.5, 8.6 and 8.7 (involving characteristic strengths and material factors) to obtain CSCT design resistance  $R_{d, CSA}$  but by using the advanced LoA approach (with compressive membrane action, refer to section 9.3). The design load/action,  $F_d$  remains the same as defined in Eq. 8.12. The results are shown in Table 8.11.

Table 8.11 Comparison of the ultimate capacity and the applied loads of the real bridge using real dimensions.

#	TPL	Designation	$P_{FEA, RB}$	$P_{CSA, RB}$	$R_{d, FEA}$	$R_{d, CSA}$	FEA FOS	CSCT FOS
							$R_{d, FEA}/F_d$	$R_{d, CSA}/F_d$
	[MPa]		[kN]	[kN]	[kN]	[kN]		
1.	1.25	P1M	958	1128	639	791	2.84	3.52
2.	2.5	P1M	1229	1228	819	875	3.64	3.89
			<b>Average Factor of Safety (FOS)</b>				<b>3.24</b>	<b>3.70</b>

### Conclusion

For the model bridge deck, a factor of safety (FOS) of 3.65, 3.56 and 3.93 is obtained by using the actual results of experiments, the FEA, and the CSCT, respectively. For the real bridge deck, a factor of safety (FOS) of 3.05, 2.96 and 3.28 is obtained from the projected results of experiments, the finite element analysis, and the CSCT, respectively. By using the real bridge analyses results, a factor of safety (FOS) of 3.24 and 3.70 is obtained from the finite element analyses and the CSCT, respectively. It is remarkable how the FOS from the model bridge calculations and that from the real bridge calculations is in the same order of magnitude.

It is to be noted that the calculations for the FOS based on the model bridge include both single and double loads applied at midspan and close to the interface (P1M, P1J, P2M and P2J), whereas, those based on the real bridge include only the typical load case of a single load at midspan (P1M). The overall factor of safety is calculated in Table 8.12 and is approximately equal to 3.25.

Table 8.12 Average factor of safety of the real bridge against the design wheel load.

Factor of safety (FOS) calculation	Model bridge projected results (Table 8.10)			Real bridge (Table 8.11)		Average FOS
	Test	FEA	CSCT	FEA	CSCT	
Load cases	14	14	14	2	2	
Average value	3.05	2.96	3.28	3.24	3.70	≈ 3.25

## 8.5 Summary and conclusions

The goal of this chapter was to carry out theoretical analyses of the model and the real bridge. The experimental and finite element results have already been presented in the previous chapters. First existing codes and methods were used to evaluate the structures under study and then the critical shear crack theory that grounds the MC2010 shear provisions has been used to make the calculations. The following important conclusions have been drawn:

- Eurocode 2 and ACI 318 give conservative results since they consider a very low contribution of the in-plane forces. Increasing the contribution of the in-plane forces improves the results from the codes leading to the conclusion that compressive membrane action should be considered at least for the assessment of old bridges.
- UKBD81/02 and CHBDC consider compressive membrane action empirically but have limited applicability for thin, prestressed decks.
- The critical shear crack theory failure criterion was verified for the current experimental data to obtain positive results.
- For the real bridge, an overall factor of safety of about 3.25 is obtained against the design wheel load. Such a high safety margin is due to the beneficial effect of compressive membrane action that gives a reserve capacity for old bridges.
- For most cases, an elementary LoA (or Level II LoA from MC2010) using CSCT can serve as a quick assessment of the punching shear capacity.
- The objective of using the advanced LoA is to prove the effectiveness of considering compressive membrane action in the load-rotation behavior of a structure.
- The LoA approach involving compressive membrane action can also be used for reinforced concrete slabs or deck slabs, provided sufficient restraint is available.

# CHAPTER 9

## Recommendations for practice

This chapter outlines the recommendations for practicing engineers to calculate the punching shear capacity of deck slabs based on the Model Code 2010 punching shear provisions (critical shear crack theory) and incorporating compressive membrane action.

## 9.1 Introduction

It is difficult, if not impossible, to analytically calculate the magnitude of compressive membrane action developed in laterally restrained slabs and deck slabs. Over the years, several approaches to calculate the compressive membrane forces have been formulated, mostly requiring complex analytical calculations that may not be easy to adapt in practice. The goal of this chapter is to provide guidelines to practicing engineers for calculating the punching shear capacity of slabs or deck slabs using the Model Code 2010 punching shear provisions and by considering compressive membrane action through the proposed Levels of Approximation (LoA) approach.

## 9.2 Proposed LoA approach to the critical shear crack theory incorporating compressive membrane action

In Chapter 8, a methodology to incorporate compressive membrane action (CMA) in the prediction of punching shear capacity of slabs or deck slabs has been proposed. The technique involves a combination of finite element analysis and the punching shear provisions of the Model Code 2010 based on the critical shear crack theory. The step-by-step procedure carried out to calculate the punching shear capacity considering compressive membrane action is summarized below:

- A 3D solid finite element model of the bridge was constructed using the DIANA software package. A layer of composed elements was provided around the loaded area to calculate the normal distributed forces arising from the compressive membrane action. An initial prestressing load was applied and a nonlinear analysis was carried out until failure.
- For the theoretical calculations, the failure criterion of the standard Model Code 2010 or the CSCT was employed.
- A level of approximation approach based on the Model Code 2010 was used to calculate the punching shear capacities. An elementary level of approximation using only the transverse prestressing force as the normal force and an advanced level of approximation using the total in-plane force (arising from transverse prestressing and compressive membrane action) as the normal force were proposed to calculate the load-rotation behavior.
- The transverse prestressing force in the elementary level of approximation depended upon the level of prestressing applied. The total in-plane force in the advanced level of approximation was obtained from the composed element output for distributed in-plane force.

- A MATLAB program was developed based on the punching shear provisions of the Model Code 2010 or the critical shear crack theory. Iterative calculations for the elementary and advanced level of approximation were made and the resulting load-rotation curves were intersected with the failure criterion of the CSCT to obtain the punching shear load.
- The elementary level of approximation gave the lower bound and the advanced level of approximation gave the upper bound of the punching shear capacity.

In the current research, a 3D solid model was used for carrying out the nonlinear analysis and calculating the compressive membrane forces. In practice, or in design codes, a 3D shell element model (2½D model) may be sufficient for calculating the compressive membrane forces. This would lead to saving in time and computational costs. Since a 3D finite element model has the capacity of predicting the punching shear failure including compressive membrane action on its own and does not necessarily require any further theoretical calculations, therefore, a shell element model which cannot predict a punching shear failure independently is considered suitable for this approach.

### 9.3 Design formulation of the proposed LoA approach

In the following section, a design formulation of the proposed LoA approach to calculate the punching shear capacity of slabs without shear reinforcement using the critical shear crack theory is made. Punching shear provisions of the Model Code 2010 (*fib* 2012) are used as the basis. The general design equation is as follows:

$$V_{Rd} = V_{Rd,c} \geq V_{Ed} \quad (9.1)$$

For no shear reinforcement in the member, the shear resistance attributed to concrete  $V_{Rd,c}$  is equal to the total shear resistance  $V_{Rd}$  which must be greater than or equal to the design punching shear force (acting shear). See section 7.3.5.3 and 7.3.5.4 of the Model Code 2010 for the complete definition of the variables involved in the following sections.

#### 9.3.1 Design shear resistance

The design shear resistance attributed to concrete is given by the failure criterion of the Critical Shear Crack Theory (CSCT):

$$V_{Rd,c} = k_w \frac{\sqrt{f_{ck}}}{\gamma_c} b_0 d_v \quad [SI \text{ Units : } N, mm] \quad (9.2)$$

$$k_{\psi} = \frac{1}{1.5 + 0.9k_{dg}\psi d} \leq 0.6 \quad (9.3)$$

In Eq. 9.2,  $b_0$  is the length of the control perimeter at  $d_v/2$  of the edge of the supported area,  $d_v$  is the shear-resisting effective depth of the member,  $f_{ck}$  is the characteristic compressive cylinder strength of the concrete and  $\gamma_c$  is the partial safety factor for concrete. In Eq. 9.3,  $k_{\psi}$  is the rotation parameter depending upon the opening and the roughness of the cracks,  $d$  is the (flexural) effective depth for the x and y-directions,  $k_{dg}$  can be taken as  $k_{dg} = 1.0$  when the maximum size of the aggregate  $d_g$  is not less than 16 mm. If concrete with a maximum aggregate size smaller than  $d_g = 16$  mm is used, the value of  $k_{dg}$  can be calculated as:  $32/(16+d_g) \geq 0.75$ .

### 9.3.2 Load-rotation relationship

The rotation at failure ( $\psi$  in Eq. 9.3) can be evaluated by using the Levels of Approximation (LoA) approach. Four levels of approximation are proposed: LoA II, LoA III, LoA IV and LoA V. LoA II and III are similar to the current punching shear provisions of the Model Code 2010 with the LoA II being the elementary LoA used in the previous chapter. The LoA IV is similar to the advanced LoA used in the previous chapter incorporating compressive membrane action and the LoA V is a completely new recommendation.

#### Level of approximation II

For prestressed slabs, the rotation can be calculated as:

$$\psi = 1.5 \frac{r_s}{d} \frac{f_{yd}}{E_s} \left( \frac{m_{sd} - m_{pd}}{m_{Rd} - m_{pd}} \right)^{1.5} \quad (9.4)$$

where,  $r_s$  can be calculated according to section 8.3.1. For bridge deck slabs,  $r_s$  can be estimated as  $\approx B/4$  where B is the span of the slab in the direction where rotations are maximum.  $f_{yd}$  is the design yield strength of the flexural reinforcement.  $E_s$  is the modulus of elasticity of flexural steel.  $m_{sd}$  is the average design moment per unit length for the calculation of the flexural reinforcement in the support strip and can be calculated as  $m_{sd} \approx V_{Ed}/8$ , for inner columns without unbalanced moments. For other cases, reference is made to the section 7.3.5.4 of the Model Code 2010.  $m_{Rd}$  is the average design flexural strength per unit length in the support strip which can be calculated by assuming that both flexural and prestressing reinforcement are yielding at failure.  $m_{pd}$  denotes the average decompression moment over the width of the support strip due to prestressing and can be taken as  $m_{pd} = n(h/2 - d/3 + e)$ , where  $n$  is the normal force per unit length arising only

from the initial prestressing and  $e$  is the eccentricity of the prestressing force from the center of gravity of the section. The decompression moment is considered positive when it leads to compressive stresses on the top side of the slab. Constrained forces and moments and losses due to shrinkage, creep and relaxation are to be taken into account.

### **Level of approximation III**

This Level of Approximation is recommended for irregular slabs or for flat slabs where the ratio of the span lengths ( $L_x/L_y$ ) is not between 0.5-2.0. The coefficient 1.5 in Eq. 9.4 can be replaced by 1.2 if  $r_s$  and  $m_{sd}$  are calculated from a linear elastic (uncracked) model.

### **Level of approximation IV**

A 3D shell finite element model (also called 2½D model) can be constructed conforming to the guidelines given in RTD 1016 (2012) or based on engineering judgment that has the capability of calculating the local normal distributed forces. The rotation  $\psi$  can be calculated on the basis of a nonlinear flexural analysis of the structure and accounting for cracking, tension-stiffening effects, yielding of the reinforcement and any other nonlinear effect relevant for providing an accurate assessment of the structural bearing capacity (*fib* 2012). Such an approach is suitable for practicing engineers.

For research purposes, where it is important to determine the contribution of compressive membrane action in the punching shear capacity, the in-plane (normal) force  $n$  at the slab or the deck slab edge can be obtained as an output of the nonlinear analysis of the shell element model. If lateral restraint is available, the in-plane force  $n$  will include the initial prestressing (if present) and compressive membrane forces and can be used to calculate the decompression moment  $m_{pd}$ . Finally, the rotation is calculated from Eq. 9.4.

### **Level of approximation V**

According to this LoA, the punching shear resistance is calculated directly by an appropriate nonlinear finite element program. A 3D solid finite element model can be constructed conforming to the guidelines given in RTD 1016 (2012) or based on engineering judgment. A nonlinear punching shear analysis can be carried out on such a model to predict the ultimate capacity. Since the punching shear failure can very well be obtained by the nonlinear analysis of a 3D solid model, no further calculations are required.

In order to determine the contribution of compressive membrane action in the punching shear capacity, the in-plane (normal) force  $n$  arising from the initial prestressing and

compressive membrane action can be obtained via the composed elements. Eq. 9.4 can then be used to obtain the rotation.

### 9.3.3 Analysis procedure

When the purpose of investigation is the analysis of a structure, the load rotation relationship obtained from the desired level of approximation is intersected with the failure criterion to calculate the punching load, where  $V_{Rd,c} = V_{Ed}$ . This process is iterative in nature and can be programmed for ease in the calculation procedure since the acting punching shear  $V_{Ed}$  is unknown and therefore the rotation  $\psi$  and the shear resistance  $V_{Rd,c}$  are also unknown.

## 9.4 Conclusion

In this chapter, a code-like formulation of the proposed Level of Approximation (LoA) approach from Chapter 8 was made using the punching shear provisions of the Model Code 2010 based on the critical shear crack theory. The load-rotation relationship can be determined at LoA II and III for a quick assessment without considering compressive membrane action. For including the beneficial effect of compressive membrane action in the punching shear capacity, a LoA IV has been proposed based on a 3D shell element model of the structure to determine the load-rotation relationship. Finally, a LoA V has been recommended in which a 3D solid model of the structure is analyzed nonlinearly. The contribution of compressive membrane action in the punching shear capacity can be determined by using the in-plane forces (arising from the prestressing and the compressive membrane action) to calculate the rotations at either LoA IV or V. The punching failure is thus obtained by intersecting the load-rotation curve with the failure criterion.

# **CHAPTER 10**

## **Conclusions and Future Recommendations**

This chapter concludes the dissertation based on the findings of experimental, numerical and theoretical research. Recommendations for future work are also given.

## 10.1 Summary and conclusions

In this research, an attempt has been made to study the behavior of transversely prestressed concrete decks and investigate the ultimate bearing capacity considering compressive membrane action. A summary of the research program is given in the following sections along with the main conclusions drawn from the investigation.

### 10.1.1 The scientific hypothesis

In the beginning of the dissertation, the hypothesis of the research was declared as below:

*“The in-plane compressive forces from transverse prestressing in combination with the compressive membrane forces arising from the lateral restraint will enhance the bearing capacity of bridge decks.”*

Based on the literature review regarding punching shear in transversely prestressed decks considering compressive membrane action, a strategy consisting of experimental, numerical and theoretical approaches was devised to work on the scientific hypothesis. The research was formulated comprising a 1:2 scale model of the Van Brienenoord bridge in Rotterdam with the objective of magnifying the results of the prototype to the real bridge using laws of similitude and considering size effects. In the following sections, a brief overview of each component of the research strategy is given explaining what steps were taken to prove the scientific hypothesis and general conclusions are made in this regard.

### 10.1.2 Experimental analysis

The experimental aspect of the research included static tests on a half scale model of a real bridge resulting in punching shear failure of the transversely prestressed deck slabs. In Chapter 3, the design and construction of the model bridge was briefly described and an overview of the experimental program and the test setup was given. Then, in chapter 4, results from 19 tests carried out on the bridge deck were summarized. The ultimate capacity, the failure mode and cracking pattern, the load-deflection behavior, state of stresses and strains at the top and bottom of the loaded area, and the vertical and horizontal displacements of the deck slab were some of the important observations. The main conclusions drawn from the experimental results are the following:

- All the tests showed failure in punching shear. Failure always occurred in the span of the slab regardless of the number and position of the loads. The interface between the girders and the deck slab remained safe.

## Conclusions and Future Recommendations

- Although the governing mode of failure was brittle punching, flexural punching was also observed in some cases when the transverse prestressing level was too low or when the single loads were applied above a duct at midspan. Flexural punching was also observed when double loads were applied at midspan.

The experimental results were further analyzed in the Chapter 5 by carrying out a parametric analysis. The main findings are summarized below:

- The transverse prestressing level enhanced the ultimate bearing capacity and the cracking loads were also higher for higher TPLs.
- For tests failing in brittle punching, a load position close to the interface gave a higher capacity than at the midspan.
- A higher punching shear capacity was observed when the deck slab was loaded directly above a prestressing duct compared to a position in-between the ducts.
- Double loads combined give a higher capacity as compared to single loads regardless of the position of the load; at midspan or close to the interface, or the TPL.
- Generally, the skewness of the interface/joint, loading the exterior or interior panels, or the longitudinal position of the load within a deck slab panel had negligible influence on the punching shear capacity.

### 10.1.3 Numerical analysis

A 3D, solid, 1:2 scaled model of a real bridge was developed in the finite element software DIANA and nonlinear analyses were performed to simulate the experiments done in the laboratory. Chapter 6 includes a basic analysis comprising eight test cases. The overall load-deflection behavior, ultimate loads and mode of failure, cracking loads and cracking pattern, stress distribution and compressive membrane action were the main results. Following important conclusions can be drawn from the finite element study:

- A nonlinear finite element analysis of a 3D solid bridge model can simulate the punching shear behavior of deck slab with good accuracy.
- The governing failure mode in the finite element analyses was punching shear similar to the experimental observations.
- The higher the transverse prestressing level (TPL), the higher was the initial cracking load.
- Use of composed elements proved to be a beneficial modeling technique. Substantial compressive membrane action was found to occur in the finite element

## Conclusions and Future Recommendations

model bridge deck and was established by the in-plane compressive force distribution of the loaded area and its surroundings.

- A default (in-built) compressive membrane action existed even for very low levels of prestressing and was dependent on the level of external restraint arising from the structural and geometrical configuration of the deck slab.
- Increasing the TPL increased the in-plane compressive force and as a result an increase in the ultimate bearing (punching shear) capacity was observed. A linear relationship was found to exist between the in-plane force and the punching shear capacity as well as between the initial transverse prestressing level and the punching shear capacity.

In order to validate the 3D solid finite element model, a detailed parametric study was carried out in Chapter 7. A comparison with the experimental results was also made, where available. The main observations are highlighted below:

- The levels of transverse prestressing were increased from two in the basic analysis to four (0.5, 1.25, 2.5 and 4.5 MPa) in the parametric analysis to confirm the previous experimental and numerical analysis observations. An increase in the TPL linearly increases the punching shear capacity when loads were applied at midspan and at the interface. Cracking loads are also increased with increasing TPLs.
- Generally, a higher bearing capacity was observed when the loads were increased in number (from single to double) or applied close to the interface or above the ducts, as compared to when they were applied at midspan or in-between the ducts. Increasing the loading area by increasing its transverse length also increased the punching shear capacity.
- The load position on the exterior or the interior deck slab panels had negligible influence on the punching shear capacity although a slight increase in stiffness and capacity was observed when interior panels were loaded.
- The larger the size of the ducts, the lower was the punching shear capacity because of the reduction in the cross-sectional area of the slab and in the volume of concrete.
- Increasing the fracture energy increased the deformation capacity of the deck slab as well as the ultimate loads. MC 90 (1993) and MC2010 (*fib* 2012) show a large difference in the calculation with regard to the fracture energy.
- A higher concrete strength led to an improved behavior of the deck slab. The tensile strength of the concrete had a larger influence on the punching shear capacity than the compressive strength.

- A 3D real bridge model was constructed to investigate the size effect. The fracture energy was increased assuming a larger aggregate size for a larger thickness, but still some size effect was seen when the results of the model bridge were projected using the scale factor. It was also observed that the size factor varied with the level of transverse prestressing. A smaller size effect was observed for higher TPLs or in other words for higher in-plane compressive forces.
- The average ratio of the ultimate loads observed in tests to the ultimate loads observed in the finite element analysis for all the test cases ( $P_T/P_{FEA}$ ) was found to be 1 with a standard deviation of 0.10 and the coefficient of variation of 10%.

### 10.1.4 Theoretical analysis

A theoretical analysis of the model and the real bridge was made by employing existing codes and methods to calculate the ultimate capacity of the two structures. The critical shear crack theory that grounds the MC2010 shear provisions was also used to carry out the calculations. The following important conclusions are drawn from the analysis.

- Eurocode 2 and ACI 318 gave conservative results since they do not consider compressive membrane action in their provisions. A coefficient of 0.7 instead of the default value ( $k_f = 0.08$  in the background report 25.5-02-37-prENV 1992-1-1 equation<sup>21</sup> and 0.3 in the ACI code equation<sup>22</sup>) was found to be sufficient to increase the contribution of the in-plane forces in the punching shear equations and improve the comparison between the experimental results and the code predictions. However, this needs further validation by considering a larger number of experimental cases.
- The elementary level of approximation, LoA (or LoA II from MC2010) using CSCT was devised to calculate the punching shear capacity considering only the prestressing forces.
- The advanced LoA using CSCT was devised to calculate the punching shear capacity considering the compressive membrane action in addition to the prestressing. In this way, the positive influence of compressive membrane action in the load-rotation behavior of a structure was turned into benefit.
- An overall factor of safety of about 3.25 was calculated for the full scale, real bridge against the design wheel load of Eurocode 2. Such a high safety margin was

---

<sup>21</sup>  $v_{Rd,c} = C_{Rd,c} k (100 \rho_l f_{ck})^{1/3} + k_1 \sigma_{cp}$ ,  $V_r = v_{rd,c} u d$

<sup>22</sup>  $V_{c,ACI} = (0.29 \sqrt{f_{cm}} + 0.3 \sigma_{cp}) b_0 d$

obtained by virtue of the beneficial effects of compressive membrane action and transverse prestressing.

### 10.1.5 Important research findings and conclusions

The following important findings have been obtained after the detailed research carried out on the ultimate bearing capacity of transversely prestressed decks.

- A design and analysis method to incorporate compressive membrane action into the punching shear provisions of the Model Code 2010 based on the critical shear crack theory has been presented in Chapter 9.
- The critical shear crack theory has been found to be versatile in catering to different types of structures and loading conditions as well as incorporating the beneficial effects of the compressive membrane action on the punching shear capacity. Not only it is suitable for research purposes but the proposed Levels-of-Approximation approach makes it helpful for practicing engineers.
- The behavior of a bridge deck with regard to both serviceability and ultimate limit state can be improved if the deck slab is prestressed in the transverse direction and sufficient lateral restraint exists to develop compressive membrane action in the deck slab.
- Most of the experimental and finite element analyses are performed with the load applied in-between the ducts and on exterior panels. The prestressing bars were unbonded in the experiments and the ducts were considered hollow in the finite element model. All these measures along with the ones mentioned in section 3.1.3 lead to conservative ultimate capacities observed in the analyses.
- Using a higher value of the fracture energy for a larger aggregate size (like in some fracture energy based models) is insufficient to properly address the size effect. An overall size effect has to be introduced for thicker structural members.
- A size factor of 1.2 is conservatively obtained after the numerical and the theoretical analyses, where:

$$\text{Real bridge punching capacity} = \frac{\text{Model bridge punching capacity} \times \text{Scale factor}}{\text{Size factor}}$$

- For research purposes, sufficient saving in cost can be realized if calibrated numerical models are employed to investigate existing structures rather than doing expensive experimental studies.

## Conclusions and Future Recommendations

The experimental, numerical and theoretical analyses have given sufficient proof for the hypothesis of the research stating that the in-plane compressive forces from the transverse prestressing in combination with the compressive membrane forces arising from the lateral restraint will enhance the bearing capacity of bridge decks. The detailed research results have led to the conclusion that the conventional bridge deck design and analysis methods are quite conservative and existing bridge decks have sufficient residual strength available to satisfy the modern traffic demands.

### **10.2 Recommendations for future research**

The current research deals with static loads applied to bridge decks. It will be interesting to observe the behavior of deck slabs under fatigue or dynamic loading and to see the development of compressive membrane action with the loading history. Research should also be done on skewed bridge decks or composite deck slabs made up of layered reinforced concrete and precast prestressed panels.

The dependency of size effect on the in-plane forces arising from the transverse prestressing level or the restraining action needs further research.

In the experimental research of this study, a single large size specimen with the same concrete strength was cast. Experimentation with varying material properties can also help to study the effect of concrete properties on the punching shear strength. Similarly, higher levels of transverse prestressing can be used in the bridge deck to further verify the linearity of the relationship between the TPL (or the overall in-plane compressive membrane forces) and the punching shear strength found in this study.

For future research work, it is recommended to quantify the compressive membrane action for different types of structures with varying boundary conditions. This will further simplify the proposed approach of using a nonlinear finite element analysis to determine the compressive membrane action.

## Conclusions and Future Recommendations

## References

- AASHTO (1987), *Standard specification for highway bridges*, American Association of State Highway and Transportation Officials, 14<sup>th</sup> edition, Washington DC, USA.
- Abendroth, R. E. (1993), *Nominal strength of composite prestressed concrete bridge deck panels*, *Journal of Structural Engineering*, Volume 121, No. 2, pp. 307-318.
- ACI (1971), *Cracking, deflection and ultimate load of concrete slab systems*, Publication SP-30, Detroit, American Concrete Institute, Farmington Hills, Michigan, USA, 382 pp.
- ACI Committee 318 (1983), *Building Code Requirements for Reinforced Concrete (ACI 318-83) and Commentary (ACI 318R-83)*, American Concrete Institute, Farmington Hills, Michigan, USA.
- ACI Committee 318 (2011), *Building Code Requirements for Structural Concrete (ACI 318-11) and Commentary (ACI 318R-11)*, American Concrete Institute, Farmington Hills, Michigan, USA.
- Amir, S.; van der Veen, C.; Walraven, J. C.; de Boer, A. (2014), *Bearing capacity of prestressed concrete deck slabs*, Proceedings of the fib congress 2014, Mumbai, India .
- ASCE-ACI Committee 426 (1974), *The shear strength of reinforced concrete members-slabs*, *Journal of the Structural Division, ASCE*, Volume 100, No. 8, pp. 1543-1591.
- Background report 25.5-02-37-prENV 1992-1-1:2002, Section 6.4 (2002), J. C. Walraven, Delft University of Technology, the Netherlands.
- Bakht, B.; Csagoly, R. P. (1979), *Bridge testing*, Ontario Ministry of Transportation and Communications, Research Report No. SRR-79-10, Ontario, Canada, 127 pp.
- Bakht, B.; Jaeger, L. G. (1992), *Ultimate load test of slab-on-girder bridge*, *Journal of Structural Engineering, ASCE*, Volume 118, No. 6, pp. 1608-1624.
- Batchelor, B. de V. (1990), *Membrane Enhancement in Top Slabs of Concrete Bridges*, *Concrete Bridge Engineering, Performance and advances*, pp. 189-213.
- Bazant, Z. P.; Gambarova, P. (1980), *Rough cracks in reinforced concrete*, *Journal of Structural Engineering, ASCE*, Volume 106, No. 4, pp. 819-842.
- Bazant, Z. P.; Cao, Z. (1987), *Size effect in punching shear failure of slabs*, *ACI Structural Journal*, Volume 84, pp. 44-53.
- Birkle, G.; Dilger, W. H. (2008), *Influence of Slab Thickness on Punching Shear Strength*, *ACI Structural Journal*, Volume 105, No. 2, pp. 180-188.

## References

- Braestrup, M. W.; Nielsen, M. P.; Jensen, B. C. (1976), *Axisymmetric punching of plain and reinforced concrete*, Report No. R-75, Structural Research Laboratory, Technical University of Denmark, Copenhagen, Denmark.
- Broms, C. E. (2006), *Concrete flat slabs and footings: Design method for punching and detailing for ductility*, Royal Institute of Technology, Stockholm, Sweden, 114 pp.
- Brotchie, J. F. (1963), *A refined theory for reinforced concrete slabs*, Journal of the Institute of Engineers, Australia, Volume 35, pp. 292-296.
- BS5400 (1978): Parts 2 & 4, *British Standard for the Design of Steel, Concrete and Composite Bridges*, British Standards Institute, London.
- CAN/CSA-S6-06 (2006), Canadian Standard Association: *Canadian Highway Bridge Design Code (CHBDC)*, Canada.
- CEB-FIP Model Code 1990 (1993), MC90, Thomas Telford Ltd, London, UK.
- CEN (2002), Eurocode 0 - *Basis of structural design* NEN-EN 1990-1-1, Comité Européen de Normalisation, Brussels, Belgium.
- CEN (2003), Eurocode 1 – *Actions on Structures - Part 2: Traffic loads on bridges*, NEN-EN 1991-2, Comité Européen de Normalisation, Brussels, Belgium, 168 pp.
- CEN (2005), Eurocode 2 – *Design of Concrete Structures - Part 1-1: General Rules and Rules for Buildings*, NEN-EN 1992-1-1, Comité Européen de Normalisation, Brussels, Belgium, 229 pp.
- Cervenka, C. (2013), *Reliability-based non-linear analysis according to fib Model Code 2010*, Structural Concrete, Volume 14, No. 1, pp. 19-28.
- Christiansen, K. P. (1963), *The effect of membrane stresses on the ultimate strength of an interior panel in a reinforced concrete slab*, The Structural Engineer, Volume 41, No. 8, pp. 261-265.
- Clément, T.; Ramos, A. P.; Fernández Ruiz, M.; Muttoni, A. (2013), *Design for punching of prestressed concrete slabs*, Structural Concrete, Volume 14, pp. 157-167.
- Collins, M. P.; Kuchma, D. (1999), *How safe are our large, lightly reinforced concrete beams, slabs, and footings?*, ACI Structural Journal, Volume 9, No. 4, pp. 482-490.
- Cornelissen, H. A. W.; Hordijk, D. A.; Reinhardt, H. W. (1986), *Experimental determination of crack softening characteristics of normal weight and lightweight concrete*, HERON, Delft University of Technology, the Netherlands, Volume 31, No. 2, pp. 45-56.

## References

- Csagoly, P. F.; Holowka, M.; Dorton, R. (1978), *The true behavior of thin concrete bridge slabs*, Transportation Research Record, No. 664, Transportation Research Board, Washington D.C.
- de Borst, R.; Nauta, P. (1985), *Non-orthogonal cracks in a smeared finite element model*, Engineering Computations 2, pp. 35-46.
- DIANA (2012), TNO DIANA user's manual - Release 9.4.4. Delft: TNO Building and Construction Research.
- DIN 4227 (1978) Teil 1 Spannbeton; *Bauteile aus Normalbeton mit beschränkter oder voller Vorspannung* (Prestressed concrete; structural members made of normal-weight concrete, with limited concrete tensile stresses or with concrete tensile stresses), Deutsches Institut für Normung, Berlin.
- DYWIDAG-Systems International B.V. Dywidag prestressing steel threadbar system. <http://www.dywidag-systems.com>.
- Edalatmanesh, R.; Newhook, J. P.; *Behavior of externally restrained noncomposite concrete bridge deck panels*, ACI Structural Journal, Volume 109, No. 2, pp. 161-169.
- Elstner, R.; Hognestad, E. (1953), *An investigation of reinforced concrete slabs failing in shear*, Mimeographed Report, Department of Theoretical and Applied Mechanics, University of Illinois, USA, 84 pp.
- Elstner, R.; Hognestad, E. (1956), *Shearing Strength of Reinforced Concrete Slabs*, ACI Structural Journal, Volume 28, No. 1, pp. 29-58.
- Fang, I. K. (1985), *Behavior of Ontario-type bridge deck on steel girders*, PhD thesis, University of Texas, Austin, USA.
- Fang, I. K.; Lee, J. H.; Chen, C. R. (1994), *Behavior of partially restrained slabs under concentrated load*, ACI Structural Journal, Volume 91, No. 2, pp. 133-139.
- Fang, I. K.; Worley, J.; Burns, N. H.; Klinger, R. E. (1990), *Behavior of isotropic concrete bridge decks on steel girders*, Journal of Structural Engineering, ASCE, Volume 116, No. 3, pp. 659-678.
- Feenstra, P. H. (1993), *Computational aspects of biaxial stress in plain and reinforced concrete*, PhD thesis, Delft University of Technology, the Netherlands, 151 pp.
- Feenstra, P. H.; Rots, J. G.; Arnesen, A.; Teigen, J. G.; Hoiseth, K. V. (1998), *A 3D Constitutive Model for Concrete Based on a Co-rotational Concept*. In de Borst et al. (eds), *Computational modelling of concrete structures*, Proceedings of the EURO-C 1998 Conference on Computational Modelling of Concrete Structures, Badgastein, Austria, pp. 13-22.

## References

- Fernández Ruiz M.; Muttoni A. (2009), *Applications of the critical shear crack theory to punching of R/C slabs with transverse reinforcement*, ACI Structural Journal, Volume 106, No. 4, pp. 485-494.
- fib (2001), *Punching of Structural Concrete Slabs*, Bulletin 12, Lausanne, Switzerland, 307 pp.
- fib (2012), *Model Code 2010-Final Draft Volume I and II*, fib Bulletin 65 and 66.
- Furuuchi, H.; Takahashi, Y.; Ueda, T.; Kakuta, Y. (1998), *Effective width for shear failure of RC deep slabs*, Transactions of the Japan Concrete Institute, Volume 20, pp. 209-216.
- Gang, W.; Qung-xiang, W.; Zhong-jun, L. (2011), *Membrane action in lateral restraint reinforced concrete slabs*, Journal of Central South University of Technology, Volume 18, No. 2, pp. 550-557.
- Graddy, J. C.; Burns, N. H.; Klingner, R. E. (1995), *Factors affecting the design thickness of bridge slabs*, Research Report 1305-3F, Center for Transportation Research, The University of Texas at Austin, USA, 186 pp.
- Guandalini S.; Burdet O.; Muttoni A. (2009), *Punching tests of slabs with low reinforcement ratios*, ACI Structural Journal, Volume 106, No.1, pp. 87-95.
- Guidotti R. (2010), *Punching of flat slabs subjected to large column loading* (in French: Poinçonnement des planchers-dalles avec colonnes superposées fortement sollicitées), PhD thesis, EPFL No. 4812, Lausanne, Switzerland , 230 pp.
- Hallgren, M. (1996), *Punching shear capacity of reinforced high strength concrete slabs*, PhD thesis, Royal Institute of Technology, Stockholm, Sweden, 206 pp.
- Hassan, A.; Kawakami, M.; Niitani, K.; Mise, A. (2010), *Cracking and ultimate strength of externally prestressed steel-free concrete deck slabs*, Proceedings of Concrete Institute (コンクリート工学年次論文集), Volume 23, No. 3, pp. 511-516.
- Hassan, A.; Kawakami, M.; Niitani, K.; Yoshioka, T. (2002), *An experimental investigation of steel-free deck slabs*, Canadian Journal of Civil Engineering, Volume 29, No. 6, pp. 831-841.
- He, W. (1992), *Punching behaviour of composite bridge decks with transverse prestressing*. PhD thesis, Queen's University, Kingston, Ontario, Canada, 228 pp.
- Hewitt, B. E. (1972), *An investigation of the punching strength of restrained slabs with particular reference to the deck slabs of composite I-beam bridges*, PhD thesis, Queen's University, Kingston, Ontario, Canada.
- Hewitt, B. E.; Batchelor, B deV. (1975), *Punching shear strength of restrained slabs*, Journal of the Structural Division, ASCE, Volume 101, No. 9, pp. 1837-1853.

## References

- Hon, A. (2003), *Compressive membrane action in reinforced concrete beam-and-slab bridge decks*, PhD thesis, Monash University, Australia, 413 pp.
- Hon, A.; Taplin, G.; Al-Mahaidi, R. S. (2005), *Strength of reinforced concrete bridge decks under compressive membrane action*, ACI Structural Journal, Volume 102, No. 3, pp. 393-401.
- Hognestad, E. (1953), *Shearing strength of reinforced concrete column footings*, ACI Structural Journal, Volume 50, No. 11, pp. 189-208.
- Hordijk, D. A. (1991), *Local Approach to Fatigue of Concrete*, PhD thesis, Delft University of Technology, the Netherlands, 210 pp.
- Hwang, H.; Yoon, H.; Joh, C.; Kim, B.S. (2010), *Punching and fatigue behavior of long-span prestressed concrete deck slabs*, Engineering Structures, Volume 32, Issue 9, pp. 2861-2872.
- Kani, G. N. J. (1967), *How safe are our large reinforced concrete beams*, ACI Journal Proceedings, Volume 64, No. 3, pp. 128-141.
- Kinnunen, S. (1963), *Punching of concrete slabs with two-way reinforcement*, Transactions of the Royal Institute of Technology, No. 198, Stockholm, Sweden, 109 pp.
- Kinnunen, S.; Nylander, H. (1960), *Punching of concrete slabs without shear reinforcement*, Transactions of the Royal Institute of Technology, No. 158, Stockholm, Sweden, 112 pp.
- Kirkpatrick, J.; Long, A. E.; Thompson, A. (1982), *Load distribution characteristics of M-Beam bridge decks*, Structural Engineer, Volume 60b, No. 2, pp. 34-43.
- Kirkpatrick, J.; Rankin, G. I. B.; Long, A. E. (1984), *Strength evaluation of M-beam bridge deck slabs*, Structural Engineer, Volume 62b, No. 3, pp. 60-68.
- Kirkpatrick, J.; Rankin, G. I. B.; Long, A. E. (1986), *The influence of compressive membrane action on the serviceability of beam and slab bridge deck*, Structural Engineer, Volume 64b, No. 1, pp. 6-9 and 12.
- Lantsoght, E.O.L. (2013), *Shear in reinforced concrete slabs under concentrated loads close to supports*, PhD thesis, Delft University of Technology, the Netherlands, 306 pp.
- Liebenberg, A. C. (1966), *Arch action in concrete slabs*, National Building Research Institute, Report 234, Bulletin 40. South African Council for Scientific and Industrial Research.
- Litton, R. W. (1974), *A contribution to the analysis of concrete structures under cyclic loading*, PhD thesis, University of California, Berkeley, USA.

## References

- Long, A.E. (1975), *A two-phase approach to the prediction of the punching strength of slabs*, ACI Structural Journal, Volume 72, No. 2, pp. 37-45.
- Long, A. E.; Kirkpatrick, J.; Rankin, G. I. B. (1995), *Enhancing influences of compressive membrane action in bridge decks*, Bridge Modification Conference Proceedings, Ch. 21, pp. 217-227.
- Long, A.E.; Rankin, G.I.B. (1989), *Real strength and robustness of reinforced concrete structures*, Conservation of Engineering Structures, Thomas Telford, London, UK, pp. 47-58.
- Mahdal, A. (2013), *Idealisation of arching action forces in laterally restrained reinforced concrete slab*, Wikimedia commons.
- Masterson, D. M.; Long, A.E. (1974), *The punching strength of slabs, a flexural approach using finite elements*, ACI SP 42, Volume 2, Part 4, pp.747-768
- Marshe, S. (1997), *Punching behavior of composite bridge decks transversely prestressed with carbon fibre reinforced plastic tendons*, Master's thesis, Queen's University, Ontario, Canada, 173 pp.
- Marshe, S.; Green, M. F. (1999), *Punching behavior of composite bridge decks transversely prestressed with carbon fibre reinforced polymer tendons*, Canadian Journal of Civil Engineering, Volume 26, pp. 618-630.
- MATLAB and Statistics Toolbox Release 2012b (2012), The MathWorks, Inc., Natick, Massachusetts, USA.
- McDowell. E.L.; McKee, K.E.; Sevin. E. (1956), *Arching action theory of masonry walls*, *Journal of the Structural Division*, ASCE, Volume 82, No. 2, pp. 915-1 – 915-18.
- Menétrey, Ph. (1994), *Numerical analysis of punching failure in reinforced concrete structures*, PhD thesis, EPFL No. 1279, Lausanne, Switzerland, 179 pp.
- Microsoft Excel (2010), Microsoft. Redmond, Washington, USA.
- Mitchell, D.; Cook, W. D.; Dilger, W. (2005), *Effects of size, geometry and material properties on punching shear resistance*, *Punching Shear in Reinforced Concrete Slabs*, ACI SP-232-3, pp. 39-56.
- Moe, J. (1961), *Shearing strength of reinforced concrete slabs and footings under concentrated loads*, Bulletin D47, Portland Cement Association, Skokie, IL, 135 pp.
- Moll, E. L. (1984), *Investigation of transverse stressing in bridge decks*, Master's thesis, McMaster University, Hamilton, Ontario, Canada.

## References

- Mosalam, K.M.; Paulino, G. H. (1997), *Evolutionary characteristic length method for smeared cracking finite element models*, Finite Element in Analysis and Design, Vol. 27, No. 1, pp. 99-108.
- Mostafaei, H.; Vecchio, F.; Gauvreau, P.; Semelawy, M. (2011), *Punching Shear Behavior of Externally Prestressed Concrete Slabs*, Journal of Structural Engineering, Volume 137, No. 1, pp. 100-108.
- Mufti, A. A.; Jaeger, L. G.; Bakht, B; Wegner, L.D. (1993), *Experimental investigation of fibre reinforced concrete deck slabs without internal steel reinforcement*, Canadian Journal of Civil Engineering, Volume 20, No.3, pp. 398-406.
- Muttoni, A. (1985), *Punching shear – Draft code proposal*, SIA 162, Working Group 5, Swiss Society of Engineers and Architects, Zürich, 15 pp.
- Muttoni, A. (1989), *The applicability of the theory of plasticity in the design of reinforced concrete* (in German, *Die Anwendbarkeit der Plastizitätstheorie in der Bemessung von Stahlbeton*), Institut für Baustatik und Konstruktion, Report Nr. 176, ETH, Zürich, 159 pp.
- Muttoni, A. (2008), *Punching shear strength of reinforced concrete slabs without transverse reinforcement*, ACI Structural Journal, Volume 105, No. 4, pp. 440-450.
- Muttoni, A.; Fernández Ruiz, M. (2010), *MC2010: The Critical Shear Crack Theory as a mechanical model for punching shear design and its application to code provisions*, fib Bulletin 57, Workshop Shear and punching shear in RC and FRC elements, Salò, Italy, pp 31-60.
- Muttoni, A.; Fernández Ruiz, M. (2012a), *The levels-of-approximation approach in MC 2010: application to punching shear provisions*, Structural Concrete, Volume 13, pp. 32-41.
- Muttoni, A.; Fernández Ruiz, M. (2012b), *Levels-of-Approximation Approach in Codes of Practice*, Structural Engineering International, Volume 22, No. 2, pp. 190-194.
- Muttoni, A.; Fernández Ruiz, M.; Bentz, E. C.; Foster, S. J.; Sigrist, V. (2013), *Background to fib Model Code 2010 shear provisions - Part II Punching Shear*, Structural Concrete, Volume 14, No. 3, pp. 204–214.
- Muttoni A.; Schwartz J. (1991), *Behaviour of beams and punching in slabs without shear reinforcement*, IABSE Colloquium Stuttgart, Volume 62, IABSE, Zurich, Switzerland, pp. 703-708.
- Muttoni, A.; Thürlimann, B. (1986), *Shear tests on beams and slabs without shear reinforcement* (in German, *Schubversuche an Balken und Flachdecken ohne Schubbewehrung*), Institut für Baustatik und Konstruktion, ETH, Zürich, 12 pp.

## References

- NEN 6720:1995, Regulations for concrete: *Structural requirements and calculation methods* (in Dutch), Dutch Normalisation Institute (NEN).
- NEN-EN 1990+A1+A1/C2:2011/NB:2011, National Annex to NEN-EN 1990+A1+A1/C2: Eurocode: *Basis of structural design*, 37 pp.
- Niblock, R. (1986), *Compressive membrane action and the ultimate capacity of uniformly loaded reinforced concrete slabs*, PhD thesis, Queen's University, Belfast, Northern Ireland, UK, 318 pp.
- Ockleston, A. J. (1955), *Load tests on a three-storey reinforced concrete building in Johannesburg*, The Structural Engineer, Volume 33, pp. 304-322.
- Ockleston, A. J. (1958), *Arching action in reinforced concrete slabs*, The Structural Engineer, Volume 36, No. 6, pp. 197-201.
- OHBDC (1979), *Ontario Highway Bridge Design Code*, 1<sup>st</sup> edition, Ontario Ministry of Transportation (OMTC), Highway Engineering Division, Ontario, Canada.
- OHBDC (1983), *Ontario Highway Bridge Design Code*, 2<sup>nd</sup> edition, Ontario Ministry of Transportation (OMTC), Highway Engineering Division, Ontario, Canada.
- OHBDC (1991), *Ontario Highway Bridge Design Code*, 3<sup>rd</sup> edition, Ontario Ministry of Transportation (MTO), Highway Engineering Division, Ontario, Canada.
- Park, R. (1964), *Ultimate strength of rectangular concrete slabs under short-term uniform loading with edges restrained against lateral movement*, Proceedings of the Institution of Civil Engineers, Structures and Buildings, Volume 28, pp. 125-150.
- Park, R.; Gamble, W. (2000), *Reinforced concrete slabs*, John Wiley & Sons, New York, USA, 716 pp.
- Poston, R.W.; Phipps, A. R.; Almustafa, R. A.; Breen, J. E.; Carrasquillo, R. L. (1988), *Effects of transverse prestressing in bridge decks*, Journal of Structural Engineering, Volume 114, No. 4, pp. 743-762.
- Pucher, A. (1964), *Influence surfaces of elastic plates*, Springer – Verlag, Wien, Austria.
- Ramos, A. P.; Lúcio, V.; Regan, P. E. (2011), *Punching of flat slabs with in-plane forces*, Engineering Structures, Volume 33, No. 3, pp. 894–902.
- Ramirez, J. A.; Aguilar, G. (2010), *Experimental evaluation and implementation of post-tensioning in concrete bridge decks*, Report FHWA/IN/JTRP-2010/28 (SPR-2944), 46 pp.
- Ramirez, J. A.; Smith-Pardo, J. P. (2002), *An investigation on transversely prestressed concrete bridge decks*, Report FHWA/IN/JTRP/2002-26 (SPR-2409), 168 pp.

## References

- Rankin, G.I.B. (1982), *Punching failure and compressive membrane action in reinforced concrete slabs*, PhD Thesis, Queen's University Belfast, Northern Ireland, UK, 334 pp.
- Rankin, G. I. B.; Long, A. E. (1987), *Predicting the enhanced punching strength of conventional slab-column specimens*, Proceedings of the Institution of Civil Engineers, Structures and Buildings, Volume 82, pp. 1165-1186.
- Rankin, G. I. B.; Long, A. E. (1997), *Arching action strength enhancement in laterally restrained slab strips*, Proceedings of the Institution of Civil Engineers, Structures and Buildings, Volume 122, pp. 461 - 467.
- Rashid, Y. R. (1968), *Analysis of prestressed concrete pressure vessels*, Nuclear Engineering and Design, Volume 7, No. 4, pp. 334-344.
- Regan, P. E. (1971), *Behavior of reinforced and prestressed concrete subjected to shear forces*, Proceedings of the Institution of Civil Engineers, Structures and Buildings, Paper 7411S, pp. 337 - 364.
- Regan, P. E. (1981), *Behavior of reinforced concrete flat slabs*, CIRIA Report No.89, Construction Industry Research and Information Association, London, UK, 89 pp.
- Regan, P. E. (1982), *Shear resistance of concrete slabs at concentrated loads close to supports*, Engineering Structures Research Group, Polytechnic of Central London, London, UK, 24 pp.
- Regan, P. E. (1985), *The punching resistance of prestressed concrete slabs*, Proceedings of the Institution of Civil Engineers, Structures and Buildings, Volume 79, No. 4, pp. 657 - 680.
- Richart, F. E. (1948), *Reinforced concrete walls and column footings*, parts 1 and 2, ACI Structural Journal, Volume 45, No. 2, pp. 97-127 and No. 3, pp. 237-260.
- Riggs, H. R.; Powell, G. H. (1986), *Rough crack model for analysis of concrete*, Journal of Engineering Mechanics, ASCE, Volume 112, No. 5, pp. 448-464.
- Rosignoli, M. (2002), *Bridge launching*, Thomas Telford Publishing, London, UK, 342 pp.
- Rots, J. G. (1988), *Computational modeling of concrete fracture*, PhD thesis, Delft University of Technology, the Netherlands.
- Rots, J. G. (2002), *Comparative study of crack models*, Proceedings of Third DIANA World Conference, Tokyo, Japan, pp. 17-28.
- Rots, J. G.; Blaauwendraad, J. (1989), *Crack Models for Concrete: Discrete or Smeared? Fixed, Multi-Directional or Rotating?*, HERON, Delft University of Technology, the Netherlands, Volume. 34, No.1, 56 pp.

## References

- RTD 1016 (2012), *Guidelines for nonlinear finite element analysis of concrete structures*, Rijkswaterstaat Technisch Document (RTD) 1016:2012.
- RTD 1006 (2013), RBK, *Richtlijnen Beoordeling Kunstwerken*, Rijkswaterstaat Technisch Document (RTD) 1006:2013.
- Savides, P. (1989), *Punching strength of transversely prestressed deck slabs of composite I-beam bridges*, Master's thesis, Queen's University, Kingston, Ontario, Canada, 217 pp.
- Semelawy, M. (2007), *Effects of axial prestress on the punching behaviour of plain and fibre reinforced concrete slabs*, Master's thesis, University of Tokyo, Japan, 180 pp.
- Shehata, I. A. (1982), *Punching of prestressed and nonprestressed reinforced concrete flat slabs*, M. Phil thesis, Polytechnic of Central London, UK.
- Shehata, I. A. (1985), *Theory of punching in concrete slabs*, PhD thesis, Polytechnic of Central London, UK.
- Shehata, I. A.; Regan, P. E. (1989), *Punching in R.C. slabs*, Journal of Structural Engineering, ASCE, Volume 115, No. 7, pp 1726-1740.
- SIA 262 (2003), *Code 262 for Concrete Structures*, Swiss Society of Engineers and Architects, Zürich, Switzerland, 94 pp.
- Stefanou, G. D. (1993), *Punching shear resistance of prestressed concrete slabs*, Engineering Fracture Mechanics, Volume 44, No. 1, pp. 137-153.
- Stevin Report No. 25.5.13-06, Amir, S.; van der Veen, C. (2013), *Bearing capacity of transversely prestressed concrete decks*, Delft University of Technology, The Netherlands, 243 pp.
- Strauss, A.; Bergmeister, K.; Santa, U.; Pukl, R.; Cervenka, V.; Novák, D. (2003), *Nondestructive reliability analysis of concrete structures numerical concepts and material models for existing concrete structures*, Deutsche Gesellschaft für Zerstörungsfreie Prüfung: International Symposium (NDT-CE 2003) NonDestructive Testing in Civil Engineering 2003, Berlin, Germany.
- Talbot, A. (1973), *Reinforced concrete wall footings and column footings*, University of Illinois, 114 pp.
- Taylor, S. E. (2000), *Compressive membrane action in high strength concrete bridge deck slab*, PhD thesis, Queen's University, Belfast, Northern Ireland, UK.
- Taylor, S. E.; Rankin, G. I. B.; Cleland, D. J. (2002), *Guide to Compressive Membrane Action in Bridge Deck Slabs*, Technical Paper 3, Concrete Bridge Development Group, Camberley, Surrey, UK, 46 pp.

## References

- Taylor, S.; Rankin, G. I. B.; Cleland, D. J. (2003), *Real strength of high performance concrete bridge deck slabs*, Proceedings of the Institution of Civil Engineers, Bridge Engineering, Volume 156, No. 2, pp. 81-90.
- Taylor, S.; Rankin, G. I. B.; Cleland, D. J.; Kirkpatrick, J. (2007), *Serviceability of bridge deck slabs with arching action*, ACI Structural Journal, Volume 104, No. 1, pp. 39-48.
- Tedesko, A. (1976), *Bridge decks: transverse post-tensioning and other successful experiences*, ACI Structural Journal, Volume 73, No. 12, pp. 665-670.
- Thorenfeldt, E.; Tomaszewicz, A.; Jensen, J. J. (1987), *Mechanical properties of high-strength concrete and applications in design*, Proceedings of the symposium on Utilization of High-Strength Concrete, Tapir, Trondheim, Norway, pp. 14-159.
- Tong, P. Y.; Batchelor, B. dev. (1971), *Compressive membrane enhancement in two-way bridge slabs*, ACI Publication SP-30, pp. 271-286.
- Transit New Zealand Ararau Aotearoa (2003), *New Zealand Bridge Manual*, 2nd Edition.
- UK Highways Agency BD 37/01 (2001), *Loads for Highway bridges*, Design Manual for Roads and Bridges, Volume 1, Section 3, part 14, 123 pp.
- UK Highways Agency BD 81/02 (2002), *Use of Compressive Membrane Action in bridge decks*, Design Manual for Roads and Bridges, Volume 3, Section 4, part 20, 20 pp.
- Vaz Rodrigues, R. (2007), *Shear strength of reinforced concrete bridge deck slabs*, PhD thesis, EPFL No. 3739, Lausanne, Switzerland, 271 pp.
- Vaz Rodrigues, R.; Fernández Ruiz. M.; Muttoni, A. (2008), *Punching shear strength of R/C bridge cantilever slabs*, Engineering Structures, Elsevier, Volume 30, No. 11, pp. 3024-3033.
- Vecchio, F. J.; Collins, M. P. (1986), *The modified compression field theory for reinforced concrete elements subjected to shear*, ACI Structural Journal, Volume 83, No. 2, pp. 219-231.
- Vugts, M. W. J. (2012), *Experimental determination of bearing capacity of transversely prestressed concrete deck slabs*, Master's thesis, Delft University of Technology, the Netherlands.
- Walraven, J. C. (1981), *Fundamental analysis of aggregate interlock*, Journal of Structural Engineering, ASCE, Volume 107, No. 11, pp. 2245-2270.
- Wei, X. (2008), *Assessment of real loading capacity of concrete slabs*, Master's thesis, Delft University of Technology, the Netherlands, 102 pp.

## References

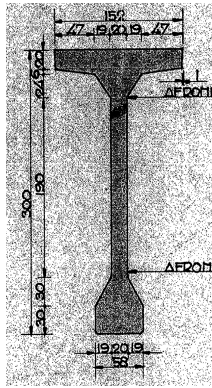
- Whitney, C. S. (1957), *Ultimate shear strength of reinforced concrete flat slabs, footings, beams and frame members without shear reinforcement*, ACI Structural Journal, Volume 54, No. 4, pp 265-298.
- Witteveen+Bos (2009), *Materiaalonderzoek betonnen kunstwerken 37h-006-01 van brienenoord oost (tussenstorten)*, Technical report (in dutch), the Netherlands.
- Wood, R. H. (1961), *Plastic and elastic design of slabs and plates*, Thames and Hudson, London, 344 pp.
- Young, D. M. (1965), *The strength of two-way slabs with fixed edges subjected to concentrated loads*, Master's thesis, Queen's University, Kingston, Ontario, Canada.
- Zheng, Y, Robinson, D, Taylor, S.; Cleland, D. (2009), *Finite element investigation of the structural behaviour of deck slabs in composite bridges*, Engineering Structures, Volume 31, No. 8, pp. 1762-1776.
- Zheng, Y.; Robinson, D.; Taylor, S.; Cleland, D. (2010), *Investigation of the ultimate strength of deck slabs in steel-concrete bridges*, ACI Structural Journal, Volume 107, No. 1, 107-S09, pp. 82-91.

## **Appendix A : Girders**

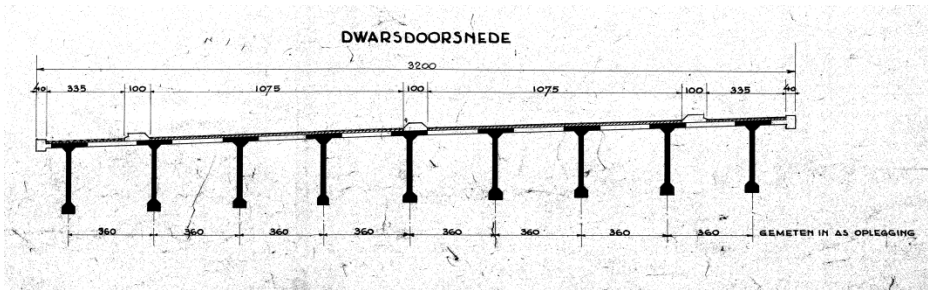
- A1. Old draft drawings of Van Brienoord Bridge
- A2. Reinforcement of the model bridge girders (Spanbeton)
- A3. Preparation of precast, prestressed model bridge girders

## Appendix A

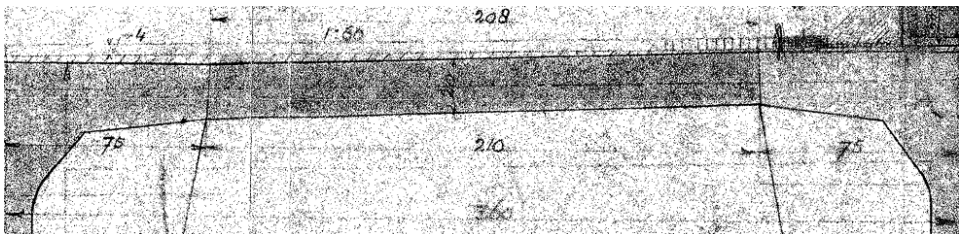
### A1. Old draft drawings of the Van Brienoord Bridge



(a)



(b)



(c)

Fig. A1-1 Old draft drawings of the Van Brienoord Bridge: a) Girder cross-section at midspan of the deck; b) Bridge deck cross section at midspan; c) Deck slab panel cross-section between two girders.

A2. Reinforcement of the model bridge girders (Spanbeton)

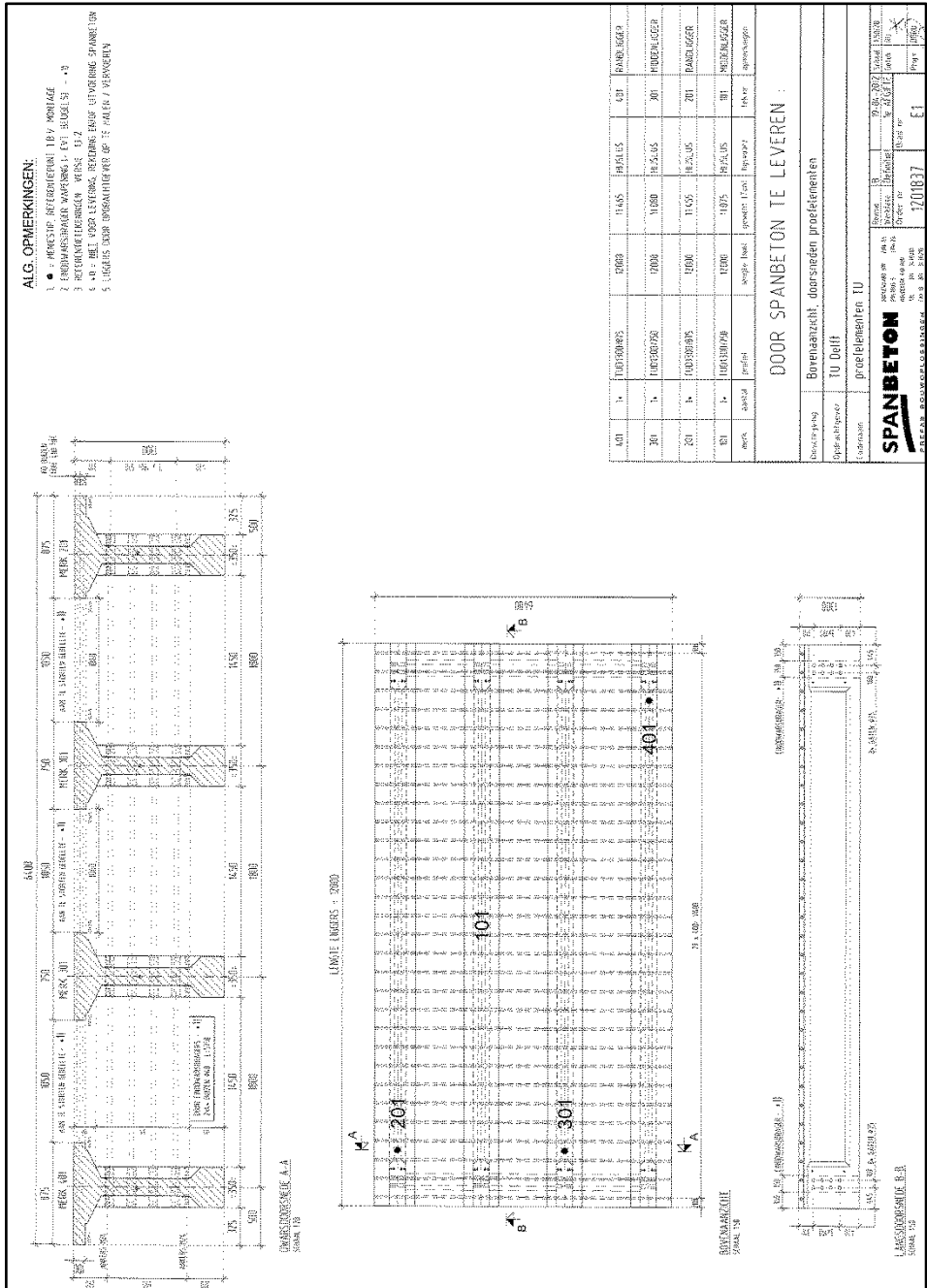


Fig. A2-1 Overview of the model bridge.

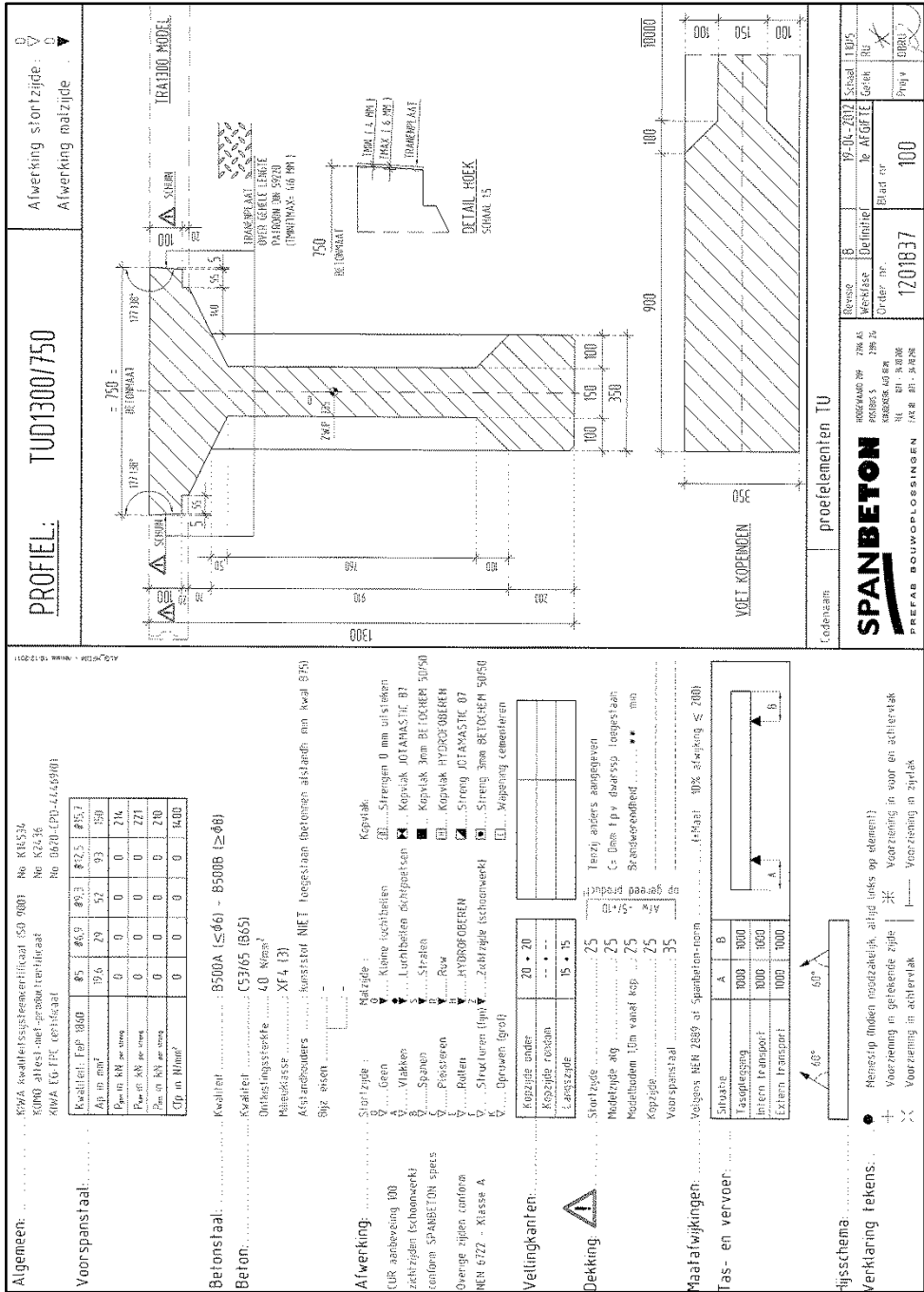


Fig. A2-2 Cross-section of a typical interior girder.



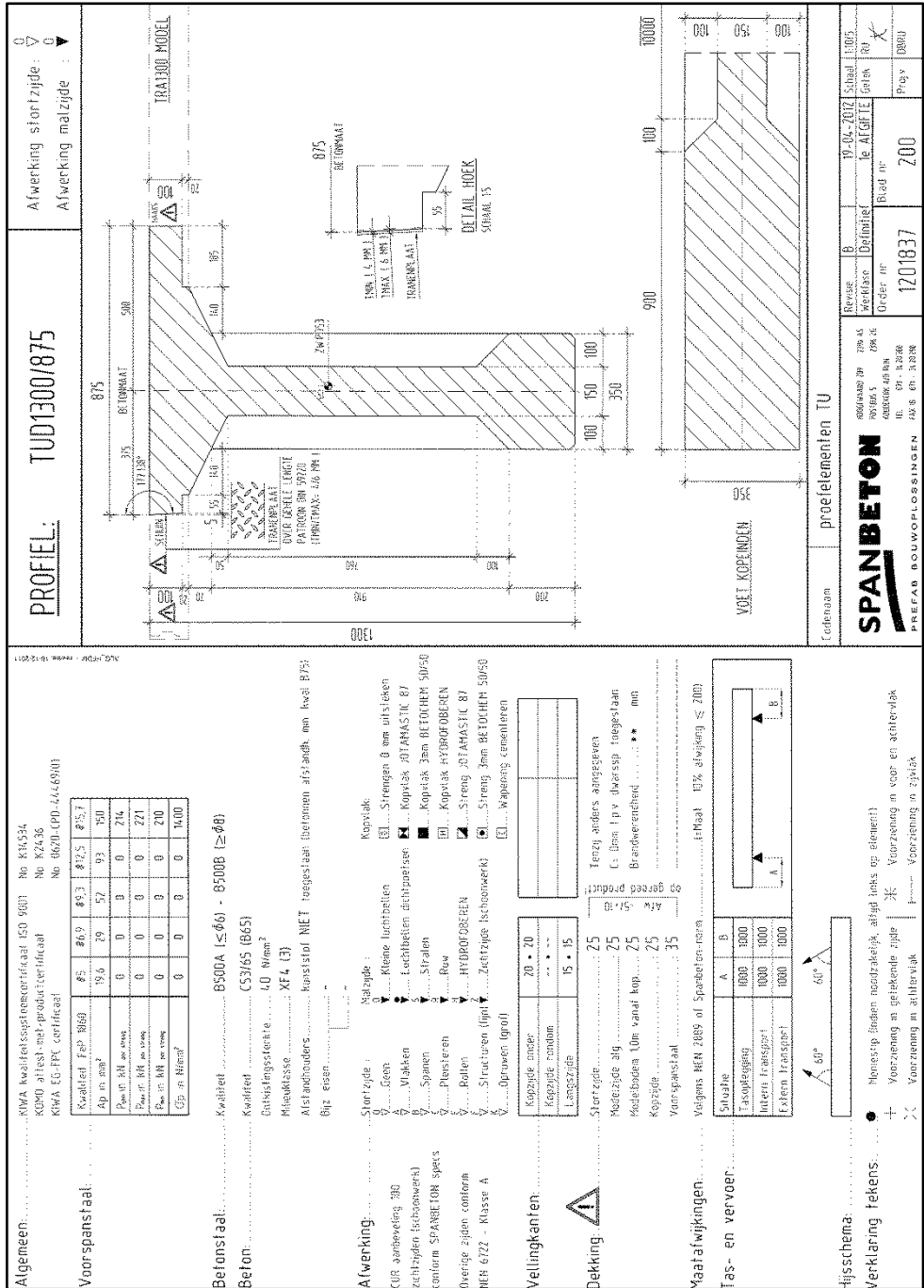


Fig. A2-4 Cross-section of a typical exterior girder.

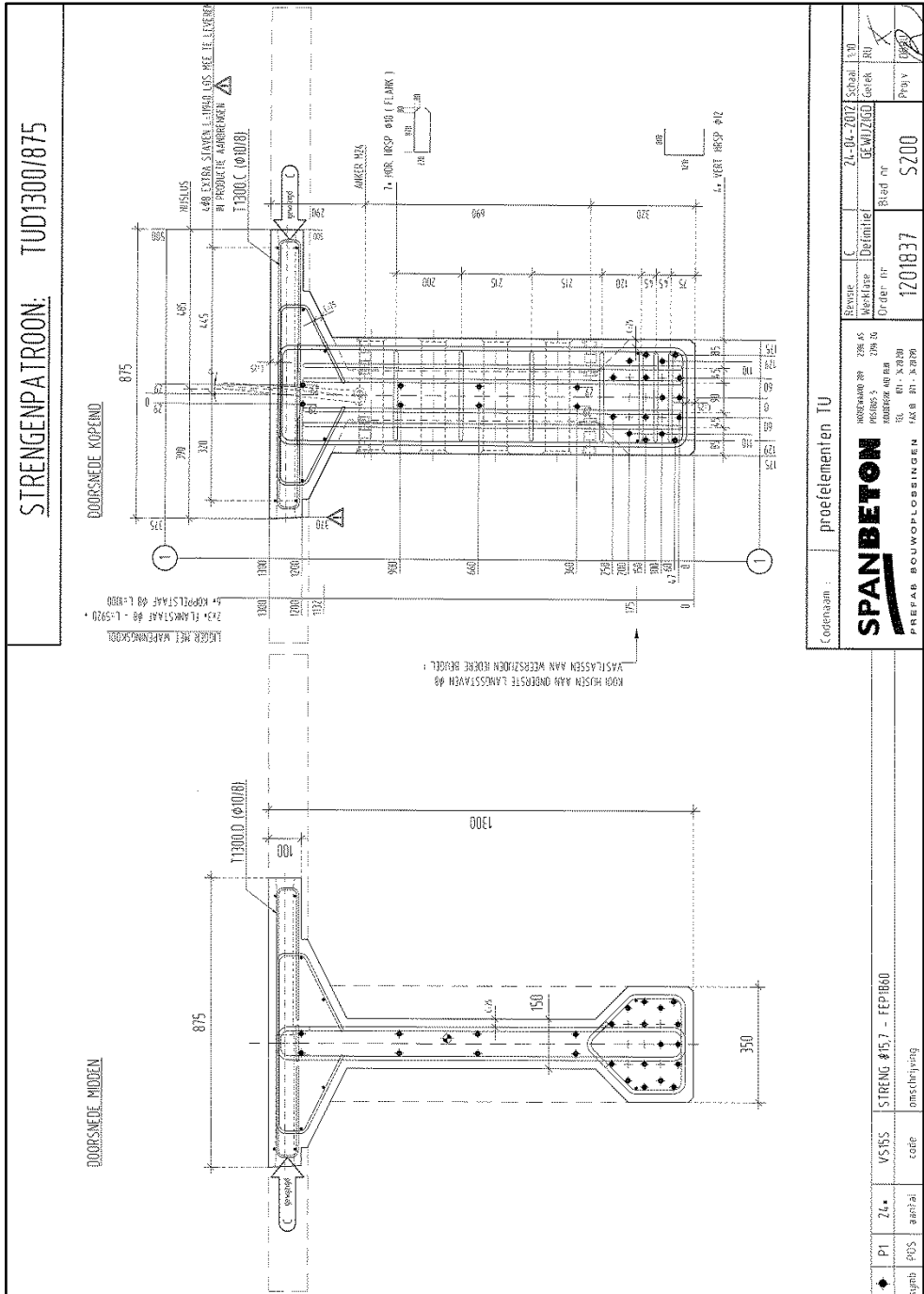


Fig. A2-5 Reinforcement of a typical exterior girder.

Appendix A

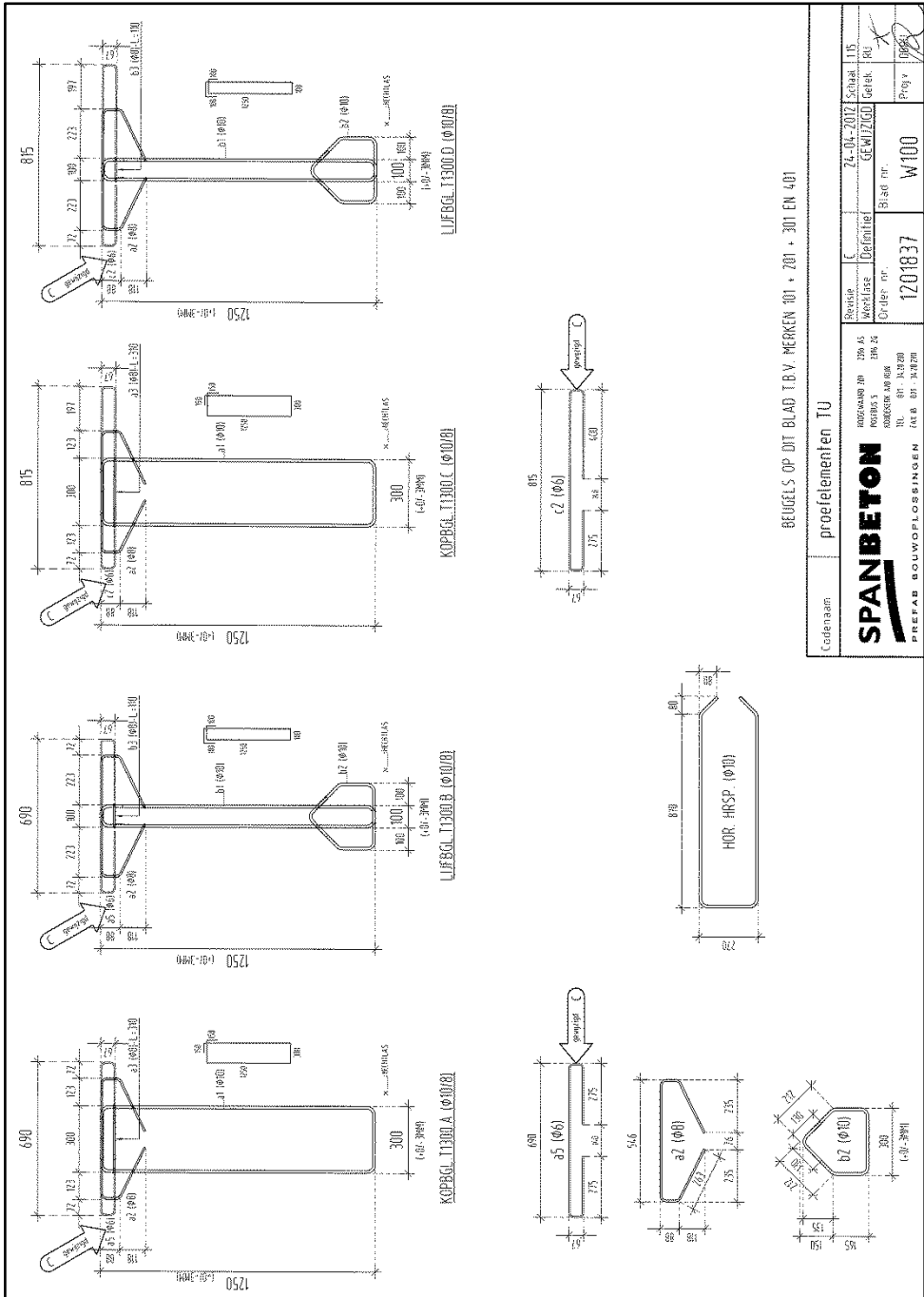


Fig. A2-6 Shear reinforcement of typical interior and exterior girders.

BEUGELS OP DIT BLAD T.B.V. MERKEN 401 + 201 + 301 EN 401

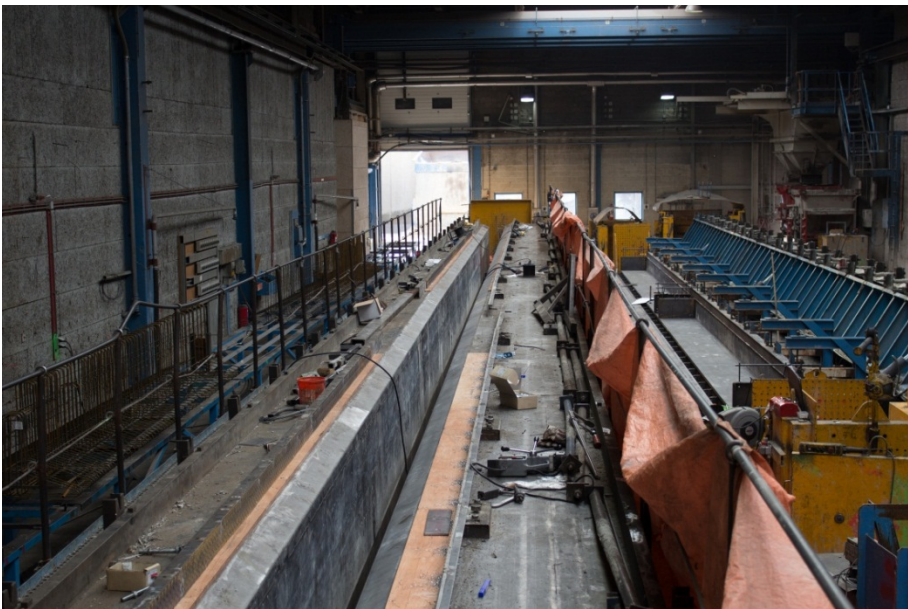
Codenaam	proeielementen TU		
	Revisie wijzigse	Definitie	Schaal
Order nr.	1201837		Blad nr.
	W100		Proj. no.
SPANBETON PREFAB SOUWFOFFLOSSINGEN			
ROZSAKAP P10 100 AS P100 B13 P100 C100 AS 600 TU 81-10-2020 R4 B 01-10-2020		21-04-2017 GEWIZZIGD	Schaal 1/15 Getek. JRU Proj. 1000

## Appendix A

### A3. Preparation of precast, prestressed model bridge girders



(a)



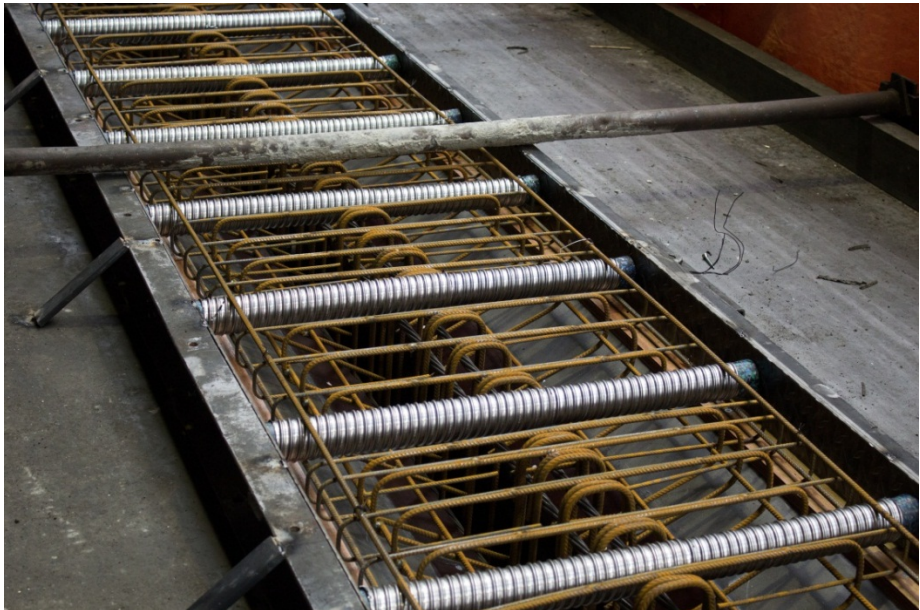
(b)

Fig. A3-1 Preparation of girders in Spanbeton: a) Steel reinforcement; b) Preparing the mold.

Appendix A



(a)



(b)

*Fig. A3-2 Preparation of girders in Spanbeton: a) Steel reinforcement being put inside the mold; b) Ducts inserted in the flanges for transverse prestressing bars of the deck to be cast later on.*

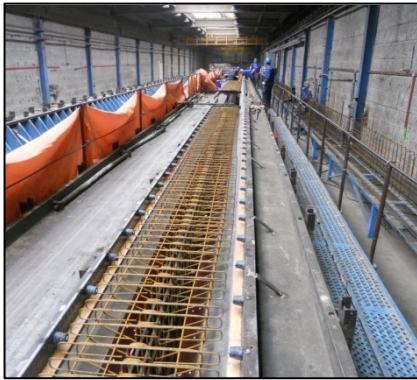
## Appendix A



(a)



(b)



(c)



(d)

*Fig. A3-3 Preparation of girders in Spanbeton: a) Introducing skewed interface template at the flanges; b) Wooden formwork; c) Layout of the girder mold; d) Fixing the ducts in the mold.*

## Appendix A

## **Appendix B: Model bridge deck slab and transverse beams**

- B1. Reinforcement detail of the deck slab
- B2. Deck slab before casting of concrete
- B3. Reinforcements detail of the transverse beams

## Appendix B

### B1. Reinforcement detail of the deck slab

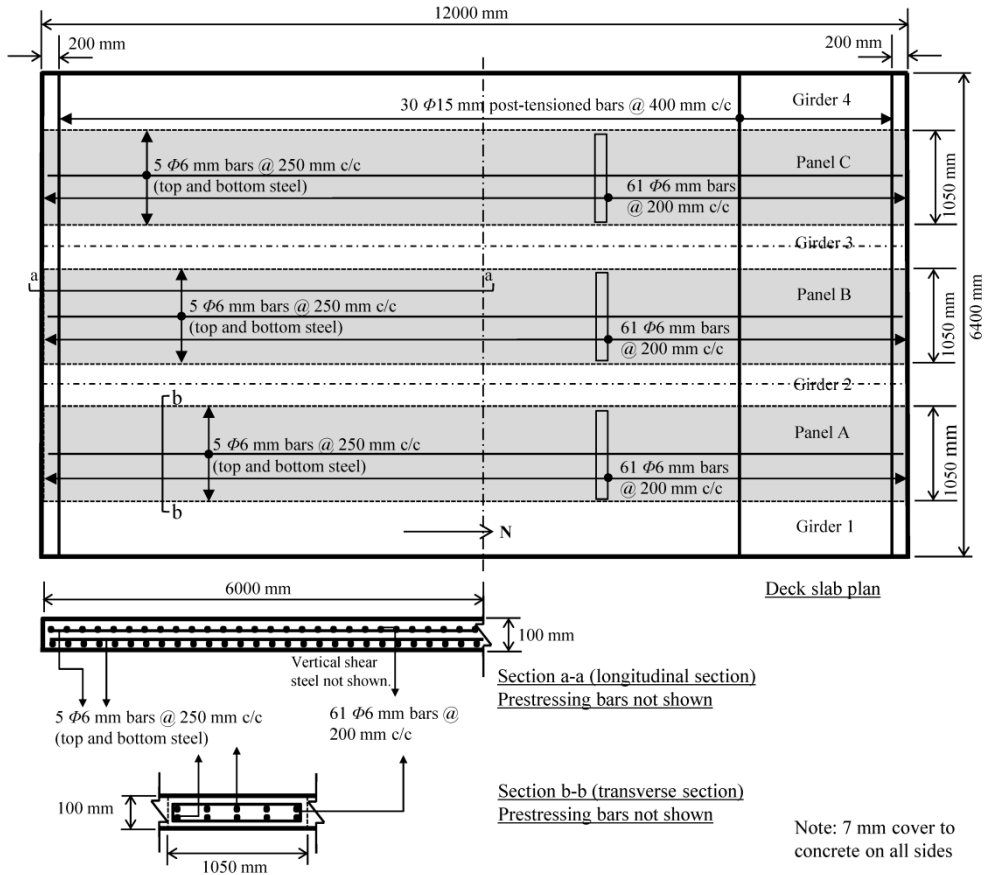
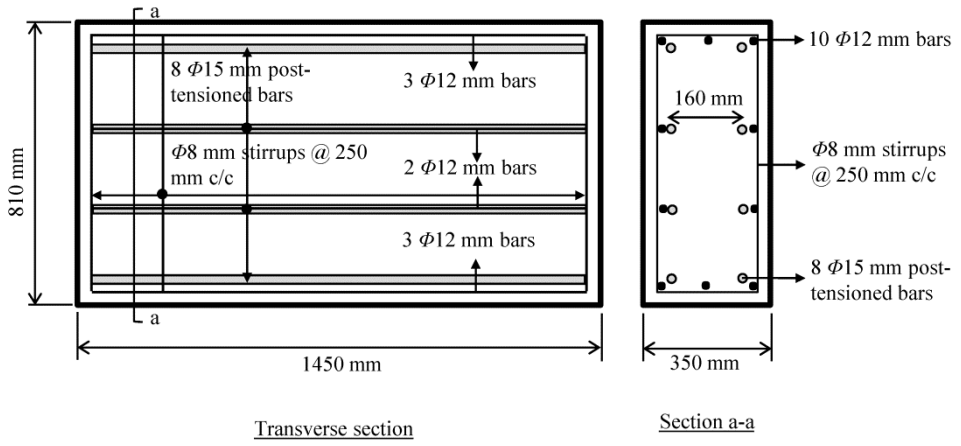


Fig. B1-1 Reinforcement detail of the deck slab.

**B2. Deck slab before casting of concrete**



Note: 20 mm cover to concrete on all sides

*Fig. B2-1 Ordinary steel reinforcement detailing of the deck slab.*

**B3. Reinforcement detail of the transverse beams**

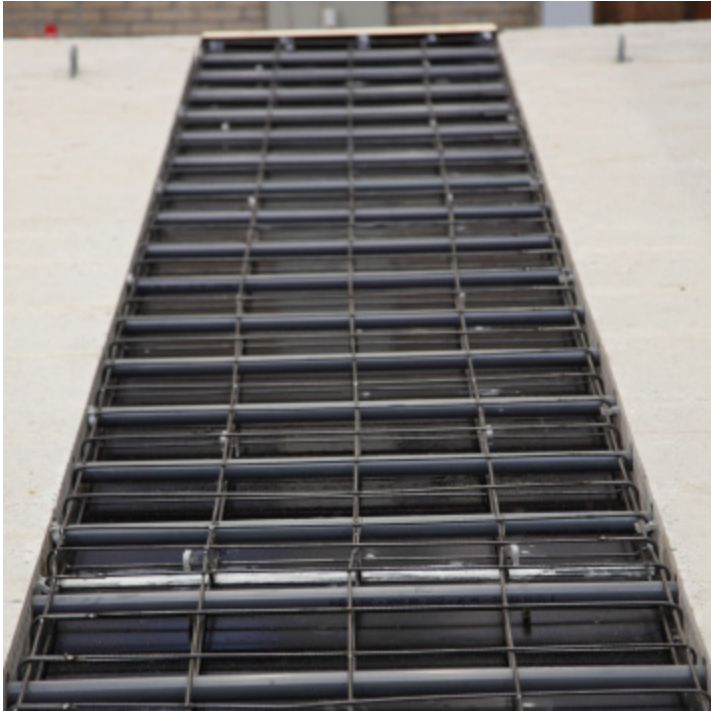


*Fig. B3-1 Ordinary steel reinforcement detailing of the transverse beams.*

## **Appendix C : Theoretical Analysis**

- C1. Park's flexural theory (Wei 2008)
- C2. Size factor by Mitchel et al. (2005)
- C3. MATLAB Program – Critical Shear Crack Theory
- C4. Sample calculation – Critical Shear Crack Theory

**C1. Park's flexural theory (Wei 2008)**

Consider a partially restrained slab strip acted upon by a concentrated load at the midspan.

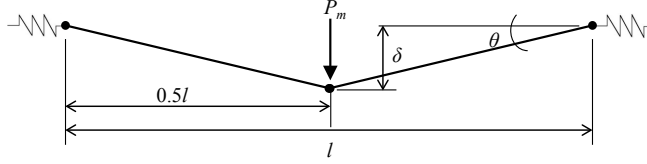


Fig. C1-1 Concentrated load acting at midspan of a partially restrained slab strip.

The original Park's theory (Park and Gamble 2000) has been derived for a partially restrained slab strip with uniformly loaded conditions considering compressive membrane action. According to Wei (2008), the flexural capacity of such a slab strip but with a concentrated load at midspan is:

$$\frac{P_m l}{4} = 0.8 f_{cm} \beta_1 h \left[ \begin{aligned} & \frac{h}{2} \left( 1 - \frac{\beta_1}{2} \right) + \frac{\delta}{4} (\beta_1 - 3) + \frac{l^2}{8\delta} (\beta_1 - 1) \left( \varepsilon + \frac{2t}{l} \right) \\ & + \frac{\delta^2}{8h} \left( 2 - \frac{\beta_1}{2} \right) + \frac{l^2}{8h} \left( 1 - \frac{\beta_1}{2} \right) \left( \varepsilon + \frac{2t}{l} \right) \\ & - \frac{\beta_1 l^4}{64h\delta^2} \left( \varepsilon + \frac{2t}{l} \right)^2 \end{aligned} \right] + d \rho f_{sy} (2d - h + \delta) \quad (1)$$

$$\varepsilon + \frac{2t}{l} = \frac{\left( \frac{1}{hE_c} + \frac{2}{lS} \right) \left[ 0.8 f_{cm} \beta_1 \left( \frac{h}{2} - \frac{\delta}{4} \right) - d \rho f_{sy} \right]}{1 + 0.1 \frac{f_{cm} \beta_1 l^2}{\delta} \left( \frac{1}{hE_c} + \frac{2}{lS} \right)} \quad (2)$$

Units: SI [N, mm]

where,  $P_m$  is the flexural capacity of the slab considering CMA,  $l$  is the length of the slab strip,  $h$  is the depth of the slab strip,  $d$  is the effective depth of the slab strip,  $\varepsilon$  is the strain caused by the horizontal forces,  $t$  is the lateral displacement of the boundary,  $\delta$  is the deflection at midspan,  $\beta_1$  is the ratio of the depth of the equivalent rectangular stress block to the depth of the neutral axis,  $\rho$  is the steel reinforcement ratio,  $f_{cm}$  is the mean cylinder strength of concrete,  $f_{sy}$  is the yield strength of the reinforcement,  $E_c$  is the modulus of elasticity of concrete and  $S$  is the lateral restraint stiffness ( $\infty$  for rigid restraint).

Note: An equivalent steel ratio for the prestressing steel was used for the calculations. No material factors have been applied. Mean strengths have been used.  $S = 10000$  N/mm (assumed).

C2. Size factor by Mitchel et al. 2005

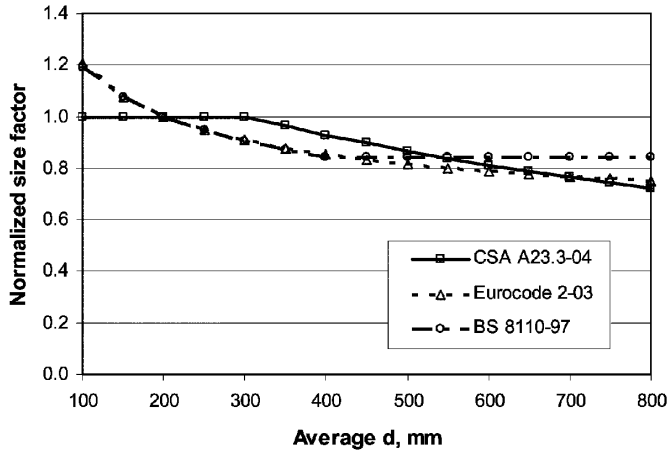


Fig. C2-1 Size effect factors normalized to an average effective depth of 200 mm.

**C3. MATLAB Program – Critical Shear Crack Theory**

```

clear all;
clc;
close all;
%bc = transverse dimension of the loading plate [mm]
%cc = longitudinal dimension of the loading plate [mm]
%bo = critical shear perimeter [mm]
%B = size of the square slab [mm]
%rs = distance from the axis of the column to the line of the contra-flexure of bending
moments [mm]
%h = depth of the slab [mm]
%d = average effective depth of the slab [mm]
%rhops = equivalent steel reinforcement ratio
%dg = maximum aggregate size [mm]
%dg0 = reference aggregate size [mm]
%fcm = compressive strength of concrete [MPa]
%Es = Youngs modulus for steel steel [MPa]
%fpe = effective prestress [MPa]
%sai = Guess sai [-]
%Ap = Area of prestressing steel [mm2/mm]
%Fp = Inplane force [N/mm]
%SigmaP = Compressive stress in concrete [MPa]
%mr = flexural strength [Nmm/mm]
%mp = decompression moment [Nmm/mm]

% Starting input data
% Change data for a different slab
h = 100;
d = 87;
B = 1050;
bc = 200;
cc = 200;
fcm = 65;
SigmaP = 2.5; %Change value for LoA
Ap = 0.4425;
rhops = 0.004425;
Es = 2 * 10^5;
dg = 20;

```

## Appendix C

```
dgo = 16;
e = 0;
c1 = 0.75;
c2 = 15;

%calculated parameters
bo = ((2 * bc) + (2 * cc)) + (3.1416*d);
rs = 250;
n = SigmaP * h;
fpe = Fp/Ap;
mr = rhops * fpe * d^2 * (1-(rhops * fpe / 2 / fcm));
mp = n * ((h/2)-(d/3)+ e);
mrp = mr - mp;

%Starting assumption
sai = 0;
%outer loop
j=0;
% -----code-----

saveThisSai=[];
saveThisJ=[];

% select the x-axis and resolution = sai vector and its resolution
sai=0:0.00001:0.15;

% iterate over each value of sai with variable j= 1 to number_of_elements in sai_vector
for j=1:numel(sai)

    % calculate ms for each value of sai
    ms(j) = (((sai(j)/1.5*d/rs*Es/fpe)^(2/3))*(mrp))+ mp);

    %calculate Vrs
    Vrs(j) = 8 * ms(j)/(1e6);
    % calculate Vrf
    Vrf(j) = ((bo * d * ((fcm)^0.5) * c1)/(1 + ((c2 * sai(j) * d)/(dg + dgo)))/(1e6);

    % calculate distance between the Vrs and Vrf
```

## Appendix C

```
diff(j)=(abs(Vrs(j)-Vrf(j)));
threshold=0.0001;

%Note: Vrs and Vrs are in 'megaNewton'

if(diff(j)<threshold)
saveThisSai=sai(j);
saveThisJ=j;
end

end

% interpolated graph of Vrs Vs. sai
% 'linewidth' property sets : thickness of plot lines
plot(sai,Vrs,'b','linewidth',1.5)
hold on
% interpolated graph of Vrf Vs. sai
plot(sai,Vrf,'r','linewidth',1.5)
hold on

%*****

ylim([0 0.8])
xlim([0 0.05])
xlabel ('Rotation [rad]');
ylabel ('Load [MN]');
grid on
```

#### C4. Sample calculation for a TPL of 2.5 MPa

The equations related to the critical shear crack theory are as follows. The variables are defined in section 8.3. Mean material strengths and SI units ( $N$ ,  $mm$ ) will be used in the calculation.

Failure criterion according to the critical shear crack theory:

$$\frac{V_R}{b_0 d_v \sqrt{f_c}} = \frac{3/4}{1 + 15 \frac{\psi d}{d_{g0} + d_g}} \quad (1)$$

which can be rewritten as ( $d = d_v$ ,  $f_c = f_{cm}$ ):

$$V_{rf} = V_R = \frac{0.75 b_0 d \sqrt{f_{cm}}}{1 + 15 \frac{\psi d}{d_{g0} + d_g}} \quad (2)$$

Load-rotation relationship:

$$\psi = 1.5 \frac{r_s}{d} \frac{f_{sy}}{E_s} \left( \frac{m_s - m_p}{m_R - m_p} \right)^{1.5} \quad (3)$$

which can be rewritten as ( $f_{sy} = f_{pe}$ ,  $\rho = \rho_{ps}$ ):

$$m_s = \left[ \left( \frac{\psi}{1.5} \frac{d}{r_s} \frac{E_s}{f_{pe}} \right)^{1.5} (m_R - m_p) \right] + m_p \quad (4)$$

where,  $m_R = \rho_{ps} f_{pe} d^2 (1 - 0.5 \rho_{ps} f_{pe} / f_{cm})$ ,  $m_p = n (h/2 - d/3 + e)$

$$V_{rs} = V = 8 m_s \quad (5)$$

As shown in the figure below, the intersection of the load-rotation curve (Eq. 5) with the failure criterion (Eq. 2) gives the punching load ( $V_{rf} = V_{rs}$ ). The calculation is iterative in nature since the rotation  $\psi$  at which the two curves intersect is unknown in the beginning. Here, the calculation corresponding to  $\psi = 0.034$  that gives the punching shear capacity for a transverse prestressing level of 2.5 MPa is shown. It is the point where the MATLAB program shows the intersection of the load-rotation curve with the failure criterion with negligible error.

## Appendix C

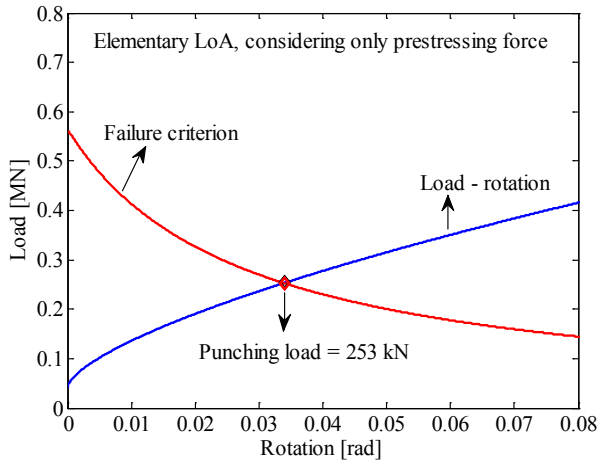


Fig. C4-1 Punching load as calculated by CSCT by an Elementary LoA for a TPL of 2.5 MPa.

### Input parameters:

$h = 100 \text{ mm}$   
 $d = 87 \text{ mm}$   
 $B = 1050 \text{ mm}$   
 $b_c = c_c = 200 \text{ mm}$   
 $f_{cm} = 65 \text{ MPa}$   
 $\sigma_p = 2.5 \text{ MPa}$   
 $A_p = 0.4425 \text{ mm}^2/\text{mm}$   
 $\rho_{ps} = 0.004425$   
 $E_s = 200000 \text{ MPa}$   
 $d_g = 20 \text{ mm}$   
 $d_{g0} = 16 \text{ mm}$   
 $e = 0 \text{ mm}$   
 $c_1 = 0.75$   
 $c_2 = 15$   
 $r_s = 250 \text{ mm}$

### Calculated parameters:

$b_0 = 4 b_c + \pi d = 4 (200) + \pi (87) = 1073.18 \text{ mm}$   
 $n = \sigma_p h = 2.5 \times 100 = 250 \text{ N/mm}$   
 $f_{pe} = n / A_p = 250 / 0.4425 = 565 \text{ MPa}$   
 $m_R = \rho_{eq} d^2 f_{pe} (1 - 0.5 \rho_{ps} f_{pe} / f_{cm})$   
 $m_R = 0.004425 \times 87^2 \times 565 (1 - 0.5 \times 0.004425 \times 565 / 65) = 18558.5 \text{ N-mm/mm}$   
 $m_p = n (h/2 - d/3 + e) = 250 (100/2 - 87/3 + 0) = 5250 \text{ N-mm/mm}$

## Appendix C

Critical shear crack theory parameters:

For  $\psi = 0.034$ :

Load-rotation relationship:

$$m_s = \left[ \left( \frac{\psi}{1.5} \frac{d}{r_s} \frac{E_s}{f_{pe}} \right)^{1.5} (m_R - m_p) \right] + m_p$$

Putting all the values,

$$m_s = \left[ \left( \frac{0.034}{1.5} \frac{87}{250} \frac{200000}{565} \right)^{1.5} (18558.5 - 5250) \right] + 5250$$

$$m_s = 31640.24 \text{ N-mm/mm}$$

$$V_{rs} = V = 8m_s = 253122 \text{ N} = 253.12 \text{ kN} \quad (6)$$

Failure-criterion:

$$V_{rf} = V_R = \frac{0.75 b_0 d \sqrt{f_c}}{1 + 15 \frac{\psi d}{d_{g0} + d_g}}$$

Putting all values,

$$V_{rf} = V_R = \frac{0.75 \times 1073.18 \times 87 \sqrt{65}}{1 + 15 \frac{0.034 \times 87}{16 + 20}}$$

$$V_{rf} = 252882 \text{ N} = 252.9 \text{ kN} \quad (7)$$

Punching shear capacity =  $V_{rs} = V_{rf} \approx 253 \text{ kN}$ .

## Appendix C

## Appendix D: Details of other experimental programs used to verify CSCT

Notations:

$h$  = total depth of the slab

$d$  = Flexural effective depth of the slab. If negligible reinforcement is present,  $d = 0.9 h$ .

$B$  = Transverse span of the slab.

$b \times c$  = Size of the loading plate.

$f_c$  = Concrete compressive strength.

$A_p$  = Area of prestressing steel. Calculated for a unit length, if not directly given.

$\sigma_{cp}$  = Prestress.

$F_p$  = In-plane force due to *inbuilt* compressive membrane action (if present). If not given, assumed proportionally to the current model bridge values given by the finite element analyses. For Advanced LoA, a combined action of  $\sigma_{cp}$  and  $F_p$  is applied.

$d_g$  = Maximum size of the aggregate. If not given, assumed proportional to the scale of the experiments.

$f_{pe}$  = Effective prestress.

$M_r$  = Flexural capacity, if given.

$P_T$  = Ultimate punching load in the test.

$P_{CSA}$  = Punching load by CSCT at advanced LoA if enough lateral restraint is present. For simple supports, calculation is only made at elementary LoA.

## Appendix D

Table D1. Detail of the experimental cases analyzed by CSCT using advanced LoA.

Test	$h$	$d$	$b \times c$	$f_c$	$A_p$	$\sigma_{cp}$	$F_p$	$P_T$	$P_{CSA}$	$P_T/P_{CSA}$
#	mm	mm	mm $\times$ mm	MPa	mm <sup>2</sup> /mm	MPa	N/mm	kN	kN	
<b>Savides (1989), <math>B = 569</math> mm, elliptical loading area, <math>d_g = 10</math> mm</b>										
<b>Concrete deck slab acting compositely with steel girders by shear studs.</b>										
CE-1	43	39	130 $\times$ 90	47	0.19	4.37	185	94.12	75	1.25
NE-2	43	39	130 $\times$ 90	47	0.19	4.37	185	92.28	75	1.23
NW-3	43	39	130 $\times$ 90	47	0.19	4.37	185	80.11	75	1.07
CW-4	43	39	130 $\times$ 90	47	0.19	4.37	185	82.66	75	1.10
SE-5	43	39	130 $\times$ 90	47	0.19	4.37	185	87.3	75	1.16
SW-6	43	39	130 $\times$ 90	47	0.19	4.37	185	92.23	75	1.23
<b>He (1992), <math>B = 569</math> mm, elliptical loading area, <math>d_g = 10</math> mm</b>										
<b>Concrete deck slab acting compositely with steel girders by shear studs.</b>										
SW-1	43	39	130 $\times$ 90	46.55	0.0869	1.84	185	53.1	53.8	0.99
SE-1	43	39	130 $\times$ 90	46.55	0.0869	1.84	185	53.04	53.8	0.99
CW-2	43	39	130 $\times$ 90	43.15	0.105	2.15	185	54.82	55.6	0.99
CE-2	43	39	130 $\times$ 90	43.15	0.105	2.15	185	57.26	55.6	1.03
NW-2	43	39	130 $\times$ 90	43.15	0.1198	2.5	185	63.85	58.1	1.10
NE-2	43	39	130 $\times$ 90	43.15	0.1198	2.5	185	48.7	58.1	0.84
CE-1	43	39	130 $\times$ 90	46.55	0.14	2.91	185	74.43	62.5	1.19
CW-1	43	39	130 $\times$ 90	46.55	0.14	2.91	185	65.82	62.5	1.05
SE-2	43	39	130 $\times$ 90	43.15	0.1549	3.32	185	66.31	63.1	1.05
SW-2	43	39	130 $\times$ 90	43.15	0.1549	3.32	185	72.97	63.1	1.16
NE-1	43	39	130 $\times$ 90	46.55	0.176	3.88	185	80.54	67.6	1.19
NW-1	43	39	130 $\times$ 90	46.55	0.176	3.88	185	77.52	67.6	1.15
<b>Abendroth (1995), <math>B = 1980</math> mm. RC deck cast over a thin PC deck. <math>f_{pc} = 1395</math> MPa</b>										
<b><math>f_c</math> taken of the RC layer. <math>d</math> calculated till flexural reinforcement. Simply supported edges.</b>										
<b>Precast panels. Flexural strength given. <math>\sigma_{cp}</math> not needed separately. No <math>F_p</math>. <math>d_g = 32</math> mm</b>										
Test	$h$	$d$	$b \times c$	$f_c$	$A_p$	$M_r$	$F_p$	$P_T$	$P_{CSE}$	$P_T/P_{CSE}$
#	mm	mm	mm $\times$ mm	MPa	mm <sup>2</sup> /mm	kNmm/mm	N/mm	kN	kN	
1-U1	201	140	203 $\times$ 508	43.7	0.236	134	-	645	698.8	0.92
2-U1	189	125.5	203 $\times$ 508	48.9	0.236	117.7	-	667	627.7	1.06
2-U2	189	125.5	203 $\times$ 508	48.9	0.236	120	-	689	632	1.09
3-U1	214	150.5	203 $\times$ 508	44.2	0.236	146.9	-	778	763.5	1.02
3-U2	214	150.5	203 $\times$ 508	44.2	0.236	143.3	-	778	755	1.03
4-U1	214	150.5	203 $\times$ 508	49.6	0.236	142.5	-	756	779.6	0.97
4-U2	214	150.5	203 $\times$ 508	49.6	0.236	141.2	-	734	776.7	0.95
5-U1	205	141.5	203 $\times$ 508	43.7	0.236	124.8	-	712	680.4	1.05
5-U2	205	141.5	203 $\times$ 508	43.7	0.236	125.4	-	681	681	1.00
<b>Graddy et al. (1995), <math>B = 1830</math> mm, two RC, two RC/PC panels. <math>F_p</math> given. <math>d_g = 32</math> mm</b>										
<b>Concrete deck slab acting compositely with steel girders by shear studs.</b>										
Test	$h$	$d$	$b \times c$	$f_c$	$A_p$	$\sigma_{cp}$	$F_p$	$P_T$	$P_{CSA}$	$P_T/P_{CSA}$
#	mm	mm	mm $\times$ mm	MPa	mm <sup>2</sup> /mm	MPa	N/mm	kN	kN	
RC1	191	108	406 $\times$ 610	41	-	-	260	770	809.8	0.95
RC2	191	108	406 $\times$ 610	41	-	-	307	912	893	1.02
PC1	191	138	406 $\times$ 610	32.7	0.467	2.83	158	467	480.4	0.97
PC2	191	138	406 $\times$ 610	32.7	0.467	2.83	173	512	486.2	1.05

Appendix D

Test #	$h$ mm	$d$ mm	$b \times c$ mm $\times$ mm	$f_c$ MPa	$A_p$ mm <sup>2</sup> /mm	$\sigma_{cp}$ MPa	$F_p$ N/mm	$P_T$ kN	$P_{CSA}$ kN	$P_T/P_{CSA}$
<b>Marshe (1997), <math>B = 569</math> mm, elliptical loading area, <math>d_g = 10</math> mm, CFRP tendons (higher local restraint)</b>										
<b>Concrete deck slab acting compositely with steel girders by shear studs.</b>										
CW-6	43	39	130 $\times$ 90	48.6	0.096	2.15	250	79	66.7	1.18
CE-3	43	39	130 $\times$ 90	48.6	0.096	2.15	250	82	66.7	1.23
NW-5	43	39	130 $\times$ 90	48.6	0.096	2.5	250	78	67.4	1.16
NE-4	43	39	130 $\times$ 90	48.6	0.096	2.5	250	72	67.4	1.07
SW-1	43	39	130 $\times$ 90	48.6	0.145	3.32	250	92	75.9	1.21
SE-2	43	39	130 $\times$ 90	48.6	0.145	3.32	250	95	75.9	1.25
<b>Hassan et al. (2002), <math>B = 2200</math>, Externally prestressed, steel free deck. <math>d_g = 32</math> mm</b>										
<b>Concrete deck slab acting compositely with steel girders by shear studs.</b>										
DS1	170	170	200 $\times$ 400	37.8	0.454	0	300	554.6	517.3	1.07
DS2	170	170	200 $\times$ 400	37.4	0.454	0.38	300	746.2	690.1	1.08
DS3	170	170	200 $\times$ 400	38.4	0.454	0.49	300	730.9	701.4	1.04
DS3'	170	170	200 $\times$ 400	36.1	0.454	0.48	300	696.1	688.1	1.01
DS4	170	170	200 $\times$ 400	90.7	0.454	0	300	862.9	851.4	1.01
DS5	170	170	200 $\times$ 400	94	0.454	0.59	300	853.2	908	0.94
DS6	170	170	200 $\times$ 400	88.4	0.454	0.85	300	980.5	911.1	1.08
<b>Hwang et al. (2010), <math>B = 2700</math> mm, Steel girders, <math>d_g = 20</math> mm</b>										
<b>Concrete deck slab acting compositely with steel girders by shear studs.</b>										
FS-1	115	102	77 $\times$ 192	47.8	0.536	4.07	300	257.3	312	0.82
FS-2	115	102	77 $\times$ 192	53.2	0.536	4.07	300	325.4	322.2	1.01
P1S	115	102	77 $\times$ 192	54.2	0.536	2.69	300	316.3	305.5	1.04
P2S	115	102	77 $\times$ 192	52	0.536	1.32	300	320	281.3	1.14
MS	115	102	77 $\times$ 192	49.8	0.536	0.67	300	216.2	267	0.81
NS	115	102	77 $\times$ 192	57.6	0.536	0	300	308.3	265	1.16
<b>Mostafaiei et al. (2011), <math>B = 1500</math> mm. Externally prestressed, fibre-reinforced. <math>d_g = 20</math> mm</b>										
<b>Slab resting on continuous roller supports. No <math>F_p</math>. Average <math>\sigma_{cp}</math> is considered.</b>										
P1	127	104	200 $\times$ 200	65.4	2.13	7.15	-	488	458.6	1.06
P2A	130	101.6	200 $\times$ 200	68.5	2.13	5.85	-	390	412.8	0.94
P3	130	101.6	200 $\times$ 200	68.5	2.13	4.8	-	239	346.7	0.69
F1	130	101.6	200 $\times$ 200	59.9	2.13	7.35	-	503	452.6	1.11
F2	130	101.6	200 $\times$ 200	54.8	2.13	6.5	-	457	426.1	1.07
F3	130	101.6	200 $\times$ 200	56.2	2.13	4.75	-	419	395.7	1.06
Specimen P3 is not considered in the calculations due to failure in flexure.										

## Appendix D

## **Acknowledgements**

And by the grace of God, with this dissertation, I conclude my five years of research at the Delft University of Technology. The journey has had its ups and downs but ultimately has ended in bringing me perhaps the greatest achievement of my life.

This research was funded by multiple institutions and organizations. I gratefully acknowledge the support of my alma mater, University of Engineering and Technology Lahore, in extending me the Faculty Development Scholarship. I am also thankful to the section of Concrete Structures at TU Delft and SOOB (the Netherlands) for providing me with additional financial aid, and the Dutch ministry of Infrastructure and the Environment for providing the funds for the experimental part of my research.

This work would not have been possible without the guidance of my promotor Prof. Joost Walraven. It has been an honor to work under his supervision. I am extremely grateful to him for advising me throughout the course of this study and for helping me write this dissertation. I have learnt a lot from him, and not just related to my research. He has taught me how to think out of the box – something I had never done in my life before.

If there is one person who has been the utmost guide to me in my research, it has to be my daily supervisor and copromotor Dr. Cor van der Veen. I am extremely thankful to him for supervising me in this research, for keeping me “on track” whenever I was struggling in my work, and to be always there to help me whenever I needed his opinion on my thesis.

I am also grateful to all the reviewers of my thesis for giving me their valuable input. I’d especially like to thank Dr. Ane de Boer for his input and guidance regarding my finite element model. Thank you Prof. Dick Hordijk and Prof. Jan Rots for the helpful discussions on my thesis. Much appreciation for Dr. Barry Rankin and Prof. Mikael Hallgren for travelling from abroad and being part of my thesis defense committee.

To my teachers from Defense Public School and Kinnaird College, and to my professors from UET Lahore: You all have played an important role in my education. I’d like to express my sincere gratitude towards Prof. Dr. Muhammad Ilyas for supervising me in my B.Sc. and M.Sc. thesis. I also appreciate the encouragement I received from Prof. Dr. Muhammad Ashraf (late), Prof. Dr. Abdul Shakir, and most importantly, the Vice Chancellor UET Lahore, Gen (retd) Muhammad Akram, to do a PhD from abroad.

A research is not just the effort of one person. In fact, there are a lot of people who work behind the scenes and play an important role in its success. I’d like to take this opportunity

to thank all the laboratory staff that has helped me in the preparation of the test setup and in carrying out the experiments.

To my colleagues at TU Delft, thank you for providing me a great environment to work in. Marjo, thank you for all your support and help in practical matters. To my fellow PhD students, I have learnt a lot from all of you. Thank you Kassahun, Andrija, Reza, Yuguang and Patrick, for the jokes we shared during the departmental excursions and other occasions. Thank you Andrija for the back cover picture of this thesis. Many thanks to Yuguang for the helpful tips in the numerical modeling part of my research.

To Ella Fasel and Luz-Ton Estrada: Thank you for all the help and support that you provided me. I am indebted to you for a lifetime.

To Dr. Shahid Suddle: You have been like a mentor to me. Thank you for your kindness and generosity and for advising me during the course of my research.

To my friends in the Netherlands: you are too many to name but I'd like to thank you all for making my stay here a pleasant experience. Amarjeet: Delft has been fun with you around. Thank you for being my friend. Maham, Asma, Aisha, Umer, Adeel, Ali: Thank you for all the fun times, get-togethers and political debates. Farideh and Zdenka, you girls are awesome. It has been a pleasure sharing our house together.

To my friends, Shehzeen, Khadija, Ahmad Hassan, Bilal Zia and Nadeem Mohsin: How lucky I am to have friends like you in my life. Thank you for everything.

To Ejaz: You believed in me when I doubted myself. Thank you for always being there for me. I have no words to express my gratitude towards you.

To Shirin: You are the sister I never had. I am so grateful to you for your support and for making me feel at home in the Netherlands.

And lastly, I'd like to thank my family and friends in Pakistan for supporting me while I completed my study abroad. To my brothers, Daniyal and Mohid: You have been my greatest source of strength. To my dear parents: You have always encouraged me to follow my life's dreams. I owe everything to you and I love you with all my heart.

This PhD has been an eventful and interesting journey for me. I have found the strength in me that I never knew I possessed. Living away from home has been challenging but it has provided me with the cultural exposure that I needed to become the person I am today. Thank you Delft University of Technology for making this "Dutch" experience a memorable one.

## About the author

Sana Amir was born on December 10<sup>th</sup>, 1983 in Lahore, Pakistan. She completed her secondary school studies in 1999 from Defense Public School Lahore. She did her F.Sc. pre-Engineering from Kinnaird College Lahore in 2001. In 2006, she graduated from the University of Engineering and Technology Lahore as a B.Sc. Civil Engineer. Soon after graduation, she started working as a Lecturer in the University of Engineering and Technology Lahore and taught a variety of subjects related to Structural Engineering. She obtained her M.Sc. degree in Civil (Structural) Engineering from the University of Engineering and Technology Lahore in 2008. In 2009, she came to the Delft University of Technology, the Netherlands, to do her PhD on Compressive Membrane Action in Prestressed Concrete Deck Slabs. In her free time, Sana likes to read and write. She is also an aspiring chef in international cuisine.



